Peat erosion: processes, patterns and rates

Changjia Li

Submitted in accordance with the requirements for the degree of
Doctor of Philosophy

The University of Leeds
School of Geography

January 2019

The candidate confirms that the work submitted is his own, except where work which has formed part of jointly-authored publications has been included. The contribution of the candidate and the other authors to this work has been explicitly indicated below. The candidate confirms that appropriate credit has been given within the thesis where reference has been made to the work of others.

The work in Chapter two of the thesis has appeared in a journal publication as follows:

Changjia Li, Richard Grayson, Joseph Holden, Pengfei Li. Erosion in peatlands: recent research progress and future directions. *Earth-Science Reviews*. **185**: 870-886, DOI: 10.1016/j.earscirev.2018.08.005

Changjia Li was responsible for the literature review, data analysis, preparation of figures and tables, and writing the manuscript. Richard Grayson and Joseph Holden provided advice, guidance and feedback throughout. Pengfei Li contributed with critical feedback on a draft of the manuscript.

The work in Chapter three of the thesis has appeared in a journal publication as follows:

Changjia Li, Joseph Holden, Richard Grayson. 2018. Effects of rainfall, overland flow and their interactions on peatland interrill erosion processes. *Earth Surface Processes and Landforms*. **43** (7): 1451-1464, DOI: 10.1002/esp.4328

Changjia Li was responsible for the study design, data collection and analysis, preparation of figures, and writing the manuscript. Joseph Holden and Richard Grayson contributed to the study design, critical feedback and comments on draft manuscripts.

The work in Chapter four of the thesis has appeared in a journal publication as follows:

Changjia Li, Joseph Holden, Richard Grayson. Effects of needle ice on peat erosion processes during overland flow events. *Journal of Geophysical Research: Earth Surface*. DOI: 10.1029/2017JF004508

Changjia Li was responsible for the study design, data collection and analysis, preparation of figures, and writing the manuscript. Joseph Holden and Richard Grayson contributed to the study design, suggested ways of interpreting the data, critical feedback and comments on draft manuscripts.

The work in Chapter five of the thesis has been acceted to *Earth Surface Processes and Landforms*:

Changjia Li, Richard Grayson, Mark Smith, Joseph Holden. Patterns and drivers of peat topographic changes determined from Structure-from-Motion photogrammetry at field plot and laboratory scales. *Earth Surface Processes and Landforms* (accepted).

Changjia Li was responsible for the study design, data collection and analysis, preparation of figures, and writing the manuscript. All other authors contributed to critical feedback and made suggestions for use of different types of software and made comments on draft manuscripts.

The work in Chapter six of the thesis has been submitted to a journal and is under review:

Changjia Li, Joseph Holden, Richard Grayson. Sediment and fluvial particulate carbon flux from an eroding peatland catchment in northern England.

Changjia Li was responsible for the study design, data collection and analysis, preparation of figures, and writing the manuscript. Joseph Holden and Richard Grayson contributed to the critical feedback and commented on draft manuscripts.

Thesis by alternative format - rationale

This thesis is submitted in accordance with the Faculty of Environment's alternative style of doctoral thesis including published material. This format is apposite for this thesis because the literature review chapter and two out of the four research chapters have already been published in peer-reviewed journal, while one chapter is currently under review with a journal and the other is ready for submission to a journal.

This thesis has a short introduction (Chapter 1), including an outline of the main research questions and research strategy; a critical literature review (Chapter 2, published); four research articles (Chapter 3 and Chapter 4 published, Chapter 5 under review and Chapter 6 ready for submission); and a section for research synthesis and conclusions (Chapter 7) which intertwines the findings of all four data chapters, placing them in the context of the objectives and the literature, providing critical discussion and including ideas for future work. The format described above is in line with the University of Leeds guidelines for the alternative style of doctoral thesis including published material.

Acknowledgements

I am extremely grateful to my supervisors, Joseph Holden and Richard Grayson, for valuable advice and guidance and continued support during the past four years. Without their expertise, enthusiasm and valuable contributions this project would not have been so productive and enjoyable. Their encouragement and help, not only for my research but also for life and career development, made my four year's living, studying and working in Leeds greatly valuable with unforgettable memories for the rest of my life.

I would like to sincerely acknowledge my Research Support Group (RSG) members (Mark Smith and Brian Irvine) for their help and support. Mark Smith introduced SfM to my PhD project, provided help in my RSG meetings and kindly provided help when I had problems processing data with Agisoft Photoscan and CloudCompare software.

Laboratory work was very important in this project. David Ashley is gratefully acknowledged for his assistance in preparing the laboratory experimental materials. I would like to thank people from other schools or universities who helped. Susanne Patel from the School of Chemical and Process Engineering (University of Leeds) kindly provided use of the Malvern Morphologi G3S. Jeff Warburton from the Department of Geography (Durham University) is thanked for his support in providing the rainfall simulator and advice for the design of sediment traps used in this study. Many thanks to Damian Lawler from the Centre for Agroecology, Water and Resilience, Coventry University who provided helpful suggestions through emails about how to produce needle ice under laboratory conditions.

Field data collection played a vital role in this project. Field trips to Oxenhope Moor and Marsden Moor with Karen Scott and Michael Dorrington greatly improved my understanding about peatlands, including knowledge about peatland hydrology, vegetation cover and peat erosion features and processes. Field work at Moor House National Nature Reserve involved significant contributions from Joseph Holden and Richard Grayson who helped collect undisturbed peat blocks for laboratory experiments. Field work at Fleet Moss lasted for more than one year with 17 field trips. The work would not have been possible without the support given by the laboratory, field store and technical staff within the School of Geography and this is much appreciated. David Ashley helped a lot with the field set-up. I would also like to thank everyone who endured many days and ably assisted

with field work at Fleet Moss: Santiago Clerici, Sarah Hunt and David Wilson. Their hard work in extremely harsh upland weather conditions are fully acknowledged. I am grateful to David Roe and Dominic Emery for making field equipment available. Demonstrations from Josh Greenwood for water sample (POC) analysis in the laboratory was much appreciated.

I am hugely grateful to everyone in my School who provided help for my PhD project. Jonathan Carrivick and Lee Brown are thanked for providing the Geodimeter and tinytags used in this study. Duncan Quincey, Scott Watson, Joe Mallalieu, Owen King are thanked for providing advice on using Agisoft Photoscan and CloudCompare to undertake data analysis. Claudio Bravo and Yi-Min Chang Chien are thanked for providing help in using Matlab and R to do data analysis. Mike Kirkby and Taco Regensburg also provided helpful discussions and suggestions for my work in River Basin Processes & Management cluster meetings. I am grateful to Jacob A. Morgan (Colorado State University, USA) for providing help in data visualization.

The work was funded by the China Scholarship Council (File No. 201406040068) and the University of Leeds. I would like to thank the River Basin Processes & Management cluster, School of Geography (University of Leeds) for providing me with financial support for sample analysis and meeting attendance. The financial aid from the British Geomorphology Society for attending EGU 2018 General Assembly is also gratefully acknowledged.

I would like to thank my friends and colleagues in Leeds for their physical and mental support and great friendship. There are a lot of unforgettable memories for us getting together for travelling UK and European countries, sports (squash, tennis and badminton), drinks (tea and beer) and food. These nice people are listed in alphabetical order: Dian Li, Faith Chan, Mingyang Lv, Jiren Xu, Junfan Lin, Pengfei Li, Qing Sui, Ru Xu, Yiting Duan, Yue Cao.

Finally, special thanks to my family for their great love!

Abstract

Improved understanding of peat erosion processes and rates of erosion at different scales are urgently needed to better predict future peat erosion under climate and land management changes. This laboratory and field study on UK blanket peat showed that both raindrop impact and the interaction between rainfall and flow driven erosion processes were important in affecting peat overland flow and erosion processes for gentle slopes and shallow overland flow conditions. Raindrop impact contributed significantly to increasing sediment yields (47%). Needle-ice (NI) processes dramatically increased peat erodibility and reduced peat stability, producing six times higher peat losses than control treatments. NI significantly reduced surface flow velocity (32–44%) but increased overland flow shear stress (55–85%). Net topographic change measured using Structure-from-Motion (SfM) was –14 to +30 mm yr^{-1} for field plots (peat hagg, gully wall, riparian area, gully head) and –27 mm yr^{-1} over a 598 m^2 catchment. Repeated SfM surveys showed spatial patterns of erosion and deposition could be driven by event-scale processes that may not be observed with surveys conducted between long intervals. Surface roughness was a significant predictor of topographic change at both field plot scale and laboratory macroscale. SfM produced significantly different topographic change values compared to sediment traps in nested catchments in the field and sediment yield sampling on laboratory peat blocks. The greatest sediment and particulate organic carbon losses from a 1.7 ha study catchment were found during the autumn and much of the available sediment appeared to be derived from weathering during dry weather earlier in the year. The research shows that where bare peat is subject to weathering by needle ice and desiccation, and is subsequently splashed by raindrops a large supply of sediment can be mobilised by overland flow, particularly where flow concentrates producing interrill, rill and gully erosion.

Table of contents

List of tables

List of figures

List of common abbreviations used

SY	Sediment yield rate (t km^{-2} yr^{-1}, mg m^{-2} h^{-1} or mg m^{-2} min^{-1})
SC	Sediment concentration (mg l^{-1})
SRR	Surface retreat rate (mm yr^{-1})
OD	Outside diameter (mm) of the drop former (Tygon tubing)
ID	Inside diameter (mm) of the drop former (Tygon tubing)
D_{50}	Median raindrop size (mm)
I	Rainfall intensity (mm hr^{-1})
θ	Slope (º)
F	Upslope inflow rate (mm hr^{-1})
R_i	*i*th overland flow volume collected (mL)
S	Plot area (cm^2)
t	Time interval between the collection of successive overland flow samples (min)
V_s	Surface flow velocity (cm s^{-1})
V	Mean flow velocity (cm s^{-1})
k	A coefficient which is 0.33 for shallow flows on bare peat surfaces under gentle slopes
h	Mean flow depth for the whole plot (cm)
q	Unit discharge (cm^2 s^{-1})
Q	The overland flow volume during *t* duration (ml)
b	The width of water-crossing section (cm)
n	The Manning's friction coefficient
f	The Darcy–Weisbach friction factor
J	The *sine* of the bed slope (m m^{-1})
τ	Flow shear stress (Pa)
Ω	Stream power (W m^{-2})
ρ	The density of water (kg m^{-3})
$I_{raindrop}$ *(SC)*	The raindrop impact on sediment
Interaction (SC)	Effect of the interaction between rainfall- and flow-driven erosion on sediment concentration
$SC_{Rainfall}$	The average sediment concentration in *Rainfall* experiments
SC_{Inflow}	The average sediment concentration in *Inflow* experiments
$SC_{Rainfall + Flow}$	The sediment concentration in *Rainfall* + *Flow* experiment
IS	The initial overland flow stage
SSRS	The steady-state overland flow stage

WS	The whole experimental stage
AS	Peat anti-scouribility capacity (L g^{-1})
W	The weight of the oven-dried peat mass (g)
NI	Peat blocks subject to needle ice processes
Non-NI	Peat blocks not subject to needle ice processes
SfM	Structure-from-Motion photogrammetry
GCPs	Ground Control Points
RMSE	Root mean squared error
M3C2	Model to Model Cloud Comparison algorithm
E_{norm}	Normal error (%)
D	The normal scale
d	The projection scale
σ	Roughness
n(i)	The normal scale *D* divided by the roughness σ
$LoD_{95\%}$	Level of Detection threshold for a 95% confidence level
σ_1 *and* σ_2	The roughness of each point in sub-clouds of diameter *d* and size n_1 and n_2,
reg	The user-specified registration error
SS	Suspended sediment
POC	Particulate organic carbon
DOC	Dissolved organic carbon
EC	Electro-conductivity
SSC	Suspended sediment concentration
Q_s	Suspended sediment yield (kg d^{-1})
Q_{POC}	Particulate organic carbon yield (kg d^{-1})

Chapter 1
General introduction

1.1 Project rationale

Peatlands, where organic-rich peat slowly accumulates (Charman, 2002), cover approximately 2.84% of the world's land area (Xu et al., 2018b). Peatlands serve as important terrestrial carbon sinks, storing one-third to half of the world's soil carbon (Yu, 2012). Quantification of the carbon flux from peatland systems is therefore vital to fully understand global carbon cycling (Evans and Warburton, 2007, Pawson et al., 2008). Peatlands provide a wide range of important ecosystem services including water supply (Xu et al., 2018a), recreation and biodiversity (Bonn et al., 2016). Peatlands are fragile ecosystems as the conditions required for peatland initiation and ongoing survival are relatively narrow. In addition, they are sensitive to a wide range of external and internal pressures such as climate change, atmospheric pollution, grazing, burning, artificial drainage, afforestation and infrastructure (Ise et al., 2008, Fenner and Freeman, 2011, Parry et al., 2014, Noble et al., 2017, Holden et al., 2007).

Peat erosion is a natural process driven primarily by the actions of water and wind. However, slight changes in conditions driven by human action can lead to accelerated erosion and degradation (Parry et al., 2014). Blanket peatlands are rain-fed and usually occur on sloping terrain and thus could be more vulnerable to water erosion (Li et al., 2017). Many blanket peatlands have experienced severe erosion (Evans and Warburton, 2007, Grayson et al., 2012, Li et al., 2016b) and are under increasing erosion risk from future climate change (Li et al., 2016a, Li et al., 2017). The erosion of peat with high carbon content will enhance losses of terrestrial carbon in many regions. Sediment loss from peatlands represents a significant removal of carbon, compromising a peatland's ability to maintain ecosystem function as a terrestrial carbon sink (Evans and Lindsay, 2010).

Peatland erosion has previously been studied (Bower, 1960, Evans and Warburton, 2007, Li et al., 2016b), but some of the processes still remain poorly understood (Li et al., 2018). Prevention and control of peat erosion risk relies on designing and applying appropriate conservation strategies and management techniques, which in turn requires a thorough understanding of processes and rates. Improved understanding of spatial and temporal peat

erosion dynamics and more data on rates of erosion at different scales are urgently needed.

1.2 Aim and research objectives

This research aims to investigate mechanisms and controls of some important peat erosion processes (i.e. interrill erosion, needle-ice formation and thawing, water erosion processes); and to measure peat erosion rates using a range of techniques (laboratory simulation experiments, Structure-from-Motion photometric techniques, sediment traps and catchment stream sampling) at different spatial scales (very fine and fine plot, mini-catchment and catchment scales). Four research objectives have been structured that allow the broader research aim to be achieved. The specific objectives are identified below, together with an outline of the research strategy.

1.2.1 Objective1 (Chapter 3): To determine how rainfall, overland flow and their interaction affect peat interrill erosion processes

1.2.1.1 Rationale

Blanket peatlands are rain-fed and thus rainsplash is an important sediment supply mechanism, with raindrops providing the primary force to initiate low-density peat particle detachment. In addition, raindrop impact is important in affecting overland flow hydraulics and sediment transport as overland flow depths are typically shallow, in the order of a few millimeters (Holden et al., 2008, Holden and Burt, 2002). However, rather limited attention has been given to peat erosion on hillslopes that are affected by mechanisms of raindrop impact, overland flow and their interaction. The first aim of this thesis is to understand the importance of each of these mechanisms and how they interact. The specific objectives are: (i) to assess how rainfall impact affects overland flow hydraulics and erosion processes for shallow overland flow; (ii) to examine the effects of interactions of rainfall and flow on sediment yield and flow hydraulics; and (iii) to investigate the effects of slope gradient and upslope inflow on peat hillslope overland flow and erosion.

1.2.1.1 Research strategy

Laboratory simulation experiments were conducted on peat blocks under two slopes (2.5° and 7.5°) and three treatments: *Rainfall*, where rainfall with an intensity of 12 mm hr^{-1} was simulated; *Inflow*, where upslope overland flow at a rate of 12 mm hr^{-1} was applied; and *Rainfall* + *Inflow* which combined both *Rainfall* and *Inflow*. Overland flow, sediment loss and

overland flow velocity data were collected and splash cups were used to measure the mass of sediment detached by raindrops. The effects of rainfall, overland flow and their interaction were determined as the differences in the sediment collected at the exit from the flume among the *Rainfall*, *Inflow* and *Rainfall* + *Inflow* events.

1.2.2 Objective 2 (Chapter 4): To determine how needle ice formation and thawing affect peat erosion processes during overland flow events

1.2.2.1 Rationale

Peat has a high volumetric heat capacity but much lower conductivity, and thus a strong thermal gradient can develop between a cold peat surface and warmer peat at depth. The significant temperature gradients together with abundant moisture supply are ideal for needle-ice formation that has been widely reported to be important in producing eroding peat faces. However, little quantitative work has been conducted on how surface roughness and overland flow are affected by needle-ice formation and melting, nor on quantifying how these effects impact upon peat erosion. The aim of Chapter 4 is to measure how needle-ice processes affect peat erodibility, overland flow hydraulic characteristics and sediment production processes through a series of experiments.

1.2.2.2 Research strategy

To quantify the effects of needle-ice on peat physical properties, overland flow hydraulics and erosion processes, physical overland flow simulation experiments were conducted on bare blanket peat with and without needle-ice processes (NI). For each treatment with NI and Non-NI, overland flow rates of 0.5, 1.0 and 2.0 L min^{-1} and slopes of 2.5° and 7.5° were applied. Peat erodibility, sediment concentration and sediment yield were significantly elevated in treatments subjected to needle-ice processes.

1.2.3 Objective 3 (Chapter 5): To assess peat erosion rates, patterns and drivers using Structure-from-Motion

1.2.3.1 Rationale

Peat erosion or deposition can be measured by numerous methods including erosion pins and bounded plots, and more recently through high resolution topographic surveying methods to improve quantification of erosion. Erosion plots are used commonly to measure soil erosion over short and medium time periods. Bounded plots are usually equipped with troughs

or sediment traps to catch exported sediment directly under natural precipitation or rainfall simulations. While plot scale or catchment yield studies have supported understanding of peat erosion they usually allow the measurement of the soil loss reaching the plot or catchment outlet, which is then averaged for the entire plot area (Parsons et al., 2006). The data integrate all upslope processes at a single point (Smith and Vericat, 2015). Therefore it is difficult to assess the spatial variation of erosion and deposition and the drivers within the plot due to the lack of sufficient data. Direct measurements of surface denudation with high accuracy would therefore be preferable if we are to understand more about erosion processes.

1.2.3.2 Research strategy

Structure-from-Motion (SfM) photogrammetry was used to study event-based and seasonal changes in peatland topography on field plots. Over a 12 month period, 11 repeated SfM surveys were conducted on four geomorphological sites of 18–28 m^2 (peat hagg, gully wall, riparian area and gully head) in a blanket peatland in northern England. Repeat SfM surveys were conducted to examine the spatial and temporal variability of erosion and deposition patterns on the four sites. In the laboratory, peat blocks with slopes of 2.5° and 7.5° were subject to simulated rainfall and upslope inflow treatments. The peat losses quantified by traditional sediment yield sampling were compared with the SfM derived topographic data.

1.2.4 Objective 4 (Chapter 6): To quantify sediment and fluvial particulate carbon flux from an eroding peatland catchment in northern England and to compare these data to spatial patterns of topographic change within the catchment

1.2.4.1 Rationale

Assessing the temporal patterns of sediment and POC from eroding peatlands has the potential to provide insight into the controls on fluvial carbon flux from these systems (Pawson et al., 2012). Multi-scale studies to improve understanding of connections between different spatial scales and upscaling of erosion rates are necessary. Chapter 6 aims to assess the sediment and POC loss from a degraded, eroding blanket peat catchment and nested smaller catchments to determine how this relates to spatial patterns of topographic change across the catchment over the course of a year. Specific objectives are: (i) to measure fluvial suspended sediment and POC fluxes from an eroding headwater peatland system; (ii) to describe the

dynamics of suspended sediment transport at different temporal scales (seasonal and monthly); (iii) to compare peat erosion rates measured by different techniques (sediment traps, SfM photogrammetry, sediment sampling) at different scales (plot, nested catchment and small headwater catchment).

1.2.4.2 Research strategy

Field-based SfM photogrammetry, sediment traps and sediment sampling in the stream flowing from a headwater blanket peat catchment were used to compare the rate of peat surface topographic change and the rates of suspended sediment and POC losses. The fieldwork enabled both a temporal and spatial assessment of peat sediment dynamics at different scales.

1.3 Thesis outline

This thesis is structured as follows:

1. Chapter 2 provides a detailed literature review that covers: i) peat erosion processes across different scales; ii) techniques used to measure peat erosion; iii) factors affecting peat erosion; and iv) meta-analyses of reported peat erosion rates. Further research needs were identified on basic peat erosion processes, application of new and integrated measurement of different variables and the impact of drivers or mitigation techniques that may affect peat erosion.
2. Chapter 3 provides the first experimental work designed and conducted to investigate mechanisms of raindrop impact, overland flow and their interaction perform on a peat soil. Laboratory experiments of rainfall simulation, upslope inflow simulation and a combination of rainfall and upslope inflow simulation were conducted on peat blocks. The research objectives were addressed by comparing overland flow and sediment yield processes and flow hydraulic characteristics among different treatments.
3. Chapter 4 addresses objective 2 and provided the first quantitative analysis of the effects of needle ice on peat physical properties, overland flow hydraulics and erosion processes by physical overland flow simulation experiments.
4. Chapter 5 addresses objective 3 by examining the spatial and temporal variability of peat erosion and topographic and weather-

related drivers at field plot scale; and by comparing peat losses quantified by traditional sediment yield sampling with the SfM derived topographic data on laboratory peat blocks.

5. Chapter 6 addresses objective 4 by measuring fluvial suspended sediment and POC fluxes from an eroding headwater peatland system; and by examining the dynamics of suspended sediment and POC transport at different temporal scales (seasonal and monthly). It also compared peat erosion rates measured by different techniques (sediment traps, SfM photogrammetry, sediment sampling) at different scales (plot, mini-catchment and catchment).

6. Chapter 7 provides a synthesis of the main findings in this thesis. It draws together the findings in Chapters 3–6 and discusses the wider implications of the findings. The limitations of the study and directions for future work are also discussed. The chapter ends with a summary of the conclusions from the thesis.

References

BONN, A., ALLOTT, T., EVANS, M., JOOSTEN, H. & STONEMAN, R. 2016. *Peatland restoration and ecosystem services: science, policy and practice*, Cambridge University Press.

BOWER, M. 1960. Peat erosion in the Pennines. *Advancement of Science,* 64**,** 323-331.

CHARMAN, D. 2002. *Peatlands and environmental change,* Chichester, UK, John Wiley & Sons Ltd.

EVANS, M. & LINDSAY, J. 2010. High resolution quantification of gully erosion in upland peatlands at the landscape scale. *Earth Surface Processes and Landforms,* 35**,** 876-886.

EVANS, M. & WARBURTON, J. 2007. *Geomorphology of upland peat: erosion, form and landscape change,* Oxford, UK, John Wiley & Sons.

FENNER, N. & FREEMAN, C. 2011. Drought-induced carbon loss in peatlands. *Nature Geoscience,* 4**,** 895.

GRAYSON, R., HOLDEN, J., JONES, R., CARLE, J. & LLOYD, A. 2012. Improving particulate carbon loss estimates in eroding peatlands through the use of terrestrial laser scanning. *Geomorphology,* 179**,** 240-248.

HOLDEN, J. & BURT, T. 2002. Infiltration, runoff and sediment production in blanket peat catchments: implications of field rainfall simulation experiments. *Hydrological Processes,* 16**,** 2537-2557.

HOLDEN, J., KIRKBY, M. J., LANE, S. N., MILLEDGE, D. G., BROOKES, C. J., HOLDEN, V. & MCDONALD, A. T. 2008. Overland flow velocity and roughness properties in peatlands. *Water Resources Research,* 44**,** W06415.

HOLDEN, J., SHOTBOLT, L., BONN, A., BURT, T., CHAPMAN, P., DOUGILL, A., FRASER, E., HUBACEK, K., IRVINE, B. & KIRKBY, M.

2007. Environmental change in moorland landscapes. *Earth-Science Reviews,* 82**,** 75-100.

ISE, T., DUNN, A. L., WOFSY, S. C. & MOORCROFT, P. R. 2008. High sensitivity of peat decomposition to climate change through water-table feedback. *Nature Geoscience,* 1**,** 763.

LI, C., GRAYSON, R., HOLDEN, J. & LI, P. 2018. Erosion in peatlands: Recent research progress and future directions. *Earth-Science Reviews,* 185**,** 870-886.

LI, P., HOLDEN, J. & IRVINE, B. 2016a. Prediction of blanket peat erosion across Great Britain under environmental change. *Climatic Change,* 134**,** 177-191.

LI, P., HOLDEN, J., IRVINE, B. & GRAYSON, R. 2016b. PESERA‐PEAT: a fluvial erosion model for blanket peatlands. *Earth Surface Processes and Landforms,* 41**,** 2058-2077.

LI, P., HOLDEN, J., IRVINE, B. & MU, X. 2017. Erosion of Northern Hemisphere blanket peatlands under 21st‐century climate change. *Geophysical Research Letters,* 44**,** 3615-3623.

NOBLE, A., PALMER, S. M., GLAVES, D. J., CROWLE, A., BROWN, L. E. & HOLDEN, J. 2017. Prescribed burning, atmospheric pollution and grazing effects on peatland vegetation composition. *Journal of Applied Ecology,* 55**,** 559-569.

PARRY, L. E., HOLDEN, J. & CHAPMAN, P. J. 2014. Restoration of blanket peatlands. *Journal of Environmental Management,* 133**,** 193-205.

PARSONS, A. J., WAINWRIGHT, J., BRAZIER, R. E. & POWELL, D. M. 2006. Is sediment delivery a fallacy? *Earth Surface Processes and Landforms,* 31**,** 1325-1328.

PAWSON, R., EVANS, M. & ALLOTT, T. 2012. Fluvial carbon flux from headwater peatland streams: significance of particulate carbon flux. *Earth Surface Processes and Landforms,* 37**,** 1203-1212.

PAWSON, R., LORD, D., EVANS, M. & ALLOTT, T. 2008. Fluvial organic carbon flux from an eroding peatland catchment, southern Pennines, UK. *Hydrology and Earth System Sciences,* 12**,** 625-634.

SMITH, M. W. & VERICAT, D. 2015. From experimental plots to experimental landscapes: topography, erosion and deposition in sub‐humid badlands from structure‐from‐motion photogrammetry. *Earth Surface Processes and Landforms,* 40**,** 1656-1671.

XU, J., MORRIS, P. J., LIU, J. & HOLDEN, J. 2018a. Hotspots of peatland-derived potable water use identified by global analysis. *Nature Sustainability,* 1**,** 246.

XU, J., MORRIS, P. J., LIU, J. & HOLDEN, J. 2018b. PEATMAP: Refining estimates of global peatland distribution based on a meta-analysis. *Catena,* 160**,** 134-140.

YU, Z. 2012. Northern peatland carbon stocks and dynamics: a review. *Biogeosciences,* 9**,** 4071-4085.

Chapter 2
Erosion in peatlands: recent research progress and future directions

Changjia Li, Richard Grayson, Joseph Holden, Pengfei Li. 2018. Erosion in peatlands: recent research progress and future directions. *Earth-Science Reviews*. **185**: 870-886. DOI: 10.1016/j.earscirev.2018.08.005

2.1 Abstract

Peatlands cover approximately 2.84% of global land area while storing one third to one half of the world's soil carbon. While peat erosion is a natural process it has been enhanced by human mismanagement in many places worldwide. Enhanced peat erosion is a serious ecological and environmental problem that can have severe on-site and off-site impacts. A 2007 monograph by Evans and Warburton synthesized our understanding of peatland erosion at the time and here we provide an update covering: i) peat erosion processes across different scales; ii) techniques used to measure peat erosion; iii) factors affecting peat erosion; and iv) meta-analyses of reported peat erosion rates. We found that over the last decade there has been significant progress in studying the causes and effects of peat erosion and some progress in modelling peat erosion. However, there has been little progress in developing our understanding of the erosion processes. Despite the application of new peat surveying techniques there has been a lack of their use to specifically understand spatial and temporal peat erosion dynamics or processes in a range of peatland environments. Improved process understanding and more data on rates of erosion at different scales are urgently needed in order to improve model development and enable better predictions of future peat erosion under climate change and land management practices. We identify where further research is required on basic peat erosion processes, application of new and integrated measurement of different variables and the impact of drivers or mitigation techniques that may affect peat erosion.

Keywords: peatlands; erosion; processes; measurements; rates; restoration

2.2 Introduction

Peat is a slowly-accumulating organic-rich soil composed of poorly decomposed remains of plant materials (Charman, 2002). Peatlands are areas with a surface peat accumulation and they can be broadly subdivided into bogs, fens and some types of swamps (Joosten, 2016). Bogs, which can be subdivided into blanket peatlands and raised bog (Charman, 2002), are ombrotrophic and receive water and nutrients primarily from precipitation. Fens and swamps are minerotrophic and receive water and nutrients from groundwater. To initiate and develop, peatlands require water-saturated conditions. However, peatlands occur in a broad range of climatic conditions from the warm tropics through to the cold, high latitudes and in total they cover approximately 4.23 million km^2 (2.84%) of the world's land area (Xu et al., 2018). Peatlands serve as important terrestrial carbon sinks, storing carbon equivalent to more than two thirds of the atmospheric store (Yu et al., 2010). Quantification of the carbon flux from peatland systems is therefore vital to fully understand global carbon cycling (Evans and Warburton, 2007, Pawson et al., 2008). In addition, peatlands provide a wide range of important ecosystem services including water supply, recreation and biodiversity (Bonn et al., 2009, Osaki and Tsuji, 2015). The conditions required for peatland initiation and ongoing survival are relatively narrow and as a result they are fragile ecosystems that are sensitive to a wide range of external and internal pressures, including changes in topography due to peat growth, climate change, atmospheric pollution, grazing, burning, artificial drainage, afforestation and infrastructure (Ise et al., 2008, Fenner and Freeman, 2011, Parry et al., 2014, Noble et al., 2017, Holden et al., 2007c).

Peat erosion is a natural process driven primarily by actions of water and wind, but slight changes in conditions driven by human action can lead to accelerated erosion and degradation (Parry et al., 2014). Wind erosion can occur where the peat surface is largely bare and is common in windy uplands and peat mining areas (Foulds and Warburton, 2007b, Foulds and Warburton, 2007a). Erosion by water can occur through a number of different processes (both on and below the surface), with the scale of erosion varying by peatland type as well as how degraded they are. Rainsplash and runoff energy can cause erosion on bare peat surfaces. Where flow accumulates, both in artificial ditches and natural channels, further erosion can take place. In peatlands that have been drained ditch erosion often occurs while channel bank collapse may occur on all peatlands

(Marttila and Kløve, 2010a). Erosion under the peat surface can also occur with piping being common in many peatlands globally (Jones, 2010).

Rain-fed blanket peatlands cover 105,000 km^2 of the Earth's surface (Li et al., 2017a) and occur on sloping terrain, with slope angles as high as 15°. As a result, blanket peatlands are potentially more vulnerable to water erosion than other types of peatlands occurring in landscapes with very little surface gradient (Li et al., 2017a). It has been reported that many blanket peatlands have experienced severe erosion (Evans and Warburton, 2007, Grayson et al., 2012, Li et al., 2016b) and are under increasing erosion risk from future climate change (Li et al., 2016a, Li et al., 2017a). The erosion of peat with high carbon content will enhance losses of terrestrial carbon in many regions. The main erosion processes affecting blanket peat can be broadly divided into sediment supply processes (e.g., freeze–thaw and desiccation), sediment transfer from hillslopes (e.g., interrill erosion, rill erosion and gully erosion), bank failures and mass movement (Bower, 1961, Francis, 1990, Labadz et al., 1991, Evans and Warburton, 2007, Warburton and Evans, 2011, Li et al., 2018a). Figure 2.1 shows some typical peat erosion features and processes in the uplands of northern England.

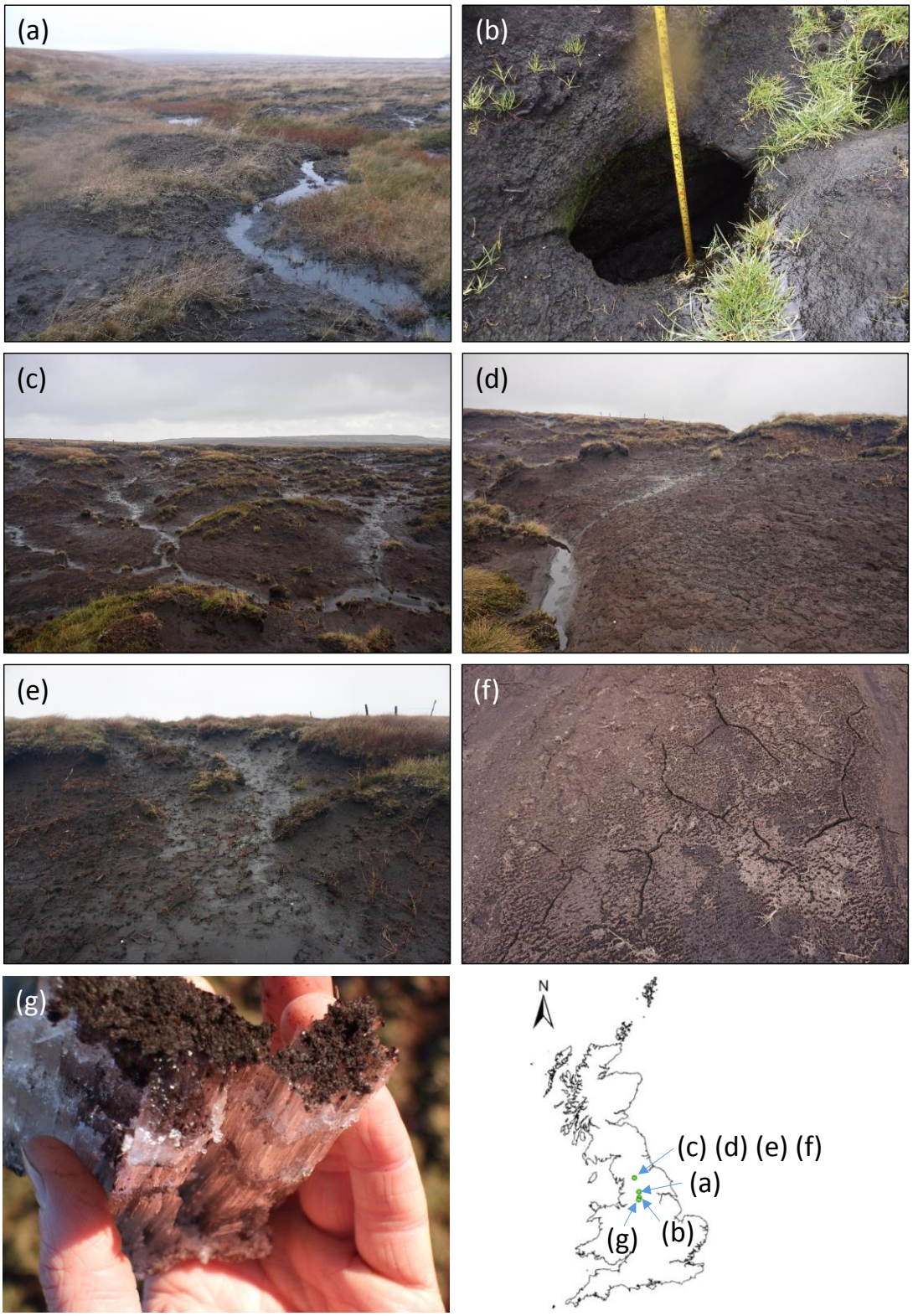

Figure 2.1 Evident examples of erosion features and processes in blanket peatlands of northern England: (a) rill erosion; (b) pipe erosion; (c) eroded bare hillslopes; (d) gully wall; (e) gully head; (f) desiccation; (g) needle ice production.

Extensive erosion of many blanket peatlands potentially compromises their ability to maintain ecosystem functions (Evans and Lindsay, 2010a) and has been found to have adverse impacts on landscapes (Holden et al., 2007c), reservoir sedimentation (Labadz et al., 1991), water quality (Rothwell et al., 2008b, Shuttleworth et al., 2015, Rothwell et al., 2008a, Rothwell et al., 2010, Daniels et al., 2008, Crowe et al., 2008), carbon dynamics (Holden, 2005b, Worrall et al., 2011) and other ecosystem services (Osaki and Tsuji, 2015).

As a proportion of dry mass, blanket peat is typically around 50% carbon (e.g. Dawson et al. (2004)). Thus sediment loss from peatlands also represents a significant removal of carbon. However, most research on peatland carbon budgets has focussed on gas flux with less effort on aquatic carbon fluxes from peatlands (Holden et al., 2012c). Where aquatic carbon fluxes from peatlands have been measured, the dissolved organic carbon (DOC) flux tends to be several times greater than that of particulate organic carbon (POC) (e.g. Hope et al. (1997); Dinsmore et al. (2010); Holden et al. (2012c)). However, in more severely eroding peatlands the POC flux has been shown to be greater than that of DOC (Pawson et al., 2012, Pawson et al., 2008).

Despite peatland erosion having been studied for more than sixty years some of the processes remain poorly understood (Bower, 1960, Evans and Warburton, 2007, Li et al., 2016b). The prevention and control of peat erosion risk relies on designing and applying appropriate conservation strategies and management techniques, which in turn requires a thorough understanding of processes. Traditionally the bulk of soil erosion research has focussed on understanding mineral soils, with much less known about erosion of organic soils. While soil erosion remains a major concern in mineral agricultural soils (Li et al., 2017c), erosion of peat is of particular concern due to the increased risk of carbon loss to the atmosphere once peat sediment is moved from its original location (Palmer et al., 2016).

On 12th November 2017, a bibliographic search was conducted to analyze the evolution and trends in peatland erosion studies with the aim of identifying new lines of investigation. The search used Thomson Reuters© Web of Science® bibliographic databases. Using the key words ‘peat’ and ‘erosion’ 683 items were retrieved over the period 1900 to the present (12/11/2017). The indexed articles cover both qualitative and quantitative investigations of peat erosion processes, rates and the impacts of different factors on peat erosion (Figure 2.2). Between 1960 and 1980 the number of

peat erosion related publications remained low, however since 1990 there has been a rapid increase in associated research and resulting publications; this has resulted in exponential growth in the number of citations. Evans and Warburton (2007) synthesized our understanding of upland peat erosion at the time of their monograph. Developments in direct and indirect methods for measuring soil erosion processes and rates since 2007 and a greater appreciation for the detrimental impacts of peat erosion have resulted in an increase in the number of articles published annually, with a peak of 50 articles per year in 2016. Here we provide an updated review of recent developments. Our review therefore focuses on new research over the last decade, but refers to older research where necessary to provide background context or where that material was not originally covered by Evans and Warburton (2007).

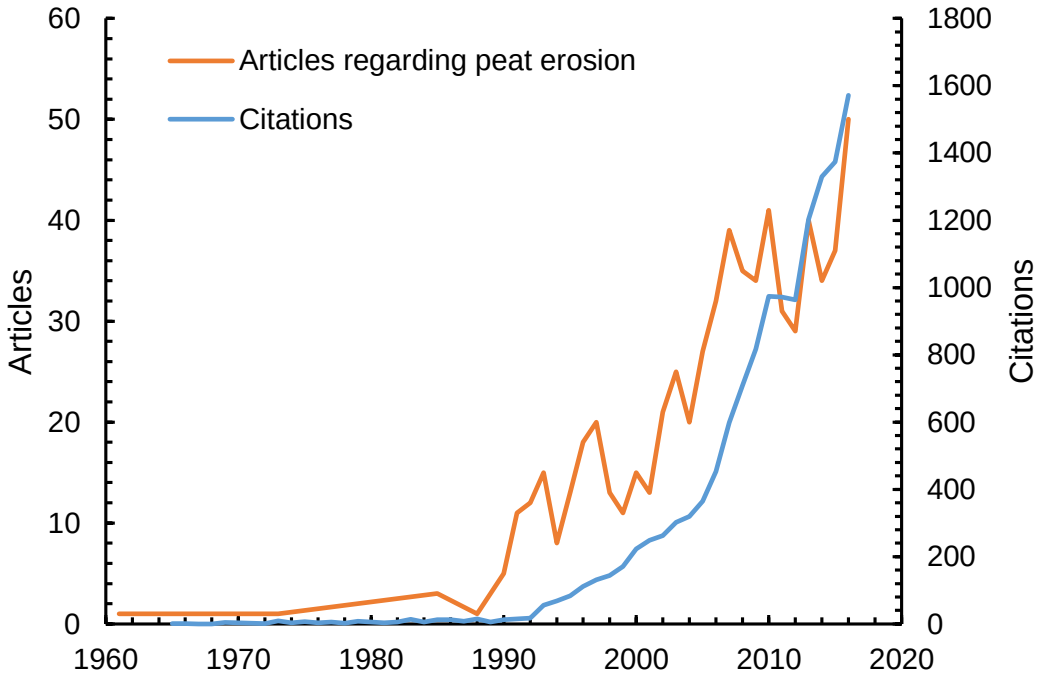

Figure 2.2 Annual evolution of the number of publications on peat erosion from 1960 to 2017 (indexed in Web of Science 12/11/2017) and the number of citations.

Although there may be some grey literature (unpublished research, theses or reports), much of the recently published peat erosion literature is geographically limited to blanket peatlands in the British Isles, and peatlands in Finland, North America and tropical areas, primarily due to concerns over peat erosion in these locations and programs to address these concerns.

Therefore this review of updates over the last decade will necessarily have more concentrated information relating to those systems, however the findings will have broader implications for peatlands globally. The literature covered in this review primarily consists of peer-reviewed papers, books and book chapters drawn from the Web of Science® database, but also includes publically available academic theses and reports (e.g., IUCN UK Committee Peatland Programme reports).

This paper is structured to provide the following:

1. Review of the dominant erosion processes at a range of scales and their interactions in peatland environments.
2. Review of the techniques used to measure peat erosion.
3. A discussion of the factors affecting erosion processes in peatlands.
4. A database and meta-analyses of peat erosion rates measured at different temporal and spatial scales.
5. A synthesis of unanswered research questions on peat erosion.

2.3 Peat erosion processes

A discussion of the characteristics of critical erosion processes active in peatlands is essential in predicting and mitigating the effects of erosion. Peat erosion can be seen as a two-phase process that consists of: 1) the supply of erodible peat particles by weathering processes, and; 2) their subsequent transport by agents such as water and wind (Li et al., 2016b). Weathering processes such as freeze–thaw and desiccation (Figure 2.1 (f)–(g)) are important for producing a friable and highly erodible peat surface layer for transport by water and wind (Evans and Warburton, 2007, Li et al., 2018a, Lindsay et al., 2014). Rainsplash and runoff energy are active erosion agents for water erosion processes involving splash erosion, interrill erosion, rill erosion, pipe erosion and ditch/channel erosion (Li et al., 2018b, Evans and Warburton, 2007, Holden, 2006). Dry peat with a low density is potentially highly susceptible to erosion and transport by wind through dry blow or wind-driven rainsplash (Warburton, 2003, Foulds and Warburton, 2007b, Foulds and Warburton, 2007a, Evans and Warburton, 2007).

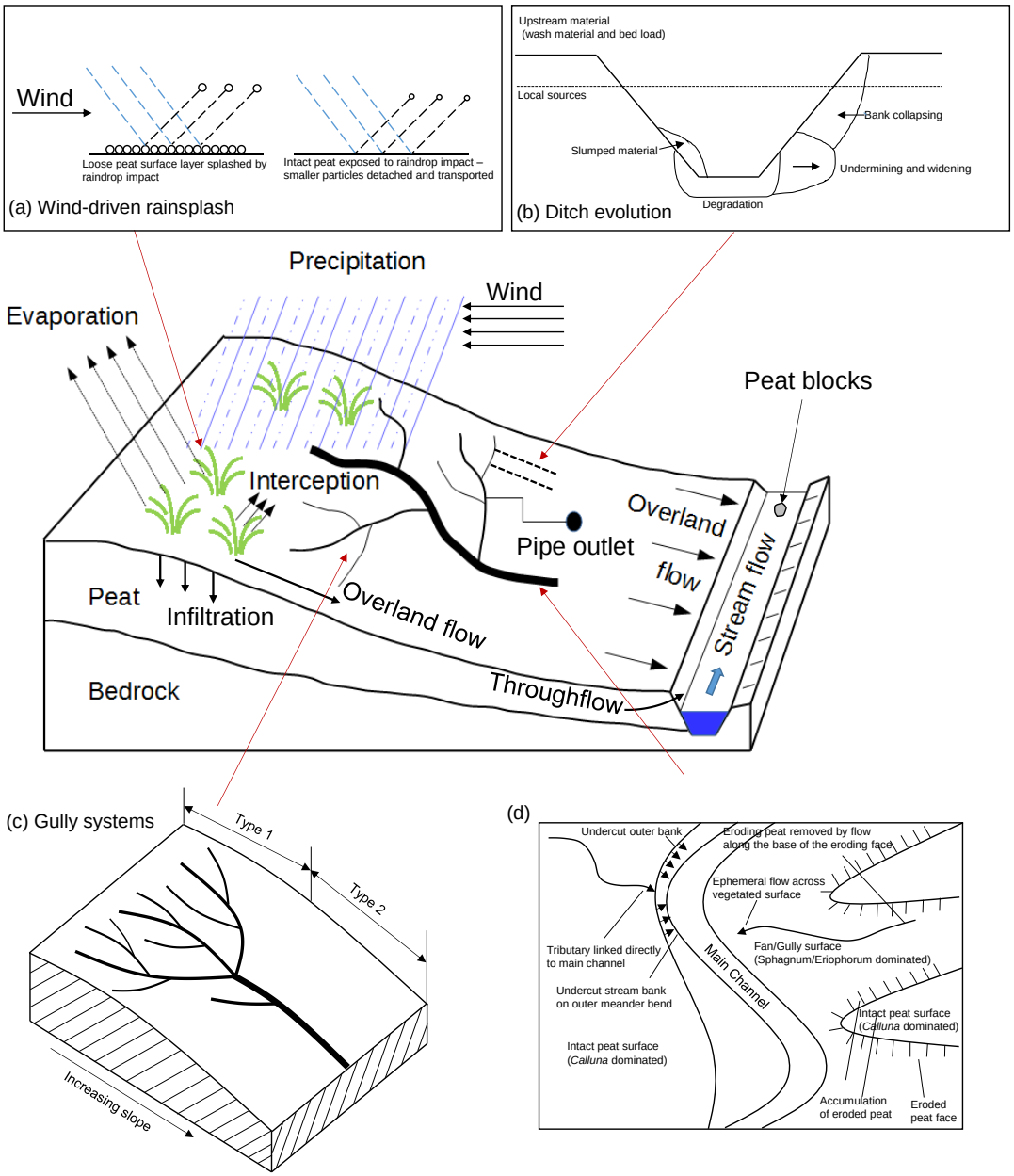

Figure 2.3 Sketch illustrating water flow paths and main water and wind erosion processes on peatland systems: (a) Conceptual diagram showing two-phase mechanism of bare peat erosion by wind-driven rain, deduced from the particle size and shape (after Baynes (2012)); (b) Conceptual model of drainage channel evolution, and sediment and erosion dynamics in a peatland forest ditch (after Marttila and Kløve (2010a)). (c) *Type* 1 and *Type* 2 dissection of gully systems (after Bower (1961)); (d) Diagram showing the main channel of a stream in an eroding peatland with erosion and revegetation processes operating in the catchment (after Evans and Burt (2010)).

2.3.1 Weathering processes

2.3.1.1 Frost action

Frost weathering resulting from the freezing and thawing of water between peat particles is common in cool high latitude or high altitude climates which support many peatlands, and plays a vital role in breaking the peat surface during winter months (Francis, 1990, Labadz et al., 1991, Evans and Warburton, 2007, Li et al., 2018a). Compared to mineral soils peat has a higher volumetric heat capacity but much lower conductivity and as a result has a significantly different thermal response during wetting or drying periods (FitzGibbon, 1981). On cold days, a strong thermal gradient can develop between a cold peat surface and warmer peat at depth (Evans and Warburton, 2007) which together with an abundant moisture supply make ideal conditions for needle ice formation (Figure 2.1 (g)) (Outcalt, 1971). Needle-ice is important in producing eroding peat faces (Tallis, 1973, Luoto and Seppälä, 2000, Grab and Deschamps, 2004) with ice crystal growth gradually weakening and finally breaking peat soil aggregates and the subsequent warming and thawing weakening or loosening the fractured peat. The growth of needle ice can lead to a 'fluffy' peat surface that is loose and granular and vulnerable to being flushed off by overland flow events (Li et al., 2018a, Evans and Warburton, 2007).

Despite the important role of needle-ice formation in preparing the peat surface for erosion, very little has been done to understand the actual process and quantify the effects on erosion (Li et al., 2018a). Li et al. (2018a) conducted physical overland flow simulation experiments on peat with needle ice treatments. Using a cooling rate of −1.3 °C hr^{-1} to a minimum of −1.0 °C, Li et al. (2018a) successfully formed needle-ice within the upper layer of peat blocks and provided the first quantitative analysis demonstrating that needle-ice production and thaw is a primary process contributing to upland peat erosion by enhancing peat erodibility during runoff events following thaw. It should be noted that Li et al. (2018a) used simulated upslope inflow and excluded responses to raindrop impact, while under natural rainfall conditions raindrops provide the primary force to initiate peat particle detachment (Li et al., 2018b). Thus, more significant effects of freeze–thaw on increasing peat erosion could be expected under combined rainfall and overland flow conditions and exploration of these processes could be undertaken in future work.

2.3.1.2 Desiccation

Surface desiccation during extended periods of dry weather is another important weathering process for producing erodible peat (Evans et al., 1999, Francis, 1990, Holden and Burt, 2002a, Burt and Gardiner, 1984). Desiccation of surface peat can lead to development of hydrophobicity (Eggelsmann et al., 1993). Where desiccation occurs the surface layer is typically platy with a dried upper crust that is concave in shape and is detached from the intact peat below (Evans and Warburton, 2007); this dry crust layer could impede infiltration (Holden et al., 2014). On the other hand, a desiccated peat surface can be susceptible to shrinkage and cracking (Holden and Burt, 2002a) that actually promotes delivery of surface water to the subsurface hydrological system (Holden et al., 2014).

Li et al. (2016a) modelled the effect of future climate change on UK peatlands and found that peat shrinkage and desiccation may become more important in blanket peatlands as a result of warmer summers and the resulting lowering of water tables. Given projected global climate change, desiccation of the peat surface might be exacerbated across many low-latitude peatland areas (Li et al., 2017a). In addition, field observations have shown that desiccation of the peat surface contributes to increasing surface roughness (Smith and Warburton, 2018).

2.3.2 Sediment transport processes

Transport of sediment from hillslopes to channels where it is more accessible to fluvial processes is of great importance in geomorphology (Bryan, 2000b, Evans and Warburton, 2007). Many erosional processes are active on peat hillslopes (Figure 2.3), including water erosion (Bower, 1961), wind erosion (Warburton, 2003, Foulds and Warburton, 2007a, Foulds and Warburton, 2007b) and mass movements such as peat slides and bog bursts (Evans and Warburton, 2001, Warburton et al., 2004, Evans and Warburton, 2007, Crowe and Warburton, 2007, Warburton and Evans, 2011). Bank erosion is an important process in some peatlands, contributing to stream sediment loads (Evans and Warburton, 2001). Peat transported within channels is typically in the form of fine suspended sediment or larger low-density peat blocks which may remain in situ until they float off in storms or roll along the bed and quickly break up once mobilized (Evans and Warburton, 2007, Warburton and Evans, 2011).

2.3.2.1 Water erosion

Interrill erosion processes

For interrill erosion, the dominant processes are detachment by raindrop impact and transport by raindrop-impacted sheet flow (Kinnell, 2005). Raindrops affect interrill erosion processes in two ways. First, raindrops provide the primary force to initiate low-density peat particle detachment; with the importance of raindrop impact on sediment detachment having been shown under both laboratory and field conditions (Li et al., 2018b, Holden and Burt, 2002a, Kløve, 1998). Li et al. (2018b) found that without raindrop impact shallow interrill overland flow had little entrainment capacity, with raindrop impact increasing peat surface erosion by 47% (Li et al., 2018b). Second, raindrop impact is important in affecting overland flow hydraulics and sediment transport as overland flow depths are typically shallow, in the order of a few millimeters (Holden et al., 2008a, Holden and Burt, 2002a). Li et al. (2018b) found that raindrop impacts increased flow resistance which reduced overland flow velocities by 80–92%. Overland flow hydraulics as modified by raindrop impact are important in defining and modelling overland flow erosion processes (Bryan, 2000a); further work should be carried out to explore these interactions.

For interrill erosion areas, soil detachment and sediment transport are simultaneously influenced by rainfall-driven and flow-driven erosion processes and their interaction (Li et al., 2018b). However, rather limited attention has been given to the importance of the interaction between rainfall- and flow-driven processes and the interaction is usually ignored when modelling interrill processes (May et al., 2010). Li et al. (2018b) found a negative interaction, with the total sediment concentration for both rainfall and runoff treatments being lower than the sum of the combined rainfall and runoff treatments. This interaction substantially reduced sediment concentration as a result of significantly increased flow resistance caused by the retardation effect of raindrops on shallow overland flow.

Saturation-excess overland flow and near-surface throughflow are dominant in many (but not all) types of peatland including blanket peatland (Evans et al., 1999, Holden and Burt, 2002a, 2003c) and are a result of shallow water tables and low hydraulic conductivity throughout most of the peat depth (Holden and Burt, 2003a, Holden and Burt, 2003b, Rosa and Larocque, 2008). The hydraulic conditions of overland flow (e.g., flow velocity, depth and resistance) determine the erosive forces acting on the peat in interrill areas. Runoff hydraulics including flow velocity, flow depth and friction

coefficients, and their empirical relationships have been reported at the plot scale on blanket peat slopes (Holden et al., 2008a). Holden et al. (2008a) found a region of shallow flows in which there is a gradual increase of roughness (reducing $f^{-0.5}$) with depth, and a deeper region of flows with significantly decreasing roughness (logarithmically) with depth.

Rill erosion processes

Rill processes are affected by concentrated flow and soil resistance (Govers et al., 2007, Knapen et al., 2007). Li et al. (2018a) conducted laboratory flume experiments on blanket peat with and without needle ice processes. The physical overland flow simulation experiments showed that rills were not produced in intact peat without needle ice production and thaw. However, visual observations of the needle ice treatments showed that micro-rills and headcuts occurred and caused localized micro-waterfalls (Li et al., 2018a). For the needle-ice treatments with rill initiation, stepwise linear regression showed that stream power was the only factor that predicted erosion (Li et al., 2018a). Although recent research has focused on the mechanisms of peat interrill and rill erosion (Li et al., 2018b, Li et al., 2018a) little is known about the threshold hydraulic conditions for the transition from interrill to rill processes. There is a dearth of evidence on how the two erosive agents interact with each other, and how their interactions impact on peatland hillslope development.

Pipe erosion

Piping is commonly found in peatlands (Holden and Burt, 2002c, Holden, 2006, Holden et al., 2012c, Rapson et al., 2006, Price and Maloney, 1994, Woo and DiCenzo, 1988, Norrström and Jacks, 1996). Peat pipes connect the shallow and deep layers of the peat profile (Holden, 2005b, Holden, 2005a, Billett et al., 2012) and act as significant sources and pathways for water, carbon and sediment transport. In addition, pipe collapse is common, often being associated with gully head retreat (Jones, 2004, Verachtert et al., 2011). However, pipe erosion is less well studied compared with surface soil erosion by water due to its subsurface nature (Holden, 2005a). Geophysical techniques (e.g., ground-penetrating radar) (Holden et al., 2002) have helped improve the identification of pipe networks, but studies have generally focused on pipe distribution and hydrology (Holden and Burt, 2002c, Holden, 2005a, Holden, 2006, Holden, 2009a, Holden, 2009b, Holden et al., 2012b, Holden et al., 2012c, Smart et al., 2013). Holden and Burt (2002c) found that around 10% of stream discharge was derived from pipe networks in Little Dodgen Pot Sike, a deep blanket peat catchment in

the North Pennines of England. In the nearby Cottage Hill Sike catchment, Smart et al. (2013) found that pipes contributed 13.7% of the streamflow. Jones (2004) showed that piped areas produced more sediment to the stream than areas without piping. Pipe outlets delivered an amount of aquatic carbon equivalent to 22% of the aquatic carbon flux at the outlet of Cottage Hill Sike catchment (Holden et al., 2012c) with POC flux observed at the pipe outlets equivalent to 56−62% of the annual stream POC flux (Holden et al., 2012b, 2012c). Despite these valuable results, quantification of the contribution of piping to peat loss is still limited to a few case studies in a limited number of environments.

2.3.2.2 Wind erosion

Windy conditions are typical of many exposed peatland environments. The impacts of wind action on peatlands differs between dry and wet conditions (Evans and Warburton, 2007). During drought periods dry blow is of great importance in transporting eroded peat as dry peat with a low density has a high potential susceptibility to erosion and transport by wind (Warburton, 2003, Foulds and Warburton, 2007a, 2007b, Campbell et al., 2002). In contrast under wet and windy conditions, wind-driven rain is important in peat surface erosion through the detachment and transport of peat particles (Warburton, 2003, Foulds and Warburton, 2007a). Baynes (2012) identified a two-phase erosion process of bare peat by wind-driven rain (Figure 2.3 (a)). Phase 1 includes large loose surface peat particles that are produced by frost action or surface desiccation and are mobilized by raindrop impact and transported by wind. The removal of the top layer exposes the intact peat surface to raindrop impact which erodes smaller particles (Phase 2). Li et al. (2018b) found that raindrop impact plays a key role in affecting overland flow, flow hydraulics and soil loss under lower rainfall intensity conditions. However, more significant effects could be expected with higher kinetic energy levels closer to those experienced where natural rainfall is driven by strong wind. Future work could examine overland flow interactions with wind-driven rainsplash erosion and its contribution to total erosion, as rainfall on exposed peatlands is often associated with strong winds (Evans and Warburton, 2007).

2.3.2.3 Ditch erosion

Artificial drainage on peatlands and the associated changes in peat structure, hydrological flow paths and erosion have been widely reported in upland Britain (Holden et al., 2004, Holden et al., 2006, Holden et al., 2007b, Armstrong et al., 2009) and Finland (Kløve, 1998, Marttila and Kløve, 2008,

Marttila and Kløve, 2010a, Stenberg et al., 2015b, Tuukkanen et al., 2016, Haahti et al., 2014, Stenberg et al., 2015a). Holden et al. (2007b) found that drain networks that were well connected to stream channels were important contributors of suspended sediment to the stream network. Ditch creation and maintenance contribute to increased erosion and suspended sediment yields by undermining and bank collapse (Marttila and Kløve, 2010a, Stenberg et al., 2015b, Stenberg et al., 2015a, Tuukkanen et al., 2016). Field and laboratory observations in Finland have shown that erosion of deposited peat sediment from main ditches is the main suspended sediment source in peat extraction areas during individual summer storm events (Marttila and Kløve, 2008, Tuukkanen et al., 2014). Marttila and Kløve (2010a) presented a conceptual model of the processes in the drainage channel, where suspended sediment production in the channel is a result of flow erosion, sheet wash, sidewall collapse and undercutting. Sediment from upstream areas can be stored in the main drain during smaller flow events, indicating a physical process limited by the transport capacity. The deposited sediment in the ditch bottom can be released to be transported during larger flow events, and this process can either be supply- or transport-limited (Marttila and Kløve, 2010a). Stenberg et al. (2015a) outlined a conceptualisation where bank erosion occurs in the area of a seepage face and the material is eroded due to different mechanisms (e.g. seepage, gravitational forces, and freeze–thaw processes) and deposited on the bottom of the ditch and the lower parts of the ditch bank. They concluded that the main mechanism causing bank erosion was plausibly the seepage and wetting-induced loosening of the peat material, as most of the erosion took place during the time when groundwater levels were highest.

2.3.2.4 Other erosion processes

Other commonly observed erosion forms in peatlands are gully erosion, mass movements and in-stream transport processes, and an extensive body of literature has been published on these subjects (see Evans and Warburton (2007) for a concise review). Little additional work has been published in the last decade on these processes. Warburton and Evans (2011) found large peat blocks in alluvial river systems could significantly contribute to stream sedimentation, and this contribution might be greater than those from other fluvial erosion forms such as rill and gully erosion, particularly over short timescales and in a local context. The effects of peat blocks on downstream sediment load were found to depend on channel width (Warburton and Evans, 2011). For narrow channels, peat blocks act as

natural and economical dams to block the flow and sediment pathways, which may lead to the upstream accumulation of bed material; while for wider channels the blocks tend to be stored on the river bed in isolation and are of less importance in controlling sedimentation (Warburton and Evans, 2011). Once peat blocks begin to move they break down at a relatively rapid speed through abrasion and disaggregation, which may release a large quantity of fine sediments in stream systems (Evans and Warburton, 2007, Evans and Warburton, 2001). Little is known about the hydraulic thresholds required for peat blocks to be entrained, transported and deposited, nor the factors impacting the dispersal and persistence of peat blocks in streams (Warburton and Evans, 2011).

2.3.3 Interactions among different peat erosion processes

The three most common sediment supply processes affecting peatlands (e.g., frost action, desiccation and rainsplash) seldom occur independently of each other (Figure 2.4). Peat is usually 'puffed up' by frost in winter, contracted by desiccation in summer, and buffeted year-round by wind-driven rain (Warburton, 2003). Rainsplash plays an important role in detaching peat particles for flow transport (Li et al., 2018b). However, antecedent conditions such as antecedent freeze–thaw or desiccation activity are very important in controlling peat erodibility and thus erosional response to a given rainfall event. In addition, desiccation is closely related to the frost effect in terms of the formation of segregation ice at the peat surface and this could initiate desiccation of the surface layer (Evans and Warburton, 2007).

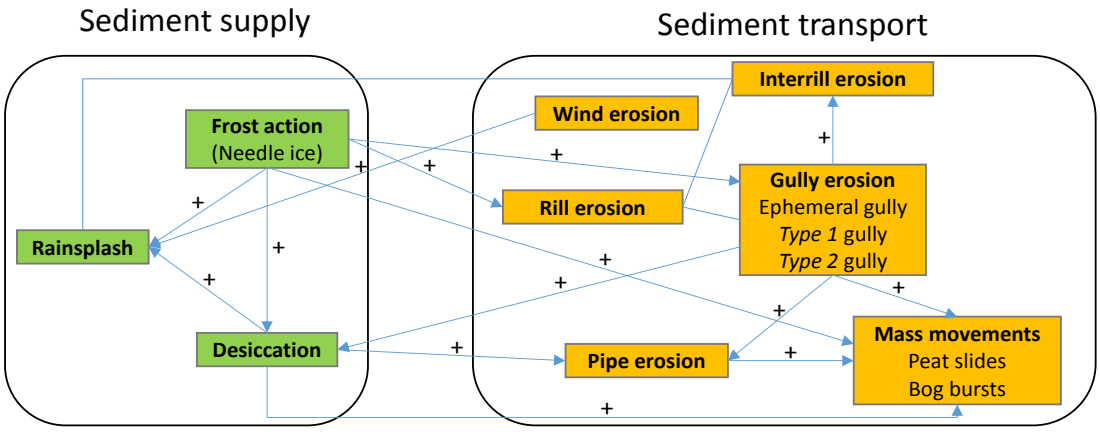

Figure 2.4 Interactions among sub-processes of sediment supply and sediment transport processes in peatlands.

Active sediment transport processes strongly interact with each other in some areas of peatlands (Figure 2.4). There are links between the development of interrill erosion and gully erosion. Interrill erosion is widely spread on summits of *Type 1* gully dissection systems, where large areas of bare peat are exposed (Bower, 1961). Once gullies develop, mass wasting and slope instability can be triggered and piping can also be enhanced. Holden et al. (2002) found through ground-penetrating radar survey of pipe frequency that pipes were often found at the head of gullies. In turn, pipes have the potential to initiate or impact gully system development through roof collapse or channel extension (Tomlinson, 1981, Holden and Burt, 2002c). Pipe collapse is potentially associated with initiation of *Type 2* gullies (Evans and Warburton, 2007). However, there are no direct observations or quantitative analysis linking pipe features and gully initiation in peatlands. Peat mass movements have also been linked to gully formation (Evans and Warburton, 2007).

Strong links would be expected between sediment supply and sediment transport processes in peatland environments. For example, needle-ice formation resulting from freeze–thaw cycles could result in damage to gully walls (Imeson, 1971, Evans and Warburton, 2007). Freeze–thaw action would also be associated with deep cracking on the bank face and peat mass failure (Wynn et al., 2008). Desiccation cracking may promote delivery of surface water to the subsurface hydrological system promoting elevated pore pressures and peat mass failure (Hendrick, 1990). Gully systems are particularly vulnerable to desiccation process, due to exposed faces drying quickly and particles being rapidly removed by wind and gravity (Holden et al., 2007a). The desiccation of the peat surface, has the potential to encourage soil pipe development and pipe erosion (Holden, 2006, Jones, 2004). New routes created by shrinking and cracking of the desiccated peat for bypassing flow, may initiate the ephemerally flowing pipe networks, when abundant sourcing water flows through the preferential flow pathways (Holden, 2006).

2.3.4 Scale-dependency of peat erosion processes

A conceptual model of the active sources and sinks of sediment in peatlands can be developed based on De Vente and Poesen (2005). Different peat erosion processes are active at different spatial scales. For example, rainsplash, interrill and rill erosion are the dominant erosion processes studied at fine scales (erosion plots) (Holden et al., 2008a, Li et al., 2018b, Li et al., 2018a, Holden and Burt, 2002a, Grayson et al., 2012). For larger

hillslope and small and medium-size catchment scale, gully erosion and mass movements become more important, yielding large quantities of sediment (Evans and Warburton, 2007, Evans et al., 2006, Evans and Warburton, 2005). At the large basin scale long-term erosion and sediment deposition processes are more important due to large sediment sinks (footslopes and floodplains) (De Vente and Poesen, 2005). Riverine POC is also potentially transformed to DOC by in-stream degradation or mineralized to CO_2 during periods of floodplain storage (Pawson et al., 2012).

2.4 Methodological approaches for assessing erosion in peatlands

2.4.1 Measuring techniques

Numerous direct and indirect methods have been used to measure and monitor peat erosion. Traditionally these have included: erosion pins (Grayson et al., 2012), bounded plots (Holden et al., 2008a, Li et al., 2018b, Li et al., 2018a), gauging stations, bathymetric surveys in reservoirs (Yeloff et al., 2005) and some of these have been combined as part of sediment budgeting (Evans and Warburton, 2005, Evans et al., 2006). However, more recently modern high resolution topographic surveying methods have been applied to peatlands to improve quantification of erosion (Evans and Lindsay, 2010a, Rothwell et al., 2010, Evans and Lindsay, 2010b, Grayson et al., 2012, Glendell et al., 2017).

2.4.1.1 Erosion pins

Erosion pins are widely used to measure erosion and deposition directly through observed changes in the peat surface at a given point (Grayson et al., 2012, Tuukkanen et al., 2016). Surface retreat rates measured by erosion pins are the combined effects of wind erosion, water erosion and peat wastage (oxidative peat loss) (Francis, 1990, Evans and Warburton, 2007, Evans et al., 2006). The point measurements are usually interpolated over relatively small areas. However, interpreting erosion rates based on erosion pins should be treated with caution as the accuracy and precision can be affected by: i) peat soil expansion and contraction during weathering processes (freeze–thawing and wetting–drying cycles) (Labadz, 1988, Kellner and Halldin, 2002); ii) significant spatial variation even over small areas (Grayson et al., 2012); iii) increasing erosion or trapping eroded material (Benito and Sancho, 1992, Couper et al., 2002); iv) interference

from grazing animals like sheep; v) disturbance and damage to the peat surface caused by installation and repeated pin measurement.

2.4.1.2 Erosion plots

Erosion plots are one of the most widely applied methods for measuring peat erosion rates over short and medium time periods (Holden and Burt, 2002a, Grayson et al., 2012, Li et al., 2018b). Erosion plots include closed plots that are usually ≤10 m^2, and open plots which are larger. Closed plots are normally equipped with troughs, runoff and sediment collectors and are employed together with rainfall simulation or upslope inflow simulation experiments (Holden and Burt, 2002a, Holden and Burt, 2002b, Holden and Burt, 2003b, Clement, 2005, Holden et al., 2008a, Li et al., 2018b, Li et al., 2018a). Closed plots have the advantages of allowing a comparison of different responses at the same spatial scale (Boix-Fayos et al., 2006). However, Holden and Burt (2002a) and Li et al. (2018b) showed that closed erosion plots reduce erosion rates with rainfall simulation due to a change from transport-limited to detachment-limited conditions. Open plots are usually used in the field (Grayson et al., 2012) and they have the advantage of better representation of natural conditions.

2.4.1.3 Sediment transport measurements at gauging stations

Sediment concentration measurements at gauging stations allow the calculation of sediment yield rate and its temporal variability (Nadal-Romero et al., 2011). A wide range of equipment and techniques (e.g., sediment traps, sampling) are generally used to measure sediment flux at the catchment outlet at larger spatial and temporal scales (Labadz et al., 1991, Francis, 1990, Holden et al., 2012c, Pawson et al., 2012). Sediment sampling is usually used in combination with the rating curve technique (Francis, 1990, Labadz et al., 1991). It is important to consider sampling intervals as peat systems often have flashy regimes and hence many sampling strategies (e.g., daily sampling) may miss important sediment transport events such as storm (Pawson et al., 2008). Antecedent conditions and hysteresis in the sediment – discharge relationship are also important factors to consider when designing sampling campaigns. Turbidity meters have often been used to measure suspended sediment concentrations in mineral catchments. However, their application in peatland catchments should be treated with caution and calibration is required since turbidity is sensitive to variations in particle size distribution, water colour and the proportion of organic and inorganic contents (Marttila et al., 2010, Lewis, 1996).

2.4.1.4 Bathymetric surveys in reservoirs

Repeat bathymetric surveys of reservoirs or check dams provide insights into sediment yield at the catchment scale over long periods of time (Nadal-Romero et al., 2011). Compared to other techniques, analyzing reservoir sedimentation is generally a cheaper and more reliable way to estimate net erosion rate (Verstraeten et al., 2006). However, the bathymetric survey method is constrained by determinations of trap efficiency, dry sediment bulk density and spatial analysis being rather challenging (Boix-Fayos et al., 2006, Verstraeten and Poesen, 2002).

2.4.1.5 Sediment budget

Sediment budgeting within a catchment acts as a framework for identifying sediment yield processes, sediment transport processes and linkages (Parsons, 2011). Several studies have reported sediment budgets for blanket peat catchments (Evans and Warburton, 2005, Evans et al., 2006, Baynes, 2012). Evans and Warburton (2005) constructed a sediment budget over a four-year monitoring period in the Rough Sike catchment that is an eroded but partially re-vegetated system in north Pennines of England. They reported that hillslope sediment supply to the catchment outlet was significantly reduced due to re-vegetation of eroding gullies. Re-vegetation of the slope-channel interface, which acts as a vegetated filter strip, reduced the sediment connectivity between the hillslopes and channels. However, there may be a limited capacity for how much sediment can be trapped over a given time period as overland flow may still flush out redeposited sediment on vegetated areas. More research is needed to evaluate the effectiveness of different vegetative filter strip characteristics (e.g. vegetation type, width) in reducing sediment delivery efficiency in peatland environments.

2.4.1.6 Topographic surveys of soil surfaces

Topographic surveys and fine-resolution topographic data allow the determination of peat erosion or deposition (Grayson et al., 2012, Glendell et al., 2017). Remote-sensing technologies employing high-resolution airborne and terrestrial LiDAR (Light Detection and Ranging) for measuring peat surface changes have been reported in blanket peatlands (Rothwell et al., 2010, Evans and Lindsay, 2010a, Evans et al., 2005, Grayson et al., 2012). Grayson et al. (2012) compared the use of terrestrial laser scanning and erosion pins across a blanket bog; contrasting results were obtained from the two different methodologies. A net surface increase of 2.5 mm was calculated from the terrestrial laser scans (included areas of erosion and

deposition), compared with a net decrease in peat surface height of 38 mm measured using pins (eroding areas only) during the same study period (Grayson et al., 2012).

The cost-effective and flexible photogrammetric surveying technique called ‘Structure-from-Motion’ (SfM) provides a cheaper alternative to the established airborne and terrestrial LiDAR (Smith and Vericat, 2015, Smith et al., 2016). Currently, through the SfM technique, it is possible to produce high-resolution DEMs from multi-stereo images without expert knowledge in photogrammetry, by using consumer-grade digital cameras, including those compatible with unmanned aerial vehicles (UAVs) (Glendell et al., 2017). UAVs allow large areas to be covered without disturbing the investigated plot (Glendell et al., 2017). High-resolution topographic data obtained from SfM techniques may provide new insights into erosion dynamics that affect peatlands at field scales (Glendell et al., 2017, Smith and Warburton, 2018). Wider application of the SfM technique is recommended to enable a better understanding of erosion processes and their spatial and temporal dynamics.

2.4.2 Modelling techniques

Blanket peat erosion has been estimated using numerical models such as the Universal Soil Loss Equation (USLE) (May et al., 2010), Cellular Automaton Evolutionary Slope and River (CAESAR) model (Coulthard et al., 2000) and the grid version of the Pan–European Soil Erosion Assessment (PESERA–GRID) model (Li et al., 2016b). May et al. (2010) applied USLE to model soil erosion and transport in a typical blanket peat-covered catchment on the northwest coast of the Ireland. Coulthard et al. (2000) used CAESAR model in an upland catchment partially covered by peat to assess the effects of climate and land-use change on sediment loss. The USLE model assumes that entrainment is primarily caused by rainsplash energy while the CAESAR model assumes that entrainment is caused by overland flow (Coulthard et al., 2000). However, these models ignore the dominant weathering processes such as freeze–thaw and desiccation in blanket peatlands. Li et al. (2016b) developed a process-based model of peatland fluvial erosion (PESERA–PEAT) by modifying the PESERA–GRID model (Kirkby et al., 2008) through the addition of modules describing both freeze–thaw and desiccation. Temperature and water table were chosen as indicators to parameterize freeze–thaw and desiccation (Li et al., 2016b). PESERA–PEAT has been shown to be robust in predicting blanket peat erosion (Li et al., 2016b) and it has been successfully applied to examine the

response of fluvial blanket peat erosion to future climate change, land management practices and their interactions at regional, national and global scales (Li et al., 2016b, Li et al., 2016a, Li et al., 2017a, Li et al., 2017b).

2.5 Factors affecting erosion in peatlands

2.5.1 Climatic conditions

Climatic conditions are important for peatland stability. Li et al. (2016b) found via modelling work and sensitivity analysis that with a climate scenario of the annual rainfall total being initially low, annual peat erosion increases if climate change causes increased precipitation, whereas for a scenario whereby annual precipitation is initially high, annual erosion decreases with increased annual precipitation. This demonstrates that when rainfall is above a threshold value there is a shift from supply-limited to transport-limited erosion patterns (Li et al., 2016b).

Modelled erosion rate in cold months (from October to February in Great Britain) has been found to decrease with increasing air temperature, while in warm months (from March to September) erosion increased with increasing temperature (Li et al., 2016a). The effects of temperature are associated with its significant control on freeze–thaw and desiccation weathering processes. Holden and Adamson (2002) showed that a small change in the mean annual temperature at Moor House, from 5.2 ˚C (1931–1979) to 5.8 ˚C (1991–2000), led to a decrease in the mean number of freezing days from 133 to 101 per year. Therefore, a minor change in near-surface air temperature has the potential to significantly impact sediment availability (Holden, 2007) due to the vital preparatory role of freeze–thaw cycles.

Peatland development is highly susceptible to climate change (Ise et al., 2008, Fenner and Freeman, 2011, Parry et al., 2014). During the Medieval warm period between 950 CE and 1100, a decrease in rainfall and an increase in temperature resulted in drying of peat surfaces and promotion of erosion (Ellis and Tallis, 2001, Tallis, 1997). Bioclimatic modelling suggests a retreat of bioclimatic space suitable for blanket peatlands due to climatic change in the 21st century (Gallego-Sala and Prentice, 2013, Gallego-Sala et al., 2010, Clark et al., 2010). Li et al. (2017a) found that future climatic change will begin to affect sediment release from increasingly large areas of blanket peatland in the Northern Hemisphere.

2.5.2 Peat properties

The physical properties of peat (e.g., degree of humification, shear strength, bulk density) affect peat erosion and sediment delivery (Svahnbäck, 2007, Carling et al., 1997, Marttila and Kløve, 2008, Tuukkanen et al., 2014). Carling et al. (1997) showed that intact peat (not yet loosened or weathered) is highly resistant to water erosion, suggesting a high flow velocity of 5.7 m s^{-1} was needed for continuous erosion of unweathered peat material. Svahnbäck (2007) found a positive relationship between the degree of humification and suspended sediment concentration (SSC) through sprinkler experiments in the laboratory. Tuukkanen et al. (2014) examined whether peat physical properties including the degree of humification, bulk density, ash content, and shear strength affect peat erodibility and found that well-decomposed peat generated higher SSC than slightly or moderately decomposed, fiber-rich peat. The degree of humification affects peat erodibility and sediment transport in two ways. First, the critical shear stress required for peat particle entrainment decreases with increasing degree of humification. Second, there is a higher risk of rill formation in well-decomposed peat extraction areas (Tuukkanen et al., 2014). As a consequence, well-decomposed peat with low fiber content is more likely to cause increased transport of organic suspended matter, compared with poorly decomposed peat (Tuukkanen et al., 2014).

Marttila and Kløve (2008) conducted laboratory flume experiments on peat sediments and found that deposited sediment formed a loose layer overlaid by more stabilized layers with stabilization time ranging from 15 min to 10 days. An increase in stabilization time resulted in increased erosion rates. Critical shear stress was 0.01 ± 0.002 N m^{-2} for the loose surface peat layer, and was 0.059 ± 0.001 N m^{-2} for the entire peat deposited peat sediment (Marttila and Kløve, 2008). Two linear equations can be fitted to explain the erosion across the critical shear stress. The critical shear stress for deposited ditch sediment was about 0.1 N m^{-2} (Marttila and Kløve, 2008) which was much lower than 0.6 N m^{-2} for well-decomposed peat and 4–6 N m^{-2} for poorly decomposed peat (Tuukkanen et al., 2014). The difference in critical shear stress between intact soil and ditch sediment indicated that deposited ditch sediment was much more susceptible to erosion than intact peat. Bulk density affects peat erosion and sediment transport through changes in runoff generation, rather than through its effect on peat erodibility (Tuukkanen et al., 2014). The tendency for overland flow is greater in peat with higher bulk density since the saturated hydraulic conductivity of peat

often (but not always) decreases with increasing bulk density (Chow et al., 1992).

Peat erodibility in the physically-based PESERA–PEAT model represents the erodibility of available peat materials weathered by freeze–thaw and desiccation (Li et al., 2016b). The erodibility of weathered peat was reported to be 2–3 times that of intact peat (Mulqueen et al., 2006). In addition, Li et al. (2018a) conducted physical overland flow simulation experiments on highly frost-susceptible blanket peat with and without needle ice processes. They defined peat anti-scouribility capacity (*AS*) as the resistance of peat to overland flow scouring. The higher the peat *AS*, the lower the peat erodibility, with *AS* significantly increasing in treatments subjected to needle ice processes, indicating that needle ice processes significantly increased peat erodibility (Li et al., 2018a).

2.5.3 Vegetation cover

Vegetation cover in blanket peatlands is dominated by slow-growing vascular plants and bryophytes (Holden et al., 2015), such as bog mosses (*Sphagnum* spp.), cotton-grass (sedges) (*Eriophorum* spp.) and shrubs such as common heather (*Calluna* spp.). These types of vegetation cover act as both indicators and creators of blanket peat conditions. Vegetation cover impacts both sediment supply and transport processes in peatlands (Li et al., 2016a). Vegetation cover protects bare peat surface against weathering processes (Lindsay et al., 2014, Holden et al., 2007b, Holden et al., 2007c, Shuttleworth et al., 2015), rainsplash and overland flow erosion (Holden et al., 2008a), and mass movements (Warburton et al., 2004, Evans and Warburton, 2007). The removal of vegetation cover increases the thermal gradient between cold surfaces and warmer peat at depth during winter (Brown et al., 2015), making the peat surface susceptible to needle ice weathering processes (Li et al., 2016b). Peat surfaces with sparse vegetation cover are also more vulnerable to desiccation in summer (Brown et al., 2015).

In addition, vegetation cover reduces overland flow velocity (Holden et al., 2008a, Holden et al., 2007b) and sediment connectivity from sediment source zones to river channels (Evans et al., 2006, Evans and Warburton, 2007). Holden et al. (2008a) demonstrated that vegetation cover dissipated overland flow energy by imparting roughness, and therefore substantially reduced velocity of running water across the peat surface compared to bare peat surfaces. Grayson et al. (2010) analyzed long-term (1950s to 2010s) hydrograph data from the Trout Beck blanket peat catchment, northern

England, and found that revegetation of eroded peat contributed to reduced flood peak, with hydrographs being flashier and more narrow-shaped with higher peaks during the more eroded periods. Recent modelling studies have also suggested that surface vegetation cover is important in affecting the timing of the flood peaks from upland peatlands (Ballard et al., 2011, Lane and Milledge, 2013). A spatially-distributed version of TOPMODEL developed by Gao et al. (2015) simulated how restoration and the associated land-cover change impact river peak flow. They reported that a catchment with a cover of *Eriophorum* and *Sphagnum* had much lower peak flows than that with bare peat (Gao et al., 2015, Gao et al., 2016, Gao et al., 2017).

Vegetation removal driven by land management practices (e.g., burning, overgrazing) (Parry et al., 2014) and atmospheric pollution (Smart et al., 2010) is normally associated with the first stage of the onset of blanket peat erosion (Lindsay et al., 2014, Parry et al., 2014, Shuttleworth et al., 2015). In modelling peat erosion using PESERA–GRID, a vegetation growth module was used to estimate gross primary productivity, soil organic matter and vegetation cover based on the biomass carbon balance (Kirkby et al., 2008, Li et al., 2016b). Li et al. (2016a) found that modelled peat erosion increased significantly with decreased vegetation coverage. For example, predicted peat erosion for the Trout Beck study catchment increased by 13.5 times when vegetation coverage was totally removed as a scenario (Li et al., 2016a).

2.5.4 Land management practices

Peatlands can be destabilized by changes in hydrology that may be brought about by a wide range of land management practices, including peat extraction, artificial drainage, grazing, burning (prescribed burning or wild fire), afforestation and infrastructure (Parry et al., 2014, Ramchunder et al., 2009).

Grazing has received increasing attention due to its important impacts on peat condition, vegetation and hydrological processes (Worrall et al., 2007a, Holden et al., 2007a, Evans, 2005, Worrall and Adamson, 2008). Unsustainable levels of grazing have adverse effects on peatland hydrological and erosion processes. Meyles et al. (2006) reported increased hydrological connectivity of hillslopes with channels resulting from grazing practices which led to increased flood peaks. The high risk of vegetation damage and exposure of bare soils by grazing make the bare peat surface vulnerable to weathering processes (Evans, 1997). Compaction of soils by

trampling decreases soil infiltration and may enhance erosion sensitivity due to increased hydrological connectivity by animal tracks (Meyles et al., 2006, Zhao, 2008).

Fire is a common occurrence in peatlands throughout the world (Turetsky et al., 2015, Ramchunder et al., 2013), both naturally and for management purposes. Prescribed burning has been practiced in many peatlands to mitigate wildfire risks (Holden et al., 2007c, Hochkirch and Adorf, 2007), to clear land for plantations or agriculture (Gaveau et al., 2014) and to promote changes in heather structure for food production to support grouse habitats and the rural gun-sports industry (Holden et al., 2012a, Grant et al., 2012, Ramchunder et al., 2013). Managed fire practice attempts to avoid consumption of the underlying peat by keeping the fire under control (Holden et al., 2015). However, the soil properties and surface conditions can be affected in the aftermath of the fire with enhanced surface drying, increased bulk density and associated water retention in the near-surface peat (Brown et al., 2015, Holden et al., 2015). This may lead to decreased evapotranspiration (Bond-Lamberty et al., 2009), enhanced overland flow production and exacerbated surface erosion (Pierson et al., 2008, Smith and Dragovich, 2008, Holden et al., 2014, Holden et al., 2015).

There have been several recent studies examining the effects of prescribed burning on peatland vegetation communities (Noble et al., 2017), hydrological processes (Holden et al., 2014, Holden et al., 2015, Clay et al., 2009a), thermal regime of the soil mass (Brown et al., 2015), soil solution chemistry (Clay et al., 2009b, Worrall et al., 2007a) and fluvial carbon loads (Worrall et al., 2013, Worrall et al., 2011, Holden et al., 2012a). Imeson (1971) reported that burning not only exposed the peat surface to erosion and accelerated the loss of surface material, but also increased the rate and intensity of infiltration and throughflow that promotes gully formation and development (e.g. Maltby et al. (1990)). Rothwell et al. (2007) found that approximately 32% of the total lead export from a peatland catchment may have been released during a discrete erosion event soon after a wildfire, and accidental wildfires and the subsequent release of highly contaminated peat may increase under future climate change. Worrall et al. (2011) measured the POC release from peat-covered sites after restoration, following degradation by past wildfires. They found that unrestored, bare peat sites had mean POC flux at 181 t C km^{-2} yr^{-1} which was much higher than that of the restored sites (18 t C km^{-2} yr^{-1}) and the intact vegetated control sites without wildfire impact (21 t C km^{-2} yr^{-1}). Note that as peat sediment is

around half organic carbon, then, crudely, the above values can be doubled to estimate sediment flux.

Several recent modelling studies have been conducted to examine the effects of land-management practices on controlling erosion. Li et al. (2016a) found that a shift in land-management practices that reduce drainage density, grazing and vegetation burning intensity can mitigate the impacts of future climate change on blanket peat erosion, and promote the resilience of systems. Li et al. (2017b) used land-management scenarios including intensified and extensified grazing, artificial drainage and prescribed burning in modelling blanket peat erosion, and found that less intensive management reduced erosion but potentially enhanced the risk of more severe wildfires.

2.5.5 Peatland conservation techniques

Numerous studies have examined the techniques available for restoring degraded blanket peatlands (Crowe et al., 2008, Holden et al., 2008b, Armstrong et al., 2009, Parry et al., 2014), and the role of conservation techniques on stream peak flow (Grayson et al., 2010, Lane and Milledge, 2013, Gao et al., 2015, Gao et al., 2016, Gao et al., 2017), water table and hydrological processes (Worrall et al., 2007b, Allott et al., 2009, Wilson et al., 2010, Holden et al., 2011) and sediment and particulate organic carbon (Holden et al., 2007b, Holden et al., 2008a, Wilson et al., 2011, Ramchunder et al., 2012, Shuttleworth et al., 2015). Restoration practices that result in stabilization and revegetation are recommended as vegetation cover is capable of reducing erosion by: i) significantly reducing overland flow velocity by 32–70% (Holden et al., 2008a); ii) reducing hydrological connectivity (Gao et al., 2015, Gao et al., 2016, Gao et al., 2017) and sediment connectivity (Evans et al., 2006, Evans and Warburton, 2007); iii) protecting peat surfaces from the effects of rainsplash (Li et al., 2018b), freeze–thaw action and desiccation (Brown et al., 2015, Li et al., 2016b); and iv) enhancing the organic matter and microbiological function of peat. In turn, areas with enhanced peat erosion and good hydrological connectivity would make it more difficult for the peat to host vegetation as seeds or small plants would be readily washed away during rainfall events (Holden, 2005b).

Traditional techniques for controlling gully erosion are the establishment of check dams to slow down water flows and control the expansion of the gully network, and reprofiling of the sides of gullies to reduce the slope steepness of gully walls (Parry et al., 2014). Following reprofiling, revegetating gully sides (natural or artificial revegetation) is frequently used to decrease the sediment connectivity of the landscape, resulting in reduced sediment

delivery to the channel system (Evans and Warburton, 2005, Parry et al., 2014).

Management techniques that aim to control channel processes are important for reducing flow erosion, undercutting and ditch bank collapse (Marttila and Kløve, 2010a, Holden et al., 2007b). Holden et al. (2007b) found that blocking drains with periodic dams was successful at reducing sediment yield by more than 50-fold. Practices such as peak runoff control dams (Marttila and Kløve, 2009, Kløve, 2000) that allow temporarily ponding of water above erodible bed deposits during low flows, have been found to be effective in reducing peak flows, sediment and nutrient transport at peat harvesting sites and in peatland forestry management (Marttila and Kløve, 2010b, Marttila and Kløve, 2009, Marttila and Kløve, 2008, Kløve, 1998). In addition, treatment wetland systems, or overland flow areas, are sometimes constructed downstream to purify the peat extraction runoff by retaining sediment and nutrient loads (Postila et al., 2014).

2.6 A meta-analysis of peat erosion rates

2.6.1 Data collection and statistical analysis

Data on peat erosion rates was searched for within the existing published literature identified in the Web of Science described above. A total of 38 publications provided erosion rate data with 61 erosion rate records obtained within these publications (Table 2.1). The dataset compiled included: (i) erosion rates and/or peat loss; (ii) study area; (iii) spatial scale, (iv) temporal scale, (v) measurement method. Erosion rates in the literature tend to be expressed as mg m^{-2} h^{-1} for data collected at very fine scale during short periods (minutes or hours) (Arnaez et al., 2007, Morvan et al., 2008); and as mm yr^{-1} for data collected at fine scale; or as t km^{-2} yr^{-1} for data collected at hillslope and field scales over longer periods (up to several years) (Cerdan et al., 2010, Prosdocimi et al., 2016). We report data at these scales as presented in the literature. However, it is worth noting that it is possible to convert between units by using reported values of peat bulk density. While peat bulk density varies, it is typically very low. Hobbs (1986) reported bulk density values for British peats of ~ 1g cm^{-3}. Therefore, an erosion rate of 1 t km^{-2} yr^{-1} is equivalent to 10 mm of peat loss, or 0.5 t km^{-2} yr^{-1} of carbon. Spatial scale is classified as very fine (microplots < 1 m^2), fine (1–1000 m^2), hillslope (1000 m^2 – 1 ha) and field (> 1 ha) scale (Boix-Fayos et al., 2006, Verheijen et al., 2009). Temporal scale is classified as event (up to several days), monthly, seasonal, long-term (> 1 year) scale. Methods used to obtain

erosion data included erosion pins, bounded plots, sediment transport measurements through sampling or at gauging stations, bathymetric surveys in reservoirs, topographic surveys and sediment budgeting. Correlation analysis and regression analysis were used to identify the relationship between area and sediment yield rate. Test results were considered significant at $p < 0.05$.

Table 2.1 Erosion rates in peatlands reported in publications since 1957.

Region	Spatial scale	Temporal scale	Methods*	Erosion rate**	Reference
Strines Reservoir, S Pennines, England	Catchment (11.15 km^2)	Long-term (87 years)	d	SY1: 39.4	Young (1957)
Catcleugh Reservoir, N England	Catchment (40 km^2)	Long-term (4 years)	d	SY1: 43.1	Hall (1967)
Moor House, N Pennines, England	Catchment (0.83 km^2)	Long-term (1 year)	c	SY1: 110.8 SRR: 10.0	Crisp (1966)
Featherbed Moss, N England	Catchment (0.03 km^2)	Long-term (1 year)	c	SY1: 12.0–40.0	Tallis (1973)
North York Moors, N England	Fine	Long-term (2 years)	a	SRR: 40.9	Imeson (1974)
Hopes Reservoir, SE Scotland	Catchment (5 km^2)	Long-term (35 years)	d	SY1: 25.0	Ledger et al. (1974)
North Esk Reservoir, S Scotland	Catchment (7 km^2)	Long-term (121 years)	d	SY1: 26.0	Ledger et al. (1974)
North York Moors, N England	Catchment	–	–	SY1: 2.0–30.0	Arnett (1979), cited in Robinson and Blyth (1982)
Snake Pass, S Pennines, England	Fine	Long-term (1 year)	a	SRR: 7.8	Philips et al. (1981)
Moor House, N Pennines, England	Fine	Long-term (1 year)	a	SRR: 10. 5	Philips et al. (1981)
Holme Moss, S Pennines, England	Fine	Long-term (1 year)	a	SRR: 73. 8	Philips et al. (1981)
Snake Pass, S Pennines, England	Fine	Long-term (1 year)	a	SRR: 5.4	Philips et al. (1981)
Coalburn, N England	Catchment (1.5 km^2)	Long-term (1.5 year)	c	SY1: 3.0	Robinson and Blyth (1982)
Holme Moss, S Pennines, England	Fine	Long-term (2 years)	a	SRR: 33.5	Tallis and Yalden (1983)
Cabin Clough, S Pennines, England	Fine	Long-term (2 years)	a	SRR: 18.5	Tallis and Yalden (1983)
Doctors Gate, S Pennines, England	Fine	Long-term (2 years)	a	SRR: 9.6	Tallis and Yalden (1983)
Glenfarg reservoir, Scotland	Catchment (5.82 km^2)	Long-term (56 years)	d	SY1: 26.3	McManus and Duck (1985)
Glenquey reservoir, Scotland	Catchment (5.58 km^2)	Long-term (73 years)	d	SY1: 31.3	McManus and Duck (1985)
Peak District Moorland, N England	Fine	Long-term (1 year)	a	SRR: 18.4–24.2	Anderson (1986)
Monachyle, C Scotland	Catchment (7.7 km^2)	–	c	SY1: 43.8	Stott et al. (1986)
Plynlimon, Mid Wales	Fine	Long-term (5 years)	a	SRR: 30.0	Robinson and Newson (1986)
Wessenden Moor, S Pennines, N. England	Catchment	–	c	SY1: 55.0	Labadz (1988)

Region	Spatial scale	Temporal scale	Methods*	Erosion rate**	Reference
Chew Reservoir, S Pennines, N. England	Catchment (3.06 km^2)	–	d	SY1: 212.7	Labadz (1988)
Mid Wales	Fine	Long-term (1.4 years)	a	SRR: 23.4	Francis and Taylor (1989)
Ceunant Ddu, Mid Wales	Catchment (0.34 km^2)	Seasonal	c	SY1: 3.7	Francis and Taylor (1989)
Ceunant Ddu (Ploughing), Mid Wales	Catchment (0.34 km^2)	Seasonal	c	SY1: 9.0	Francis and Taylor (1989)
Nant Ysguthan, Mid Wales	Catchment (0.14 km^2)	Long-term (1.4 years)	c	SY1: 1.1	Francis and Taylor (1989)
Nant Ysguthan (Ploughing), Mid Wales	Catchment (0.14 km^2)	Seasonal	c	SY1: 3.1	Francis and Taylor (1989)
Earlsburn Reservoir, Scotland	Catchment (2.85 km^2)	–	d	SY1: 68.2	Duck and McManus (
North Third Reservoir, Scotland	Catchment (9.31 km^2)	–	d	SY1: 205.4	Duck and McManus (
Carron Valley Reservoir, Scotland	Catchment (38.7 km^2)	–	d	SY1: 141.9	Duck and McManus (
Pinmacher Reservoir, Scotland	Catchment (0.425 km^2)	–	d	SY1: 50.9	Duck and McManus (
Holl Reservoir, Scotland	Catchment (3.99 km^2)	–	d	SY1: 72.3	Duck and McManus (
Harperleas Reservoir, Scotland	Catchment (3.44 km^2)	–	d	SY1: 13.8	Duck and McManus (
Drumain Reservoir, Scotland	Catchment (1.53 km^2)	–	d	SY1: 3.9	Duck and McManus (
Plynlimon, Mid Wales	Fine	Long-term (2 years)	a	SRR: 16.0	Francis (1990)
Upper Severn, Mid Wales	Catchment (0.94 km^2)	Long-term (2 years)	c	SY1: 34.4	Francis (1990)
Abbeystead Reservoir, N. England	Catchment (48.7 km^2)	Long-term (2 years)	d	SY1: 34.8	Labadz et al. (1991)
Wessenden Head Moor, N. England	Catchment (2.4 km^2)	Long-term (2 years)	c	SY1: 38.8	Labadz et al. (1991)
Shetland, N. Scotland	Fine	Long-term (5 years)	a	SRR: 10.0–40.0	Birnie (1993)
Forest of Bowland, N. England	Fine	Long-term (1 year)	a	SRR: 20.4	Mackay and Tallis (1994)
Howden Reservoir, N. England	Catchment (32.0 km^2)	Long-term (75 years)	d	SY1: 128.0	Hutchinson (1995)
Abbeystead Reservoir, N. England	Catchment (48.7 km^2)	Long-term (140 years)	d	SY1: 35.5	Rowan et al. (1995)
77 Reservoirs in Yorkshire, N. England	Catchment	–	d	SY1: 124.5	White et al. (1996)
Harrop Moss, Pennines, N. England	Fine	Long-term (7 years)	a	SRR: 13.2	Anderson et al. (1997)
Monachyle, C. Scotland	Fine	Long-term (2 years)	a	SRR: 59.0	Stott (1997)
Haapasuo peat mine, C. Finland	Fine	Event	b	SY2: 20.0–7060.6	Kløve (1998)
Burnhope Reservoir, N.	Catchment (17.8 km^2)	Long-term (62 years)	d	SY1: 33.3	Holliday (2003)

Region	Spatial scale	Temporal scale	Methods*	Erosion rate**	Reference
England					
Moor House, N. Pennines, N. England	Fine	Long-term (4 years)	a	SRR: 19.3	Evans and Warburton (2005)
Moor House, N. Pennines, N. England	Catchment (0.83 km^2)	Long-term (4 years)	f	SY1: 44.6	Evans and Warburton (2005)
Upper North Grain, S. Pennines, N. England	Catchment (0.38 km^2)	Long-term (1 year)	c	SY1: 161.6	Yang (2005)
March Haigh Reservoir, N. England	Catchment	–	d	SY1: 2–28	Yeloff et al. (2005)
Upper North Grain, S. Pennines, England	Fine	Long-term (1 year)	a	SRR: 34.0	Evans et al. (2006)
Upper North Grain, S. Pennines, England	Catchment (0.38 km^2)	Long-term (1 year)	f	SY1: 195.2	Evans et al. (2006)
Oughtershaw Beck, N. England	Catchment	Long-term (1 year)	c	SY1: 16.9	Holden et al. (2007b)
Flow Moss, N. Pennines, N. England	Fine	Seasonal	a	SRR: 1.03	Baynes (2012)
Harthope Head, N. England	Fine	Seasonal	a	SRR: 38.0	Grayson et al. (2012)
Harthope Head, N. England	Fine	Seasonal	e	SRR: –6.6~ –2.5	Grayson et al. (2012)
Cottage Hill Sike, Moor House, N. England	Catchment (0.17 km^2)	Long-term (3 years)	c	SY1: 2.8	Holden et al. (2012c)
Moor House, N. Pennines, N. England	Very fine	Event	b	SY2: 188.8–72,061.8	Li et al. (2018b)
Moor House, N. Pennines, N. England	Very fine	Event	b	SY2: 28.6–299.2	Li et al. (2018a)

*Methods used: a = erosion pins; b = bounded plots; c = sediment transport measurements through sampling or at gauging stations; d = bathymetric surveys in reservoirs; e = topographic surveys; f = sediment budgeting.
**Erosion rates are summarized in forms of sediment yield (SY1, t km^{-2} yr^{-1} and SY2, mg m^{-2} h^{-1}) or surface retreat rate (SRR, mm yr^{-1}).

2.6.2 Scale-dependency of peat erosion rates and the controls

Figure 2.5 (a) shows the median sediment yield measured at different spatial scales. Sediment yields ranged from 251 to 3,711,055 t km^{-2} yr^{-1} at the very fine scale, from –6600 to 73,800 t km^{-2} yr^{-1} at fine scale, and from 3 to 213 t km^{-2} yr^{-1} at the catchment scale. The significant range at the very fine scale is mainly associated with differences in plot size, rainfall intensity and peat properties utilized in different studies (Kløve, 1998, Li et al., 2018b, Li et al., 2018a). The sediment yields reported at catchment scales tend to cluster quite closely, perhaps because of the close range of climates within which peatlands are formed. A comparison of sediment yields at different scales indicated significant differences between scales, probably caused by

extrapolating data from very fine and fine scales to catchment scales. Different erosion processes are active at different spatial scales, and different sediment sinks and sources appear from plot to catchment scale. In addition, the processes at one spatial or temporal scale interact with processes at another scale. Erosion or deposition rate measured directly by pins are usually interpolated over relatively small areas. Measured erosion rates from erosion plot studies ranged from 20.0 to 72,061.8 mg m^{-2} min^{-1} (Kløve, 1998, Li et al., 2018b, Li et al., 2018a). The temporal pattern of erosion typically displays a positive hysteresis in the relationship between suspended sediment concentration and overland rate, with peak sediment concentration occurring during the rising limb of the overland flow hydrograph (Holden and Burt, 2002a, Clement, 2005, Li et al., 2018b, Kløve, 1998). The positive hysteresis is a result of sediment exhaustion (Li et al., 2018b). The laboratory experiments by Li et al. (2018a) revealed that antecedent conditions such as needle-ice formation is very important in controlling peat erodibility and thus erosional response to a given rainfall event. In fact at the plot scale, without the impacts of rainsplash and weathering processes (freeze–thaw and desiccation), sheet or rill flow has limited effect on increasing peat erosion (Li et al., 2018b, Li et al., 2018a). The presence or absence of vegetation is considered as the other critical factor determining the hydrological and erosion response at the finest temporal and spatial scales (Holden et al., 2008a, Holden and Burt, 2002a, Clement, 2005).

The spatial patterns of topography and vegetation are key factors controlling the response of hillslopes to generation of runoff and the transfer of sediments. Holden and Burt (2003c) found that the source area for overland flow on a hillslope varied depending on the topography and time since rainfall. Gentle slopes, especially footslopes, are dominated by saturation-excess overland flow, whereas steeper midslope sections are dominated by shallow subsurface flow (Holden, 2005b). The majority of sediment produced by interrill and rill erosion on hillslopes is usually deposited at the foot of hillslopes or trapped by vegetation surrounding bare peat areas, and therefore does not reach the channel systems.

Catchment sediment yields reflect the combined effect of all active and interacting erosion and sediment deposition processes. Figure 2.5 (b) shows the relationship between catchment area (A) and mean annual sediment yield (SY) for a total of 19 catchments, based on published reservoir sedimentation measurements (Small et al., 2003, Labadz et al., 1991, Yeloff

et al., 2005); there is wide variation and high degree of scatter, with no statistically significant correlation (Spearman's correlation test, p = 0.898). It has been widely reported that sediment yields decrease with increasing area (De Vente et al., 2007) due to decreasing sediment delivery ratios (Walling and Webb, 1996). However, different behavior has been reported from upland peat catchments (Small et al., 2003) with channel bank erosion being suggested as the dominant sediment source. It can be inferred that gully and bank erosion and mass movements form an important part of the catchment sediment budget in these environments. This is further confirmed by modelling, field measurement and tracer studies demonstrating a significant contribution to sediment yield from gully erosion, bank erosion and mass movements (Evans and Warburton, 2007, Evans et al., 2006). At the catchment scale where all erosion and sediment deposition processes are active and interactive, sediment yield can either increase or decrease with increasing area.

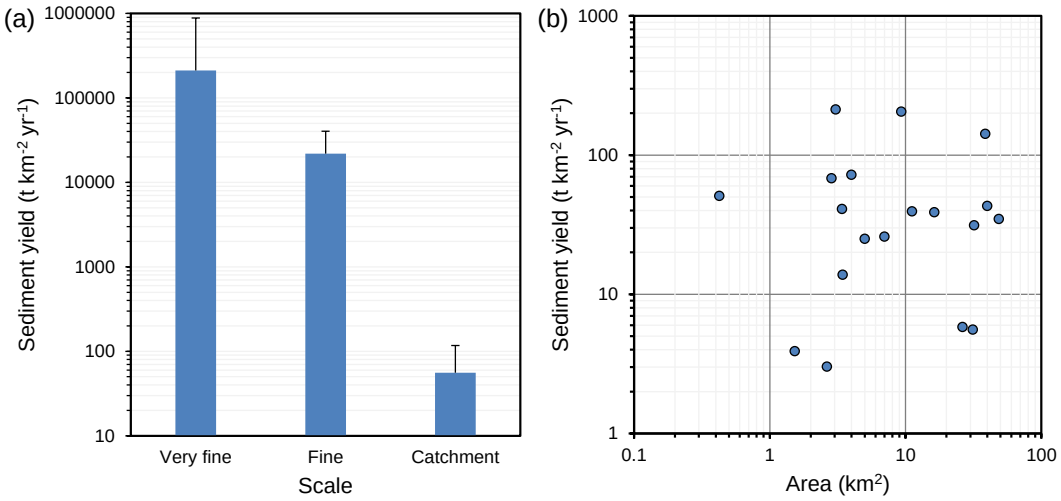

Figure 2.5 (a) Erosion rates obtained from different spatial scales. The sediment yield data obtained from very fine and fine scales was directly extrapolated to a catchment scale for comparison purposes only; (b) Relationship between catchment area and sediment yield for catchment-scale peatland sediment studies.

2.7 Main gaps and prospects in peat erosion research

Since peat erosion consists of complex interacting process that are variable in both space and time and are influenced by numerous internal and external factors, there are still many unanswered questions. More peat erosion research is required in three key areas: i) further study of the known basic peat erosion processes and their incorporation into peat erosion modelling; ii) studies of how peat erosion measurement techniques compare and what types of new information can be gleaned from new techniques; iii) more studies in a range of peatland environments on how erosion drivers or mitigation techniques influence peat erosion.

2.7.1 Peat erosion processes and incorporation into peat erosion models

Some important issues that remain to be addressed include how basic erosion processes such as freeze–thaw weathering, wind-driven rainsplash and pipe erosion function and how they interact with each other. In addition, incorporating some of the important erosion processes into peat erosion models remains a challenge either due to difficulties in the parametrisation of processes that are not fully understood or, as is often the case, a lack of field data for model calibration and validation. For example, the contributions of wind erosion, gully erosion, bank erosion, pipe erosion and mass movements to catchment sediment budgets are usually under-represented in erosion models, although field data clearly demonstrate their importance (Li et al., 2016b). More attention should be focused on process-based studies of these erosion forms to directly inform future model development:

(1) Needle ice production has been observed to be a vital agent of freeze–thaw weathering in producing erodible peat materials (Evans and Warburton, 2007, Grayson et al., 2012, Li et al., 2018a). Studies of the mechanisms controlling needle ice formation (e.g., cooling rate, freezing point, number and frequency of freeze–thaw cycles and moisture content at freezing) are urgently required to enhance the representation of freeze–thaw processes within peatland sediment supply models.

(2) Limited attention has been given to quantitative study of rainsplash erosion, wind-driven rainsplash as well as interactions between rainfall- and flow-driven processes (Li et al., 2018b). Spatially-

distributed models of peatlands which can incorporate these important controls for interrill erosion would be useful for predicting future slope development in peatlands. In addition, the effect of raindrop impact on detachment capacity is highly related to rainfall properties (e.g., rainfall type and intensity, drop size, velocity and kinetic energy and impact gradient of falling drops) (Salles and Poesen, 2000, Singer and Blackard, 1982, Torri and Poesen, 1992), that are usually modified by wind in many peatland environments (Warburton, 2003, Foulds and Warburton, 2007a, Foulds and Warburton, 2007b). These controls on rainsplash detachment should also be reflected in further peat erosion models development.

(3) Piping has been widely observed in peatland landscapes. However, the complete understanding of pipe initiation mechanisms, the interaction of environmental factors controlling the development of pipe networks, roof collapse and gully development, and the influence of piping on catchment water and sediment response needs to be considered.

(4) Despite the importance of wind erosion in upland peat, surprisingly few studies have examined aeolian erosion processes compared with those on fluvial processes in peatland landscapes. Of the few studies available most have focused on the UK north Pennines and are temporally limited with less than two years monitoring (Warburton, 2003, Foulds and Warburton, 2007a, 2007b). Future long-term observations of wind erosion are required in a range of geomorphological locations, to gain a full understanding of peatland aeolian system dynamics and erosion rates.

(5) Floodplain sediment storage may be an important component of the carbon balance of eroding peatlands (Pawson et al., 2012). Future work is required to ascertain the fate of floodplain carbon (and the downstream fate of POC in the fluvial system more generally) in terms of rates and fluxes of loss to DOC or CO_2.

(6) Peat erosion processes interact with one another. Further exploration of the combined effects of sediment supply (rainsplash, freeze–thaw and desiccation) and sediment transport (water erosion, wind erosion, mass movements) processes could be undertaken in future studies that couple laboratory-based experiments and field monitoring to reveal the relative importance of these controls.

(7) Further research is needed on thresholds for connectivity of water and sediment flows at all scales and the role of streams as sediment sources and (temporal) sinks. Multi-scale studies to facilitate spatial upscaling of runoff and erosion rates and provide data on the spatial connections between different units at each scale are necessary.

(8) Finally, peat erosion models should be coupled to peatland landform development models (e.g. DigiBog; Baird et al. (2012); Young et al. (2017)) that can be run under different climate, land management and topographic configurations so that predictions of peat mass growth and decay can include the erosion components.

2.7.2 Peat erosion measurements

Traditional methods of peat erosion measurement using erosion pins, sediment traps and erosion plots have the disadvantage of disturbance and damage to the peat surface during installation and repeated measurements. Photogrammetric measuring techniques are instead recommended where possible. By using measurement techniques such as SfM (Glendell et al., 2017) or remote sensing (Rothwell et al., 2010, Evans and Lindsay, 2010a, Grayson et al., 2012), micro-topographical changes can be compared by using time-series data and mapping important erosion processes (e.g., gully erosion) or erosion affected by needle ice production, desiccation or extreme rainfall events.

In addition, measuring peat erosion is restricted by the temporal scale involved as most monitoring programs are typically limited to a few years (Table 2.1). Short-term measurements may not be representative of long-term fluctuations (Boix-Fayos et al., 2006), such as seasonal and interannual variations in measured peat erosion rates at both the catchment (Francis, 1990, Labadz et al., 1991, Evans and Warburton, 2007) and plot scale (Holden and Burt, 2002a). Long-term systematic measurements under real field conditions are recommended to reduce the temporal uncertainty of erosion plot experiments and to provide numeric models (Li et al., 2016a) with reliable data. In addition, continuous and prolonged monitoring of peat erosion processes should utilize standardized procedures to allow comparisons of data obtained from different study areas (Prosdocimi et al., 2016).

Peat loss measured at one scale may not be representative of those at other scales. Therefore, direct extrapolation of plot scale interrill and rill erosion rates up the catchment scale can be problematic (De Vente and Poesen,

2005, Parsons et al., 2006). There is a need for monitoring, experimental and modelling studies as a basis for scaling erosion rates from one specific area to larger or smaller areas.

2.7.3 Factors (drivers or mitigation techniques) influencing peat erosion

2.7.3.1 Effects of drivers

Changes in micro-climatic factors such as air temperature and moisture content impact the actions and interactions of freeze–thaw and wet–dry cycles and the associated weathering processes of the peat surface. Without intensive weathering processes, running water is unlikely to wash off large quantities of peat (Evans and Warburton, 2007, Li et al., 2018a). More direct investigations are required to reveal the importance of interactions between temperature and moisture controls on sediment supply processes.

In addition to the normally observed peat properties (e.g., degree of humification, shear strength, bulk density) that affect peat erosion (Svahnbäck, 2007, Carling et al., 1997, Marttila and Kløve, 2008, Tuukkanen et al., 2014), other physical and geochemical properties (e.g., grain size distribution and form, moisture) also impact peat erodibility. For example, it has been hypothesized that peat particle size distribution and form impacts the resistance of peat to wind erosion process (Warburton, 2003). Any increase in moisture content is likely to enhance peat hillslope instability due to reduced cohesion and saturation of the basal peat (Warburton et al., 2004, Evans and Warburton, 2007). More attempts are needed to assess how these peat properties influence sediment yield and transport.

Numerous studies have demonstrated that vegetation cover can reduce peat erosion. However, there are several related research questions remaining unanswered. For example, what is the effectiveness of a plant cover in reducing splash erosion rates through interception of raindrops and by decreasing the kinetic energy of raindrops approaching the peat surface? Are weathering processes (freeze–thaw cycle and wet–drying cycle) for the bare soil surfaces different for vegetated peat surfaces? How does vegetation cover impact wind erosion by imparting roughness to the air flow and reducing the shear velocity of wind? To what extent does vegetation cover contribute to peat slope stability reducing mass movements?

In addition, management practices such as artificial drainage, prescribed burning and grazing can result in changes to vegetation cover and sediment connectivity from sources areas to channels (Evans et al., 2006). However,

there have been limited measurements of how peatland hillslope erosion processes respond to changes of vegetation cover that are associated with these management practices (Li et al., 2016a, Li et al., 2017b). Integrated research into the interaction of peat hillslope erosion processes and different vegetation cover conditions that are associated with different states of degradation and re-vegetation will help inform future functioning of peatlands.

Local disturbances such as installation of infrastructure (e.g., windfarms, tracks, footpaths, pipelines) (Parry et al., 2014), may also affect peatland runoff and sediment production (Holden, 2005a, Robroek et al., 2010). More long term studies of peatland runoff and erosion are needed to understand the impacts of these land management practices.

2.7.3.2 Effects of peatland conservation techniques

In recent years there has been a significant increase in the number of peatland restoration projects and amount of funding to reduce the negative consequences of peatland degradation on ecosystem services (Holden et al., 2008b, Parry et al., 2014). Fewer studies have evaluated the effectiveness of conservation measures (e.g., check-dams in gullies and streams) at catchment or regional scales, therefore more attention is required in future studies, particularly to help ensure that erosion prevention is accounted for in carbon accounting processes as part of land management change (LULUCF, 2014) under the United Nations Framework Convention on Climate Change.

2.8 Conclusions

From this review of peatland erosion research a number of research themes have emerged as requiring further attention in the near future. Firstly, there is a need to increase understanding of the basic erosion processes operating in peatlands (e.g., freeze–thaw weathering, wind-driven rainsplash, and piping erosion) and how they interact with one another. Secondly, it is important to establish long-term and multi-scale in-situ monitoring programmes that combine both traditional and new methods (e.g. SfM techniques) that offer improved resolution and spatial coverage. These should adopt standardized procedures to allow comparisons of data derived from different sites but should also be investigative to help our understanding of process dynamics. Process studies and new datasets will enable improved model parameterization through the incorporation of basic

erosion processes that are currently under-represented in erosion models. Finally there is a need to collect more spatially-distributed data, across a wider range of peatland environments to help improve our understanding of the effects of environmental factors and land management practices on peat erosion processes and rates, not least as this will be beneficial for determining the most feasible and sustainable conservation techniques, and support reporting for LULUCF as part of UN climate change commitments.

Acknowledgements

The work was jointly funded by the China Scholarship Council and the University of Leeds (File No. 201406040068).

References

ALLOTT, T., EVANS, M., LINDSAY, J., AGNEW, C., FREER, J., JONES, A. & PARNELL, M. 2009. Water tables in Peak District blanket peatlands. *Report to the Moors for the Future Partnership,* 17.

ANDERSON, P. 1986. Accidental moorland fires in the Peak District: a study of their incidence and ecological implications. *Report to the Peak District Moorland Restoration Project Peak District Planning Board***,** 164.

ANDERSON, P., TALLIS, J. & YALDEN, D. 1997. Restoring moorland: Peak District moorland management project phase 3 report. *Peak District National Park Authority***,** 153.

ARMSTRONG, A., HOLDEN, J., KAY, P., FOULGER, M., GLEDHILL, S., MCDONALD, A. & WALKER, A. 2009. Drain-blocking techniques on blanket peat: A framework for best practice. *Journal of Environmental Management,* 90**,** 3512-3519.

ARNAEZ, J., LASANTA, T., RUIZ-FLAÑO, P. & ORTIGOSA, L. 2007. Factors affecting runoff and erosion under simulated rainfall in Mediterranean vineyards. *Soil and Tillage Research,* 93**,** 324-334.

ARNETT, R. 1979. The use of differing scales to identify factors controlling denudation rates. *Geographical approaches to fluvial processes.* Norwich, UK: Geo Books.

BAIRD, A. J., MORRIS, P. J. & BELYEA, L. R. 2012. The DigiBog peatland development model 1: rationale, conceptual model, and hydrological basis. *Ecohydrology,* 5**,** 242-255.

BALLARD, C., MCINTYRE, N., WHEATER, H., HOLDEN, J. & WALLAGE, Z. 2011. Hydrological modelling of drained blanket peatland. *Journal of Hydrology,* 407**,** 81-93.

BAYNES, E. R. C. 2012. *Peat bog restoration: Implications of erosion and sediment transfer at Flow Moss, North Pennines.* Durham thesis, Durham University.

BENITO, G. & SANCHO, C. 1992. Erosion rates in badland areas of the central Ebro Basin (NE-Spain). *Catena,* 19**,** 269-286.

BILLETT, M., DINSMORE, K., SMART, R., GARNETT, M., HOLDEN, J., CHAPMAN, P., BAIRD, A., GRAYSON, R. & STOTT, A. 2012. Variable source and age of different forms of carbon released from natural peatland pipes. *Journal of Geophysical Research: Biogeosciences,* 117.

BIRNIE, R. V. 1993. Erosion rates on bare peat surfaces in Shetland. *The Scottish Geographical Magazine,* 109**,** 12-17.

BOIX-FAYOS, C., MARTÍNEZ-MENA, M., ARNAU-ROSALÉN, E., CALVO-CASES, A., CASTILLO, V. & ALBALADEJO, J. 2006. Measuring soil erosion by field plots: understanding the sources of variation. *Earth-Science Reviews,* 78**,** 267-285.

BOND-LAMBERTY, B., PECKHAM, S. D., GOWER, S. T. & EWERS, B. E. 2009. Effects of fire on regional evapotranspiration in the central Canadian boreal forest. *Global Change Biology,* 15**,** 1242-1254.

BONN, A., REBANE, M. & REID, C. 2009. Ecosystem services: a new rationale for conservation of upland environments. *In:* A. BONN, T. ALLOTT, K. HUBACEK & STEWART, J. (eds.) *Drivers of Environmental Change in Uplands.* Routledge, London/New York. pp. 448-474.

BOWER, M. 1960. Peat erosion in the Pennines. *Advancement of Science,* 64**,** 323-331.

BOWER, M. 1961. The distribution of erosion in blanket peat bogs in the Pennines. *Transactions and Papers (Institute of British Geographers),* 29**,** 17-30.

BROWN, L. E., PALMER, S. M., JOHNSTON, K. & HOLDEN, J. 2015. Vegetation management with fire modifies peatland soil thermal regime. *Journal of Environmental Management,* 154**,** 166-176.

BRYAN, R. B. 2000a. Soil erodibility and processes of water erosion on hillslope. *Geomorphology,* 32**,** 385-415.

BRYAN, R. B. 2000b. Soil erodibility and processes of water erosion on hillslope. *Geomorphology,* 32**,** 385-415.

BURT, T. & GARDINER, A. 1984. Runoff and sediment production in a small peat-covered catchment: some preliminary results. *Catchment Experiments in Fluvial Geomorphology* Norwich, England: Geo Books.

CAMPBELL, D. R., LAVOIE, C. & ROCHEFORT, L. 2002. Wind erosion and surface stability in abandoned milled peatlands. *Canadian Journal of Soil Science,* 82**,** 85-95.

CARLING, P. A., GLAISTER, M. S. & FLINTHAM, T. P. 1997. The erodibility of upland soils and the design of preafforestation drainage networks in the United Kingdom. *Hydrological Processes,* 11**,** 1963-1980.

CERDAN, O., GOVERS, G., LE BISSONNAIS, Y., VAN OOST, K., POESEN, J., SABY, N., GOBIN, A., VACCA, A., QUINTON, J. & AUERSWALD, K. 2010. Rates and spatial variations of soil erosion in Europe: a study based on erosion plot data. *Geomorphology,* 122**,** 167-177.

CHARMAN, D. 2002. *Peatlands and environmental change,* Chichester, UK, John Wiley & Sons Ltd.

CHOW, T., REES, H., GHANEM, I. & CORMIER, R. 1992. Compactibility of cultivated Sphagnum peat material and its influence on hydrologic characteristics. *Soil Science,* 153**,** 300-306.

CLARK, J. M., GALLEGO-SALA, A. V., ALLOTT, T., CHAPMAN, S., FAREWELL, T., FREEMAN, C., HOUSE, J., ORR, H. G., PRENTICE, I. C. & SMITH, P. 2010. Assessing the vulnerability of blanket peat to climate change using an ensemble of statistical bioclimatic envelope models. *Climate Research,* 45**,** 131-150.

CLAY, G. D., WORRALL, F., CLARK, E. & FRASER, E. D. 2009a. Hydrological responses to managed burning and grazing in an upland blanket bog. *Journal of Hydrology,* 376**,** 486-495.

CLAY, G. D., WORRALL, F. & FRASER, E. D. 2009b. Effects of managed burning upon dissolved organic carbon (DOC) in soil water and runoff water following a managed burn of a UK blanket bog. *Journal of Hydrology,* 367**,** 41-51.

CLEMENT, S. 2005. *The future stability of upland blanket peat following historical erosion and recent re-vegetation.* PhD thesis, Durham University.

COULTHARD, T., KIRKBY, M. & MACKLIN, M. 2000. Modelling geomorphic response to environmental change in an upland catchment. *Hydrological Processes,* 14**,** 2031-2045.

COUPER, P., STOTT, T. & MADDOCK, I. 2002. Insights into river bank erosion processes derived from analysis of negative erosion ‐ pin recordings: observations from three recent UK studies. *Earth Surface Processes and Landforms,* 27**,** 59-79.

CRISP, D. 1966. Input and output of minerals for an area of Pennine moorland: the importance of precipitation, drainage, peat erosion and animals. *Journal of Applied Ecology,* 3**,** 327-348.

CROWE, S., EVANS, M. & ALLOTT, T. 2008. Geomorphological controls on the re-vegetation of erosion gullies in blanket peat: implications for bog restoration. *Mires & Peat,* 3.

CROWE, S. & WARBURTON, J. 2007. Significance of large peat blocks for river channel habitat and stream organic budgets. *Mires & Peat,* 2**,** 1-15.

DANIELS, S., EVANS, M., AGNEW, C. & ALLOTT, T. 2008. Sulphur leaching from headwater catchments in an eroded peatland, South Pennines, UK. *Science of the Total Environment,* 407**,** 481-496.

DAWSON, J. J., BILLETT, M. F., HOPE, D., PALMER, S. M. & DEACON, C. M. 2004. Sources and sinks of aquatic carbon in a peatland stream continuum. *Biogeochemistry,* 70**,** 71-92.

DE VENTE, J. & POESEN, J. 2005. Predicting soil erosion and sediment yield at the basin scale: Scale issues and semi-quantitative models. *Earth-Science Reviews,* 71**,** 95-125.

DE VENTE, J., POESEN, J., ARABKHEDRI, M. & VERSTRAETEN, G. 2007. The sediment delivery problem revisited. *Progress in Physical Geography,* 31**,** 155-178.

DINSMORE, K. J., BILLETT, M. F., SKIBA, U. M., REES, R. M., DREWER, J. & HELFTER, C. 2010. Role of the aquatic pathway in the carbon and greenhouse gas budgets of a peatland catchment. *Global Change Biology,* 16**,** 2750-2762.

DUCK, R. & MCMANUS, J. Relationships between catchment characteristics, land use and sediment yield in the Midland Valley of Scotland. *In:* BOARDMAN, J., FOSTER, I. D. L. & DEARING, J. A., eds. Soil erosion on agricultural land. Proceedings of a workshop

sponsored by the British Geomorphological Research Group, Coventry, UK, January 1989. Chichester: John Wiley & Sons Ltd, 285-299.

EGGELSMANN, R., HEATHWAITE, A., GROSSE-BRAUCKMANN, G., KUSTER, E., NAUCKE, W., SCHUCH, M. & SCHWEICKLE, V. 1993. Physical processes and properties of mires. *In:* DEPARTMENT FOR ENVIRONMENT, F. A. R. A. (ed.). John Wiley and Sons Ltd.

ELLIS, C. J. & TALLIS, J. H. 2001. Climatic control of peat erosion in a North Wales blanket mire. *New Phytologist,* 152**,** 313-324.

EVANS, M., ALLOTT, T., HOLDEN, J., FLITCROFT, C. & BONN, A. 2005. Understanding gully blocking in deep peat. *Moors for the Future Report.* Derbyshire.

EVANS, M., BURT, T., HOLDEN, J. & ADAMSON, J. 1999. Runoff generation and water table fluctuations in blanket peat: evidence from UK data spanning the dry summer of 1995. *Journal of Hydrology,* 221**,** 141-160.

EVANS, M. & LINDSAY, J. 2010a. High resolution quantification of gully erosion in upland peatlands at the landscape scale. *Earth Surface Processes and Landforms,* 35**,** 876-886.

EVANS, M. & LINDSAY, J. 2010b. Impact of gully erosion on carbon sequestration in blanket peatlands. *Climate Research,* 45**,** 31-41.

EVANS, M. & WARBURTON, J. 2001. Transport and dispersal of organic debris (peat blocks) in upland fluvial systems. *Earth Surface Processes and Landforms,* 26**,** 1087-1102.

EVANS, M. & WARBURTON, J. 2005. Sediment budget for an eroding peat - moorland catchment in northern England. *Earth Surface Processes and Landforms,* 30**,** 557-577.

EVANS, M. & WARBURTON, J. 2007. *Geomorphology of upland peat: erosion, form and landscape change,* Oxford, UK, John Wiley & Sons.

EVANS, M., WARBURTON, J. & YANG, J. 2006. Eroding blanket peat catchments: global and local implications of upland organic sediment budgets. *Geomorphology,* 79**,** 45-57.

EVANS, M. G. & BURT, T. P. 2010. Erosional Processes and Sediment Transport in Upland Mires. *In:* BURT, T. P. & ALLISON, R. J. (eds.) *Sediment Cascades: An Integrated Approach.*

EVANS, R. 1997. Soil erosion in the UK initiated by grazing animals: a need for a national survey. *Applied Geography,* 17**,** 127-141.

EVANS, R. 2005. Curtailing grazing-induced erosion in a small catchment and its environs, the Peak District, Central England. *Applied Geography,* 25**,** 81-95.

FENNER, N. & FREEMAN, C. 2011. Drought-induced carbon loss in peatlands. *Nature Geoscience,* 4**,** 895.

FITZGIBBON, J. 1981. Thawing of seasonally frozen ground in organic terrain in central Saskatchewan. *Canadian Journal of Earth Sciences,* 18**,** 1492-1496.

FOULDS, S. A. & WARBURTON, J. 2007a. Significance of wind-driven rain (wind-splash) in the erosion of blanket peat. *Geomorphology,* 83**,** 183-192.

FOULDS, S. A. & WARBURTON, J. 2007b. Wind erosion of blanket peat during a short period of surface desiccation (North Pennines,

Northern England). *Earth Surface Processes and Landforms,* 32**,** 481-488.

FRANCIS, I. 1990. Blanket peat erosion in a mid ‐ wales catchment during two drought years. *Earth Surface Processes and Landforms,* 15**,** 445-456.

FRANCIS, I. & TAYLOR, J. 1989. The effect of forestry drainage operations on upland sediment yields: A study of two peat ‐ covered catchments. *Earth Surface Processes and Landforms,* 14**,** 73-83.

GALLEGO-SALA, A., CLARK, J., HOUSE, J., ORR, H., PRENTICE, I. C., SMITH, P., FAREWELL, T. & CHAPMAN, S. 2010. Bioclimatic envelope model of climate change impacts on blanket peatland distribution in Great Britain. *Climate Research,* 45**,** 151-162.

GALLEGO-SALA, A. V. & PRENTICE, I. C. 2013. Blanket peat biome endangered by climate change. *Nature Climate Change,* 3**,** 152-155.

GAO, J., HOLDEN, J. & KIRKBY, M. 2015. A distributed TOPMODEL for modelling impacts of land ‐ cover change on river flow in upland peatland catchments. *Hydrological Processes,* 29**,** 2867-2879.

GAO, J., HOLDEN, J. & KIRKBY, M. 2016. The impact of land ‐ cover change on flood peaks in peatland basins. *Water Resources Research,* 52**,** 3477-3492.

GAO, J., HOLDEN, J. & KIRKBY, M. 2017. Modelling impacts of agricultural practice on flood peaks in upland catchments: an application of the distributed TOPMODEL. *Hydrological Processes,* 31**,** 4206-4216.

GAVEAU, D. L., SALIM, M. A., HERGOUALC'H, K., LOCATELLI, B., SLOAN, S., WOOSTER, M., MARLIER, M. E., MOLIDENA, E., YAEN, H. & DEFRIES, R. 2014. Major atmospheric emissions from peat fires in Southeast Asia during non-drought years: evidence from the 2013 Sumatran fires. *Scientific Reports,* 4**,** 6112.

GLENDELL, M., MCSHANE, G., FARROW, L., JAMES, M. R., QUINTON, J., ANDERSON, K., EVANS, M., BENAUD, P., RAWLINS, B. & MORGAN, D. 2017. Testing the utility of structure ‐ from ‐ motion photogrammetry reconstructions using small unmanned aerial vehicles and ground photography to estimate the extent of upland soil erosion. *Earth Surface Processes and Landforms,* 42**,** 1860-1871.

GOVERS, G., GIMÉNEZ, R. & VAN OOST, K. 2007. Rill erosion: Exploring the relationship between experiments, modelling and field observations. *Earth-Science Reviews,* 84**,** 87-102.

GRAB, S. W. & DESCHAMPS, C. L. 2004. Geomorphological and geoecological controls and processes following gully development in alpine mires, Lesotho. *Arctic, Antarctic, and Alpine Research,* 36**,** 49-58.

GRANT, M. C., MALLORD, J., STEPHEN, L. & THOMPSON, P. S. 2012. The costs and benefits of grouse moor management to biodiversity and aspects of the wider environment: a review. RSPB Research Report Number 43.

GRAYSON, R., HOLDEN, J., JONES, R., CARLE, J. & LLOYD, A. 2012. Improving particulate carbon loss estimates in eroding peatlands through the use of terrestrial laser scanning. *Geomorphology,* 179**,** 240-248.

GRAYSON, R., HOLDEN, J. & ROSE, R. 2010. Long-term change in storm hydrographs in response to peatland vegetation change. *Journal of Hydrology,* 389**,** 336-343.

HAAHTI, K., YOUNIS, B. A., STENBERG, L. & KOIVUSALO, H. 2014. Unsteady flow simulation and erosion assessment in a ditch network of a drained peatland forest catchment in eastern Finland. *Water Resources Management,* 28**,** 5175-5197.

HALL, D. G. 1967. The pattern of sediment movement in the River Tyne.

HENDRICK, E. 1990. A bog flow at Bellacorrick forest, Co. Mayo. *Irish Forestry*.

HOBBS, N. 1986. Mire morphology and the properties and behaviour of some British and foreign peats. *Quarterly Journal of Engineering Geology and Hydrogeology,* 19**,** 7-80.

HOCHKIRCH, A. & ADORF, F. 2007. Effects of prescribed burning and wildfires on Orthoptera in Central European peat bogs. *Environmental Conservation,* 34**,** 225-235.

HOLDEN, J. 2005a. Controls of soil pipe frequency in upland blanket peat. *Journal of Geophysical Research: Earth Surface (2003–2012),* 110.

HOLDEN, J. 2005b. Peatland hydrology and carbon release: why small-scale process matters. *Philosophical Transactions of the Royal Society A: Mathematical, Physical and Engineering Sciences,* 363**,** 2891-2913.

HOLDEN, J. 2006. Sediment and particulate carbon removal by pipe erosion increase over time in blanket peatlands as a consequence of land drainage. *Journal of Geophysical Research: Earth Surface (2003–2012),* 111.

HOLDEN, J. 2007. A plea for more careful presentation of near‐surface air temperature data in geomorphology. *Earth Surface Processes and Landforms,* 32**,** 1433-1436.

HOLDEN, J. 2009a. Flow through macropores of different size classes in blanket peat. *Journal of Hydrology,* 364**,** 342-348.

HOLDEN, J. 2009b. Topographic controls upon soil macropore flow. *Earth Surface Processes and Landforms,* 34**,** 345-351.

HOLDEN, J. & ADAMSON, J. 2002. The Moor House long‐term upland temperature record: New evidence of recent warming. *Weather,* 57**,** 119-127.

HOLDEN, J. & BURT, T. 2002a. Infiltration, runoff and sediment production in blanket peat catchments: implications of field rainfall simulation experiments. *Hydrological Processes,* 16**,** 2537-2557.

HOLDEN, J. & BURT, T. 2002b. Laboratory experiments on drought and runoff in blanket peat. *European Journal of Soil Science,* 53**,** 675-690.

HOLDEN, J. & BURT, T. 2002c. Piping and pipeflow in a deep peat catchment. *Catena,* 48**,** 163-199.

HOLDEN, J. & BURT, T. 2003a. Hydraulic conductivity in upland blanket peat: measurement and variability. *Hydrological Processes,* 17**,** 1227-1237.

HOLDEN, J. & BURT, T. 2003b. Hydrological studies on blanket peat: the significance of the acrotelm‐catotelm model. *Journal of Ecology,* 91**,** 86-102.

HOLDEN, J., BURT, T. & VILAS, M. 2002. Application of ground‐penetrating radar to the identification of subsurface piping in blanket peat. *Earth Surface Processes and Landforms,* 27**,** 235-249.

HOLDEN, J. & BURT, T. P. 2003c. Runoff production in blanket peat covered catchments. *Water Resources Research,* 39.

HOLDEN, J., CHAPMAN, P., EVANS, M., HUBACECK, K., KAY, P. & WARBURTON, J. 2007a. Vulnerability of organic soils in England and Wales. *Final report for DEFRA Project SP0532.*

HOLDEN, J., CHAPMAN, P. & LABADZ, J. 2004. Artificial drainage of peatlands: hydrological and hydrochemical process and wetland restoration. *Progress in Physical Geography,* 28**,** 95-123.

HOLDEN, J., CHAPMAN, P., PALMER, S., KAY, P. & GRAYSON, R. 2012a. The impacts of prescribed moorland burning on water colour and dissolved organic carbon: a critical synthesis. *Journal of Environmental Management,* 101**,** 92-103.

HOLDEN, J., EVANS, M., BURT, T. & HORTON, M. 2006. Impact of land drainage on peatland hydrology. *Journal of Environmental Quality,* 35**,** 1764-1778.

HOLDEN, J., GASCOIGN, M. & BOSANKO, N. R. 2007b. Erosion and natural revegetation associated with surface land drains in upland peatlands. *Earth Surface Processes and Landforms,* 32**,** 1547-1557.

HOLDEN, J., KIRKBY, M. J., LANE, S. N., MILLEDGE, D. G., BROOKES, C. J., HOLDEN, V. & MCDONALD, A. T. 2008a. Overland flow velocity and roughness properties in peatlands. *Water Resources Research,* 44**,** W06415.

HOLDEN, J., PALMER, S. M., JOHNSTON, K., WEARING, C., IRVINE, B. & BROWN, L. E. 2015. Impact of prescribed burning on blanket peat hydrology. *Water Resources Research,* 51**,** 6472-6484.

HOLDEN, J., SHOTBOLT, L., BONN, A., BURT, T., CHAPMAN, P., DOUGILL, A., FRASER, E., HUBACEK, K., IRVINE, B. & KIRKBY, M. 2007c. Environmental change in moorland landscapes. *Earth-Science Reviews,* 82**,** 75-100.

HOLDEN, J., SMART, R., DINSMORE, K., BAIRD, A., BILLETT, M. & CHAPMAN, P. 2012b. Morphological change of natural pipe outlets in blanket peat. *Earth Surface Processes and Landforms,* 37**,** 109-118.

HOLDEN, J., SMART, R. P., DINSMORE, K. J., BAIRD, A. J., BILLETT, M. F. & CHAPMAN, P. J. 2012c. Natural pipes in blanket peatlands: major point sources for the release of carbon to the aquatic system. *Global Change Biology,* 18**,** 3568-3580.

HOLDEN, J., WALKER, J., EVANS, M., WORRALL, F. & BONN, A. 2008b. A compendium of UK peat restoration and management projects. *Rep. No. SP0556. Defra, London*.

HOLDEN, J., WALLAGE, Z., LANE, S. & MCDONALD, A. 2011. Water table dynamics in undisturbed, drained and restored blanket peat. *Journal of Hydrology,* 402**,** 103-114.

HOLDEN, J., WEARING, C., PALMER, S., JACKSON, B., JOHNSTON, K. & BROWN, L. E. 2014. Fire decreases near‐surface hydraulic conductivity and macropore flow in blanket peat. *Hydrological Processes,* 28**,** 2868-2876.

HOLLIDAY, V. J. 2003. *Sediment budget for a North Pennine upland reservoir catchment, UK.* Durham thesis, Durham University.

HOPE, D., BILLETT, M. F., MILNE, R. & BROWN, T. A. 1997. Exports of organic carbon in British rivers. *Hydrological Processes,* 11**,** 325-344.

HUTCHINSON, S. M. 1995. Use of magnetic and radiometric measurements to investigate erosion and sedimentation in a British upland catchment. *Earth Surface Processes and Landforms,* 20**,** 293-314.

IMESON, A. 1971. Heather burning and soil erosion on the North Yorkshire Moors. *Journal of Applied Ecology***,** 537-542.

IMESON, A. 1974. The origin of sediment in a moorland catchment with particular reference to the role of vegetation. *Institute of British Geographers Special Publication,* 6**,** 59-72.

ISE, T., DUNN, A. L., WOFSY, S. C. & MOORCROFT, P. R. 2008. High sensitivity of peat decomposition to climate change through water-table feedback. *Nature Geoscience,* 1**,** 763.

JONES, J. 2004. Implications of natural soil piping for basin management in upland Britain. *Land Degradation & Development,* 15**,** 325-349.

JONES, J. 2010. Soil piping and catchment response. *Hydrological Processes,* 24**,** 1548-1566.

JOOSTEN, H. 2016. Peatlands across the globe. *In:* A. BONN, T. ALLOTT, M. EVANS, JOOSTEN, H. & STONEMAN, R. (eds.) *Peatland Restoration and Ecosystem Services: Science, Policy and Practice.* Cambridge: Cambridge University Press.

KELLNER, E. & HALLDIN, S. 2002. Water budget and surface‐layer water storage in a Sphagnum bog in central Sweden. *Hydrological Processes,* 16**,** 87-103.

KINNELL, P. 2005. Raindrop‐impact‐induced erosion processes and prediction: a review. *Hydrological Processes,* 19**,** 2815-2844.

KIRKBY, M., IRVINE, B., JONES, R. J. & GOVERS, G. 2008. The PESERA coarse scale erosion model for Europe. I.–Model rationale and implementation. *European Journal of Soil Science,* 59**,** 1293-1306.

KLØVE, B. 1998. Erosion and sediment delivery from peat mines. *Soil and Tillage Research,* 45**,** 199-216.

KLØVE, B. 2000. Retention of suspended solids and sediment bound nutrients from peat harvesting sites with peak runoff control, constructed floodplains and sedimentation ponds. *Boreal Environment Research,* 5**,** 81-94.

KNAPEN, A., POESEN, J., GOVERS, G., GYSSELS, G. & NACHTERGAELE, J. 2007. Resistance of soils to concentrated flow erosion: A review. *Earth-Science Reviews,* 80**,** 75-109.

LABADZ, J., BURT, T. & POTTER, A. 1991. Sediment yield and delivery in the blanket peat moorlands of the Southern Pennines. *Earth Surface Processes and Landforms,* 16**,** 255-271.

LABADZ, J. C. 1988. *Runoff and sediment production in blanket peat moorland studies in the Southern Pennines.* Unpublished PhD thesis, Huddersfield Polytechnic.

LANE, S. N. & MILLEDGE, D. G. 2013. Impacts of upland open drains upon runoff generation: a numerical assessment of catchment‐scale impacts. *Hydrological Processes,* 27**,** 1701-1726.

LEDGER, D., LOVELL, J. & MCDONALD, A. 1974. Sediment yield studies in upland catchment areas in south-east Scotland. *Journal of Applied Ecology,* 11**,** 201-206.

LEWIS, J. 1996. Turbidity‐controlled suspended sediment sampling for runoff‐event load estimation. *Water Resources Research,* 32**,** 2299-2310.

LI, C., HOLDEN, J. & GRAYSON, R. 2018a. Effects of needle ice production and thaw on peat erosion processes during overland flow events. *Journal of Geophysical Research: Earth Surface,* 123**,** 2107-2122

LI, C., HOLDEN, J. & GRAYSON, R. 2018b. Effects of rainfall, overland flow and their interactions on peatland interrill erosion processes. *Earth Surface Processes and Landforms,* 43**,** 1451-1464.

LI, P., HOLDEN, J. & IRVINE, B. 2016a. Prediction of blanket peat erosion across Great Britain under environmental change. *Climatic Change,* 134**,** 177-191.

LI, P., HOLDEN, J., IRVINE, B. & GRAYSON, R. 2016b. PESERA‐PEAT: a fluvial erosion model for blanket peatlands. *Earth Surface Processes and Landforms,* 41**,** 2058-2077.

LI, P., HOLDEN, J., IRVINE, B. & MU, X. 2017a. Erosion of Northern Hemisphere blanket peatlands under 21st‐century climate change. *Geophysical Research Letters,* 44**,** 3615-3623.

LI, P., IRVINE, B., HOLDEN, J. & MU, X. 2017b. Spatial variability of fluvial blanket peat erosion rates for the 21st Century modelled using PESERA-PEAT. *Catena,* 150**,** 302-316.

LI, P., MU, X., HOLDEN, J., WU, Y., IRVINE, B., WANG, F., GAO, P., ZHAO, G. & SUN, W. 2017c. Comparison of soil erosion models used to study the Chinese Loess Plateau. *Earth-Science Reviews,* 170**,** 17-30.

LINDSAY, R., BIRNIE, R. & CLOUGH, J. 2014. Peat bog ecosystems: weathering, erosion and mass movement of blanket bog. Edinburgh: International Union for the Conservation of Nature.

LULUCF. 2014. *Land Use, Land-Use Change and Forestry (LULUCF)* [Online]. http://unfccc.int/land_use_and_climate_change/lulucf/items/1084.php. [Accessed].

LUOTO, M. & SEPPÄLÄ, M. 2000. Summit peats ('peat cakes') on the fells of Finnish Lapland: continental fragments of blanket mires? *The Holocene,* 10**,** 229-241.

MACKAY, A. W. & TALLIS, J. H. 1994. The recent vegetational history of the Forest of Bowland, Lancashire, UK. *New Phytologist,* 128**,** 571-584.

MALTBY, E., LEGG, C. & PROCTOR, M. 1990. The ecology of severe moorland fire on the North York Moors: effects of the 1976 fires, and subsequent surface and vegetation development. *The Journal of Ecology***,** 490-518.

MARTTILA, H. & KLØVE, B. 2008. Erosion and delivery of deposited peat sediment. *Water Resources Research,* 44.

MARTTILA, H. & KLØVE, B. 2009. Retention of sediment and nutrient loads with peak runoff control. *Journal of Irrigation and Drainage Engineering,* 135**,** 210-216.

MARTTILA, H. & KLØVE, B. 2010a. Dynamics of erosion and suspended sediment transport from drained peatland forestry. *Journal of Hydrology,* 388**,** 414-425.

MARTTILA, H. & KLØVE, B. 2010b. Managing runoff, water quality and erosion in peatland forestry by peak runoff control. *Ecological Engineering,* 36**,** 900-911.

MARTTILA, H., POSTILA, H. & KLØVE, B. 2010. Calibration of turbidity meter and acoustic doppler velocimetry (Triton ‑ ADV) for sediment types present in drained peatland headwaters: Focus on particulate organic peat. *River Research and Applications,* 26**,** 1019-1035.

MAY, L., PLACE, C., O'HEA, B., LEE, M., DILLANE, M. & MCGINNITY, P. Modelling soil erosion and transport in the Burrishoole catchment, Newport, Co. Mayo, Ireland. Freshwater Forum, 2010.

MCMANUS, J. & DUCK, R. W. 1985. Sediment yield estimated from reservoir siltation in the Ochil Hills, Scotland. *Earth Surface Processes and Landforms,* 10**,** 193-200.

MEYLES, E., WILLIAMS, A., TERNAN, J., ANDERSON, J. & DOWD, J. 2006. The influence of grazing on vegetation, soil properties and stream discharge in a small Dartmoor catchment, southwest England, UK. *Earth Surface Processes and Landforms,* 31**,** 622-631.

MORVAN, X., SABY, N., ARROUAYS, D., LE BAS, C., JONES, R., VERHEIJEN, F., BELLAMY, P., STEPHENS, M. & KIBBLEWHITE, M. 2008. Soil monitoring in Europe: a review of existing systems and requirements for harmonisation. *Science of the Total Environment,* 391**,** 1-12.

MULQUEEN, J., RODGERS, M., MARREN, N. & HEALY, M. G. 2006. Erodibility of hill peat. *Irish Journal of Agricultural and Food Research***,** 103-114.

NADAL-ROMERO, E., MARTÍNEZ-MURILLO, J. F., VANMAERCKE, M. & POESEN, J. 2011. Scale-dependency of sediment yield from badland areas in Mediterranean environments. *Progress in Physical Geography,* 35**,** 297-332.

NOBLE, A., PALMER, S. M., GLAVES, D. J., CROWLE, A., BROWN, L. E. & HOLDEN, J. 2017. Prescribed burning, atmospheric pollution and grazing effects on peatland vegetation composition. *Journal of Applied Ecology,* 55**,** 559-569.

NORRSTRÖM, A.-C. & JACKS, G. 1996. Water pathways and chemistry at the groundwater/surface water interface to Lake Skjervatjern, Norway. *Water Resources Research,* 32**,** 2221-2229.

OSAKI, M. & TSUJI, N. 2015. *Tropical peatland ecosystems,* Tokyo, Japan, Springer.

OUTCALT, S. I. 1971. An algorithm for needle ice growth. *Water Resources Research,* 7**,** 394-400.

PALMER, S. M., EVANS, C. D., CHAPMAN, P. J., BURDEN, A., JONES, T. G., ALLOTT, T. E., EVANS, M. G., MOODY, C. S., WORRALL, F. & HOLDEN, J. 2016. Sporadic hotspots for physico-chemical retention of aquatic organic carbon: from peatland headwater source to sea. *Aquatic Sciences,* 78**,** 491-504.

PARRY, L. E., HOLDEN, J. & CHAPMAN, P. J. 2014. Restoration of blanket peatlands. *Journal of Environmental Management,* 133**,** 193-205.

PARSONS, A. J. 2011. How useful are catchment sediment budgets? *Progress in Physical Geography,* 36**,** 60-71.

PARSONS, A. J., BRAZIER, R. E., WAINWRIGHT, J. & POWELL, D. M. 2006. Scale relationships in hillslope runoff and erosion. *Earth Surface Processes and Landforms,* 31**,** 1384-1393.

PAWSON, R., EVANS, M. & ALLOTT, T. 2012. Fluvial carbon flux from headwater peatland streams: significance of particulate carbon flux. *Earth Surface Processes and Landforms,* 37**,** 1203-1212.

PAWSON, R., LORD, D., EVANS, M. & ALLOTT, T. 2008. Fluvial organic carbon flux from an eroding peatland catchment, southern Pennines, UK. *Hydrology and Earth System Sciences,* 12**,** 625-634.

PHILIPS, J., TALLIS, J. & YALDEN, D. 1981. Peak District moorland erosion study: Phase 1 report. *Peak Park Joint Planning Board, Bakewell*.

PIERSON, F. B., ROBICHAUD, P. R., MOFFET, C. A., SPAETH, K. E., HARDEGREE, S. P., CLARK, P. E. & WILLIAMS, C. J. 2008. Fire effects on rangeland hydrology and erosion in a steep sagebrush‐dominated landscape. *Hydrological Processes,* 22**,** 2916-2929.

POSTILA, H., SAUKKORIIPI, J., HEIKKINEN, K., KARJALAINEN, S. M., KUOPPALA, M., MARTTILA, H. & KLØVE, B. 2014. Can treatment wetlands be constructed on drained peatlands for efficient purification of peat extraction runoff? *Geoderma,* 228**,** 33-43.

PRICE, J. & MALONEY, D. 1994. Hydrology of a patterned bog-fen complex in southeastern Labrador, Canada. *Hydrology Research,* 25**,** 313-330.

PROSDOCIMI, M., CERDÀ, A. & TAROLLI, P. 2016. Soil water erosion on Mediterranean vineyards: A review. *Catena,* 141**,** 1-21.

RAMCHUNDER, S., BROWN, L. & HOLDEN, J. 2009. Environmental effects of drainage, drain-blocking and prescribed vegetation burning in UK upland peatlands. *Progress in Physical Geography,* 33**,** 49-79.

RAMCHUNDER, S. J., BROWN, L. E. & HOLDEN, J. 2012. Catchment‐scale peatland restoration benefits stream ecosystem biodiversity. *Journal of Applied Ecology,* 49**,** 182-191.

RAMCHUNDER, S. J., BROWN, L. E. & HOLDEN, J. 2013. Rotational vegetation burning effects on peatland stream ecosystems. *Journal of Applied Ecology,* 50**,** 636-648.

RAPSON, G., SYKES, M. T., LEE, W. G., HEWITT, A. E., AGNEW, A. & WILSON, J. B. 2006. Subalpine gully‐head ribbon fens of the Lammerlaw and Lammermoor Ranges, Otago, New Zealand. *New Zealand Journal of Botany,* 44**,** 351-375.

ROBINSON, M. & BLYTH, K. 1982. The effect of forestry drainage operations on upland sediment yields: a case study. *Earth Surface Processes and Landforms,* 7**,** 85-90.

ROBINSON, M. & NEWSON, M. D. 1986. *Comparison of forest and moorland hydrology in an upland area with peat soils*.

ROBROEK, B. J., SMART, R. P. & HOLDEN, J. 2010. Sensitivity of blanket peat vegetation and hydrochemistry to local disturbances. *Science of the Total Environment,* 408**,** 5028-5034.

ROSA, E. & LAROCQUE, M. 2008. Investigating peat hydrological properties using field and laboratory methods: application to the Lanoraie peatland complex (southern Quebec, Canada). *Hydrological Processes,* 22**,** 1866-1875.

ROTHWELL, J., EVANS, M. & ALLOTT, T. 2008a. In-stream processing of sediment-associated metals in peatland fluvial systems. *Water, Air, and Soil pollution,* 187**,** 53-64.

ROTHWELL, J., EVANS, M., LIDDAMAN, L. & ALLOTT, T. 2007. The role of wildfire and gully erosion in particulate Pb export from contaminated peatland catchments in the southern Pennines, UK. *Geomorphology,* 88**,** 276-284.

ROTHWELL, J. J., EVANS, M. G., DANIELS, S. M. & ALLOTT, T. E. 2008b. Peat soils as a source of lead contamination to upland fluvial systems. *Environmental Pollution,* 153**,** 582-589.

ROTHWELL, J. J., LINDSAY, J. B., EVANS, M. G. & ALLOTT, T. E. 2010. Modelling suspended sediment lead concentrations in contaminated peatland catchments using digital terrain analysis. *Ecological Engineering,* 36**,** 623-630.

ROWAN, J., GOODWILL, P. & GRECO, M. 1995. Temporal variability in catchment sediment yield determined from repeated bathymetric surveys: Abbeystead Reservoir, UK. *Physics and Chemistry of the Earth,* 20**,** 199-206.

SALLES, C. & POESEN, J. 2000. Rain properties controlling soil splash detachment. *Hydrological Processes,* 14**,** 271-282.

SHUTTLEWORTH, E., EVANS, M., HUTCHINSON, S. & ROTHWELL, J. 2015. Peatland restoration: controls on sediment production and reductions in carbon and pollutant export. *Earth Surface Processes and Landforms,* 40**,** 459-472.

SINGER, M. J. & BLACKARD, J. 1982. Slope angle-interrill soil loss relationships for slopes up to 50%. *Soil Science Society of America Journal,* 46**,** 1270-1273.

SMALL, I., ROWAN, J. & DUCK, R. 2003. Long-term sediment yield in Crombie Reservoir catchment, Angus; and its regional significance within the Midland Valley of Scotland. *Hydrological Sciences Journal,* 48**,** 619-635.

SMART, R., HOLDEN, J., DINSMORE, K., BAIRD, A., BILLETT, M., CHAPMAN, P. & GRAYSON, R. 2013. The dynamics of natural pipe hydrological behaviour in blanket peat. *Hydrological Processes,* 27**,** 1523-1534.

SMART, S., HENRYS, P., SCOTT, W., HALL, J., EVANS, C., CROWE, A., ROWE, E., DRAGOSITS, U., PAGE, T. & WHYATT, J. 2010. Impacts of pollution and climate change on ombrotrophic Sphagnum species in the UK: analysis of uncertainties in two empirical niche models. *Climate Research,* 45**,** 163-177.

SMITH, H. & DRAGOVICH, D. 2008. Post-fire hillslope erosion response in a sub-alpine environment, south-eastern Australia. *Catena,* 73**,** 274-285.

SMITH, M., CARRIVICK, J. & QUINCEY, D. 2016. Structure from motion photogrammetry in physical geography. *Progress in Physical Geography,* 40**,** 247-275.

SMITH, M. & WARBURTON, J. 2018. Microtopography of bare peat: a conceptual model and objective classification from high‐resolution topographic survey data. *Earth Surface Processes and Landforms,* 43**,** 1557-1574.

SMITH, M. W. & VERICAT, D. 2015. From experimental plots to experimental landscapes: topography, erosion and deposition in sub‐humid badlands from structure‐from‐motion photogrammetry. *Earth Surface Processes and Landforms,* 40**,** 1656-1671.

STENBERG, L., FINÉR, L., NIEMINEN, M., SARKKOLA, S. & KOIVUSALO, H. 2015a. Quantification of ditch bank erosion in drained forested catchment. *Boreal Environment Research,* 20**,** 1-18.

STENBERG, L., TUUKKANEN, T., FINÉR, L., MARTTILA, H., PIIRAINEN, S., KLØVE, B. & KOIVUSALO, H. 2015b. Ditch erosion processes and sediment transport in a drained peatland forest. *Ecological Engineering,* 75**,** 421-433.

STOTT, T. 1997. A comparison of stream bank erosion processes on forested and moorland streams in the Balquhidder catchments, central Scotland. *Earth Surface Processes and Landforms,* 22**,** 383-399.

STOTT, T., FERGUSON, R., JOHNSON, R. & NEWSON, M. 1986. Sediment budgets in forested and unforested basins in upland Scotland. *IAHS-AISH publication***,** 57-68.

SVAHNBÄCK, L. 2007. *Precipitation-induced runoff and leaching from milled peat mining mires by peat types: a comparative method for estimating the loading of water bodies during peat pruduction.* Doctoral dissertation, University of Helsinki.

TALLIS, J. 1973. Studies on southern Pennine peats: V. Direct observations on peat erosion and peat hydrology at Featherbed Moss, Derbyshire. *The Journal of Ecology,* 61**,** 1-22.

TALLIS, J. 1997. The pollen record of Empetrum nigrum in southern Pennine peats: implications for erosion and climate change. *Journal of Ecology***,** 455-465.

TALLIS, J. & YALDEN, D. 1983. Peak District Moorland Restoration Project Phase 2 Report. *Peak District National Park Authority, Bakewell*.

TOMLINSON, R. 1981. The erosion of peat in the uplands of Northern Ireland. *Irish Geography,* 14**,** 51-64.

TORRI, D. & POESEN, J. 1992. The effect of soil surface slope on raindrop detachment. *Catena,* 19**,** 561-578.

TURETSKY, M. R., BENSCOTER, B., PAGE, S., REIN, G., VAN DER WERF, G. R. & WATTS, A. 2015. Global vulnerability of peatlands to fire and carbon loss. *Nature Geoscience,* 8**,** 11-14.

TUUKKANEN, T., MARTTILA, H. & KLØVE, B. 2014. Effect of soil properties on peat erosion and suspended sediment delivery in drained peatlands. *Water Resources Research,* 50**,** 3523-3535.

TUUKKANEN, T., STENBERG, L., MARTTILA, H., FINÉR, L., PIIRAINEN, S., KOIVUSALO, H. & KLØVE, B. 2016. Erosion mechanisms and sediment sources in a peatland forest after ditch cleaning. *Earth Surface Processes and Landforms,* 41**,** 1841-1853.

VERACHTERT, E., MAETENS, W., VAN DEN EECKHAUT, M., POESEN, J. & DECKERS, J. 2011. Soil loss rates due to piping erosion. *Earth Surface Processes and Landforms,* 36**,** 1715-1725.

VERHEIJEN, F. G., JONES, R. J., RICKSON, R. & SMITH, C. 2009. Tolerable versus actual soil erosion rates in Europe. *Earth-Science Reviews,* 94**,** 23-38.

VERSTRAETEN, G., BAZZOFFI, P., LAJCZAK, A., RÃDOANE, M., REY, F., POESEN, J. & DE VENTE, J. 2006. Reservoir and pond sedimentation in Europe. *Soil Erosion in Europe***,** 757-774.

VERSTRAETEN, G. & POESEN, J. 2002. Using sediment deposits in small ponds to quantify sediment yield from small catchments: possibilities

and limitations. *Earth Surface Processes and Landforms: The Journal of the British Geomorphological Research Group,* 27**,** 1425-1439.

WALLING, D. E. & WEBB, B. 1996. *Erosion and Sediment Yield: Global and Regional Perspectives: Proceedings of an International Symposium Held at Exeter, UK, from 15 to 19 July 1996*, IAHS.

WARBURTON, J. 2003. Wind-splash erosion of bare peat on UK upland moorlands. *Catena,* 52**,** 191-207.

WARBURTON, J. & EVANS, M. 2011. Geomorphic, sedimentary, and potential palaeoenvironmental significance of peat blocks in alluvial river systems. *Geomorphology,* 130**,** 101-114.

WARBURTON, J., HOLDEN, J. & MILLS, A. J. 2004. Hydrological controls of surficial mass movements in peat. *Earth-Science Reviews,* 67**,** 139-156.

WHITE, P., LABADZ, J. & BUTCHER, D. 1996. Sediment yield estimates from reservoir studies: an appraisal of variability in the southern Pennines of the UK. *IAHS Publications-Series of Proceedings and Reports-Intern Assoc Hydrological Sciences,* 236**,** 163-174.

WILSON, L., WILSON, J., HOLDEN, J., JOHNSTONE, I., ARMSTRONG, A. & MORRIS, M. 2010. Recovery of water tables in Welsh blanket bog after drain blocking: discharge rates, time scales and the influence of local conditions. *Journal of Hydrology,* 391**,** 377-386.

WILSON, L., WILSON, J., HOLDEN, J., JOHNSTONE, I., ARMSTRONG, A. & MORRIS, M. 2011. Ditch blocking, water chemistry and organic carbon flux: evidence that blanket bog restoration reduces erosion and fluvial carbon loss. *Science of the Total Environment,* 409**,** 2010-2018.

WOO, M.-K. & DICENZO, P. 1988. Pipe flow in James Bay coastal wetlands. *Canadian Journal of Earth Sciences,* 25**,** 625-629.

WORRALL, F. & ADAMSON, J. 2008. The effect of burning and sheep grazing on soil water composition in a blanket bog: evidence for soil structural changes? *Hydrological Processes,* 22**,** 2531-2541.

WORRALL, F., ARMSTRONG, A. & ADAMSON, J. 2007a. The effects of burning and sheep-grazing on water table depth and soil water quality in a upland peat. *Journal of Hydrology,* 339**,** 1-14.

WORRALL, F., ARMSTRONG, A. & HOLDEN, J. 2007b. Short-term impact of peat drain-blocking on water colour, dissolved organic carbon concentration, and water table depth. *Journal of Hydrology,* 337**,** 315-325.

WORRALL, F., ROWSON, J. & DIXON, S. 2013. Effects of managed burning in comparison with vegetation cutting on dissolved organic carbon concentrations in peat soils. *Hydrological Processes,* 27**,** 3994-4003.

WORRALL, F., ROWSON, J., EVANS, M., PAWSON, R., DANIELS, S. & BONN, A. 2011. Carbon fluxes from eroding peatlands–the carbon benefit of revegetation following wildfire. *Earth Surface Processes and Landforms,* 36**,** 1487-1498.

WYNN, T., HENDERSON, M. & VAUGHAN, D. 2008. Changes in streambank erodibility and critical shear stress due to subaerial processes along a headwater stream, southwestern Virginia, USA. *Geomorphology,* 97**,** 260-273.

XU, J., MORRIS, P. J., LIU, J. & HOLDEN, J. 2018. PEATMAP: Refining estimates of global peatland distribution based on a meta-analysis. *Catena,* 160**,** 134-140.

YANG, J. 2005. *Monitoring and modelling sediment flux from eroding peatland.* PhD Thesis University of Manchester.

YELOFF, D., LABADZ, J., HUNT, C., HIGGITT, D. & FOSTER, I. D. 2005. Blanket peat erosion and sediment yield in an upland reservoir catchment in the southern Pennines, UK. *Earth Surface Processes and Landforms,* 30**,** 717-733.

YOUNG, A. 1957. A record of the rate of erosion on Millstone Grit. *Proceedings of the Yorkshire Geological Society,* 31**,** 149-156.

YOUNG, D. M., BAIRD, A. J., MORRIS, P. J. & HOLDEN, J. 2017. Simulating the long‐term impacts of drainage and restoration on the ecohydrology of peatlands. *Water Resources Research,* 53**,** 6510-6522.

YU, Z., LOISEL, J., BROSSEAU, D. P., BEILMAN, D. W. & HUNT, S. J. 2010. Global peatland dynamics since the Last Glacial Maximum. *Geophysical Research Letters,* 37.

ZHAO, Y. 2008. *Livestock impacts on hydrological connectivity.* PhD thesis, University of Leeds.

Chapter 3
Effects of rainfall, overland flow and their interactions on peatland interrill erosion processes

Changjia Li, Joseph Holden, Richard Grayson. 2018. Effects of rainfall, overland flow and their interactions on peatland interrill erosion processes. *Earth Surface Processes and Landforms*. **43** (7): 1451-1464. DOI: 10.1002/esp.4328

3.1 Abstract

Interrill erosion processes on gentle slopes are affected by mechanisms of raindrop impact, overland flow and their interaction. However, limited experimental work has been conducted to understand how important each of the mechanisms are and how they interact, in particular for peat soil. Laboratory simulation experiments were conducted on peat blocks under two slopes (2.5° and 7.5°) and three treatments: *Rainfall*, where rainfall with an intensity of 12 mm hr^{-1} was simulated; *Inflow*, where upslope overland flow at a rate of 12 mm hr^{-1} was applied; and *Rainfall* + *Inflow* which combined both *Rainfall* and *Inflow*. Overland flow, sediment loss and overland flow velocity data were collected and splash cups were used to measure the mass of sediment detached by raindrops. Raindrop impact was found to reduce overland flow by 10–13%, due to increased infiltration, and reduce erosion by 47% on average for both slope gradients. Raindrop impact also reduced flow velocity (80–92%) and increased roughness (72–78%). The interaction between rainfall and flow was found to significantly reduce sediment concentrations (73–85%). Slope gradient had only a minor effect on overland flow and sediment yield. Significantly higher flow velocities and sediment yields were observed under the *Rainfall* + *Inflow* treatment compared to the *Rainfall* treatment. On average, upslope inflow was found to increase erosion by 36%. These results indicate that overland flow and erosion processes on peat hillslopes are affected by upslope inflow. There was no significant relationship between interrill erosion and overland flow, whereas stream power had a strong relationship with erosion. These

findings help improve our understanding of the importance of interrill erosion processes on peat.

KEYWORDS: overland flow; erosion; flow hydraulics; raindrop impact; peat

3.2 Introduction

During rainfall events, soil erosion processes mainly include mechanisms of soil detachment, sediment transport by raindrop impact and surface flow and sediment deposition. For interrill erosion, the dominant processes are detachment by raindrop impact and transport by raindrop-impacted sheet flow (Kinnell, 2005). Raindrop impact affects interrill erosion processes in two ways. First, raindrops provide the primary force to initiate soil particle detachment and the importance of raindrop impact on sediment detachment has been shown under both laboratory and field conditions (Salles et al., 2000). The effect of raindrop impact on detachment capacity is highly related to rainfall properties such as rainfall intensity, drop size, velocity and kinetic energy (Salles and Poesen, 2000), soil type (Quansah, 1981) and slope gradient that affects the impact gradient of falling drops (Singer and Blackard, 1982, Torri and Poesen, 1992). In addition, raindrop impact is important in affecting flow hydraulics and sediment transport as overland flow depths are typically shallow, in the order of a few millimetres (Beuselinck et al., 2002, Holden et al., 2008). The impact of raindrops on a thin water layer is highly related to the ratio of flow depth to raindrop diameter and an extensive body of literature has been published on the subject (see Gabet and Dunne (2003) for a concise review). However, little information is available on how raindrop impact affects overland flow hydraulics (Beuselinck et al., 2002) or the quantified contribution of raindrop impact to erosion rates (Vaezi et al., 2017). Knowledge about mechanisms of raindrop impact is helpful for improving interrill erosion models and equations and developing efficient landscape restoration strategies to prevent erosion.

For interrill erosion areas, soil detachment and sediment transport are simultaneously influenced by rainfall-driven and flow-driven erosion processes and their interaction. However, rather limited attention has been given to the importance of the interaction between rainfall- and flow-driven processes (Rouhipour et al., 2006, Asadi et al., 2007). In modelling the

interrill processes, physically-based erosion models such as WEPP (Nearing et al., 1989) assume that rainfall-driven erosion is the only process occurring in interrill areas, and any interaction between rainfall and flow is ignored. One possible reason for this is that the interaction is complex and requires extensive data for parameterization and validation. However, the interaction has been found to be important in affecting interrill erosion, showing both positive and negative effects (Rouhipour et al., 2006, Asadi et al., 2007). Asadi et al. (2007) investigated the interaction between erosion processes driven by rainfall and flow, and found that the interaction was generally positive for the three different soil types studied. Rouhipour et al. (2006) found a negative interaction for a loamy sand, and a positive interaction for a silty loam on gentle slopes (< 1°) with no rills present under laboratory conditions. Tian et al. (2017) conducted field experiments on plots on a steep loess hillslope (26°), applying upslope overland flow simulation with and without rainfall impact. They found that the interaction between rainfall and flow had a negative impact on erosion under low inflow conditions, decreasing total soil loss by 20%. These studies demonstrate that the interaction between interrill erosion processes driven by rainfall and flow should not be neglected, especially on low slopes and under low energy flows.

Most soil erosion work has been conducted on mineral soils, with much less known about erosion of organic soils which hold large amounts of the world's terrestrial carbon. Peatlands, where organic-rich peat slowly accumulates (Charman, 2002), cover approximately 2.84% of the world's land area (Xu et al., 2018) and are important terrestrial carbon sinks that store one-third to half of the world's soil carbon (Yu, 2012). The physical and chemical characteristics of peat can be quite different to those of mineral soils (Hobbs, 1986). Of particular concern in terms of erosion are rain-fed blanket peatlands which cover 105000 km^2 of the Earth's surface (Li et al., 2017a) and can occur on sloping terrain, with slope angles as high as 15°. As such, blanket peatlands could be more vulnerable to water erosion than other types of peatlands which may occur in landscapes with very little surface gradient. Many blanket peatlands in the Northern Hemisphere have experienced severe erosion and are under increasing erosion risk from future climate change (Li et al., 2016a, Li et al., 2017a), which will lead to enhanced losses of terrestrial carbon in many regions. The main blanket peat erosion processes include sediment supply processes (e.g., freeze–thaw and desiccation), sediment transfer from hillslopes (e.g., interrill erosion, rill erosion and gully erosion), bank failures and mass movement

(Evans and Warburton, 2007). Blanket peat erosion has adverse impacts on landscapes (Holden et al., 2007), reservoir sedimentation (Labadz et al., 1991), water quality (Rothwell et al., 2005) and carbon dynamics (Holden, 2005). Although peatland erosion has been studied for almost sixty years some of the processes remain poorly understood (Bower, 1960, Evans and Warburton, 2007, Li et al., 2016a, Li et al., 2016b, Li et al., 2017a, Li et al., 2017b). The prevention of peat erosion relies on selecting appropriate conservation strategies which in turn requires a thorough understanding of the peat erosion processes.

Most previous studies examining the effect of raindrops on shallow overland flow were conducted in arid or semi-arid environments. However, little attention has been given to northern peatlands which have very different rainfall characteristics being dominated by high frequency, low intensity rainfall. Kløve (1998) used indirect evidence of the positive hysteresis in the overland flow and sediment concentration relationship to suggest that raindrop detachment tended to decrease with increasing wetting of the peat surface. However, the effectiveness of the raindrop detachment might have been overestimated based on the extremely high intensity rainfall (35–240 mm hr^{-1}) applied (Kløve, 1998). High intensity rainfall is rare in many blanket peatlands where low intensity rainfall with small drop diameter is more common. Holden and Burt (2002) applied rainfall simulation with more realistic intensities ranging from 3 to 12 mm hr^{-1} on bare peat blocks. They found that raindrop detachment is important in supplying available sediment for overland flow transport, especially in the early stage of the rainfall simulation test. These findings suggest that rainsplash is important in sediment supply. However, current understanding is underpinned by very little quantitative research which makes it difficult to understand the mechanisms of raindrop impact on flow hydraulics and erosion processes.

Overland flow and erosion processes on hillslopes are scale dependent as soil properties, hydrology and sedimentation processes vary with slope position (Kirkby, 1978, Kirkby, 1985, Cerda, 1998). Holden and Burt (2003b) used networks of crest-stage tubes to monitor overland flow production on peatland hillslopes during storm events, and revealed the importance of spatial variation and flow accumulation in overland flow generation. Overland flow and erosion rates in downslope positions are affected by accumulated flow and sediment transported from upper slope positions. However, to date, no experimental studies have been performed to investigate the effect of

accumulation of flow on erosion processes and overland flow hydraulics in peatlands.

There are three key issues to be addressed for soil erosion which also apply directly to peatland interill erosion: (1) the effects of raindrop impact on sediment detachment, overland flow hydraulics and sediment transport processes; (2) the interaction of rainfall and shallow overland flow on interrill overland flow and erosion processes; and (3) the impacts of slope gradient and position on interrill erosion processes. This study aims to address all three of these issues using the specific example of organic-rich peatland soil. The specific objectives are:

(1) Assess how rainfall impact affects overland flow hydraulics and erosion processes at shallow overland flow.

(2) Examine the effects of interactions of rainfall and flow on sediment yield and flow hydraulics.

(3) Investigate the effects of slope gradient and upslope inflow on peat hillslope overland flow and erosion.

These research objectives were addressed by comparing overland flow and sediment yield processes and flow hydraulic characteristics under laboratory experiments of rainfall simulation, upslope inflow simulation and a combination of rainfall and upslope inflow simulation on peat blocks.

3.3 Materials and methods

3.3.1 Materials

Bare peat blocks with no vegetation cover were collected from the upper peat layer at Moor House National Nature Reserve (54°41’N, 2°23’W), a blanket peat site in the North Pennines of England. A plastic rectangular gutter (1.0 m long, 0.13 m wide and 0.08 m in depth) was pushed parallel to the peat surface into the peat, and carefully dug out to extract an undisturbed peat block. All samples were tightly sealed using plastic film to minimize peat oxidation and drying before being stored at 4 °C prior to laboratory analysis. Basic chemical and physical properties of the peat blocks were determined on subsampled peat (Table 3.1).

Peat samples were extracted from the experimental blocks and then sent to the laboratory where a Morphologi G3 instrument was used to capture two dimensional images of peat particles and to calculate various size and shape

parameters (Table 3.1). Median particle diameter was 12.27 µm, with the particle-size distribution being shown in Figure 3.1.

Table 3.1 Some basic physical and chemical characteristics of the tested peat soils.

Basic physical and chemical characteristics		Median values	Standard deviation
Bulk density (g cm^{-3})		0.19	0.01
Porosity (%)		86.5	1.0
Moisture (%)		87.2	0.9
pH		3.7	0.1
Size and shape parameters of peat particles	Length (µm)	18.4	8.9
	Width (µm)	10.8	4.6
	Perimeter (µm)	49.3	23.2
	Circularity	0.83	0.06
	Convexity	0.97	0.02
	Solidity	0.94	0.03
	Aspect Ratio	0.69	0.01
	Elongation	0.31	0.01

Circularity (0–1) quantifies how close the peat particles are to perfect circles; Convexity (0–1) measures the surface roughness of peat particles.

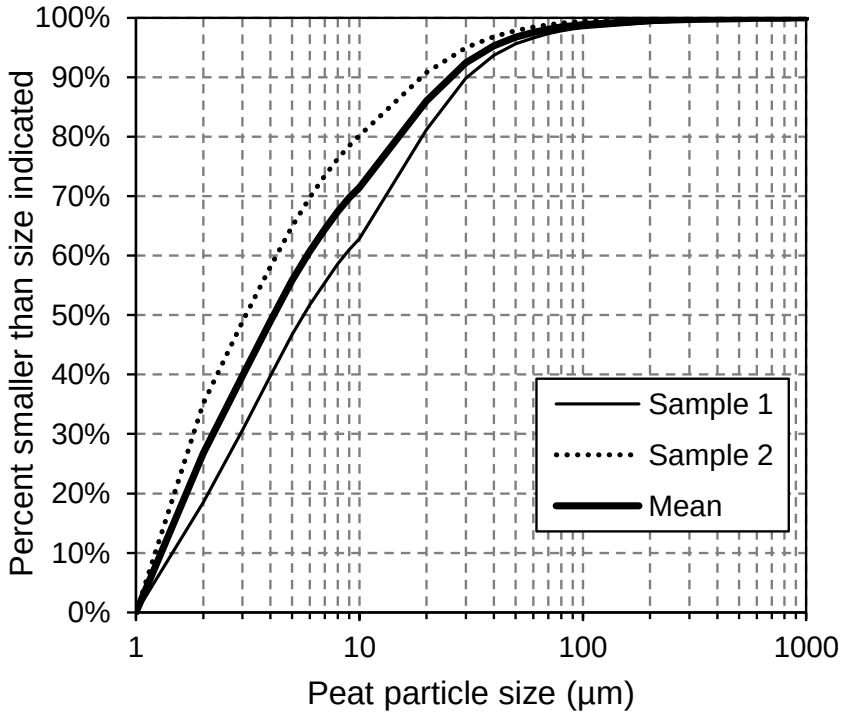

Figure 3.1 Particle-size distribution curves of the studied peat. The mean peat particle sizes were 16 µm and 8 µm for sample 1 (n = 43, 372) and sample 2 (n = 534, 485), respectively. Bold line shows the mean values of sample 1 and 2.

A ‘drip-type’ rainfall simulator was used to simulate representative precipitation. The general set-up and operating principles of the rainfall simulator are illustrated in (Bowyer-Bower and Burt, 1989). The rainfall simulator (Figure 3.2) had a height of 1.8 m with a raindrop generator plate of 1.0 m × 0.5 m consisting of 627 drop formers arranged in a 19 × 33 matrix (Holden and Burt, 2002). The drop formers were made from Tygon tubing of 2.3 mm outside diameter (OD) and 0.7 mm inside diameter (ID), through which was threaded 25 mm long, 0.6 mm OD fishing line. A 3 mm ID wire mesh hung 200 mm below the Perspex plate to break up water drops into a distribution of drop sizes closer to that of natural rainfall. Rainwater was supplied from a constant head system comprising two 25 L Mariotte bottles mounted above the Perspex drip-screen. The uniformity coefficient of rainfall (Christiansen, 1942) was determined using an array of twenty 250 mL measuring cylinders. The rainfall uniformity coefficient was 89 ± 2 % under a rainfall intensity of 12 mm hr^{-1}, which indicates a good distribution of rainfall on the plots. Rainwater was supplied with a standard electrical conductivity of 421 ± 1 µs cm^{-1} and a pH of 7.2 ± 0.1, to minimize the effects of changing water quality on the hydrological and erosion response of the peat blocks during rainfall simulation experiments. Rainfall intensity was controlled by a manometer board carefully calibrated to determine a relationship between head difference and rainfall intensity. Mean annual precipitation (records during periods of 1951–1980 and 1991–2006) at Moor House is 2012 mm (Holden and Rose, 2011), but frequency analysis of hourly rainfall intensity showed that rainfall intensities are usually low and rarely exceed an intensity of 12 mm hr^{-1} (Holden and Burt, 2002, Holden and Burt, 2003b). In this study, an intensity of 12 mm hr^{-1} was selected and calibrated by a tipping bucket rain gauge. The drop-size distribution of the simulated rainfall was measured using the flour-pellet method (Laws and Parsons, 1943), and the median raindrop size (D_{50}) of the rainfall produced by the simulator at 12 mm hr^{-1} was 1.5 mm, which aligns with natural drop-size distributions for this rainfall intensity (Holden and Burt, 2002). The mean kinetic energy was calculated as 0.069 J m^{-2} s^{-1} based on drop-size distribution data (Holden and Burt, 2002).

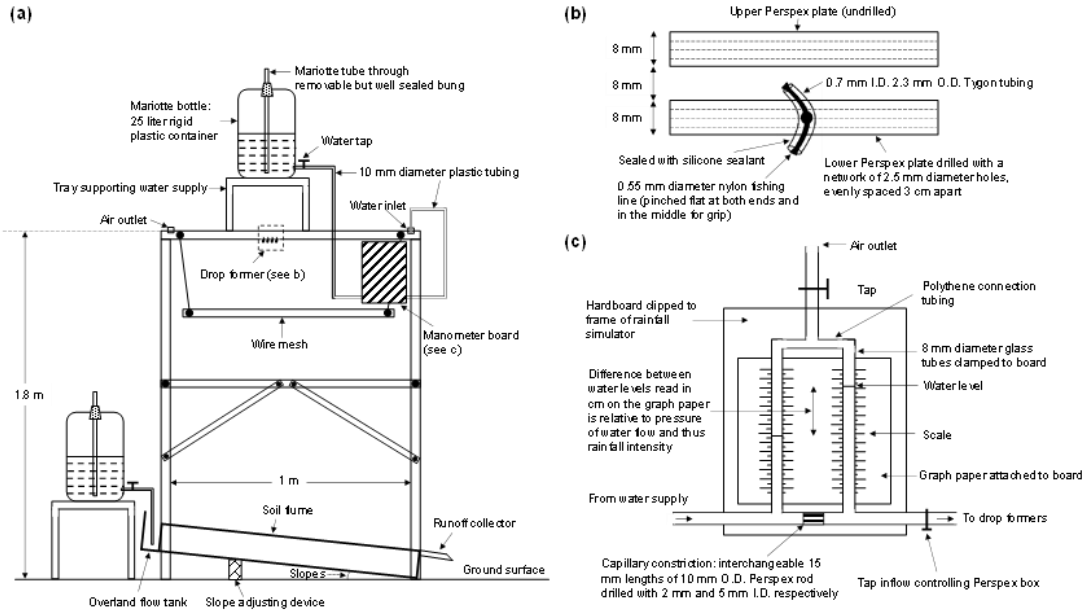

Figure 3.2 Experimental set-ups used in this study including: (a) rainfall simulator and upslope inflow simulation device; (b) drop former and (c) manometer for control of rainfall intensity. Modified from Bowyer-Bower and Burt (1989) and Holden and Burt (2002).

3.3.2 Experimental design

The experimental set-ups used (Figure 3.2) included the rainfall simulator described above, a Mariotte bottle located at the upslope plot boundary to provide upslope inflow at a constant rate and a 1.0 m long by 0.13 m wide soil flume. The peat blocks were placed inside separate flumes. The gaps between the peat blocks and the soil flumes were filled with plastic sheets, in order to prevent linkage and enable all overland flow from the peat blocks to be collected. Bower (1960) classified the gully systems in blanket peat environments into two distinct types of dissection (*Type 1* and *Type 2*). *Type 1* dissection occurs on the flatter interfluve areas where peat is usually 1.5 – 2 m in depth on slopes less than 5° (Bower, 1960). Peat gullies tend to frequently branch and intersect as an intricate dendritic network (Labadz et al., 1991). *Type 2* dissection is characterized by steeper slopes (exceeding 5°), with a system of sparsely branched drainage gullies incised through the peat to bedrock and aligned nearly parallel to each other (Bower, 1960, Labadz et al., 1991). It has been suggested that the transition between *Type 1* and *Type 2* dissection of gully systems occurs at 5° (Bower, 1960). For our experiment, the slopes were set at 2.5° and 7.5° to represent either side of this transition while also being representative of typical blanket peatland

slopes in the Pennine region of England. For each slope gradient, three treatments were conducted on the bare peat blocks (Table 3.2):

(1) *Rainfall* events to simulate rainfall-driven erosion processes: Rainfall was applied at an intensity of 12 mm hr^{-1} for a duration ranging from 60 to 120 min.

(2) *Inflow* events to simulate flow-driven erosion processes: Upslope inflow was applied with a constant rate of 26 mL min^{-1} determined by a volumetric method and which corresponded to 12 mm hr^{-1} rainfall on the studied plots.

(3) *Rainfall* + *Inflow* events to simulate the combined impacts of rainfall and flow on erosion processes. Both rainfall (12 mm hr^{-1}) and upslope inflow (26 mL min^{-1}) were applied simultaneously. Near-surface throughflow (typically upper 5 cm) and saturation-excess overland flow are dominant in blanket peatlands (Evans et al., 1999, Holden and Burt, 2002, Holden and Burt, 2003a). Therefore, in blanket peatlands the *Rainfall* + *Inflow* condition can simulate a downslope position affected by accumulated upslope inflow. The simulated upslope overland flow of 26 mL min^{-1} applied to the studied plot represents a 20 m long upslope contributing area with a rainfall intensity of 12 mm hr^{-1}. Compared with the *Rainfall* treatment, the *Rainfall* + *Inflow* treatment represents a plot 20 m downslope from the hill top.

Table 3.2 Summary of the experimental design and treatments.

Slope	Treatment	Replicate	Total Water Supply (mm hr^{-1})	Rainfall Intensity (mm hr^{-1})	Upslope Inflow Rate (mL s^{-1})	Duration* (min)
2.5°	*Rainfall*	1	12	12	0	120
		2	12	12	0	120
		3	12	12	0	60
	Inflow	1	12	0	26	120
		2	12	0	26	120
		3	12	0	26	60
	Rainfall + *Inflow*	1	24	12	26	120
		2	24	12	26	120
		3	24	12	26	60
7.5°	*Rainfall*	1	12	12	0	120
		2	12	12	0	120
		3	12	12	0	120
		4	12	12	0	60
		5	12	12	0	60
	Inflow	1	12	0	26	120
		2	12	0	26	120
		3	12	0	26	120
	Rainfall + *Inflow*	1	24	12	26	120
		2	24	12	26	120
		3	24	12	26	120
		4	24	12	26	60
		5	24	12	26	60

* Duration indicates time since overland flow generation (min).

The simulation experiments were firstly conducted with a duration of 120 minutes. Results showed that overland flow rates for those first sets of tests increased with time and then attained equilibrium. Steady-state rates of overland flow were achieved within the first 60 minutes. Suspended sediment concentrations initially increased with increasing overland flow rate, and then declined to an almost constant rate. After this point there was little variation with overland flow generation. Consequently, the duration of the subsequent experiments was shortened to 60 minutes to save time. In addition, this change in experiment duration had no impact on mean overland flow rates and sediment concentrations as once a steady-state overland flow rate was achieved the values of these parameters exhibited little variation with time.

3.3.3 Measurements

During each run the time of overland flow-initiation was recorded, after which each test lasted for between 60 and 120 minutes. Total overland flow was sampled at the plot outlet every 5 min. Overland flow volumes (mL) for each sample were determined using a measuring cylinder. Overland flow rates (mL s^{-1}) were subsequently determined by dividing these overland flow volumes by the sampling duration. Samples were then left to settle for 6 hours to allow deposition of the suspended sediment. The clear supernatant was decanted, and the remaining turbid liquid was transferred to a rectangular foil container and oven-dried at 65.0 °C until a constant weight was achieved. The dry sediment mass (mg) was calculated, and the sediment concentration (mg mL^{-1}) was determined as the ratio of dry sediment mass (mg) to the overland flow volume (mL). The sediment yield rate (mg m^{-2} s^{-1}) was defined as the ratio of dry sediment mass (mg) per unit area (m^2) per sampling duration (s).

Overland flow velocities (V_s) were determined using a fluorescein dye tracing method (Smart and Laidlaw, 1977) at 5 min intervals with 3 replicates for each plot. The time required for the leading edge of a fluorescein dye tracer to travel across a marked distance was recorded at a resolution of 0.01 s.

Splash cups were used to measure the mass of detached sediment when exposed to simulated rain (12 mm hr^{-1}) (Morgan, 1981). These comprise PVC cups with a diameter of 6.5 cm and a height of 4.5 cm with a filter at the bottom, which were filled with undisturbed peat material collected from the field; the soil surface was made flush with the rim of the cup by removing excess soil. The splash cups were placed inside an open cylindrical bucket with a diameter of 25 cm and a height of 10 cm to collect the splashed peat particles. A beaker located below the bottom end of the splash cup collected water infiltrated through the paper filter. All splashed peat and water was collected by the bucket. At the end of each run the inner wall of the bucket was carefully cleaned with deionised water in order to collect all splashed peat. The buckets were placed in an oven at 65.0 °C until a constant weight was achieved, and the mass of oven-dried splashed peat was determined.

3.3.4 Data analysis

Infiltration rates were calculated by subtracting the overland flow rates measured at the plot outlet from the inflow rate. The possible influence of evaporation was minor because of the short duration of the experiments and a relatively low room temperature (7.5 °C) for the experiments and thus was

deemed negligible. The instantaneous infiltration rates (f_i) for different experimental treatments were calculated by equations (3.1)–(3.3), respectively (Pan and Shangguan, 2006):

Under *Rainfall* conditions: $f_i = I\cos\theta - 10\,R_i / S\,t$ (3.1)

Under *Inflow* conditions: $f_i = F - 10\,R_i / S\,t$ (3.2)

Under *Rainfall* + *Inflow* conditions: $f_i = I\cos\theta + F - 10\,R_i / S\,t$ (3.3)

where I is the rainfall intensity that equals to 12 mm hr^{-1}; θ is the slope (º); F is the upslope inflow rate that equals to 12 mm hr^{-1}; R_i is the ith overland flow volume collected (mL); S is the plot area (cm^2); t is the time interval between the collection of successive overland flow samples (min) and the factor 10 is the adjusting coefficient.

For a laminar flow profile, the vertical velocity distribution is shown by a quadratic equation, with zero at the bed and a maximum for surface velocity (V_s) (Katz et al., 1995). The profile mean velocity (V) was calculated by equation (3.4):

$V = k\,V_s$ (3.4)

where V is mean flow velocity (cm s^{-1}); V_s is surface flow velocity (cm s^{-1}); k is a coefficient which is 0.33 for shallow flows on bare peat surfaces under gentle slopes (Holden et al., 2008).

The overland flow was presumed to be uniform and the average flow depth was calculated from:

$h = q / V = Q / (Vbt)$ (3.5)

where h is mean flow depth for the whole plot (cm); q is the unit discharge (cm^2 s^{-1}); Q is the overland flow volume during t duration (ml); b is the width of water-crossing section (cm).

The Manning's friction coefficient n is determined by (Pan and Shangguan, 2006):

$n = (h^{2/3} \cdot J^{1/2}) / V$ (3.6)

where J is the *sine* of the bed slope (m m^{-1}).

Flow shear stress τ (Pa) (Foster, 1982) and stream power Ω (W m^{-2}) (Bagnold, 1966) were calculated by:

$\tau = \rho g h J$ (3.7)

$\Omega = \rho g q J$ (3.8)

where ρ is the density of water (kg m^{-3}).

It is assumed that any sediment produced by the *Rainfall* experiment was the sum of the peat materials detached and transported by both the action of raindrops and flow induced processes whereas any sediment produced by the *Inflow* experiment resulted from flow induced processes only. The difference in the sediment collected at the exit from the flume between the *Rainfall* and *Inflow* events was assumed to be caused by raindrop impact:

$$I_{raindrop}\,(SC) = SC_{Rainfall} - SC_{Inflow} \tag{3.9}$$

where $I_{raindrop}$ (SC) is the raindrop impact on sediment, $SC_{Rainfall}$ and SC_{Inflow} are the average sediment concentration in *Rainfall* and *Inflow* experiments, respectively.

In terms of sediment concentration, the interaction between rainfall- and flow-driven erosion is defined as the difference between the sediment concentration resulting from the combination of rainfall and flow driven erosion (*Rainfall* + *Inflow*) and the sum of the concentrations controlled by rainfall driven erosion process (*Rainfall*) and flow driven erosion processes (*Inflow*) (Asadi et al., 2007). Thus

$$Interaction\,(SC) = SC_{Rainfall\,+\,Flow} - (SC_{Rainfall} + SC_{Inflow}) \tag{3.10}$$

where $SC_{Rainfall\,+\,Flow}$ is the sediment concentration in *Rainfall* + *Flow* experiment. Following Asadi et al. (2007), the *Interaction* (SC) > 0, = 0 and < 0 indicate a positive, zero and negative interaction of rainfall and flow driven erosion, respectively. Similarly, the effects of the interaction on other flow hydraulic parameters can be derived from equations in the same form of equations (3.10).

Datasets were tested for normality using the Anderson-Darling normality test and then either the Student t-test or the Mann-Whitney U-test were applied to test for a significant difference in the means or the medians of the studied response variables between two treatments. Parametric tests were used when both datasets being considered were normally distributed, and non-parametric tests were used for datasets when at least one of them was not normally distributed. Correlation analysis and stepwise regression analysis were used to find the relationship between overland flow hydraulics and sediment yield rate. Test results were considered significant at $p < 0.05$.

3.4 Results

3.4.1 Overland flow and infiltration

Typical overland flow and sediment concentration trends for the tests are shown in Figure 3.3. Overland flow rates in nineteen out of twenty-two cases under the *Rainfall*, *Inflow* and *Rainfall + Inflow* treatments increased with time before attaining equilibrium. Consequently, two stages were defined within a simulation test; the initial overland flow increase stage and the steady-state overland flow stage. Infiltration rates peaked early in the simulations followed by a decrease to quasi-steady state values (i.e. oscillating around a fairly stable mean value) (Figure 3.4).

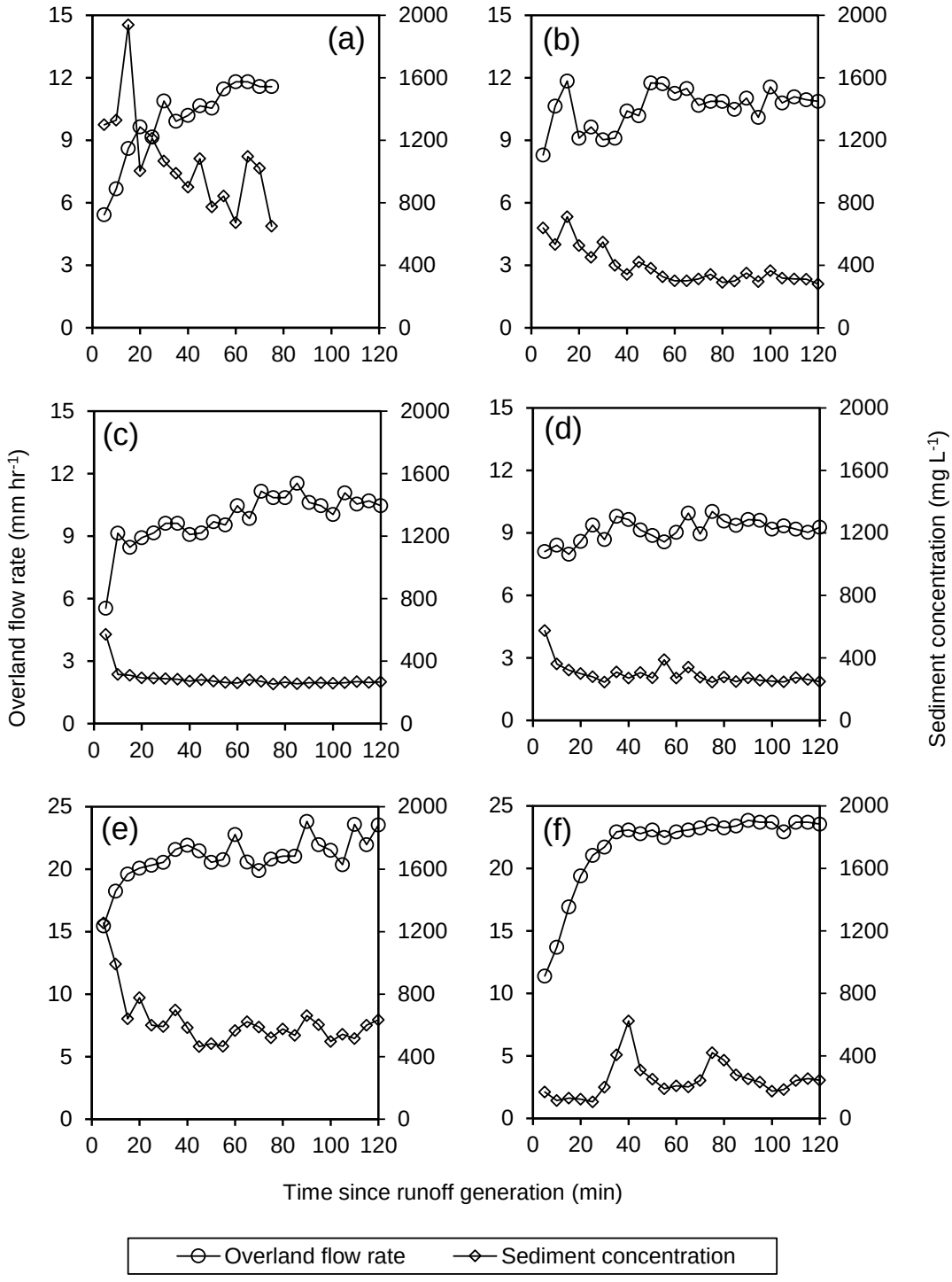

Figure 3.3 Overland flow and sediment concentration rate for representative replicates with different treatments (*Rainfall*, *Inflow* and *Rainfall*+ *Inflow*): (a) *Rainfall*, 2.5°; (b) *Rainfall*, 7.5°; (c) *Inflow*, 2.5°; (d) *Inflow*, 7.5°; (e) *Rainfall*+ *Inflow*, 2.5°; (f) *Rainfall*+ *Inflow*, 7.5°.

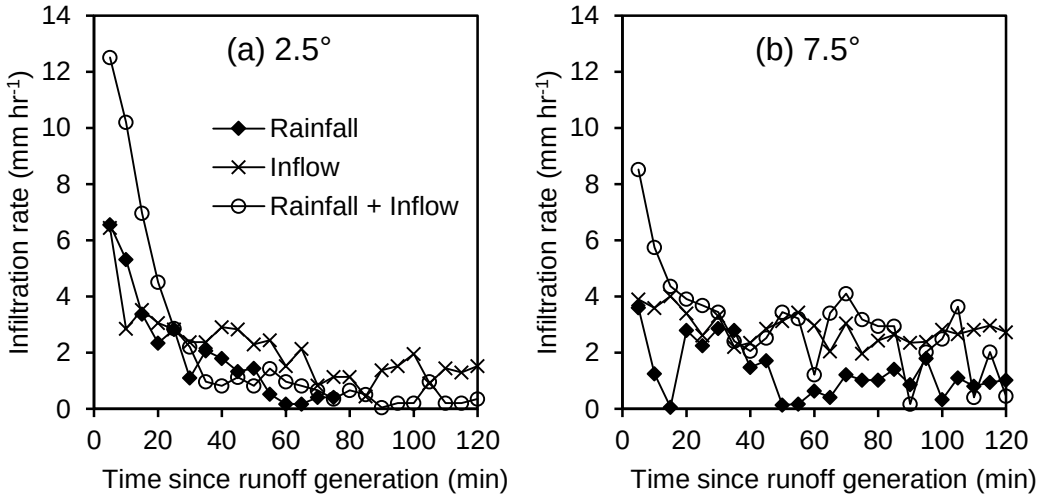

Figure 3.4 Infiltration rate for representative replicates with different treatments (*Rainfall*, *Inflow* and *Rainfall*+ *Inflow*) under (a) 2.5° and (b) 7.5° conditions, respectively.

Regardless of slope, mean overland flow rates for the *Rainfall* treatment with raindrop impact were significantly higher (Student t-test, p = 0.014) than those of the *Inflow* treatment without raindrop impact indicating that raindrop impact increased overland flow rate (Table 3.3). In comparison with the *Inflow* treatment, overland flow for the *Rainfall* treatment increased on average by 10–13% (Figure 3.5 (a)).

Table 3.3 Median overland flow and infiltration rates for the three treatments (*Rainfall*, *Inflow* and *Rainfall* + *Inflow*).

Slopes		Experimental stages	*Rainfall*	*Inflow*	*Rainfall + Inflow*
2.5°	Overland flow (mm hr^{-1})	Initial stage	8.64 ± 0.97 b	8.28 ± 0.52 b	20.75 ± 0.88 a
		Steady-state overland flow stage	11.45 ± 0.35 b	9.30 ± 1.50 c	21.61 ± 0.09 a
		Whole stage	10.31 ± 0.43 b	9.00 ± 1.21 c	21.16 ± 0.36 a
	Infiltration (mm hr^{-1})	Initial stage	3.35 ± 0.97 c	3.72 ± 0.52 b	4.27 ± 0.92 a
		Steady-state overland flow stage	0.54 ± 0.35 b	2.70 ± 1.50 a	2.38 ± 0.09 a
		Whole stage	1.68 ± 0.43 b	3.00 ± 1.21 a	2.83 ± 0.36 a
7.5°	Overland flow (mm hr^{-1})	Initial stage	9.36 ± 0.49 b	8.62 ± 1.32 c	19.25 ± 1.12 a
		Steady-state overland flow stage	11.09 ± 0.56 b	9.49 ± 0.23 c	22.45 ± 0.77 a
		Whole stage	10.35 ± 0.28 b	9.29 ± 0.43 c	21.50 ± 0.26 a
	Infiltration (mm hr^{-1})	Initial stage	2.54 ± 0.49 c	3.38 ± 1.32 b	4.65 ± 1.12 a
		Steady-state overland flow stage	0.77 ± 0.56 c	2.51 ± 0.23 a	1.45 ± 0.77 b
		Whole stage	1.59 ± 0.24 b	2.71 ± 0.43 a	2.40 ± 0.26 a

The same letter within a row (a is highest and c is lowest) indicates no significant difference based on Mann-Whitney U tests at p = 0.05.

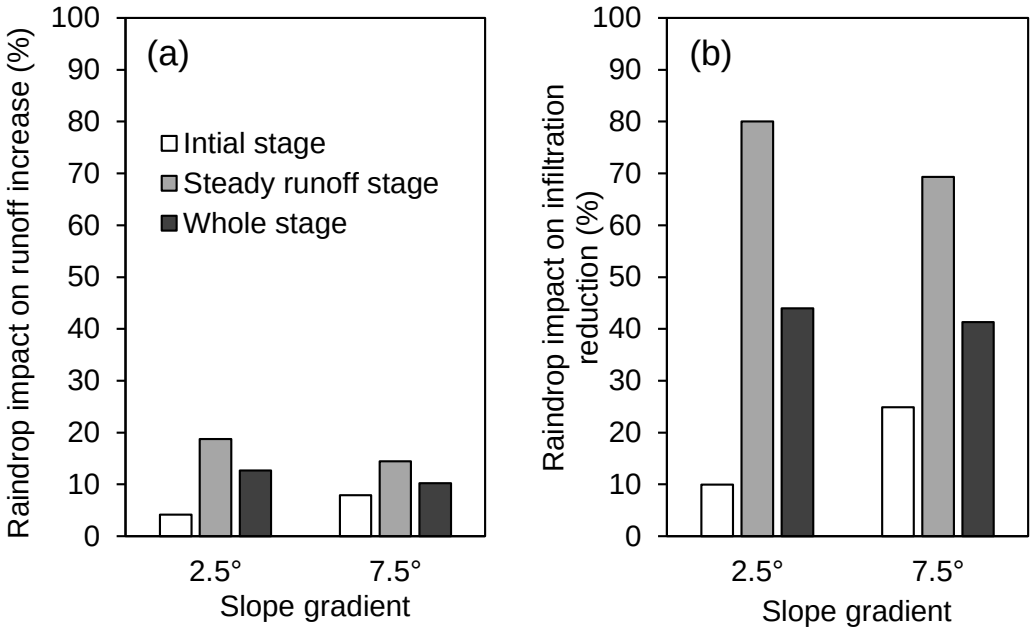

Figure 3.5 The impact of raindrops on (a) overland flow rate and (b) infiltration, during different experimental stages.

The *Rainfall* treatment produced the lowest mean infiltration rate at 1.68 ± 0.43 mm hr^{-1} and 1.59 ± 0.24 mm hr^{-1} under the 2.5° and 7.5° conditions, respectively (Table 3.3). Student t-tests showed that the mean infiltration rate produced by *Rainfall* treatments were significantly lower than those for the *Inflow* (p = 0.013) and *Rainfall* + *Inflow* (p = 0.002) treatments (Table 3.3). Compared with the *Inflow* treatment without raindrop impact, the mean infiltration rate for the *Rainfall* treatment with raindrop impact was reduced by 44% under the 2.5° slope, and by 41% for the 7.5° slope (Figure 3.5 (b)). Under steady-state overland flow the average reduction of raindrop impact was 80% and 69% under the 2.5° and 7.5° conditions, respectively (Figure 3.5 (b)).

Slope angle had no significant impact on overland flow rate (Mann-Whitney U tests, p = 0.936) and infiltration rate (Student t-test, p = 0.687).

3.4.2 Sediment yield

For both the *Rainfall* and *Rainfall* + *Inflow* treatments with raindrop impact, sediment concentrations increased during the initial stage of overland flow generation to a peak value before gradually declining (Figure 3.3). In contrast, for the *Inflow* treatment without raindrop impact, the sediment concentration was almost constant with little variation with overland flow generation.

Peat splash erosion rates measured by splash cups were 0.28 ± 0.11 g and 0.33 ± 0.09 g under the 2.5° and 7.5° slopes, respectively. The mean sediment concentration for the three treatments followed the order: *Rainfall* > *Rainfall* + *Inflow* > *Inflow* treatment (Table 3.4). Student t-tests showed that the sediment yield for the *Rainfall* treatment with raindrop impact was significantly higher than that of the *Inflow* treatment without raindrop impact (p = 0.048). The difference in sediment yield with and without raindrop impact was assumed to reflect the contribution of raindrop impact. On average, raindrop impact contributed to 62% and 31% of mean sediment yield under the 2.5° and 7.5° conditions, respectively (Table 3.5). The impact of raindrops on sediment increase in the initial overland flow stage was similar to the steady-state overland flow stage (Table 3.5). Compared with the *Rainfall* treatment, the *Rainfall* + *Inflow* produced sediment yields that were 1.4–1.7 times higher (Table 3.4). The simulated upslope inflow contributed to increasing sediment yields, with average contributions of 29% and 42% under the 2.5° and 7.5° conditions, respectively (Table 3.5).

Table 3.4 Summary of the measured sediment concentration and sediment yield rate for the three treatments (*Rainfall*, *Inflow* and *Rainfall + Inflow*) in the initial and steady-state overland flow stage.

Slope	Treatment	Replicate	Sediment Concentration (mg L^{-1})			Sediment Yield Rate (mg m^{-2} min^{-1})		
			IS*	SSRS**	WS***	IS	SSRS	WS
2.5°	*Rainfall*	1	1159.3	856.6	1058.4	261.7	252.0	258.5
		2	314.1	262.4	273.2	84.0	105.9	101.3
		3	454.0	416.7	435.3	79.9	90.2	85.1
		Mean	642.5	511.9	589.0	141.9	149.4	148.3
	Inflow	1	215.8	204.9	208.6	28.4	28.6	28.6
		2	336.4	266.1	286.6	85.9	85.0	85.3
		3	461.3	280.6	295.7	70.6	53.7	55.1
		Mean	337.8	250.5	263.6	61.6	55.8	56.3
	Rainfall + Inflow	1	327.1	303.9	308.8	168.4	150.2	153.1
		2	677.2	575.5	626.4	228.2	256.2	242.2
		3	613.9	475.6	544.8	249.2	207.8	228.5
		Mean	539.4	451.7	493.3	215.3	204.7	207.9
7.5°	*Rainfall*	1	507.5	316.0	435.1	182.7	116.4	159.5
		2	506.7	355.0	392.9	87.5	80.3	82.1
		3	748.8	390.1	494.7	172.9	94.5	117.4
		4	464.9	363.6	422.7	77.7	91.7	83.6
		5	579.2	515.3	552.6	95.3	100.8	97.6
		Mean	561.4	388.0	459.6	123.2	96.8	108.0
	Inflow	1	374.6	322.7	333.5	51.0	59.6	57.8
		2	332.4	277.2	295.6	64.4	57.2	59.6
		3	384.7	301.1	325.5	130.6	99.2	106.4
		Mean	363.9	300.3	318.2	82.0	72.0	74.6
	Rainfall + Inflow	1	177.8	275.1	246.8	54.4	109.1	93.1
		2	296.1	210.1	235.5	123.0	111.2	112.7
		3	323.2	784.5	590.3	117.2	370.9	264.1
		4	388.6	343.8	366.2	158.9	178.4	168.7
		5	575.2	688.7	660.3	248.1	316.3	299.2
		Mean	352.2	460.4	419.8	140.3	217.2	187.6

IS*, SSRS** and WS*** indicate the initial overland flow stage, steady-state overland flow stage and the whole experimental stage, respectively.

Table 3.5 Changes in sediment concentration and sediment yield due to raindrop impact, inflow impact and interaction in different stages of the experimental process.

Slopes		Stages	Raindrop Impact		Inflow Impact		Interaction	
			In rate	In percentage (%)	In rate	In percentage (%)	In rate	In percentage (%)
2.5°	SC	IS*	304.7	47	–103.1	–19	–440.9	–82
		SSRS**	261.4	51	–60.2	–13	–310.7	–69
		WS***	325.4	55	–95.7	–19	–359.3	–73
	SY	IS*	80.3	57	73.4	34	11.8	5
		SSRS**	93.6	63	55.3	27	–0.5	0
		WS***	92	62	59.6	29	3.3	2
7.5°	SC	IS*	197.5	35	–209.2	–59	–573.1	–163
		SSRS**	87.7	23	72.4	16	–227.9	–50
		WS***	141.4	31	–39.8	–9	–358	–85
	SY	IS*	41.2	33	17.1	12	–64.9	–46
		SSRS**	24.8	26	120.4	55	48.4	22
		WS***	33.4	31	79.6	42	5	3

Notes: SC and SY are sediment concentration (mg L^{-1}) and sediment yield rate (mg m^{-2} min^{-1}), respectively; IS*, SSRS** and WS*** indicate the initial overland flow stage, steady-state overland flow stage and the whole experimental stage, respectively; '–' indicates reduction; Raindrop impact, inflow impact and interaction are determined by '*Rainfall*' – '*Inflow*', '*Rainfall* + *Inflow*' – '*Rainfall*' and '*Rainfall* + *Inflow*' – '*Rainfall*' – '*Inflow*', respectively.

The mean total amount of peat loss (dry weight) was 0.98, 0.48 and 1.72 g for the *Rainfall*, *Inflow* and *Rainfall* + *Inflow* treatments, respectively, under the 2.5° condition, and was 0.97, 0.73 and 1.35 g for the *Rainfall*, *Inflow* and *Rainfall* + *Inflow* treatments, respectively, under the 7.5° condition (Figure 3.6). Student t-tests showed that the differences in the total peat loss between the 2.5° and 7.5° were not significant for all the three treatments.

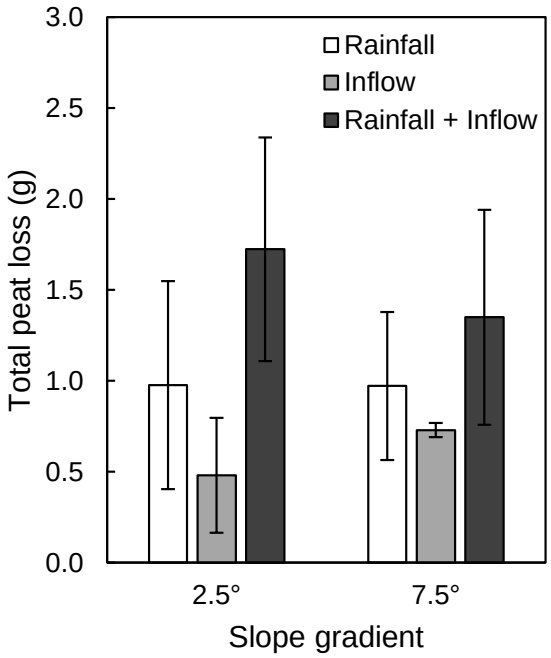

Figure 3.6 Total peat loss with different treatments (*Rainfall*, *Inflow* and *Rainfall*+ *Inflow*).

The interaction between rainfall-driven and flow-driven erosion processes defined in equation (3.10) was negative throughout the whole experimental process (Figure 3.7), with average values of –73% and –85% under the 2.5° and 7.5° conditions, respectively (Table 3.5). The contribution of the interactions to sediment concentration increase was lowest at the start of overland flow generation but increased rapidly and approached an approximately constant value (Figure 3.7). In comparison with the *Rainfall* + *Inflow* treatment, the effects of the interaction on reducing sediment concentration mainly occurred in the initial overland flow stage, with average contributions of 82% and 163% under the 2.5° and 7.5° conditions, respectively. These values were higher than those (50–69%) in the steady-state overland flow stage (Table 3.5).

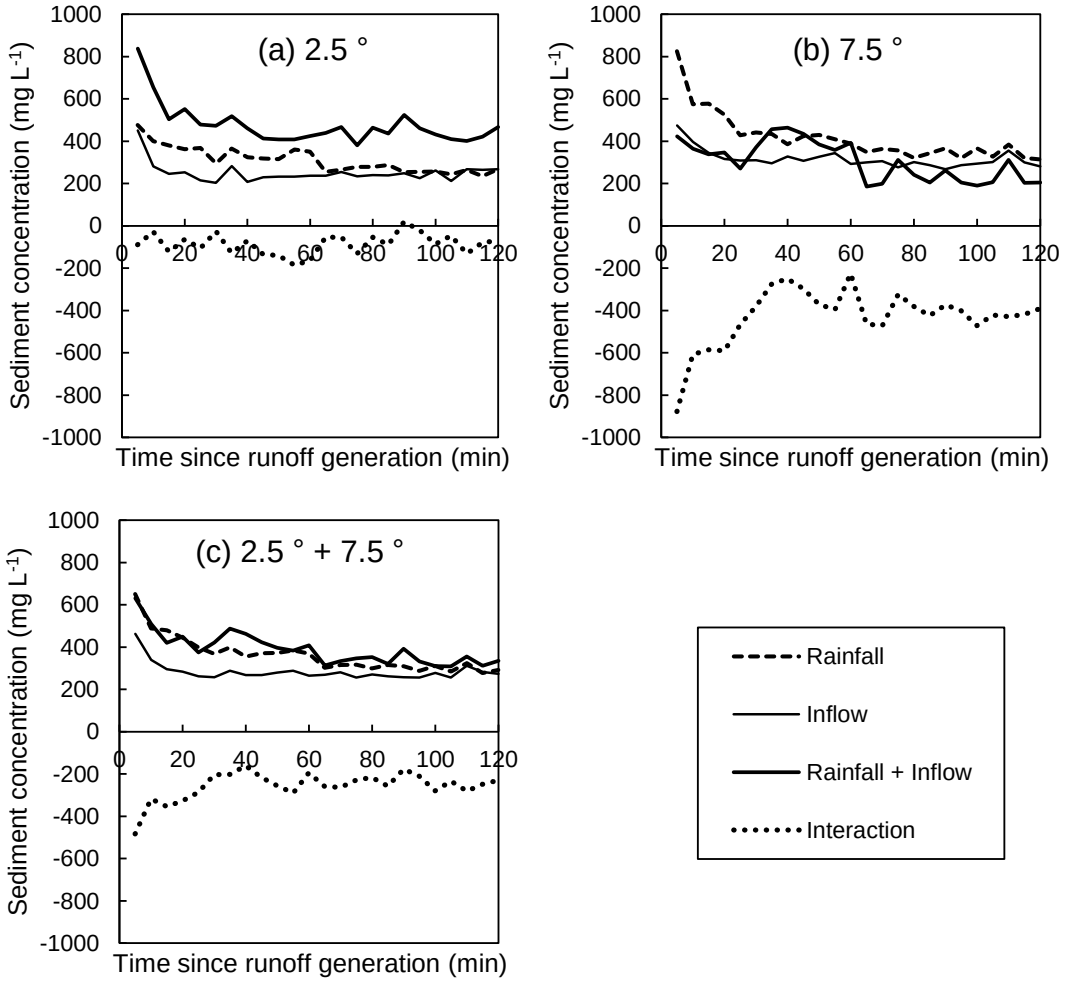

Figure 3.7 Changes with time in measured sediment concentration for each experimental treatment (*Rainfall*, *Inflow* and *Rainfall* + *Inflow*) and calculated interaction under (a) 2.5°; (b) 7.5° and (c) 2.5° + 7.5° conditions, respectively.

3.4.3 Flow hydraulics

The overland flow hydraulic parameters under the 2.5° and 7.5° conditions are shown in Table 3.6. Median overland flow velocities for the *Inflow* treatment were 1.8 cm s^{-1} and 2.5 cm s^{-1} under the under the 2.5° and 7.5° conditions, respectively. These were significantly higher (Mann-Whitney U test, $p < 0.001$) than those produced by the *Rainfall* treatment, which were 1.0 cm s^{-1} under the 2.5° condition, and 1.3 cm s^{-1} under the 7.5° condition. Raindrops impacted on mean flow velocity, with reductions of 80% and 92% under the 2.5° and 7.5° conditions, respectively, with a median reduction of 86% under both slope gradients (Table 3.7). Overland flow velocities under the *Rainfall* + *Inflow* conditions increased significantly (Mann-Whitney U test,

$p < 0.001$) compared to the *Rainfall* and Inflow conditions (Table 3.6). For all three treatments flow velocities increased with increasing slopes (Table 3.6).

Table 3.6 Median overland flow hydraulic parameters for the three treatments (*Rainfall*, *Inflow* and *Rainfall* + *Inflow*) in different experimental stages.

Slopes	Treatment	Experimental stages	V (cm s^{-1})	h (mm)	n (10^{-2})	τ	Ω (10^{-2})
2.5°	*Rainfall*	Initial stage	0.7	1.4	190	0.58	0.11
		Steady-state overland flow stage	1.1	1.0	63	0.42	0.14
		Whole stage	1.0	1.1	93	0.46	0.13
	Inflow	Initial stage	1.4	0.4	25	0.17	0.08
		Steady-state overland flow stage	1.9	0.4	18	0.15	0.09
		Whole stage	1.8	0.4	20	0.16	0.09
	Rainfall + *Inflow*	Initial stage	3.3	0.6	25	0.24	0.18
		Steady-state overland flow stage	2.1	0.7	30	0.32	0.20
		Whole stage	2.6	0.7	28	0.29	0.19
7.5°	*Rainfall*	Initial stage	1.0	1.1	106	0.49	0.12
		Steady-state overland flow stage	1.4	0.8	40	0.32	0.14
		Whole stage	1.3	0.9	60	0.37	0.14
	Inflow	Initial stage	2.5	0.4	19	0.16	0.11
		Steady-state overland flow stage	2.6	0.4	16	0.15	0.11
		Whole stage	2.5	0.4	17	0.15	0.11
	Rainfall + *Inflow*	Initial stage	3.7	0.4	15	0.18	0.16
		Steady-state overland flow stage	4.6	0.4	13	0.18	0.20
		Whole stage	4.3	0.4	13	0.18	0.19

Table 3.7 Effects of raindrop and interaction on increasing the overland flow hydraulic parameters in different experimental stages.

Slopes	Experimental stages	V (cm s^{-1})	h (mm)	n (10^{-2})	τ	Ω (10^{-2})
Raindrop impact						
2.5°	Initial stage	–0.7 (–100%)	1.0 (71%)	165 (87%)	0.41 (71%)	0.03 (27%)
	Steady-state overland flow stage	–0.8 (–73%)	0.6 (60%)	45 (71%)	0.27 (64%)	0.05 (36%)
	Whole stage	–0.8 (–80%)	0.7 (64%)	73 (78%)	0.30 (65%)	0.04 (31%)
7.5°	Initial stage	–1.5 (–150%)	0.7 (64%)	87 (82%)	0.33 (67%)	0.01 (8%)
	Steady-state overland flow stage	–1.2 (–86%)	0.4 (50%)	24 (60%)	0.17 (53%)	0.03 (21%)
	Whole stage	–1.2 (–92%)	0.5 (56%)	43 (72%)	0.22 (59%)	0.03 (21%)
Interaction						
2.5°	Initial stage	1.2 (36%)	–1.2 (–200%)	–190 (–760%)	–0.51 (–213%)	–0.01 (–6%)
	Steady-state overland flow stage	–0.9 (–43%)	–0.7 (–100%)	–51 (–170%)	–0.25 (–78%)	–0.03 (–15%)
	Whole stage	–0.2 (–8%)	–0.8 (–114%)	–85 (–304%)	–0.33 (–114%)	–0.03 (–16%)
7.5°	Initial stage	0.2 (5%)	–1.1 (–275%)	–110 (–733%)	–0.47 (–261%)	–0.07 (–44%)
	Steady-state overland flow stage	0.6 (13%)	–0.8 (–200%)	–43 (–331%)	–0.29 (–161%)	–0.05 (–25%)
	Whole stage	0.5 (12%)	–0.9 (–225%)	–64 (–492%)	–0.34 (–189%)	–0.06 (–32%)

The average flow depth for the *Rainfall* treatment was significantly higher (Mann-Whitney U test, $p < 0.001$) compared with the *Inflow* treatment (Table 3.6). Raindrop impact increased flow depths by 64% and 56% under the 2.5° and 7.5° conditions, respectively (Table 3.7).

Of the three treatments, the *Rainfall* treatment produced the highest Manning's friction factor (n) and flow shear stress (τ) (Table 3.6); and the *Rainfall* + *Inflow* treatment produced the largest stream power (Ω). Raindrop impact increased n, τ and Ω by 72–78%, 59–65% and 21–31%, respectively (Table 3.7).

3.4.4 Relationships between overland flow and sediment

Sediment yield (y) generally increased with increasing overland flow rate (x) (Figure 3.8). However, for all treatments no significant linear relationship was found between erosion and overland flow rate. A power law ($y = 1.5986x^{1.276}$, $n = 313$, $R^2 = 0.547$, $p < 0.001$) performed well in describing the relationship between sediment yield and overland flow rate.

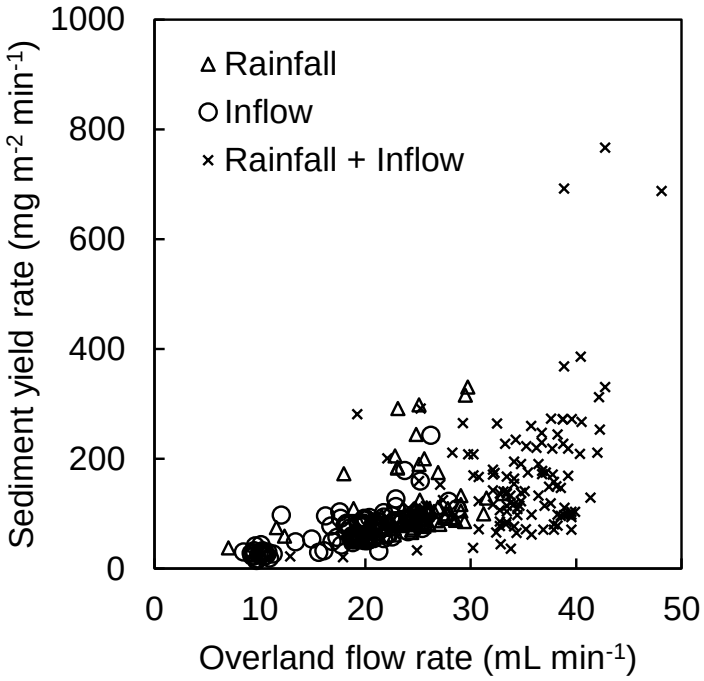

Figure 3.8 The relationship between sediment yield and overland flow.

Spearman's Rank correlation analysis was used to test for a relationship between erosion and some hydraulic parameters (Table 3.8). Under both the *Rainfall* and *Inflow* conditions, erosion rate was significantly correlated with shear stress and stream power ($p < 0.01$). Under the *Rainfall* + *Inflow* conditions, stream power had a significant role in influencing erosion ($p < 0.01$). For all treatments, the crucial hydraulic parameters affecting erosion rate were shear stress and stream power, with stream power having the largest correlation coefficient (0.711). The significantly positive erosion–stream power relation for all the three treatments demonstrated that sediment yield rate increased with an increase in stream power.

Table 3.8 Correlation matrix between erosion rate (mg m^{-2} min^{-1}) and different hydraulic parameters, including flow velocity (cm s^{-1}), shear stress (Pa) and stream power (W m^{-2}).

Parameters	Erosion rate	Flow velocity	Shear stress	Stream power
Rainfall treatment (n = 80)				
Erosion rate	1.000			
Flow velocity	–0.359**	1.000		
Shear stress	0.472**	–0.929**	1.000	
Stream power	0.391**	0.097	–0.167	1.000
Inflow treatment (n = 117)				
Erosion rate	1.000			
Flow velocity	0.032	1.000		
Shear stress	0.545**	–0.695**	1.000	
Stream power	0.705**	0.442**	0.230*	1.000
Rainfall + *Inflow* treatment (n = 115)				
Erosion rate	1.000			
Flow velocity	0.070	1.000		
Shear stress	–0.019	–0.953**	1.000	
Stream power	0.258**	0.383**	–0.152	1.000
All treatments (n = 312)				
Erosion rate	1.000			
Flow velocity	0.066	1.000		
Shear stress	0.358**	–0.809**	1.000	
Stream power	0.711**	0.331**	0.196**	1.000

* and ** indicate that correlation is significant at the 0.05 level and 0.01 level (2-tailed), respectively.

3.5 Discussion

3.5.1 Effects of rainfall on overland flow and sediment yield

Overland flow rate was significantly higher for the *Rainfall* treatment with raindrop impact than that for the *Inflow* treatment without raindrop impact. This result may be associated with peat surface sealing and crusting caused by raindrops striking the peat surface through the shallow overland flow (Burt and Slattery, 1996), leading to a decreased peat infiltration rate. In the initial stage of overland flow generation the peat infiltration capacity was high. The gradual sealing of the peat surface and increase in soil moisture contributed to reduced infiltration during the steady-state overland flow stage.

Raindrop impact significantly reduced the surface flow velocity on the gentler slope gradient. When raindrop impact was eliminated, average flow velocity increased greatly as raindrops increase surface roughness as represented by Manning's *n* friction factor. This is in agreement with Savat (1977) and Beuselinck et al. (2002) who reported that raindrop impact played a key role in disturbing overland flow and retarding flow velocity for gentle slopes and shallow overland flow conditions.

Raindrop impact significantly increased sediment yields, with an average increase of 47% for both slope gradients. The observed difference in erosion between the *Rainfall* and *Inflow* treatments primarily resulted from the effects of raindrops. For the *Rainfall* treatment, the sediment concentration rate peaked early in the rainfall simulation and then decreased to a final constant rate. The peak corresponded to the period when peat aggregates previously weathered by processes such as freeze–thaw and desiccation (Francis, 1990, Labadz et al., 1991, Shuttleworth et al., 2017) were detached and splashed by raindrop impact, and the peat soil shear strength decreased with saturation. As overland flow increased in the first few minutes, loose sediments on the surface were mobilised and exported (Figure 3.3). The erosion pattern appeared to be transport-limited in the initial stage of runoff generation. Continued raindrop impact increased the flow depth and resistance to detachment, as a result erosion rates dropped to an equilibrium level marking the balance between the erosive forces of splash and rain-impacted flow detachment and the resistance of the soil surface. The peat loss rate in the steady-state overland flow stage was generally lower compared with the initial peak rate, despite the increase in the overland flow rate and the associated transport capacity. This demonstrates that the erosion rate experienced a switch from a transported-limited to a detachment-limited system when steady state overland flow was achieved. For the *Inflow* treatment, the continuous low erosion rates with little temporal change indicated a detachment-limited system. Under the low flow velocity conditions, the impact of sheet flow without the impact of rainfall has limited effect on peat erosion as peat is fiber-rich and highly resistant to water erosion, requiring a high flow velocity before continuous erosion of peat material occurs (Carling et al., 1997).

Our study highlights the important role that raindrop impact plays in detaching peat materials for flow transport. However, the observed average contribution of raindrop impact (47%) was smaller than that reported by Guy et al. (1987) who found that the contribution exceeded 85%. The discrepancy may reflect the lower rainfall intensity used in our study. Raindrop impact has been demonstrated to play a key role in affecting overland flow, flow hydraulics and soil loss under lower rainfall intensity conditions. More significant effects could be expected with higher kinetic energy levels closer to those experienced where natural rainfall is driven by strong wind. Windy conditions are typical of many upland environments and during a drought period dry peat with a low density has a high potential susceptibility to transport by wind (Foulds and Warburton, 2007b). Under wet

and windy conditions, wind-driven rain is important in peat surface erosion through the detachment and transport of peat particles (Warburton, 2003, Foulds and Warburton, 2007a). Future work could examine overland flow interactions with wind-driven rainsplash erosion and its contribution to total erosion as rainfall on blanket peatlands is often associated with strong winds (Evans and Warburton, 2007).

3.5.2 Effects of the interaction between rainfall and inflow on soil erosion

For rainfall-driven erosion events (*Rainfall* and *Rainfall* + *Inflow* treatments), raindrop impact significantly impacted soil detachment and resulted in higher sediment yields (Table 3.4). However, the effect of shallow overland flow in the absence of rainfall on peat erosion was low.

The interaction between rainfall-driven and flow-driven erosion processes was defined as positive where the total sediment concentration produced by the *Rainfall* + *Inflow* treatment exceeded the sum of those generated by the *Rainfall* and *Inflow* treatments; and as negative where the total sediment concentration for the *Rainfall* + *Inflow* treatment was lower than the sum of those for the *Rainfall* and *Inflow* treatments. A negative interaction was observed under both the 2.5º and 7.5º slopes. Interaction was found to substantially reduce sediment concentration. This primarily results from significantly increased flow resistance caused by the retardation effect of raindrops on shallow overland flow (Table 3.7). In addition, interaction resulted in a decrease in stream power by -0.03×10^{-2} W m^{-2} and -0.06×10^{-2} W m^{-2} under the 2.5º and 7.5º slopes, respectively. This decrease was responsible for a decrease in sediment concentration as erosion was found to be positively correlated with the stream power. Rouhipour et al. (2006) and Asadi et al. (2007) found negative interaction existed in the initial stage of overland flow generation under gentle slopes and shallow overland flow conditions on silt loamy and sandy soils. However, our results contradict the positive and minor interaction effect (< 20%) reported by Tian et al. (2017) who used higher flow depths and much steeper slopes in their study of loess soil. Our results showed that the interaction between rainfall and flow driven erosion processes are important in affecting flow hydraulics and sediment, in particular under gentle slopes and shallow overland flow conditions. Consequently, to improve process-based interrill erosion modelling such as WEEP (Nearing et al., 1989) the interaction between rainfall and flow driven erosion processes should be considered. However, further work is required

to acquire an extensive dataset for parameterization across different soils and slope conditions.

3.5.3 Effects of slope gradient and upslope inflow on overland flow and erosion processes

The effect of slope gradient on overland flow and infiltration was not found to be statistically significant. Considering values normal to the surface, for both the *Rainfall* and *Rainfall + Inflow* conditions, there was a small difference (<1 %) in the raindrop energy flux density between the 7.5° and 2.5° slopes. This was insufficient to cause a significant difference in porosity near the surface resulting from compaction under raindrop impact, a factor which can be important in affecting infiltration (Mualem et al., 1990). In addition, no significant differences were found in the peat splash rate for the two slopes.

Due to the effect of upslope inflow, the average sediment yield under the *Rainfall + Inflow* condition was significantly higher than under the *Rainfall* condition. The average contribution of upslope inflow to increasing erosion was 36%. Compared with the *Rainfall* treatment, the *Rainfall + Inflow* treatment showed significantly higher flow velocity and stream power but lower Manning's *n*. These results indicate that accumulated overland flow from the upper slope positions contributes to erosion on the lower slope positions, through increasing flow velocity and stream power and decreasing surface roughness (Table 3.6). Similar findings have been reported by previous studies on semi-arid soils (Gilley et al., 1985, Parsons et al., 1994). However, the contribution of upslope inflow in our study was minor as upslope inflow rate was lower for peat detachment.

3.5.4 The relationship between overland flow and soil erosion

For the *Rainfall* and *Rainfall + Inflow* treatments, sediment concentrations typically demonstrated an initial sharp increase followed by a gradual decrease to constant level. In the early stage of the rainfall event, erosion processes were transport-limited as shown by Figure 3.3 and we observed that this raindrop detachment followed by a raindrop-induced flow transport system as suggested by (Kinnell, 2005). Peak sediment concentration usually occurred on the rising limb of the hydrograph. With increased overland flow generation, there was a shift in erosion from a transport-limited to supply-limited regime. We found that peak sediment concentration occurred during the rising limb of overland flow graphs (Figure 3.3) and this was also reported by Kløve (1998) and Holden and Burt (2002). Hence, sediment exhaustion is important in eroding blanket peat. A bare blanket

peat surface requires a period of sediment ‘preparation’ or weathering processes to produce a friable and easily erodible surface layer (Francis, 1990, Labadz et al., 1991, Shuttleworth et al., 2017). We found that rainsplash plays an important role in detaching peat particles for flow transport. However, antecedent conditions such as prior freeze–thaw or desiccation activity are very important in controlling peat erodibility and thus erosional response to a given rainfall event. Consequently, further exploration about the combined effects of rainsplash and weathering processes such as freeze–thaw and desiccation could be undertaken in future studies to reveal the relative importance of these controls.

3.5.5 Limitations

Bounded plots with rainfall and inflow simulation techniques were used in this study in order to produce quantifiable results with good levels of experimental control. The plot size (1m × 0.13m) is small but was necessary in order to obtain undisturbed peat blocks and to allow careful collection, transport and storage in the laboratory. In this study, the main active erosion process on the surface of the peat blocks was interrill erosion due to the fact that the supplied water input was insufficient for the peat surface to develop into a rill. Future work could look at rill development and also wind assisted splash effects.

It is also important to emphasize that given that accumulated inflow from upper slope positions may be loaded with sediment, more exploration with sediment-loaded inflow tests could be done in future studies to further our understanding of the effects of accumulated inflow on overland flow and erosion processes.

3.6 Conclusions

Raindrop impact was found to play an important role in affecting peat overland flow and erosion processes for gentle slopes and shallow overland flow conditions. Raindrop impact contributed significantly to increasing the sediment yield by 47% on average for both slope gradients. Compared with mineral soils peat soils were more resistant to raindrop impact forces. Raindrop impact was found to increase roughness by 72–78%, resulting in decrease in overland flow velocity by 80–92%. From a restoration perspective covering gently sloping bare peat surfaces by vegetation, brash or stabilizing geo-textiles (Parry et al., 2014) should help reduce erosion under typical rainfall intensities by weakening the impact of rainsplash.

The interaction effect of rainsplash and overland flow on sediment concentration was negative throughout the whole experimental process, with a 73–85% reduction in sediment concentration. This reduction occurred due to significantly increased flow resistance and decreased stream power. This study demonstrated that the interaction between rainfall and flow driven erosion processes was important in affecting overland flow hydraulics and sediment production on gentle peat hillslopes.

Overland flow and erosion processes on peat hillslopes are affected by slope position. The *Rainfall + Inflow* treatment produced significantly higher flow velocities and sediment yields than the *Rainfall* treatment. Sediment yield generally increased with overland flow rate but sediment exhaustion and the detachment-limited interrill erosion pattern meant no linear relationship was found. Instead, stream power was found to be a good predictor of peat erosion.

Spatially distributed models of blanket peatlands that predict stream power and which can incorporate rainsplash – flow interactions would be useful for predicting future slope development in blanket peatlands. Recent modelling projections have suggested that many blanket peatlands in the Northern Hemisphere will be more susceptible to erosion under climate change and land management practices (Li et al., 2017a). However such models do not yet incorporate processes covered in this paper and so by feeding in our process-based understanding into peat erosion models it may be possible to improve future projections.

Acknowledgements

The work was funded by the River Basin Processes & Management cluster, School of Geography (University of Leeds), and joint funding from the China Scholarship Council (File No. 201406040068) and the University of Leeds. Jeff Warburton from the Department of Geography (Durham University) is thanked for his support in providing the rainfall simulator used in this study. David Ashley from the School of Geography (University of Leeds) is gratefully acknowledged for his assistance in preparing the experimental materials. Susanne Patel from the School of Chemical and Process Engineering (University of Leeds) kindly provided use of the Malvern Morphologi G3S. We are grateful to two anonymous reviewers for providing feedback that improved the manuscript.

References

ASADI, H., GHADIRI, H., ROSE, C. & ROUHIPOUR, H. 2007. Interrill soil erosion processes and their interaction on low slopes. *Earth Surface Processes and Landforms,* 32**,** 711-724.

BAGNOLD, R. A. 1966. *An approach to the sediment transport problem from general physics*, US government printing office.

BEUSELINCK, L., GOVERS, G., HAIRSINE, P., SANDER, G. & BREYNAERT, M. 2002. The influence of rainfall on sediment transport by overland flow over areas of net deposition. *Journal of Hydrology,* 257**,** 145-163.

BOWER, M. 1960. Peat erosion in the Pennines. *Advancement of Science,* 64**,** 323-331.

BOWYER-BOWER, T. & BURT, T. 1989. Rainfall simulators for investigating soil response to rainfall. *Soil Technology,* 2**,** 1-16.

BURT, T. & SLATTERY, M. 1996. *Time-dependent changes in soil properties and surface runoff generation,* Chichester, John Wiley and Sons Ltd.

CARLING, P. A., GLAISTER, M. S. & FLINTHAM, T. P. 1997. The erodibility of upland soils and the design of preafforestation drainage networks in the United Kingdom. *Hydrological Processes,* 11**,** 1963-1980.

CERDA, A. 1998. The influence of geomorphological position and vegetation cover on the erosional and hydrological processes on a Mediterranean hillslope. *Hydrological Processes,* 12**,** 661-671.

CHARMAN, D. 2002. *Peatlands and environmental change,* Chichester, UK, John Wiley & Sons Ltd.

CHRISTIANSEN, J. E. 1942. *Irrigation by sprinkling. Resolution bulletin 670, Agricultural Experiment Station,* University of California, Berkeley, CA.

EVANS, M., BURT, T., HOLDEN, J. & ADAMSON, J. 1999. Runoff generation and water table fluctuations in blanket peat: evidence from UK data spanning the dry summer of 1995. *Journal of Hydrology,* 221**,** 141-160.

EVANS, M. & WARBURTON, J. 2007. *Geomorphology of upland peat: erosion, form and landscape change,* Oxford, UK, John Wiley & Sons.

FOSTER, G. 1982. Modeling the erosion process. *In:* CT HAAN, JOHNSON, H. & BRAKENSIEK, D. (eds.) *Hydrologic Modeling of Small Watersheds.* American Society of Agricultural Engineers.

FOULDS, S. A. & WARBURTON, J. 2007a. Significance of wind-driven rain (wind-splash) in the erosion of blanket peat. *Geomorphology,* 83**,** 183-192.

FOULDS, S. A. & WARBURTON, J. 2007b. Wind erosion of blanket peat during a short period of surface desiccation (North Pennines, Northern England). *Earth Surface Processes and Landforms,* 32**,** 481-488.

FRANCIS, I. 1990. Blanket peat erosion in a mid ‐ wales catchment during two drought years. *Earth Surface Processes and Landforms,* 15**,** 445-456.

GABET, E. J. & DUNNE, T. 2003. Sediment detachment by rain power. *Water Resources Research,* 39**,** ESG 1-1-ESG 1-12.

GILLEY, J. E., WOOLHISER, D. & MCWHORTER, D. 1985. Interril Soil Erosion, Part II. Testing and Use of Model Equations. *Biological Systems Engineering: Papers and Publications*, 134.

GUY, B., DICKINSON, W. & RUDRA, R. 1987. The roles of rainfall and runoff in the sediment transport capacity of interrill flow. *Transactions of the ASAE,* 30, 1378-1386.

HOBBS, N. 1986. Mire morphology and the properties and behaviour of some British and foreign peats. *Quarterly Journal of Engineering Geology and Hydrogeology,* 19, 7-80.

HOLDEN, J. 2005. Peatland hydrology and carbon release: why small-scale process matters. *Philosophical Transactions of the Royal Society A: Mathematical, Physical and Engineering Sciences,* 363, 2891-2913.

HOLDEN, J. & BURT, T. 2002. Infiltration, runoff and sediment production in blanket peat catchments: implications of field rainfall simulation experiments. *Hydrological Processes,* 16, 2537-2557.

HOLDEN, J. & BURT, T. 2003a. Hydraulic conductivity in upland blanket peat: measurement and variability. *Hydrological Processes,* 17, 1227-1237.

HOLDEN, J. & BURT, T. 2003b. Hydrological studies on blanket peat: the significance of the acrotelm - catotelm model. *Journal of Ecology,* 91, 86-102.

HOLDEN, J., CHAPMAN, P., EVANS, M., HUBACECK, K., KAY, P. & WARBURTON, J. 2007. Vulnerability of organic soils in England and Wales. *Final report for DEFRA Project SP0532.*

HOLDEN, J., KIRKBY, M. J., LANE, S. N., MILLEDGE, D. G., BROOKES, C. J., HOLDEN, V. & MCDONALD, A. T. 2008. Overland flow velocity and roughness properties in peatlands. *Water Resources Research,* 44, W06415.

HOLDEN, J. & ROSE, R. 2011. Temperature and surface lapse rate change: a study of the UK's longest upland instrumental record. *International Journal of Climatology,* 31, 907-919.

KATZ, D. M., WATTS, F. J. & BURROUGHS, E. R. 1995. Effects of surface roughness and rainfall impact on overland flow. *Journal of Hydraulic Engineering,* 121, 546-553.

KINNELL, P. 2005. Raindrop - impact - induced erosion processes and prediction: a review. *Hydrological Processes,* 19, 2815-2844.

KIRKBY, M. 1978. *Hillslope Hydrology*, Wiley-Interscience, Chichester.

KIRKBY, M. 1985. *Hillslope hydrology,* Chichester, Wiley.

KLØVE, B. 1998. Erosion and sediment delivery from peat mines. *Soil and Tillage Research,* 45, 199-216.

LABADZ, J., BURT, T. & POTTER, A. 1991. Sediment yield and delivery in the blanket peat moorlands of the Southern Pennines. *Earth Surface Processes and Landforms,* 16, 255-271.

LAWS, J. O. & PARSONS, D. A. 1943. The relation of raindrop - size to intensity. *Eos, Transactions American Geophysical Union,* 24, 452-460.

LI, P., HOLDEN, J. & IRVINE, B. 2016a. Prediction of blanket peat erosion across Great Britain under environmental change. *Climatic Change,* 134, 177-191.

LI, P., HOLDEN, J., IRVINE, B. & GRAYSON, R. 2016b. PESERA‐PEAT: a fluvial erosion model for blanket peatlands. *Earth Surface Processes and Landforms,* 41**,** 2058-2077.

LI, P., HOLDEN, J., IRVINE, B. & MU, X. 2017a. Erosion of Northern Hemisphere blanket peatlands under 21st‐century climate change. *Geophysical Research Letters,* 44**,** 3615-3623.

LI, P., IRVINE, B., HOLDEN, J. & MU, X. 2017b. Spatial variability of fluvial blanket peat erosion rates for the 21st Century modelled using PESERA-PEAT. *Catena,* 150**,** 302-316.

MORGAN, R. 1981. Field measurement of splash erosion. *International Association of Scientific Hydrology Publication,* 133**,** 373-82.

MUALEM, Y., ASSOULINE, S. & ROHDENBURG, H. 1990. Rainfall induced soil seal.(A) A critical review of observations and models. *Catena,* 17**,** 185-203.

NEARING, M., FOSTER, G., LANE, L. & FINKNER, S. 1989. A process-based soil erosion model for USDA-Water Erosion Prediction Project technology. *Transactions of the ASAE,* 32**,** 1587-1593.

PAN, C. & SHANGGUAN, Z. 2006. Runoff hydraulic characteristics and sediment generation in sloped grassplots under simulated rainfall conditions. *Journal of Hydrology,* 331**,** 178-185.

PARRY, L. E., HOLDEN, J. & CHAPMAN, P. J. 2014. Restoration of blanket peatlands. *Journal of Environmental Management,* 133**,** 193-205.

PARSONS, A. J., ABRAHAMS, A. D. & WAINWRIGHT, J. 1994. On determining resistance to interrill overland flow. *Water Resources Research,* 30**,** 3515-3521.

QUANSAH, C. 1981. The effect of soil type, slope, rain intensity and their interactions on splash detachment and transport. *Journal of Soil Science,* 32**,** 215-224.

ROTHWELL, J., ROBINSON, S., EVANS, M., YANG, J. & ALLOTT, T. 2005. Heavy metal release by peat erosion in the Peak District, southern Pennines, UK. *Hydrological Processes,* 19**,** 2973-2989.

ROUHIPOUR, H., GHADIRI, H. & ROSE, C. 2006. Investigation of the interaction between flow-driven and rainfall-driven erosion processes. *Soil Research,* 44**,** 503-514.

SALLES, C. & POESEN, J. 2000. Rain properties controlling soil splash detachment. *Hydrological Processes,* 14**,** 271-282.

SALLES, C., POESEN, J. & GOVERS, G. 2000. Statistical and physical analysis of soil detachment by raindrop impact: rain erosivity indices and threshold energy. *Water Resources Research,* 36**,** 2721-2729.

SAVAT, J. 1977. The hydraulics of sheet flow on a smooth surface and the effect of simulated rainfall. *Earth Surface Processes,* 2**,** 125-140.

SHUTTLEWORTH, E. L., CLAY, G. D., EVANS, M. G., HUTCHINSON, S. M. & ROTHWELL, J. J. 2017. Contaminated sediment dynamics in peatland headwater catchments. *Journal of Soils and Sediments,* 17**,** 1-11.

SINGER, M. J. & BLACKARD, J. 1982. Slope angle-interrill soil loss relationships for slopes up to 50% 1. *Soil Science Society of America Journal,* 46**,** 1270-1273.

SMART, P. & LAIDLAW, I. 1977. An evaluation of some fluorescent dyes for water tracing. *Water Resources Research,* 13**,** 15-33.

TIAN, P., XU, X., PAN, C., HSU, K. & YANG, T. 2017. Impacts of rainfall and inflow on rill formation and erosion processes on steep hillslopes. *Journal of Hydrology,* 548**,** 24-39.

TORRI, D. & POESEN, J. 1992. The effect of soil surface slope on raindrop detachment. *Catena,* 19**,** 561-578.

VAEZI, A. R., AHMADI, M. & CERDÀ, A. 2017. Contribution of raindrop impact to the change of soil physical properties and water erosion under semi-arid rainfalls. *Science of the Total Environment,* 583**,** 382-392.

WARBURTON, J. 2003. Wind-splash erosion of bare peat on UK upland moorlands. *Catena,* 52**,** 191-207.

XU, J., MORRIS, P. J., LIU, J. & HOLDEN, J. 2018. PEATMAP: Refining estimates of global peatland distribution based on a meta-analysis. *Catena,* 160**,** 134-140.

YU, Z. 2012. Northern peatland carbon stocks and dynamics: a review. *Biogeosciences,* 9**,** 4071-4085.

Chapter 4
Effects of needle ice on peat erosion processes during overland flow events

Changjia Li, Joseph Holden, Richard Grayson. Effects of needle ice on peat erosion processes during overland flow events. *Journal of Geophysical Research: Earth Surface*. DOI:10.1029/2017JF004508

4.1 Abstract

Freeze–thaw processes play a role in increasing erosion potential in upland areas, but their impact on overland flow hydraulics and fluvial erosion processes are not clearly established. We provide the first quantitative analysis demonstrating that needle ice production is a primary process contributing to upland peat erosion by enhancing peat erodibility during runoff events following thaw. To quantify the effects of needle ice on peat physical properties, overland flow hydraulics, and erosion processes, physical overland flow simulation experiments were conducted on highly frost-susceptible blanket peat with and without needle ice processes. For each treatment, overland flow rates of 0.5, 1.0, and 2.0 L min^{-1} and slopes of 2.5° and 7.5° were applied. Peat erodibility, sediment concentration, and sediment yield were significantly increased in treatments subjected to needle ice processes. Median peat losses were nearly six times higher in peat blocks subject to needle ice processes than in peat blocks not subject to needle ice processes. Needle ice processes decreased mean overland flow velocities by 32–44% via increased hydraulic roughness and changes to surface microtopographic features, with microrills and headcut development. Needle ice processes increased the hydrodynamic force of shear stress by 55–85%. Erosion rates under needle ice processes exhibited a significant linear relationship with stream power. Our findings indicate that models of overland flow-induced peat erosion would benefit from a winter component that properly accounts for the effects of needle ice processes on peat erodibility and erosion.

Keywords: erosion; freeze–thaw; needle ice; overland flow; blanket peat; wetlands

4.2 Introduction

Upland areas commonly subject to freeze–thaw processes are widely distributed in the middle-high latitudes and high-altitude areas of the world, with 66 × 10^6 km^2 of global land affected by seasonal soil freezing (Kim et al., 2011). Freeze–thaw erosion has been reported globally but particularly in parts of Europe, America, and Asia (Edwards and Burney, 1987, Labadz et al., 1991, Ferrick and Gatto, 2005, Edwards, 2013, Wang et al., 2007). While numerous studies have focused on water and wind erosion processes, much less attention has been given to freeze–thaw processes that significantly affects cohesion and strength of a frost-susceptible soil and impacts soil stability on hillslopes and resistance to running water (Gatto, 2000). A thawed surface layer overlying a frozen layer is highly susceptible to severe erosion (Wischmeier and Smith, 1978). Large amounts of eroded sediment can be produced during a thaw period and subsequent heavy rainfall (Chow et al., 2000). Freeze–thaw actions strongly interact with other erosion processes such as water erosion, wind erosion, and bank erosion (Lawler, 1986, Lawler, 2005), by preparing highly erodible soil materials for transport agents. Soil erosion is enhanced by freeze–thaw, with higher rates of sediment production and transport having been observed in areas subject to freeze–thaw cycles (Francis, 1990, Labadz et al., 1991, Lawler, 2005, Li et al., 2016). In addition, high-latitude and high-altitude regions are more likely to be affected by increases in temperature with climate change (IPCC, 2007), leading to greater seasonal or daily soil temperature variations and more frequent freeze–thaw cycles (Kværnø and Øygarden, 2006, Groffman et al., 2011) enhancing soil degradation and downstream sedimentation.

Soil freeze–thaw cycles can cause changes in several soil physical properties that play important roles in affecting soil resistance to water erosion such as soil cohesion, density, moisture content, critical shear stress, infiltration capacity, and soil aggregate stability (Oztas and Fayetorbay, 2003, Ferrick and Gatto, 2005, Van Klaveren and McCool, 2010). The magnitude of the effect is highly related to soil texture, cooling rate, freezing point, number, and frequency of freeze–thaw cycles and moisture content at freezing (Oztas and Fayetorbay, 2003, Ferrick and Gatto, 2005, Kværnø and Øygarden, 2006). Examples of studies conducted

to study the effects of freeze–thaw cycling on soil erodibility and the erosivity of overland flow are shown in Table 4.1.

Table 4.1 Experimental designs of example laboratory soil flume experiments examining the effect of freeze–thaw on runoff and soil erosion.

References	Study area	Soil type	Freezing temperature (°C)	Needle ice production	Key findings
Edwards and Burney (1987)	Canada	loam, sandy loam, fine sandy loam	–15	NA	Soil loss ↑
Edwards and Burney (1987)			–5		
Edwards and Burney (1991)			–5		
Frame et al. (1992)	Canada	fine sandy loam	–5	NA	Soil loss ↑
Edwards et al. (1995)	Canada	fine sandy loam	–5	NA	Soil loss ↑
Van Klaveren and McCool (1998)	USA	silt loam	–22 to –12	NA	Soil erodibility ↑
Gatto (2000)	USA	clayey silt	–6 to 0	Yes	Soil cohesion ↓
Ferrick and Gatto (2005)	USA	silt	–35	NA	Sediment load ↑
Van Klaveren and McCool (2010)	USA	silt loam	–22 to –12	NA	Soil erodibility ↑
Ban et al. (2016)	China	silt loam	–25 to –15	NA	Flow velocity ↓
Liu et al. (2017)	China	silt clay loam	–12	NA	Soil detachment capacity ↑

Note. Abbreviations: ↑ = an increase; ↓ = a decrease; NA = not reported in paper.

A review of the published literature reveals that despite considerable research on soil erodibility affected by freeze–thaw cycles, the relationships between soil freeze–thaw and erosion processes have received relatively little attention. In many environments, ice segregation within soil voids is considered to be an important agent of frost weathering (Lawler, 1988). Needle ice is an external form of ice segregation in which ice crystals grow orthogonally from a soil surface and propagate microcracks or macrocracks (Outcalt, 1971). Needle ice crystal growth gradually weakens and finally breaks up soil aggregates, while subsequent warming and thawing weakens or loosens this fractured soil, enhancing soil erodibility. Without needle ice growth, frozen soil remains resistant to water erosion, and only when the frost layer thaws does the soil at the surface become weakened (Van Klaveren and McCool, 2010). Soil needle ice growth and thawing, which affects surface soil properties, has been reported on all continents with several reports from key regions including the Andes and Rocky mountain chains, eastern United States, northwest and central Europe, East African

high mountains, New Zealand, and Japan (Lawler, 1988). In the 30 years since Lawler (1988) global needle ice review and mapping study, there have been almost 500 further papers reporting the needle ice phenomenon (based on a search using Thomson Reuters Web of Science). However, few studies have been conducted to quantify erosion rates or changes to flow properties associated with needle ice and thaw (Branson et al., 1996, Lawler, 1993).

The importance of overland flow hydraulic characteristics such as flow velocity, friction coefficients, and flow shear stress and their relationships with erosion have been widely reported (Govers et al., 2007). However, few studies have examined the hydraulic characteristics of overland flow on soils subject to needle ice processes. (Ban et al., 2016) found that freeze–thaw modified overland flow velocity for a clay. Any modification of overland flow velocity has important implications as it is an important parameter for modelling soil erosion, being directly related to the soil detachment and sediment transport capacity (Holden et al., 2008).

Most studies examining soil freeze–thaw erosion processes have concentrated on mineral soils, with much less known about organic soils. Peatlands that slowly accumulate organic-rich peat (Charman, 2002), cover approximately 2.84% of the world's land area (Xu et al., 2018) and are important terrestrial carbon sinks, storing one third to half of the world's soil carbon (Yu, 2012). Of particular concern in terms of erosion are rain-fed blanket peatlands, which mainly occur on sloping ground in temperate, hyperoceanic regions with high precipitation (Gallego-Sala and Prentice, 2013) and cover 105, 000 km^2 of the Earth's surface (Li et al., 2017a). Many Northern Hemisphere blanket peatlands have experienced severe erosion and are under increasing erosion risk from future climate change (Clark et al., 2010, Gallego-Sala et al., 2010, Li et al., 2017b), which will lead to enhanced losses of terrestrial carbon in many regions.

In many blanket peatlands with cool and wet climates, freeze–thaw processes are dominant sediment production mechanisms (Francis, 1990, Labadz et al., 1991, Evans and Warburton, 2007, Grayson et al., 2012, Li et al., 2016). Soil freeze–thaw processes have been evaluated through a number of laboratory and field experiments but are under-represented in the literature for blanket peat. The physical and chemical characteristics of peat can be quite different to those of mineral soils (Hobbs, 1986). Compared to mineral soils, peat has a higher volumetric heat capacity but much lower conductivity and has significantly different thermal response during wetting

or drying periods (FitzGibbon, 1981). This demonstrates that a strong thermal gradient can develop between a cold peat surface and warmer peat at depth (Evans and Warburton, 2007). The significant temperature gradients together with abundant moisture supply are ideal for needle ice formation (Outcalt, 1971). Due to the maritime location of many blanket peat environments, freezing is commonly diurnal and the effect of a single needle ice event can be multiplied many times through the winter season (Figure 4.1). The importance of needle ice formation in producing eroding peat faces has been widely reported in peatlands such as eroding upland peatlands in the United Kingdom (Tallis, 1973, Legg et al., 1992), erosion of peat remnants in Finnish Lapland (Luoto and Seppälä, 2000) and alpine mires in Lesotho (Grab and Deschamps, 2004). The growth of needle ice can lead to a *fluffy* peat surface that is loose and granular and vulnerable to being flushed off by overland flow events (Evans and Warburton, 2007), with saturation excess overland flow being a dominant flow mechanism in blanket peat systems (Holden and Burt, 2003). However, little quantitative work has been conducted on how surface roughness and overland flow are affected by needle ice formation and melting nor on quantifying how these effects impact upon peat erosion. Given the lack of quantitative data on needle ice effects on peat erosion, the aim of our study was to measure how needle ice effects soil erodibility, overland flow hydraulic characteristics and sediment production processes through a series of experiments.

Figure 4.1 Photographs taken at blanket peat field sites in northern England showing typical needle ice formation. Note the friable sediment layer on the upper surface of the ice mass. Also note different layers of ice needles indicating different consecutive nights of needle ice formation.

4.3 Materials and Methods

4.3.1 Experimental design

4.3.1.1 Sample collection

Undisturbed bare peat blocks were carefully excavated from topsoil at Moor House National Nature Reserve (NNR; 54°41′ N, 2°23′ W), a blanket peat site in northern England. The climate at Moor House is favourable for needle ice formation that is normally observed to grow within the upper peat layer during winter months (Evans and Warburton, 2007).

A plastic rectangular gutter (1.0-m long, 0.13-m wide and 0.08 m in depth) was pushed parallel to the peat surface into the peat, and carefully dug out to extract an undisturbed peat block. Samples were tightly sealed using plastic film to minimize peat oxidation and drying before being stored at 4 °C prior to laboratory analysis. Peat samples were extracted from peat blocks before and after subjecting the peat to needle ice processes and analysed in the laboratory using a Morphologi G3 to capture two-dimensional images of peat particles and to calculate size and shape parameters.

4.3.1.2 Freezing and thawing with needle ice growth and melting

Microhydrological and micrometeorological variables affecting needle ice growth include cooling rate, freezing point and duration, and soil moisture status (Branson et al., 1996, Outcalt, 1971). For laboratory-based experiments of needle ice growth, cooling rate is critical as it should be slow enough to simulate natural cooling, which is usually a result of radiative heat loss (Outcalt, 1970, Higashi and Corte, 1971). However, many laboratory experiments have failed to produce radiative cooling that enhances needle ice growth and produces erodible soil (Table 4.1). Soil aggregate stability is negatively correlated with soil moisture content at the time of freezing (Oztas and Fayetorbay, 2003) and ice crystals grow abundantly at high moisture content, which breaks bonds holding soil particles together (Ferrick and Gatto, 2005).

To ensure that freezing would occur from the peat surface downwards, the peat blocks were wrapped with heat-insulating materials on the sides and base. Peat blocks were supplied with deionised water to container capacity and then transferred from the cold store (4.0 °C) to an environmental cabinet with an initial temperature of 5.0–6.0 °C. Our preliminary tests on peat cores showed that an average cooling rate of −1.3 °C hr^{-1} contributes to ice segregation and growth. The temperature of the environmental cabinet was

subsequently set to cool at 1.3 °C hr^{-1} and finally set at −1.0 °C for 5−7 days to allow continuous growth of needle ice (Lawler, 1993). This means that the particular case we investigated was a long-duration needle ice production rather than diurnal needle ice production and thaw. Both patterns have been observed in the field (Evans and Warburton, 2007). The peat was almost saturated at the start of each freeze period, and during freezing deionised water was added periodically to provide sufficient available moisture for needle ice growth. Needle ice successfully formed within the upper layer of the peat block (Figure 4.2). Under freezing conditions, needle ice samples were carefully removed from the peat surface and photographed, with the needle ice length being measured using callipers. The peat blocks with needle ice formation were subsequently subjected to thawing at room temperature (20 °C) for approximately 2 days.

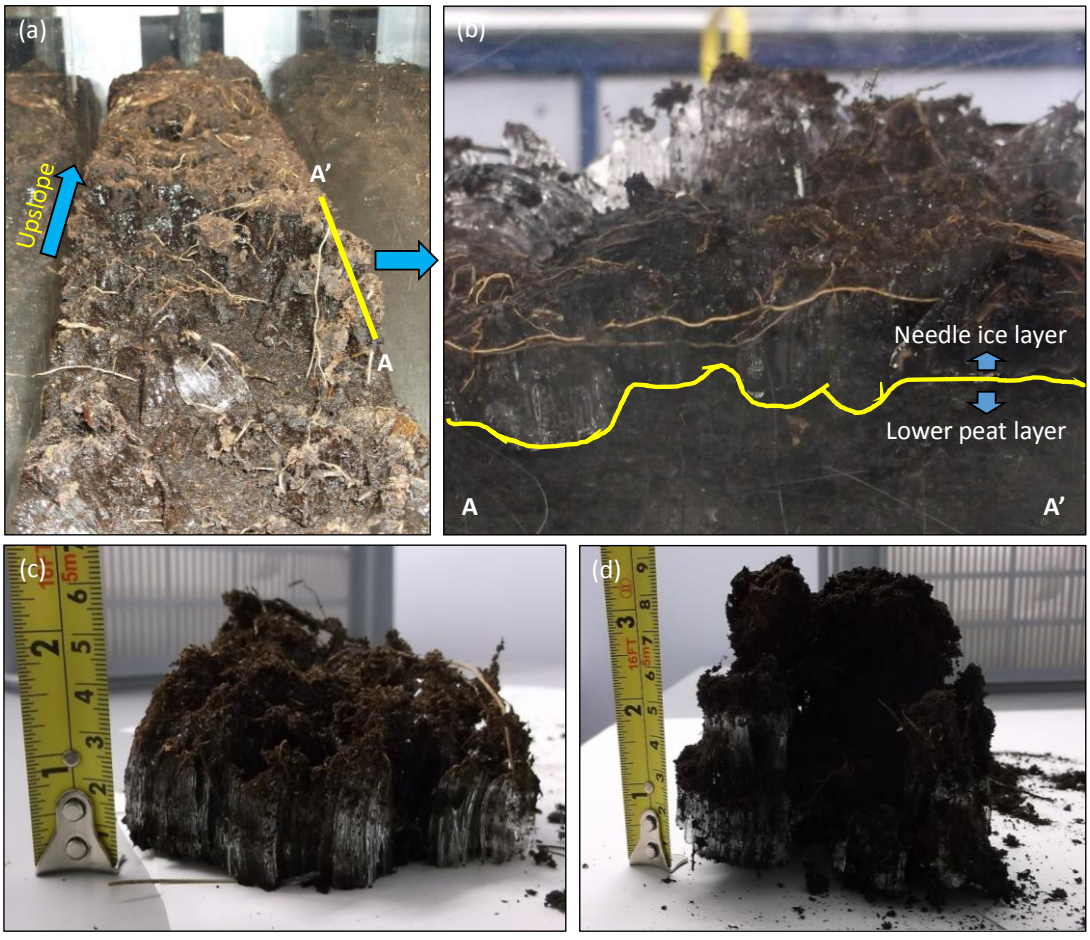

Figure 4.2 Morphology of laboratory needle ice growth: **(a)** peat block with needle-ice formation within the upper peat layers; **(b)** view from A–A' crosssection of the peat block. Two distinctive layers including the upper needle ice layer and the much denser undisturbed peat layer below were identified; **(c** and **d)** typical needle ice formations. Note the friable surface layer resulting from formation of needle ice on the upper surface of the ice mass.

Structure-from-Motion photogrammetric surveying was used to obtain high-resolution topographic data sets on peat blocks with (NI) and without (Non-NI) needle ice formation and thaw. The Multiscale Model to Model Cloud Comparison (M3C2) algorithm (Lague et al., 2013) in the open source CloudCompare software was used to compute cloud-to-cloud differencing and roughness of both clouds (NI and Non-NI).

4.3.1.3 Overland flow experiments

Peat blocks were placed inside soil flumes with an area of 0.13 m^2 (1.0 m in length and 0.13 m in width). Any gaps between the edge of the peat block and the soil flume were filled with plastic sheets in order to prevent leakage and enable all overland flow from the peat block to be collected. A pump and water distributor were used to supply uniform and steady water flow at a controlled and constant flow along the full flume width. Water was supplied from municipal water with an electrical conductivity of 421 ± 1 µs cm^{-1} and a pH of 7.2 ± 0.1, to minimize the effects of water quality on the hydrological and erosion response of the peat blocks during experiments.

Bower (1960) classified the gully systems in blanket peat environments into two distinct types of dissection (*Type 1* and *Type 2*). *Type 1* dissection occurs on the flatter interfluve areas where peat is usually 1.5 – 2.0 m in depth on slopes less than 5° (Bower, 1960). Peat gullies tend to frequently branch and intersect as an intricate dendritic network (Labadz et al., 1991). *Type 2* dissection is characterized by steeper slopes (exceeding 5°), with a system of sparsely branched drainage gullies incised through the peat to bedrock and aligned nearly parallel to each other (Bower, 1960, Labadz et al., 1991). It has been suggested that the transition between *Type 1* and *Type 2* dissection of gully system in blanket peat environments was suggested as 5° (Bower, 1960). Therefore, slope was set at 2.5° and 7.5°, respectively to characterise the peat system firmly within each *Type* category. For each slope, the experiments were conducted under three overland flow rates (i.e., 0.5, 1.0, and 2.0 L min^{-1}) for peat blocks subject to and not subject to needle ice processes with at least two replicates for each (Supplementary Table 4.1). Herein overland flow rates were selected to be appropriate to the scale of the experiments while providing sufficient range to quantify variations in peat erosion under overland flow events.

4.3.2. Flow and sediment production measurements

During each run the time of overland flow initiation was recorded, after which each test lasted for between 10 and 30 min. The durations of the simulation experiments were determined based on the time needed for steady state overland flow and sediment concentration development: a short duration for the high inflow rate but a longer duration for the low inflow rate. Total surface flow was sampled at the flume outlet every 1 or 2 min. Overland flow volumes and rates (mL s^{-1}) for each sample were measured. Samples were left to settle for 6 hr to allow deposition of the suspended sediment. The clear supernatant was decanted, and the remaining turbid liquid was transferred to a foil container and oven-dried at 65.0 °C for 48 hr prior to weighing. The dry sediment mass (mg) was calculated, and the sediment concentration (mg mL^{-1}) was calculated as the ratio of dry sediment mass (mg) to the overland flow volume (mL). The sediment yield rate (mg m^{-2} s^{-1}) was defined as the ratio of dry sediment mass (mg) per unit area (m^2) per sampling duration (s).

Surface flow velocities (V_s) were measured by injecting fluorescein solution at the uppermost positions within the plots. The time required for the leading edge of fluorescein dye tracer to travel to the outlets of the plots was recorded at a resolution of 0.01 s. Overland flow velocity was calculated by dividing the distance between the injection and outlet points by the time difference between injection of fluorescein solution and arrival to the outlets. The dye-tracing method was applied at 1 min intervals with three replicates for each.

4.3.3. Data analysis

For a laminar flow profile, the vertical velocity distribution is shown by a quadratic equation, with zero at the bed and a maximum for surface velocity (V_s; Katz et al. (1995)). The profile mean velocity (V) was calculated using equation (4.1):

$$V = k\,V_s \tag{4.1}$$

where V is mean flow velocity (cm s^{-1}); V_s is surface flow velocity (cm s^{-1}); and k is a coefficient which is 0.33 for shallow flows on bare peat surfaces under gentle slopes (Holden et al., 2008).

The overland flow was laminar and was presumed to be uniform, and the average flow depth was calculated from:

$$h = q / V = Q / (Vbt) \quad (4.2)$$

where h is mean flow depth for the whole plot (cm); q is the unit discharge ($cm^2\ s^{-1}$); Q is the overland flow volume during t duration (ml); and b is the width of water-crossing section (cm).

The Reynolds number Re (Reynolds, 1883) and Froude number Fr were calculated by

$$Re = Vh / \upsilon \quad (4.3)$$

$$Fr = V / (gh)^{1/2} \quad (4.4)$$

where g is the acceleration due to gravity ($m\ s^{-2}$); and υ is the kinematical viscosity ($cm^2\ s^{-1}$).

The Darcy-Weisbach friction factor f and Manning's friction coefficient n were determined by:

$$f = (8ghJ) / V^2 \quad (4.5)$$

$$n = (h^{2/3} \cdot J^{1/2}) / V \quad (4.6)$$

where J is the *sine* of the bed slope ($m\ m^{-1}$).

Flow shear stress τ (Pa; Foster (1982)) and stream power Ω ($W\ m^{-2}$; Bagnold (1966)) were calculated by:

$$\tau = \rho ghJ \quad (4.7)$$

$$\Omega = \rho gqJ \quad (4.8)$$

where ρ is the density of water ($kg\ m^{-3}$).

In this study, peat anti-scouribility capacity (AS) was defined to describe the resistance of peat to overland flow scouring and calculated as

$$AS = ft/W \quad (4.9)$$

where AS is the peat anti-scouribility capacity ($L\ g^{-1}$); f is discharge of scouring ($L\ min^{-1}$); t is the duration of scouring (min); W is the weight of the oven-dried peat mass (g). The higher the peat AS, the lower the peat erodibility.

Data sets were tested for normality using the Anderson-Darling normality test at the $p = 0.05$ level. Student's t test was used for testing for differences between two sets of data which were both normally distributed. The data sets that were not normally distributed were transformed and retested for normality. Mann-Whitney U tests were applied when one or both sets of response variable values were still not normally distributed. Correlation

analysis and stepwise regression analysis were used to determine the relationship between overland flow hydraulics and sediment yield. All statistical tests were considered significant at $p < 0.05$.

4.4 Results

4.4.1 Soil physical properties

Basic chemical and physical properties of the peat blocks were determined on subsampled peat (Supplementary Table 4.2). Needle ice processes (NI) increased porosity and decreased peat bulk density. Results from the Morphologi G3 analysis demonstrate that peat samples subject to NI produced particles with greater average length, width, and perimeter than those not subject to needle ice processes (Non-NI, Supplementary Table 4.2). NIs were also found to produce less rounded particles compared with Non-NI treatments.

The median particle diameter for the NI peat samples was 5.9 µm compared to 4.4 µm for the Non-NI samples. The peat soils were 92.9% and 96.7% in the grain size range from 1 to 50 µm for the NI and Non-NI treatments, respectively. Mann-Whitney *U* tests showed that needle ice processes had no significant impact on peat particle size distribution ($p = 0.397$).

Structure-from-Motion measurements showed that formation of needle ice leads to a higher peat surface, with a positive median topographic change of 0.0041 m (Supplementary Figure 4.1). The mean roughness for the NI treatment was 0.001008, which was much greater than for the Non-NI treatment (0.000887). In addition, the standard deviation of roughness on the NI treatment (0.001071) was much greater than that for the Non-NI treatment (0.000388). These results show that needle ice growth led to a rougher peat surface.

4.4.2 Sediment yield

The time for overland flow initiation from NI treatments (mean = 55.7 s, $n = 6$) was 90.7% greater than that from Non-NI blocks (mean = 29.2 s, $n = 6$). Typical overland flow and sediment concentration trends for the treatments are shown in Figure 4.3. Overland flow rates first increased with time since overland flow generation and then attained quasi steady state values (Figure 4.3). For a given slope and overland flow rate, statistical analysis showed no significant difference ($p > 0.05$) in the mean or median overland flow rate between the NI and Non-NI treatments.

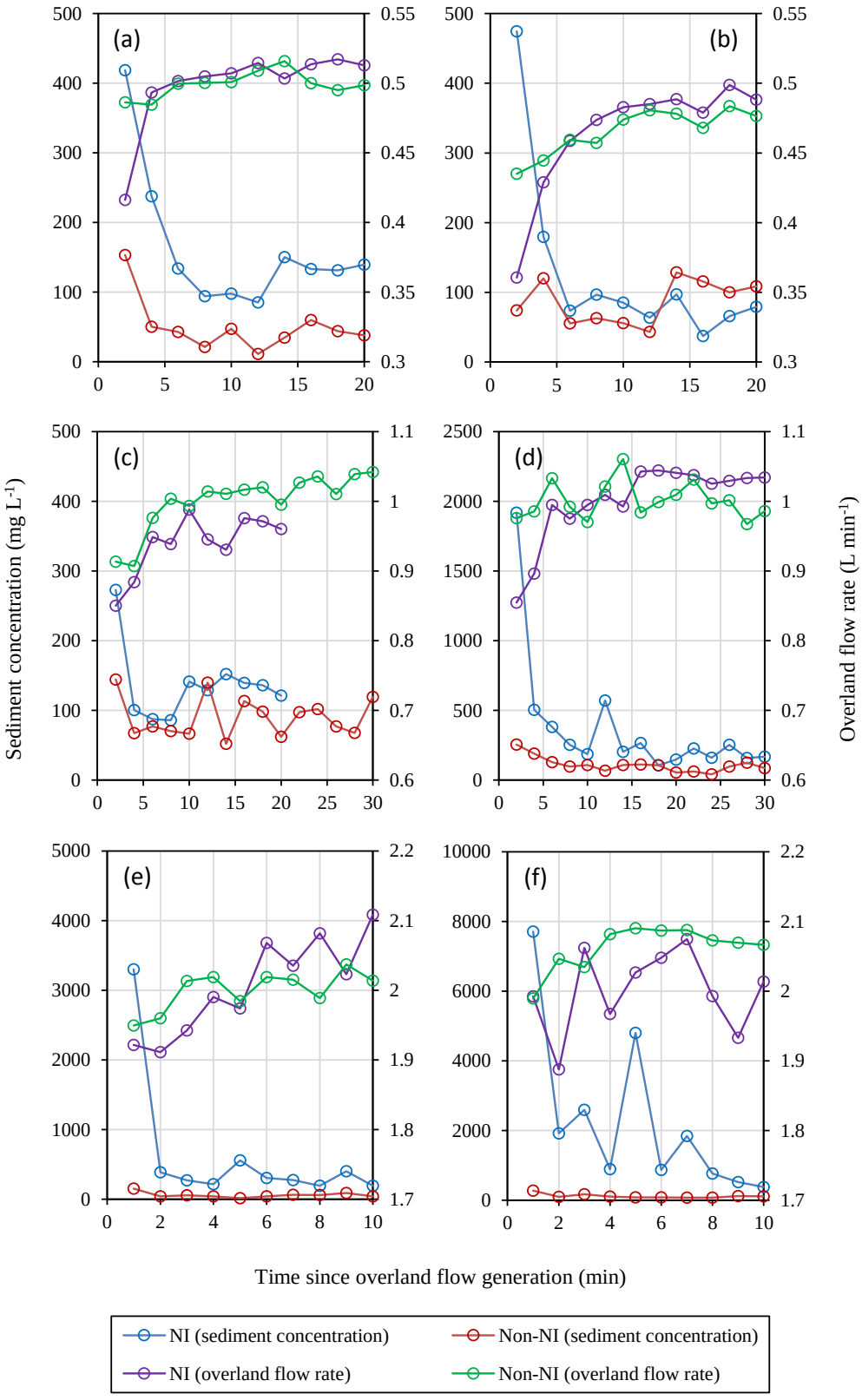

Figure 4.3 Overland flow and sediment concentration for representative NI and Non-NI treatments under different slopes and upslope inflow rates conditions: (a) 0.5 L min^{-1}, 2.5°; (b) 0.5 L min^{-1}, 7.5°; (c) 1.0 L min^{-1}, 2.5°; (d) 1.0 L min^{-1}, 7.5°; (e) 2.0 L min^{-1}, 2.5°; (f) 2.0 L min^{-1}, 7.5°. NI = those subject to needle ice processes; (Non-NI) = those not subject to needle ice processes.

For the NI treatments, sediment concentrations typically peaked during the initial stage of overland flow generation before gradually decreasing to an almost constant value (Figure 4.3) indicating that peat erosion primarily occurred during the early stage of overland flow generation. In contrast, for the Non-NI treatments, the sediment concentration was almost constant with little variation with overland flow generation. Mann-Whitney *U* test showed that the peak sediment concentration on Non-NI treatments was significantly lower (p = 0.020) than that observed on NI treatments.

The mean sediment concentration (Supplementary Table 4.3) for the NI treatment was significantly higher than that of the Non-NI treatment (Mann-Whitney *U* test, p = 0.013). Needle ice processes contributed significantly to an increase in sediment concentration, particularly at steeper slopes (7.5°; Table 4.2). Dimensionless NI/Non-NI ratios of sediment concentration are greater than 1.0 (Figure 4.4 (a)), indicating a primary effect of the needle ice processes on peat erosion. Much larger NI/Non-NI ratios of sediment concentration were found at the highest overland flow rate (2.0 L min^{-1}).

Table 4.2 The effects of needle ice processes on sediment concentration, sediment yield and peat anti-scouribility capacity under different slopes and scouring rates.

Slopes	Designed flow rate (L min^{-1})	*SC* (mg L^{-1})		*SY* (mg m^{-2} min^{-1})		*AS* (L g^{-1})	
		In rate	In percentage (%)	In rate	In percentage (%)	In rate	In percentage (%)
2.5°	0.5	58.4	97.5	230.4	92.5	–6.9	–30.7
	1.0	35.2	50.0	159.2	21.2	–5.7	–35.6
	2.0	800.2	1173.3	10929.6	774.7	–15.2	–84.9
7.5°	0.5	230.8	314.4	1844.7	666.2	–10.8	–60.7
	1.0	670.9	366.2	6003.1	322.3	–5.5	–66.3
	2.0	752.3	869.7	24818.3	1403.3	–7.7	–54.6

Note. Abbreviations: *SC*, Sediment concentration (mg L^{-1}); *SY*, Sediment yield rate (mg m^{-2} min^{-1}); *AS*, peat anti-scouribility capacity (L g^{-1}). Positive values indicate an increase for the NI treatments while negative values indicate a decrease compared to the Non-NI treatments.

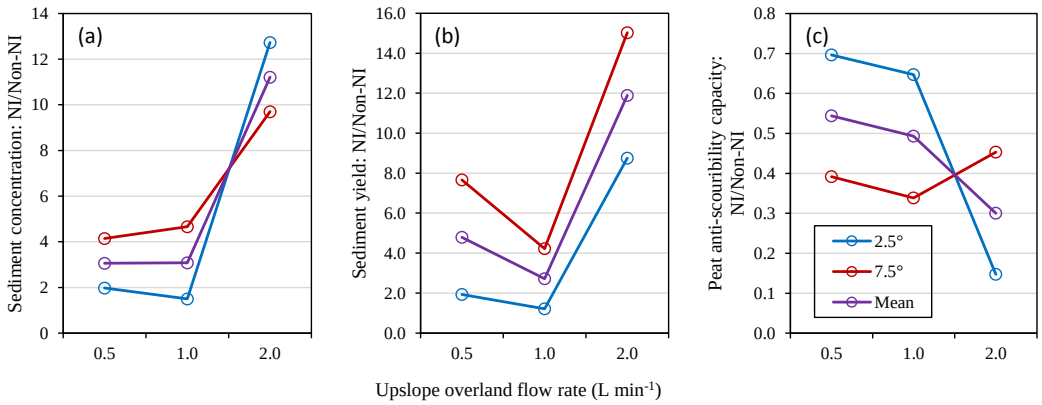

Figure 4.4 The ratios of NI treatment to Non-NI treatment in (a) sediment concentration; (b) sediment yield; and (c) peat anti-scouribility capacity under different slopes and scouring rates. NI = those subject to needle ice processes; (Non-NI) = those not subject to needle ice processes.

Peat losses from both the NI and Non-NI treatments were greater for the steeper flume slope and for the highest input flow rate (Supplementary Table 4.3). Sediment yield ratios ranged from 1.2 to 7.7 for the 0.5 and 1.0 L min^{-1} overland flow rates and up to 15.0 for the 2.0 L min^{-1} overland flow rate. The effect of needle ice processes on sediment yield was greater under the 7.5° than the 2.5° slope (Table 4.2 and Figure 4.4 (b)).

The Non-NI treatment produced a higher peat antiscouribility capacity (Supplementary Table 4.3) suggesting that needle ice processes reduce peat erodibility during overland flow events. On average, needle ice processes contributed to –50.4% and –60.5% of median peat antiscouribility capacity under the 2.5° and 7.5° conditions, respectively (Table 4.2). Dimensionless NI/Non-NI ratios of peat antiscouribility capacity were lower than 1.0, showing a primary effect of the needle ice processes on reducing peat erodibility. Peat antiscouribility capacity ratios generally decreased with an increase in overland flow rate, with the median value declining from 0.54 at the 2.0 L min^{-1}, to 0.49 at 1.5 L $min^{-1}$and to 0.30 at 0.5 L min^{-1}.

4.4.3 Overland flow hydraulics

For both the NI and Non-NI treatments overland flow velocities increased with increasing slope and upslope inflow rates (Table 4.3). Needle ice processes reduced overland flow velocity on average by 44% and 32% under the 2.5° and 7.5° conditions, respectively (Figure 4.5 (a)). The effect of needle ice processes on reducing overland flow velocity was lower under the higher inflow rate and larger slope gradient. Needle ice processes increased flow depth by 85% and 55% under the 2.5° and 7.5° conditions, respectively (Figure 4.5 (b)).

Table 4.3 Median overland flow hydraulic parameters for the treatments subject to and not subject to needle ice processes under different slopes and scouring rates.

Slopes	Designed flow rate (L min^{-1})	Treatment	*V*	*h*	*Re*	*Fr*	*f*	*n*	*τ*	*Ω*
2.5°	0.5	NI	4.7	4.2	62.0	0.1	62.0	35.4	1.8	2.8
		Non-NI	10.6	1.8	58.2	0.3	5.0	8.7	0.8	2.6
	1.0	NI	6.2	7.2	137.3	0.1	60.8	38.5	3.1	5.9
		Non-NI	13.2	3.7	133.6	0.3	14.4	14.2	1.6	6.0
	2.0	NI	12.7	6.2	243.1	0.2	12.7	17.1	2.6	11.0
		Non-NI	16.8	5.1	250.0	0.3	8.5	12.7	2.2	11.3
7.5°	0.5	NI	7.6	2.5	56.8	0.2	47.0	27.7	3.2	7.7
		Non-NI	12.3	1.5	58.9	0.3	9.6	11.9	2.0	7.9
	1.0	NI	13.5	3.4	138.1	0.3	24.2	20.3	4.4	18.6
		Non-NI	22.4	1.9	132.2	0.5	3.7	7.6	2.4	17.9
	2.0	NI	15.7	5.4	241.4	0.2	33.7	25.1	6.9	32.9
		Non-NI	19.0	4.3	254.5	0.3	11.3	15.3	5.5	34.4

Note. Abbreviations: *V* = median overland flow velocity (cm s^{-1}); *h* = median flow depth (mm); *Re* = Reynolds number; *Fr* = Froude number; *f* = Darcy-Weisbach friction factor; *n* = Manning's friction factor (10^{-2}); *τ* = flow shear stress (Pa); *Ω* = stream power (10^{-2} W m^{-2}).

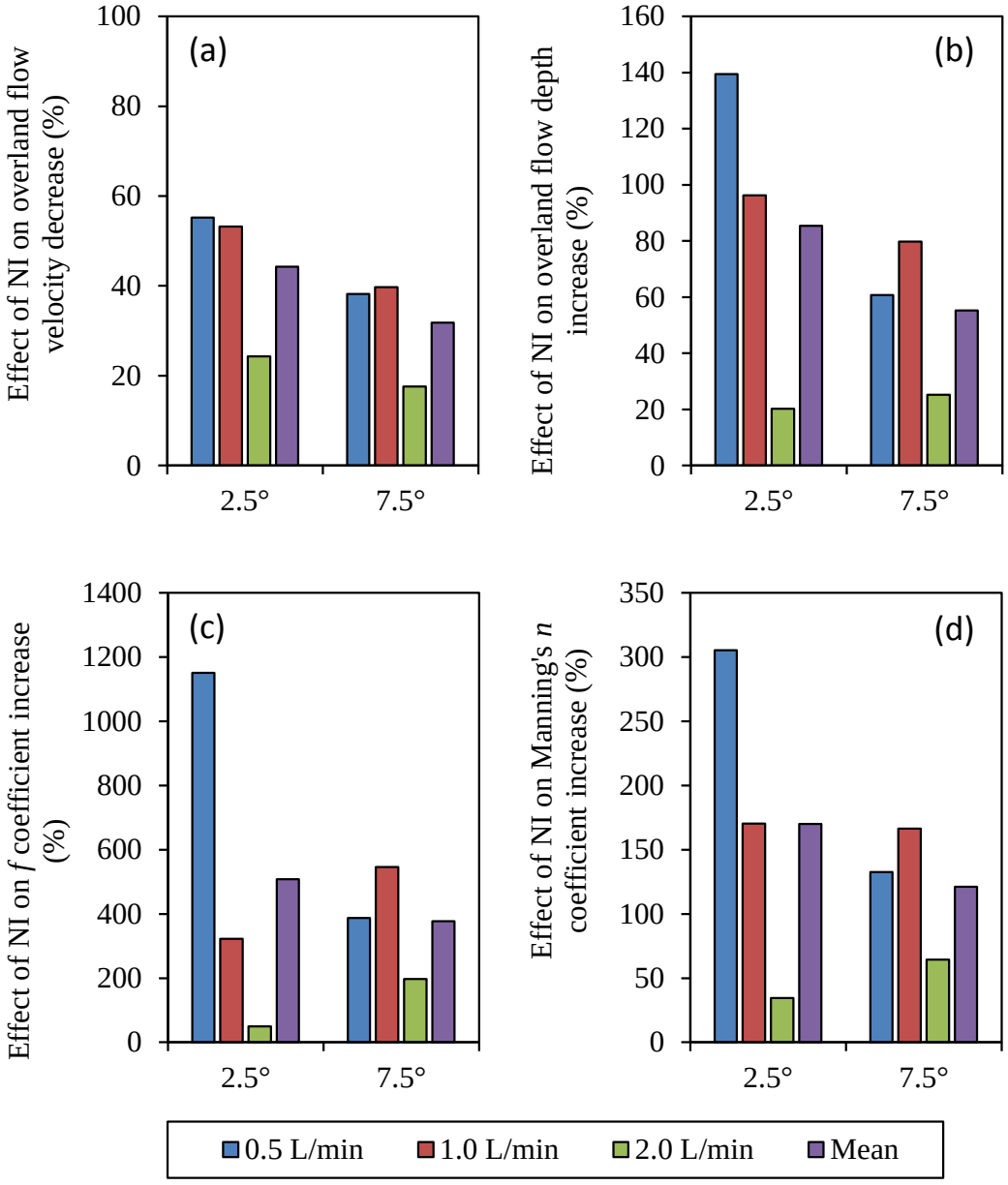

Figure 4.5 Effect of needle ice processes (NI) on (a) overland flow velocity decrease; (b) overland flow depth increase; (c) Darcy-Weisbach *f* friction factor increase; and (d) Manning's *n* friction factor increase under different slopes and scouring rates.

Overland flows were observed to be laminar with the Reynolds number (*Re*) less than 300 (Table 4.3) and subcritical (*Fr* < 1). The Darcy-Weisbach friction factor *f* and Manning's *n* friction coefficients were higher for NI treatments than Non-NI treatments. The Non-NI treatments produced *f* values ranging from 5.0 to 14.4 with a median of 9.3 under the 2.5° conditions, and from 3.7 to 11.3 with a median of 8.2 under the 7.5°

conditions. The median values were much lower than those of NI treatments, at 29.7 and 81.1 for 2.5° and 7.5° slopes, respectively. Similarly, NI treatments produced a greater (121–170%) Manning's friction factor (*n*; Figure 4.5 (d)). The higher *f* and *n* for NI treatments indicates a limited entrainment and transport capacity of the overland flow. The overland flow shear stress (*τ*) for the NI treatment was greater than that of the Non-NI treatment (Table 4.3), and needle ice processes increased *τ* by 55–85%. A similar overland flow stream power (*Ω*) was found for the NI and Non-NI treatments (Table 4.3).

4.4.4 Relationships between overland flow and sediment

Spearman's Rank correlation analysis was used to test if there was a relationship between erosion and various hydraulic parameters important for peat erosion (Figure 4.6). For the NI treatments, peat erosion rate was closely related to stream power (p = 0.016), overland flow rate (p = 0.023), and velocity (p = 0.023). The correlation coefficient between erosion and stream power was larger at 0.895 (Figure 4.6). For the Non-NI treatments, overland flow velocity had a significant role in influencing erosion (p = 0.002).

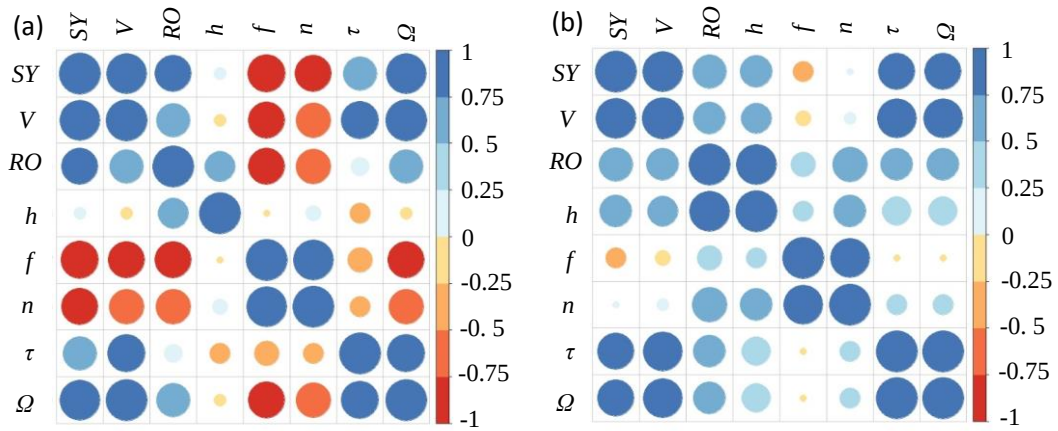

Figure 4.6 Correlation matrix between median peat erosion rate and different overland flow hydraulic parameters for NI (a) and Non-NI (b) treatments. Abbreviations: *SY* = sediment yield rate (mg m^{-2} min^{-1}); *V* = overland flow velocity (cm s^{-1}); *RO* = overland flow rate (ml min^{-1}); *h* = overland flow depth (mm); *Re* = Reynolds number; *Fr* = Froude number; *f* = Darcy-Weisbach friction factor; *n* = Manning's friction factor (10^{-2}); *τ* = flow shear stress (Pa); *Ω* = stream power (10^{-2} W m^{-2}).

For both the NI and Non-NI treatments, sediment yield generally increased with an increase in overland flow velocity, overland flow rate, flow shear stress, and stream power (Figure 4.7). For the NI treatments, stepwise linear regression showed that stream power was the only factor entered that predicted erosion, according to the criteria of probability-of-F-to-enter ≤ 0.05. The regression equation was $SY = 949.3 \times \Omega - 2{,}795.2$, with a significant ($p = 0.016$) coefficient of determination ($R^2 = 0.800$). For the Non-NI treatments, stepwise linear regression showed that overland flow velocity was a good parameter for predicating erosion, with a significant ($p = 0.002$) coefficient of determination ($R^2 = 0.935$) for the regression equation.

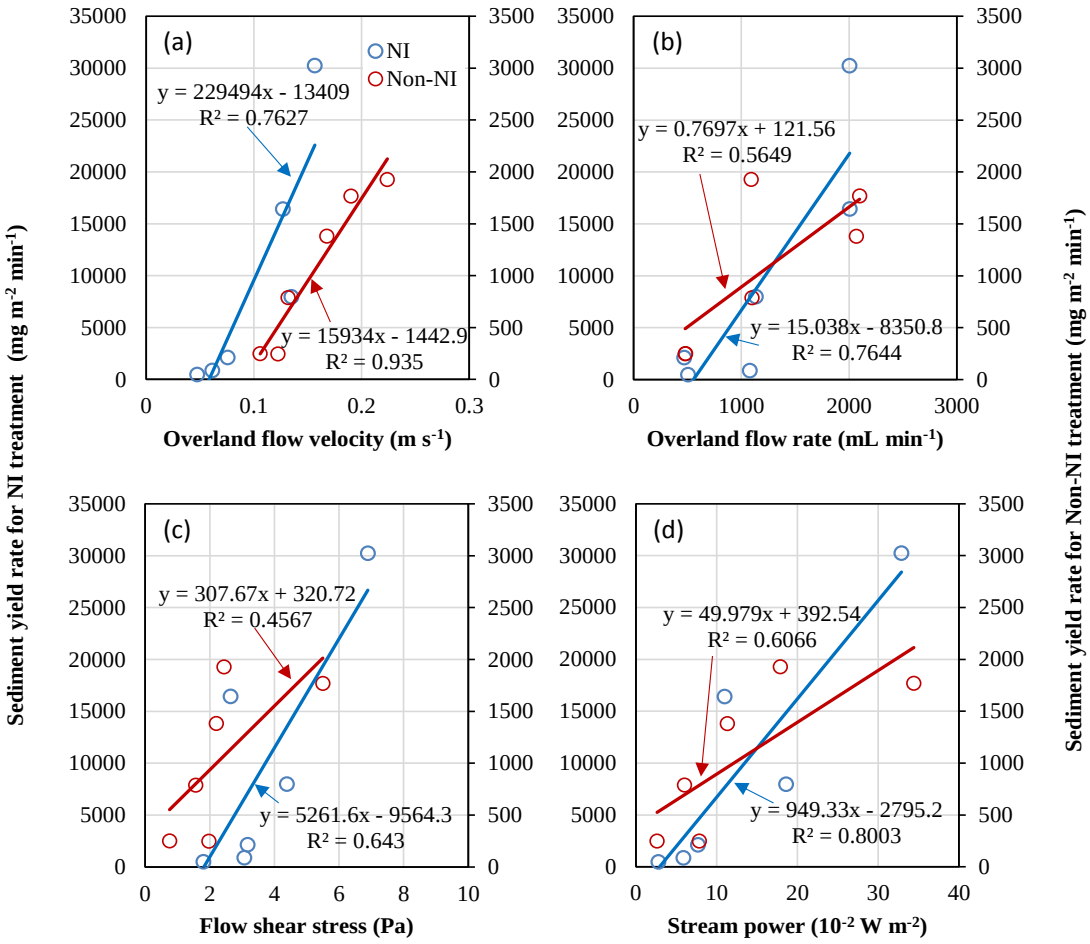

Figure 4.7 The relationships between mean sediment yield rate and (a) mean overland flow velocity; (b) mean overland flow rate; (c) mean flow shear stress, and (d) mean stream power for NI and Non-NI treatments.

The relationship between cumulative sediment yield and cumulative overland flow rate could be fitted by the power function $y = ax^b$, where y (mg) is the cumulative sediment yield, x (mL) is the cumulative overland flow rate, and a and b are regression coefficients (Table 4.4). All fitting equations were significant ($p < 0.05$). The absolute values of a for the NI treatments was much greater than those for the Non-NI treatments. However, the b coefficients of the power functions were lower for the NI treatments compared with the Non-NI treatments. These results demonstrate that the response of sediment yield to increased overland flow rates is less sensitive for the NI treatments.

Table 4.4 Regression analysis of the cumulative overland flow rate (x) and cumulative sediment yield (y) under NI and Non-NI treatments.

Treatment	Designed flow rate (L min^{-1})	Regression equation	n	R^2
NI	0.5	$y = 8.3283\ x^{0.6032}$	40	0.9983**
	1.0	$y = 235.87\ x^{0.4195}$	65	0.9810**
	2.0	$y = 260.51\ x^{0.446}$	36	0.9460**
	All	$y = 128.24\ x^{0.4672}$	141	0.7918*
Non-NI	0.5	$y = 1.7707\ x^{0.6235}$	35	0.9948**
	1.0	$y = 1.2959\ x^{0.8087}$	75	0.9724**
	2.0	$y = 10.953\ x^{0.502}$	49	0.9970**
	All	$y = 0.2414\ x^{0.9611}$	159	0.9417**

*Regression is significant at the 0.05 level.
**Regression is significant at the 0.01 level.

4.5 Discussion

4.5.1 Effects of needle ice processes on peat physical properties

Needle ice processes reduced bulk density, increased porosity, and produced larger peat particles. Less rounded particles are likely to be produced from the peat surface by recent freeze thaw; however, there was no significant effect on particle size distribution. This is contrary to the results of (Li and Fan, 2014), who found that freeze–thaw cycles usually increased the aggregates of small particle size groups and decreased the aggregates of the relatively larger particle size groups on a black soil in Northeast China. However, we only conducted one freeze–thaw cycle, whereas changes in soil particle size have been reported to increase with the number of freeze–thaw cycles (Li and Fan, 2014).

For the Non-NI treatments peat erodibility was minor; continuous low erosion rates with little temporal change indicated a detachment-limited system. The overland flow velocity on the Non-NI treatments was too low to lead to continuous erosion of peat material as peat is fiber-rich and highly resistant to water erosion (Carling et al., 1997). In contrast, peat erodibility was much higher for the NI treatments despite lower overland flow velocities being observed. In line with these findings the peat antiscouribility capacity was reduced by needle ice processes. The NI treatments produced significantly higher regression coefficient *a* values compared with the Non-NI treatments (Table 4.8) suggesting that needle ice processes decreased the inherent resistance of peat to water erosion. Needle ice growth and thaw had strong destructive effects on peat particles. Our study is in agreement with results reported by Van Klaveren and McCool (1998) and Van Klaveren and McCool (2010) who found that erodibility for a silt loam increased after freeze–thaw. It is suggested that needle ice processes should be taken into account when analysing peat erodibility and predicting peat erosion rate. Future work should be carried out to examine the effects of both the number and duration of needle ice processes on peat erodibility and the contribution to total erosion.

4.5.2 Effects of needle ice processes on overland flow hydraulics

Compared with the Non-NI treatments, NI treatments increased the time taken to generate overland flow due to enhanced peat infiltration capacity associated with greater porosity.

Overland flow velocity was significantly lower for NI treatments due to increased surface roughness. In addition, visual observations of the NI treatments showed that micro-rills and headcuts occurred and caused localized waterfalls that were responsible for lower overland flow velocities. Similar phenomena have been reported by (Ban et al., 2016) who found that headcuts on thawed slopes played an important role in retarding overland flow velocity.

The relative reduction in overland flow velocity caused by needle ice processes was lower under high scouring rate at 2.0 L min^{-1} than low scouring rate at 0.5 and 1.0 L min^{-1}. This results from a decrease in the ability for needle ice processes to increase hydraulic roughness under high flow rates. The effects of needle ice processes on reducing overland flow velocity and increasing overland flow depth and hydraulic roughness were found to be less on the steeper treatment.

4.5.3 Effects of needle ice processes on erosion processes

The NI treatments produced similar overland flow rates to Non-NI treatments but significantly greater sediment yields. The observed difference in erosion primarily resulted from the effects of needle ice processes which increased sediment concentration, sediment yield, and reduced peat antiscouribility capacity. This behaviour has been reported for other soil types (Wischmeier and Smith, 1978, Van Klaveren and McCool, 1998, Ferrick and Gatto, 2005).

Median peat losses from the NI treatments were nearly six times greater than those from the Non-NI treatments. The contribution of needle ice processes to soil loss observed in our study was significantly higher than in other flume experiments by Edwards and Burney (1987) and Frame et al. (1992) where soil losses by freeze–thaw were 90% and 24%, respectively. This difference is primarily a result of the needle ice formed in our study and the expansion reduced peat particle-to-particle bonds and increasing peat erodibility. The effect of needle ice processes on increasing peat erosion was higher at high flow rate, which is in agreement with Edwards and Burney (1987) and Ferrick and Gatto (2005) who found that the increase in soil erosion by freeze–thaw generally increased with greater overland flow.

For the NI treatment, the sediment concentration rate peaked early in the initial overland flow generation and then decreased to a final constant rate. Similar results were reported by Ferrick and Gatto (2005) who applied overland flow simulation tests with flow rates ranging from 0.4, 1.2, and 2.4 L min^{-1} on a bare silt soil following a single freeze–thaw cycle. Our observed peak probably corresponds to the period when peat aggregates subjected to needle ice processes were detached and transported by overland flow. The erosion pattern appeared to be transport-limited in the initial stage of overland flow generation as more loose sediments on the surface were available for overland flow transport as overland flow started to develop at a low rate. The peat loss rate in the steady state overland flow stage was much lower compared with the initial peak rate, despite the increase in the overland flow rate and the associated transport capacity. There are two possible reasons. First, this could be caused by exhaustion of the friable needle ice derived layer and an associated detachment-limited erosion pattern when steady state overland flow was achieved. Second, overland flow for the NI treatments was often concentrated; visual observations showed that microrills occurred. There were therefore also areas with a friable needle ice-derived peat layer but with little occurrence of overland flow, suggesting that not all friable peat materials were washed off by

running water. For the Non-NI treatment, the continuous low erosion rates with little temporal change indicated a detachment-limited system, as fresh peat is fibre-rich and highly resistant to water erosion, requiring a high flow velocity before continuous erosion of peat material occurs (Carling et al., 1997).

In this study, the main blanket peat erosion processes include sediment supply by needle ice processes and sediment transport by running water. Without sediment supply processes considered, sediment transport generally increases with an increase in overland flow velocity and the associated increased detachment capacity. Our results showed that peat blocks with needle ice treatments had greater hydraulic roughness and lower flow velocity which may indicate a lower sediment transport capacity. However, significantly greater sediment was measured on peat blocks with needle ice treatments than nonneedle ice treatments. This pattern shows that overland flow with relatively lower velocity is still capable of transporting more peat materials when more peat materials are available. The results demonstrate that where needle ice processes loosen particles from the peat surface, even small amounts of surface runoff may result in large amounts of erosion.

It has been widely reported that peatland streams have positive hysteresis in the relationship between suspended sediment concentration and discharge, showing peak suspended sediment concentration occurs ahead of peak flow (Evans and Warburton, 2007). The usual explanation for the positive hysteresis is sediment exhaustion as supply of erodible peat particles by weathering processes (e.g., rainsplash, freeze–thaw, and desiccation) is important for transport by water and wind. An alternative explanation for the positive hysteresis for areas with freeze-thaw needle ice is that overland flow on peat surfaces with needle ice formation and melting is easily spatially concentrated into efficient transport flowpaths, while areas with little occurrence of overland flow still have available friable peat layer that could be transported during future flow events.

4.5.4 Limitations

In order to produce quantifiable results with good levels of experimental control, bounded plots with inflow simulation techniques were used in this study. The size of the peat blocks we used was fairly small but meant that it was feasible to obtain undisturbed peat blocks for careful collection, transport, and storage in the laboratory. However, it should be noted that for natural peat deposits the depth of the friable upper layer disturbed by needle

ice may sometimes be 10 cm or more (Evans and Warburton, 2007), and so our experiments may underrepresent roughness effects that occur in the field, particularly where there is a much larger scale hummocky peat surface. There may also have been other effects on surface roughness if we had simulated repeated diurnal needle ice and thaw processes, and so these processes require further investigation. It should also be noted that our study used simulated upslope inflow and excluded responses to raindrop impact, while under natural rainfall conditions raindrops provide the primary force to initiate peat particle detachment (Li et al., 2018). Thus, more significant effects of needle ice processes on increasing peat erosion could be expected under combined rainfall and overland flow conditions and exploration of these processes could be undertaken in future work.

4.6 Conclusions

Overland flow derived peat erodibility was found to be minor for peat blocks not subject to needle ice processes. However, needle ice processes dramatically increased peat erodibility and reduced peat stability. Needle ice growth and expansion acts to detach particles from the otherwise resistant peat surface. Needle ice processes significantly reduced the surface flow velocity with the average reductions ranging from 32% to 44%, mainly through increased hydraulic roughness and changed surface microtopographic features, with microrills and headcuts developing. Needle ice treatments increased overland flow shear stress by 55–85%, compared with the treatments not subject to needle ice processes. Peat erosion rates for the needle ice treatments showed a significant linear relationship with stream power.

Peat erosion processes are determined by the combined effects of peat erodibility that is largely determined by needle ice processes and overland flow hydraulic characteristics. However, peat erosion processes can alter peat erodibility during a runoff event and can alter overland flow hydraulics by increasing suspended sediment content and changing surface roughness.

Median peat losses under needle ice treatments were nearly six times greater than those from treatments not subject to needle ice processes. Needle ice processes significantly increased peat erosion risk during overland flow events. This highlights that reducing bare areas of upland peat may play an important role in reducing peat erosion through protecting it from the disruptive effects of needle ice processes.

Needle ice is a primary process contributing to upland peat erosion by enhancing peat erodibility and modifying overland flow hydraulics including overland flow velocity and hydraulic roughness during run-off events that follow thaw. Models of overland flow-induced peat erosion should have a winter component that properly accounts for the effects of freeze–thaw (Li et al., 2016) and especially needle ice processes, in order to successfully predict hillslope erosion and sediment yield for watersheds in areas influenced by freezing and thawing.

Acknowledgments

The work was funded by the River Basin Processes and Management cluster, School of Geography (University of Leeds), the China Scholarship Council (File No. 201406040068) and the University of Leeds. Many thanks to Damian Lawler from the Centre for Agroecology, Water and Resilience, Coventry University (UK) who provided helpful suggestions through emails about how to produce needle ice under laboratory conditions. David Ashley from the School of Geography, University of Leeds is gratefully acknowledged for his assistance in preparing the experimental materials. Susanne Patel from the School of Chemical and Process Engineering, University of Leeds kindly provided use of the Malvern Morphologi G3S. The data used are listed in the tables in the manuscript and supplementary information.

References

BAGNOLD, R. A. 1966. *An approach to the sediment transport problem from general physics*, US government printing office.

BAN, Y., LEI, T., LIU, Z. & CHEN, C. 2016. Comparison of rill flow velocity over frozen and thawed slopes with electrolyte tracer method. *Journal of Hydrology,* 534**,** 630-637.

BOWER, M. 1960. Peat erosion in the Pennines. *Advancement of Science,* 64**,** 323-331.

BRANSON, J., LAWLER, D. & GLEN, J. 1996. Sediment inclusion events during needle ice growth: A laboratory investigation of the role of soil moisture and temperature fluctuations. *Water Resources Research,* 32**,** 459-466.

CARLING, P. A., GLAISTER, M. S. & FLINTHAM, T. P. 1997. The erodibility of upland soils and the design of preafforestation drainage networks in the United Kingdom. *Hydrological Processes,* 11**,** 1963-1980.

CHARMAN, D. 2002. *Peatlands and environmental change,* Chichester, UK, John Wiley & Sons Ltd.

CHOW, T., REES, H. & MONTEITH, J. 2000. Seasonal distribution of runoff and soil loss under four tillage treatments in the upper St. John River

valley New Brunswick, Canada. *Canadian Journal of Soil Science,* 80**,** 649-660.

CLARK, J. M., GALLEGO-SALA, A. V., ALLOTT, T., CHAPMAN, S., FAREWELL, T., FREEMAN, C., HOUSE, J., ORR, H. G., PRENTICE, I. C. & SMITH, P. 2010. Assessing the vulnerability of blanket peat to climate change using an ensemble of statistical bioclimatic envelope models. *Climate Research,* 45**,** 131-150.

EDWARDS, L., BURNEY, J. & FRAME, P. 1995. Rill sediment transport on a Prince Edward Island (Canada) fine sandy loam. *Soil Technology,* 8**,** 127-138.

EDWARDS, L. M. 2013. The effects of soil freeze–thaw on soil aggregate breakdown and concomitant sediment flow in Prince Edward Island: A review. *Canadian Journal of Soil Science,* 93**,** 459-472.

EDWARDS, L. M. & BURNEY, J. 1987. *Soil erosion losses under freeze/thaw and winter ground cover using a laboratory rainfall simulator*, National Research Council, Division of Building Research.

EDWARDS, L. M. & BURNEY, J. 1991. Sediment concentration of interrill runoff under varying soil, ground cover, soil compaction, and freezing regimes. *Journal of Environmental Quality,* 20**,** 403-407.

EVANS, M. & WARBURTON, J. 2007. *Geomorphology of upland peat: erosion, form and landscape change,* Oxford, UK, John Wiley & Sons.

FERRICK, M. & GATTO, L. W. 2005. Quantifying the effect of a freeze–thaw cycle on soil erosion: laboratory experiments. *Earth Surface Processes and Landforms,* 30**,** 1305-1326.

FITZGIBBON, J. 1981. Thawing of seasonally frozen ground in organic terrain in central Saskatchewan. *Canadian Journal of Earth Sciences,* 18**,** 1492-1496.

FOSTER, G. 1982. Modeling the erosion process. *In:* CT HAAN, JOHNSON, H. & BRAKENSIEK, D. (eds.) *Hydrologic Modeling of Small Watersheds.* American Society of Agricultural Engineers.

FRAME, P., BURNEY, J. & EDWARDS, L. 1992. Laboratory measurement of freeze thaw, compaction, residue and slope effects on rill erosion. *Canadian Agricultural Engineering,* 34**,** 143-149.

FRANCIS, I. 1990. Blanket peat erosion in a mid ‐ wales catchment during two drought years. *Earth Surface Processes and Landforms,* 15**,** 445-456.

GALLEGO-SALA, A., CLARK, J., HOUSE, J., ORR, H., PRENTICE, I. C., SMITH, P., FAREWELL, T. & CHAPMAN, S. 2010. Bioclimatic envelope model of climate change impacts on blanket peatland distribution in Great Britain. *Climate Research,* 45**,** 151-162.

GALLEGO-SALA, A. V. & PRENTICE, I. C. 2013. Blanket peat biome endangered by climate change. *Nature Climate Change,* 3**,** 152-155.

GATTO, L. W. 2000. Soil freeze–thaw-induced changes to a simulated rill: Potential impacts on soil erosion. *Geomorphology,* 32**,** 147-160.

GOVERS, G., GIMÉNEZ, R. & VAN OOST, K. 2007. Rill erosion: Exploring the relationship between experiments, modelling and field observations. *Earth-Science Reviews,* 84**,** 87-102.

GRAB, S. W. & DESCHAMPS, C. L. 2004. Geomorphological and geoecological controls and processes following gully development in alpine mires, Lesotho. *Arctic, Antarctic, and Alpine Research,* 36**,** 49-58.

GRAYSON, R., HOLDEN, J., JONES, R., CARLE, J. & LLOYD, A. 2012. Improving particulate carbon loss estimates in eroding peatlands through the use of terrestrial laser scanning. *Geomorphology,* 179**,** 240-248.

GROFFMAN, P. M., HARDY, J. P., FASHU-KANU, S., DRISCOLL, C. T., CLEAVITT, N. L., FAHEY, T. J. & FISK, M. C. 2011. Snow depth, soil freezing and nitrogen cycling in a northern hardwood forest landscape. *Biogeochemistry,* 102**,** 223-238.

HIGASHI, A. & CORTE, A. E. 1971. Solifluction: a model experiment. *Science,* 171**,** 480-482.

HOBBS, N. 1986. Mire morphology and the properties and behaviour of some British and foreign peats. *Quarterly Journal of Engineering Geology and Hydrogeology,* 19**,** 7-80.

HOLDEN, J. & BURT, T. P. 2003. Runoff production in blanket peat covered catchments. *Water Resources Research,* 39.

HOLDEN, J., KIRKBY, M. J., LANE, S. N., MILLEDGE, D. G., BROOKES, C. J., HOLDEN, V. & MCDONALD, A. T. 2008. Overland flow velocity and roughness properties in peatlands. *Water Resources Research,* 44**,** W06415.

IPCC 2007. Climate change 2007: The physical science basis. *Agenda.*

KATZ, D. M., WATTS, F. J. & BURROUGHS, E. R. 1995. Effects of surface roughness and rainfall impact on overland flow. *Journal of Hydraulic Engineering,* 121**,** 546-553.

KIM, Y., KIMBALL, J. S., MCDONALD, K. C. & GLASSY, J. 2011. Developing a global data record of daily landscape freeze/thaw status using satellite passive microwave remote sensing. *IEEE Transactions on Geoscience and Remote Sensing,* 49**,** 949-960.

KVÆRNØ, S. H. & ØYGARDEN, L. 2006. The influence of freeze–thaw cycles and soil moisture on aggregate stability of three soils in Norway. *Catena,* 67**,** 175-182.

LABADZ, J., BURT, T. & POTTER, A. 1991. Sediment yield and delivery in the blanket peat moorlands of the Southern Pennines. *Earth Surface Processes and Landforms,* 16**,** 255-271.

LAGUE, D., BRODU, N. & LEROUX, J. 2013. Accurate 3D comparison of complex topography with terrestrial laser scanner: Application to the Rangitikei canyon (NZ). *ISPRS Journal of Photogrammetry and Remote Sensing,* 82**,** 10-26.

LAWLER, D. 1986. River bank erosion and the influence of frost: a statistical examination. *Transactions of the Institute of British Geographers***,** 227-242.

LAWLER, D. 1988. Environmental limits of needle ice: a global survey. *Arctic and Alpine Research***,** 137-159.

LAWLER, D. 1993. Needle ice processes and sediment mobilization on river banks: the River Ilston, West Glamorgan, UK. *Journal of Hydrology,* 150**,** 81-114.

LAWLER, D. 2005. The importance of high-resolution monitoring in erosion and deposition dynamics studies: examples from estuarine and fluvial systems. *Geomorphology,* 64**,** 1-23.

LEGG, C., MALTBY, E. & PROCTOR, M. 1992. The ecology of severe moorland fire on the North York Moors: seed distribution and seedling establishment of Calluna vulgaris. *Journal of Ecology***,** 737-752.

LI, C., HOLDEN, J. & GRAYSON, R. 2018. Effects of rainfall, overland flow and their interactions on peatland interrill erosion processes. *Earth Surface Processes and Landforms,* 43**,** 1451-1464.

LI, G. & FAN, H. 2014. Effect of freeze-thaw on water stability of aggregates in a black soil of Northeast China. *Pedosphere,* 24**,** 285-290.

LI, P., HOLDEN, J., IRVINE, B. & GRAYSON, R. 2016. PESERA‐PEAT: a fluvial erosion model for blanket peatlands. *Earth Surface Processes and Landforms,* 41**,** 2058-2077.

LI, P., HOLDEN, J., IRVINE, B. & MU, X. 2017a. Erosion of Northern Hemisphere blanket peatlands under 21st‐century climate change. *Geophysical Research Letters,* 44**,** 3615-3623.

LI, P., IRVINE, B., HOLDEN, J. & MU, X. 2017b. Spatial variability of fluvial blanket peat erosion rates for the 21st Century modelled using PESERA-PEAT. *Catena,* 150**,** 302-316.

LIU, H., YANG, Y., ZHANG, K. & SUN, C. 2017. Soil Erosion as Affected by Freeze-Thaw Regime and Initial Soil Moisture Content. *Soil Science Society of America Journal,* 81**,** 459-467.

LUOTO, M. & SEPPÄLÄ, M. 2000. Summit peats ('peat cakes') on the fells of Finnish Lapland: continental fragments of blanket mires? *The Holocene,* 10**,** 229-241.

OUTCALT, S. I. 1970. A study of time dependence during serial needle ice events. *Archiv für Meteorologie, Geophysik und Bioklimatologie, Serie A,* 19**,** 329-337.

OUTCALT, S. I. 1971. An algorithm for needle ice growth. *Water Resources Research,* 7**,** 394-400.

OZTAS, T. & FAYETORBAY, F. 2003. Effect of freezing and thawing processes on soil aggregate stability. *Catena,* 52**,** 1-8.

REYNOLDS, O. 1883. XXIX. An experimental investigation of the circumstances which determine whether the motion of water shall he direct or sinuous, and of the law of resistance in parallel channels. *Philosophical Transactions of the Royal Society of London,* 174**,** 935-982.

TALLIS, J. 1973. Studies on southern Pennine peats: V. Direct observations on peat erosion and peat hydrology at Featherbed Moss, Derbyshire. *The Journal of Ecology,* 61**,** 1-22.

VAN KLAVEREN, R. & MCCOOL, D. 1998. Erodibility and critical shear of a previously frozen soil. *Transactions of the ASAE,* 41**,** 1315.

VAN KLAVEREN, R. W. & MCCOOL, D. K. 2010. Freeze–thaw and water tension effects on soil detachment. *Soil Science Society of America Journal,* 74**,** 1327-1338.

WANG, D.-Y., MA, W., NIU, Y.-H., CHANG, X.-X. & WEN, Z. 2007. Effects of cyclic freezing and thawing on mechanical properties of Qinghai–Tibet clay. *Cold Regions Science and Technology,* 48**,** 34-43.

WISCHMEIER, W. H. & SMITH, D. D. 1978. *Predicting rainfall erosion losses-a guide to conservation planning,* Hyattsville, Maryland USDA, Science and Education Administration

XU, J., MORRIS, P. J., LIU, J. & HOLDEN, J. 2018. PEATMAP: Refining estimates of global peatland distribution based on a meta-analysis. *Catena,* 160**,** 134-140.

YU, Z. 2012. Northern peatland carbon stocks and dynamics: a review. *Biogeosciences,* 9**,** 4071-4085.

Chapter 5
Patterns and drivers of peat topographic changes determined from Structure-from-Motion photogrammetry at field plot and laboratory scales

Changjia Li, Richard Grayson, Mark Smith, Joseph Holden. Patterns and drivers of peat erosion via using Structure-from-Motion photogrammetry at field plot and laboratory scales. *Earth Surface Processes and Landforms* (accepted).

5.1 Abstract

Little is known about the spatial and temporal variability of peat erosion nor some of its topographic and weather-related drivers. We present field and laboratory observations of peat erosion using Structure-from-Motion (SfM) photogrammetry. Over a 12 month period, 11 repeated SfM surveys were conducted on four geomorphological sites of 18–28 m^2 (peat hagg, gully wall, riparian area and gully head) in a blanket peatland in northern England. A net topographic change of –14 to +30 mm yr^{-1} for the four sites was observed during the whole monitoring period. Cold conditions in the winter of 2016 resulted in highly variable volume change (net surface topographic rise first and lowering afterwards) via freeze–thaw processes. Long periods of dry conditions in the summer of 2017 led to desiccation and drying and cracking of the peat surface and a corresponding surface lowering. Topographic changes were mainly observed over short-term intervals when intense rainfall, flow wash, needle-ice production or surface desiccation was observed. In the laboratory, we applied rainfall simulations on peat blocks and compared the peat losses quantified by traditional sediment flux measurements with SfM derived topographic data. The magnitude of topographic change determined by SfM (mean value: 0.7 mm, SD: 4.3 mm) was very different to the areal average determined by the sediment yield from the block (mean value: –0.1 mm, SD: 0.1 mm). Topographic controls on spatial patterns of topographic change were illustrated from both field and laboratory surveys. Roughness was positively correlated to positive topographic change and was negatively correlated to negative topographic

change at field plot scale and laboratory macroscale. Overall, the importance of event-scale change and the direct relationship between surface roughness and the rate of topographic change are important characteristics which we suggest are generalizable to other environments.

Keywords: peatlands; SfM; topographic change; topographic variables; roughness

5.2 Introduction

Peatlands cover approximately 2.84% of global land area (Xu et al., 2018) while storing one third to one half of the world's soil carbon (Yu, 2012). They are globally important for providing various other ecosystem services including those associated with water, food, fibre and leisure (Bonn et al., 2016). Most of these sorts of services are impaired by accelerated peat erosion (Evans and Lindsay, 2010b). Of particular concern is erosion of blanket peatlands which are rain-fed and occur on sloping terrain and thus are potentially more vulnerable to water erosion than other peatland types (Li et al., 2017). Disturbance such as atmospheric pollution, grazing pressure or fire can remove sensitive vegetation which can be followed by rapid incision (Evans and Warburton, 2007). Many blanket peatlands in the Northern Hemisphere have experienced severe erosion (Evans and Warburton, 2007, Grayson et al., 2012, Li et al., 2016b) and are under increasing erosion risk from future climate change (Li et al., 2016a, Li et al., 2017) which will enhance losses of terrestrial carbon in many regions.

The main erosion processes affecting blanket peatlands include sediment supply processes such as freeze–thaw and desiccation, and sediment transport by running water via interrill and gully erosion (Bower, 1961, Evans and Warburton, 2007, Li et al., 2018c, Li et al., 2018b, Li et al., 2018a). Freezing and thawing of water between peat particles is common in cool, high latitude or high altitude climates which support many peatlands, and plays a vital role in breaking up the peat surface during winter months (Francis, 1990, Labadz et al., 1991, Evans and Warburton, 2007, Li et al., 2018b). Surface desiccation during extended periods of dry weather is another important weathering process for producing erodible peat (Burt and Gardiner, 1984, Evans et al., 1999, Francis, 1990, Holden and Burt, 2002a). Interrill erosion is an important process acting at the hillslope scale in blanket

peatlands (Bower, 1961) and is a major source of peat and particulate carbon loss where vegetation has been damaged (Grayson et al., 2012). In addition, incision of deep gully systems into the peat surface is an extensive feature in many eroded peatlands (Bower, 1961, Evans and Warburton, 2007). Previous studies have highlighted the role of gully development and its contribution to the overall sediment yield (Evans et al., 2006, Evans and Warburton, 2007, Evans and Lindsay, 2010a).

Numerous direct and indirect methods have been used to measure peat erosion, including erosion pins (Evans and Warburton, 2005) and bounded plots (Holden et al., 2008, Li et al., 2018c, Li et al., 2018b), and more recently modern high resolution topographic surveying methods to improve quantification of erosion (Evans and Lindsay, 2010a, Rothwell et al., 2010, Evans and Lindsay, 2010b, Grayson et al., 2012, Glendell et al., 2017). Erosion plots are used commonly to measure soil erosion over short and medium time periods (Iserloh et al., 2013, Martínez-Murillo et al., 2013) and have previously been applied to peatlands (e.g. Holden and Burt (2002a), Grayson et al. (2012), Li et al. (2018c)). Bounded plots are usually equipped with troughs or sediment collectors to catch exported sediment directly under natural precipitation or rainfall simulations (Holden and Burt, 2002a, Holden and Burt, 2002b, Holden and Burt, 2003, Holden et al., 2008, Li et al., 2018c, Li et al., 2018b, Kløve, 1998). While plot scale or catchment yield studies have supported understanding of peat erosion they usually allow the measurement of the soil loss reaching the plot or catchment outlet, which is then averaged for the entire plot area (Parsons et al., 2006b). The data integrate all upslope processes at a single point (Smith and Vericat, 2015). It is difficult to assess the spatial variation of erosion and deposition and the drivers within the plot due to the lack of sufficient data. Direct measurements of surface denudation with high accuracy would therefore be preferable if we are to understand more about erosion processes.

Remote sensing techniques such as terrestrial laser scanning and digital photogrammetry provide an alternative to erosion plots by constructing 3D surfaces at set intervals and estimating the differences between these surfaces (Smith et al., 2016). Several studies have applied high resolution airborne LiDAR digital elevation models (DEMs) in combination with digital terrain analysis to identify and map landscape features, such as the extent of gully erosion in blanket peatlands (Rothwell et al., 2010, Evans and Lindsay, 2010a, Evans and Lindsay, 2010b, Evans et al., 2005). Grayson et al. (2012) examined the performance of terrestrial laser scanners (ground-based

LiDAR) in measuring peat surface retreat rate, and found that terrestrial laser scanning i) allows accurate measurements of the volume of peat lost (or gained) over time at particular test points and ii) provided high resolution spatial data on surface elevation change. However, the use of these remote sensing techniques appears to be limited by high expense and time required for set up (Morgan et al., 2017, Smith et al., 2016).

In recent years, automatic photogrammetric procedures based on SfM and Multi-View Stereo techniques (SfM-MVS) have been widely used in mapping erosion and quantifying their magnitude both in the field and in the laboratory (Prosdocimi et al., 2017, Glendell et al., 2017, Smith et al., 2016, Smith and Vericat, 2015, Micheletti et al., 2015b, Micheletti et al., 2015a, Eltner et al., 2017, Kaiser et al., 2014, Stöcker et al., 2015). However, to the best of our knowledge, there are only two studies that have been reported using and testing the application of SfM techniques in peatlands. Glendell et al. (2017) compared the cost-effectiveness and accuracy of terrestrial laser scanning, aerial (UAV-SfM) and ground-based SfM photogrammetry (GB-SfM) in quantifying the extent of gully erosion in upland landscapes. They found that GB-SfM was the best of the three techniques at measuring the volumes of erosion features at fine spatial resolution. Smith and Warburton (2018) used ground-based SfM surveys to quantify roughness for different peat surfaces and found that SfM was reliable to identify roughness signatures over bare peat plots (< 1 m^2). However, despite the application of new peat surveying techniques there has been a lack of their use to specifically understand spatial and temporal peat erosion dynamics or processes in a range of peatland environments.

This study aims to apply SfM topographic reconstruction to study dominant peat erosion processes at field plot and laboratory macro scales. The specific objectives are to:

(i) Examine the spatial and temporal variability of topographic change patterns on peat erosion sites using repeat SfM surveys.

(ii) Investigate erosional-depositional processes and their controlling topographic and weather-related drivers.

(iii) Compare peat interrill erosion rates determined by laboratory plot sediment flux and by SfM photogrammetry.

5.3 Materials and Methods

5.3.1 Field experiments

5.3.1.1 Study area

Extensive peat erosion in the UK occurs across many blanket peatlands, especially in the Pennine region of England (Bower, 1960a, Bower, 1961, Evans and Warburton, 2007). Fleet Moss (SD 86 83; 54°07´N, 2°16´W) is an area of approximately 1.0 km^2 with deep upland blanket peat at an altitude of 550–580m in the Yorkshire Dales, England (Figure 5.1 (a)). The study area is a catchment within Fleet Moss, with a large area of exposed bare peat actively eroding with sheet erosion and gullying. There are well developed and connected Type 1 and Type 2 gully systems (Li et al., 2018a): Type 1 dissection usually occurs on the flatter interfluve areas where peat is usually 1.5–2.0 m in depth on slopes less than 5° (Bower, 1960a), with gullies frequently branching and intersecting as an intricate dendritic network; Type 2 dissection dominates on steeper slopes (exceeding 5°), with a system of sparsely branched drainage gullies incised through the peat and aligned nearly parallel to each other. The vegetation is dominated primarily by *Eriophorum* vaginatum, *Calluna* vulgaris and *Empetrum* nigrum.

Four field sites across Fleet Moss with different types of erosion features were selected for survey (Figure 5.1). The peat hagg (Site 1) was an erosional escarpment with different active processes occurring in different positions (Evans and Warburton, 2007). Slump, saltation and lateral rain and wind impact are likely dominant on the upper slope; sheet wash and needle ice and freeze–thaw are probably dominant on the middle slope; while saltation and rill development are more likely along the lower slope (Evans and Warburton, 2007). Site 2 is a lateral-bank headcut on a gully wall for a ‘V’ shaped gully profile (Bower, 1960a), and Site 4 is a main headcut of the gully. Both Site 2 and Site 4 are characterized by Type II gully erosion that has unbranched channels aligned normal to the slope on steeper ground with a mean slope gradient above 17° (Bower, 1960b). Site 3 is a flat toeslope area adjacent to the stream.

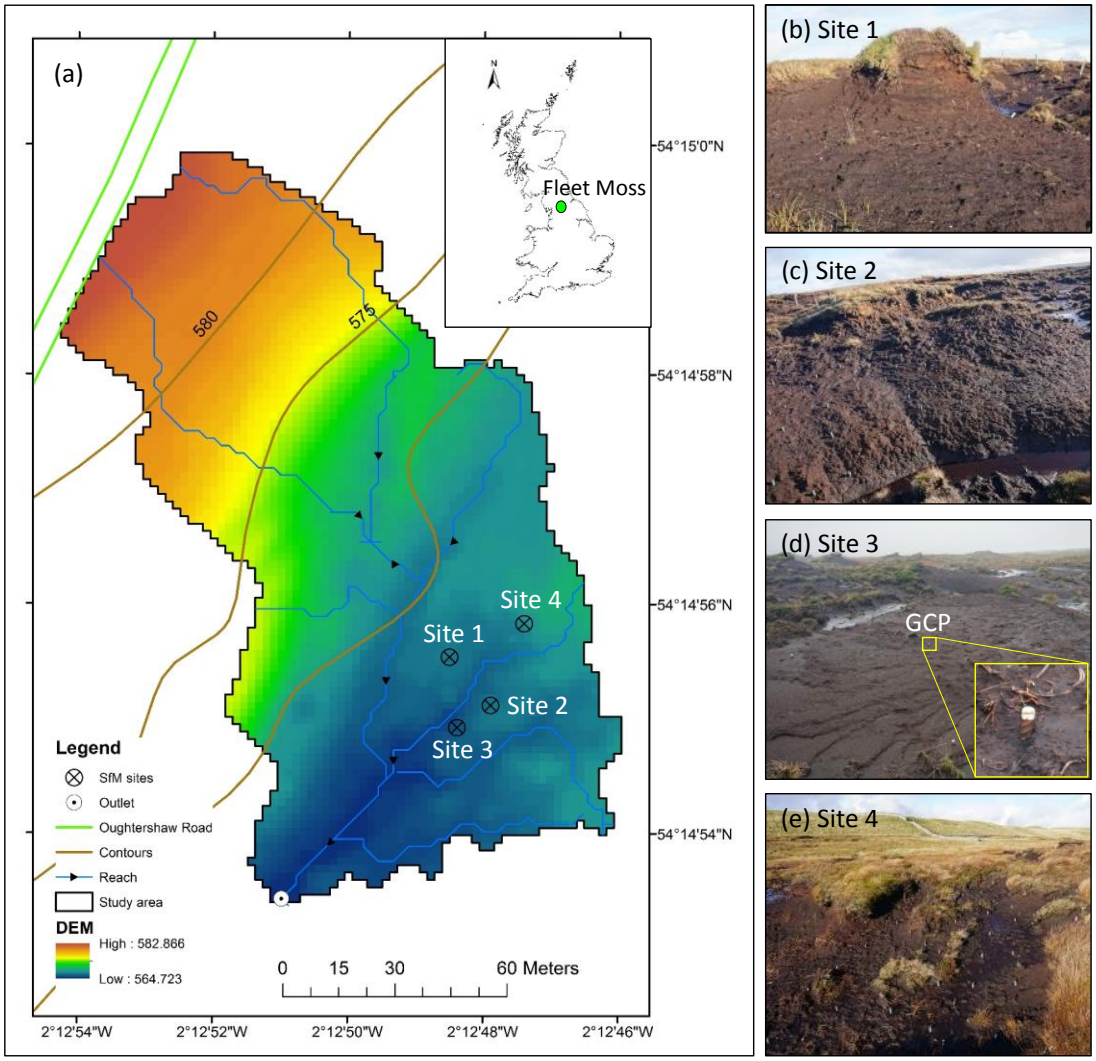

Figure 5.1 (a) Map showing the location of Fleet Moss and the distribution of SfM surveyed sites with different erosion features. A digital elevation model (DEM) across Fleet Moss was provided based on LiDAR data (2 m ground resolution, 250 mm z resolution); (b) Site 1 (21.3 m^2) is a peat hagg that is severely eroded by wind; (c) Site 2 (25.9 m^2) is a peat gully wall side; (d) Site 3 (27.5 m^2) is a flat hilltoe area adjacent to the stream. One of the GCPs used in the study can also be seen; (e) Site 4 (19.3 m^2) is a gully head.

5.3.1.2 Data acquisition

Weather data

Precipitation was measured by a digital tipping bucket raingauge at 15–minute intervals from 15/10/2016 to 15/11/2017 (Figure 5.2 (a)). Temperature loggers (Tinytag Plus 2) were used at the peat surface recording at 10–minute intervals from 26/10/2016 to 20/07/2017 (Figure 5.2 (b)). Temperature data was not recorded since 20/07/2017 due to malfunctioning loggers. Mean annual rainfall at a nearby long-term rain gauge at Snaizeholme (54°17´20´´N, 2°15´28´´W and 260 m altitude) is

1740 mm (1961–2017) with a maximum of 2667 mm and minimum of 1296 mm (UK National River Flow Archive, 2018). Rainfall during 2016 was 1655 mm at Snaizeholme and 1723 mm in 2017. Our own gauge at Fleet Moss (570 m altitude) recorded 1997 mm between 1 November 2016 and 31 October 2017 while the value was 1677 mm for Snaizeholme. While spring 2017 rainfall (329 mm at Fleet Moss) was close to the long-term Snaizeholme mean value of 319 mm, there was a dry period between 1 April and 12 May with only 23.2 mm. During 2017 the mean annual temperature for the Yorkshire Dales where Fleet Moss is located was 0.2–0.5 ºC greater than the 30-year annual mean (1981–2010). Spring 2017 was substantially warmer with a mean temperature 1.0–1.5 ºC greater than that of the 1981–2010 average (UK Met Office, 2018).

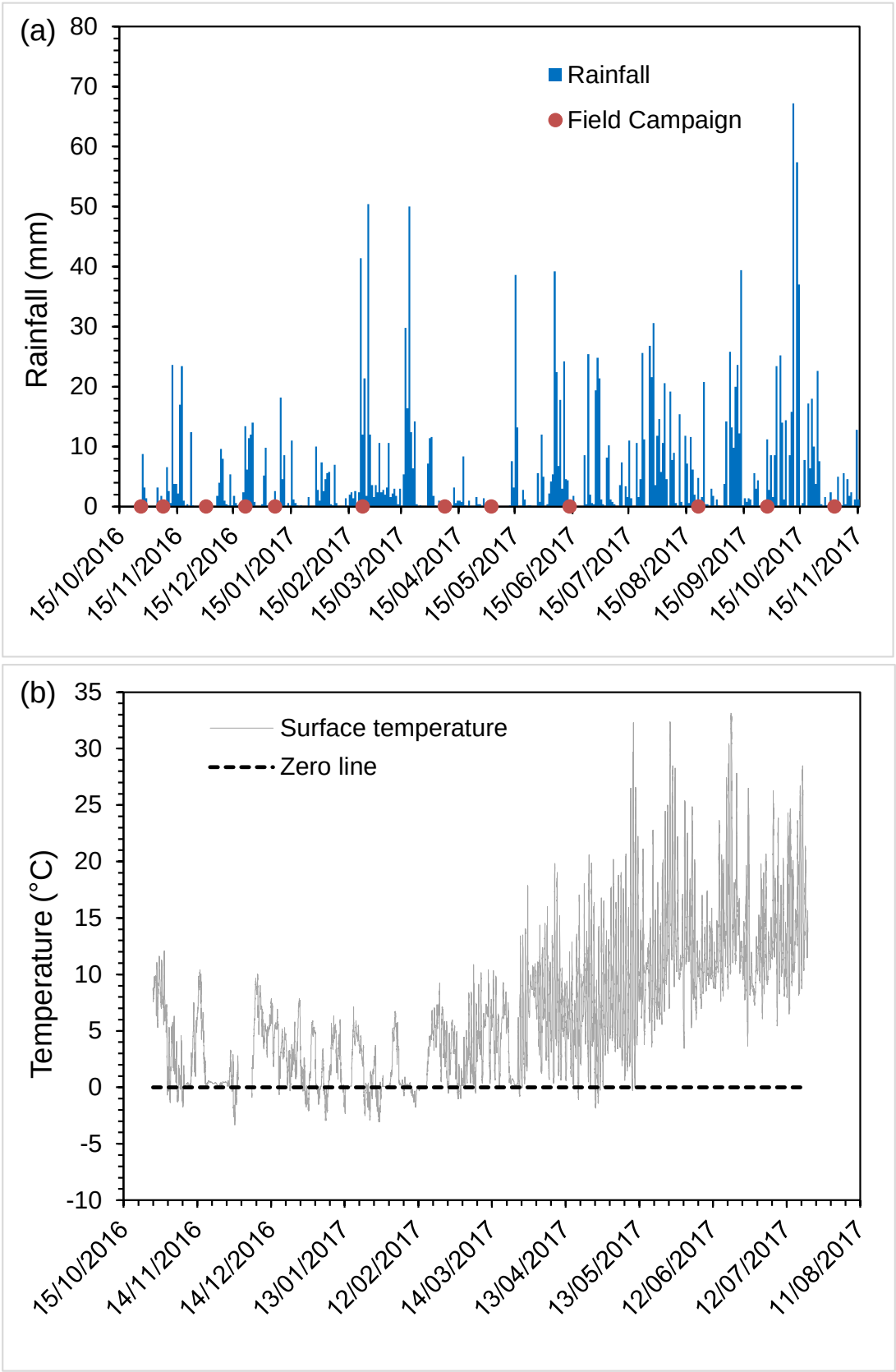

Figure 5.2 Meteorological data during the intensive survey period including (a) daily total rainfall and (b) peat surface temperature. Time of SfM measurements are indicated with red points in diagram (a). Dashed black line in diagram (b) indicates the freezing threshold (i.e. 0 °C).

SfM Photogrammetry

SfM photogrammetry calculates three-dimensional (3D) surface models from 2D images via a workflow comprising: (i) keypoint detection and matching; (ii) bundle adjustment algorithms to identify scene geometry and camera interior and exterior parameters simultaneously; (iii) georeferencing using control points identified in imagery and application of a standard seven-parameter rigid body transform; and (iv) application of multi-view stereo image matching algorithms to yield the final dense point cloud. For full details of the SfM workflow see James and Robson (2012) and Smith et al. (2016). An object of interest is observed from overlapping images acquired from different positions. From 26/10/2016 to 02/11/2017, the four sites were surveyed 11 times (Figure 5.1 (a)). Weather conditions during field campaigns can significantly influence data quality (Snapir et al., 2014, Stöcker et al., 2015). Image acquisition was mainly conducted under conditions with no strong wind, no rain or no snow cover. However, sunny weather during the November campaign (04/11/2016) produced images with shadows that resulted in decreasing contrast and some data gaps where no image points could be extracted. For the other 10 field campaigns, data acquisition was arranged to avoid sunny conditions in order to enable diffuse illumination conditions and minimize shadows.

Abundant high quality images were subsequently taken at positions and angles that have sufficient coverage of the peat erosion features of interest. In specific erosion features (i.e. gully heads, peat hagg), the density of images from additional perspectives was increased for further detailed reconstruction. The camera used was a Sony ILCE-6000 24 mega pixel digital camera with a 16 mm focal length. Camera settings varied based on light conditions, with exposure between 160 and 320 ISO, F-stop between f/4 and f/4.5 and exposure time between 1/160 and 1/80 second.

Between 8 and 12 permanent Ground Control Points (GCPs) made of rebar (0.5–1.0 m in length) were placed around and within each feature (Figure 5.1 (d) and Table 5.1). The rebar was hammered deep into the substrate below the peat with a painted white top (high contrast with the dark peat surface). A geodimeter was used and full surveys of the relative coordinates of all the GCPs were carried out at the start of the monitoring period.

Table 5.1 Summary of georeferencing errors (i.e. RMSE on control points) for the field surveys. The Six GCPs were used to reconstruct dense points for the field models. Notes refer to weather conditions on the date of survey.

Site	Survey date	No.	No. of images	Georeferencing RMSE (mm)	Notes
	26/10/2016	1	69	52.4	
	04/11/2016	2	97	53.4	
	30/11/2016	3	79	50.7	Freezing/Needle-ice
	21/12/2016	4	101	56.9	Slightly misty/ Needle-ice
	22/02/2017	5	93	56.6	Needle-ice thaw
Site 1	07/04/2017	6	88	44.4	Slight desiccation
	02/05/2017	7	74	47.4	Serious desiccation
	13/06/2017	8	79	46.8	
	21/08/2017	9	50	41.6	
	27/09/2017	10	112	59.3	
	02/11/2017	11	48	54.3	
	26/10/2016	1	47	16.5	
	04/11/2016	2	137	17.7	
	30/11/2016	3	60	23.6	Needle-ice formation
	21/12/2016	4	85	25.0	Needle-ice thawing/ misty
	22/02/2017	5	101	21.3	Needle-ice thaw
Site 2	07/04/2017	6	123	18.4	Slight desiccation
	02/05/2017	7	136	20.7	Serious desiccation
	13/06/2017	8	134	15.9	
	21/08/2017	9	107	18.8	
	27/09/2017	10	114	17.4	
	02/11/2017	11	41	18.6	
	26/10/2016	1	23	39.7	
	04/11/2016	2	68	41.6	
	30/11/2016	3	80	39.1	Freezing/Needle-ice
	21/12/2016	4	114	41.7	Misty
	22/02/2017	5	94	41.1	Needle-ice thaw
Site 3	07/04/2017	6	54	40.5	Slight desiccation
	02/05/2017	7	102	40.7	Serious desiccation
	13/06/2017	8	64	45.5	
	21/08/2017	9	73	41.9	
	27/09/2017	10	76	43.3	
	02/11/2017	11	35	38.3	
	26/10/2016	1	53	39.1	
	04/11/2016	2	52	23.1	
	22/02/2017	3	110	16.3	Needle-ice thaw
Site 4	07/04/2017	4	156	16.6	Slight desiccation
	02/05/2017	5	131	14.8	Serious desiccation
	13/06/2017	6	134	19.6	
	21/08/2017	7	90	16.1	

Site	Survey date	No.	No. of images	Georeferencing RMSE (mm)	Notes
	27/09/2017	8	79	17.2	
	02/11/2017	9	41	16.9	

5.3.2 Laboratory experiments

5.3.2.1 Material

Bare peat blocks were collected from the upper peat layer at Moor House National Nature Reserve (NNR) (54°41'N, 2°23'W), a blanket peat site in the North Pennines of England. A plastic rectangular gutter (1.0 m long, 0.13 m wide and 0.08 m in depth) was pushed into the peat parallel to the peat surface, and carefully dug out to extract an undisturbed peat block. All samples were tightly sealed using plastic film to minimize peat oxidation and drying before being stored at 4°C prior to laboratory analysis. Basic chemical and physical properties of the peat blocks were determined on subsampled peat (Li et al., 2018c).

The experiment used a 'drip-type' rainfall simulator (Bowyer-Bower and Burt, 1989, Holden and Burt, 2002a), a Mariotte bottle located at the upslope plot boundary to provide upslope inflow at a constant rate and a 1.0 m long by 0.13 m wide soil flume. The general set-ups and operating principles of the rainfall simulator, inflow device and soil flume are illustrated in Li et al. (2018c).

5.3.2.2 Experimental design

For interrill erosion on gentle peat slopes, peat particle detachment and transport are simultaneously influenced by rainfall-driven and flow-driven erosion processes and their interaction (Li et al., 2018c). In this study, the slopes were set at 2.5° and 7.5° to represent either side of the transition (5°) between Type 1 (heavily branching) and Type 2 (linear) dissection of gully systems (Bower, 1960a) and also being representative of typical blanket peatland slopes in the Pennine region of England. For each slope gradient, three treatments were conducted on the bare peat blocks (Table 5.2):

(i) Rainfall events to simulate rainfall-driven erosion processes: Rainfall was applied at an intensity of 12 mm hr^{-1} for a duration of 120 min.

(ii) Inflow events to simulate flow-driven erosion processes: Upslope inflow was applied with a constant rate of 12 mm hr^{-1} determined by a volumetric method and which corresponded to 12 mm hr^{-1} rainfall on the studied plots.

(iii) Rainfall + Inflow events to simulate the combined impacts of rainfall and flow on erosion processes. Both rainfall (12 mm hr^{-1}) and upslope inflow (12 mm hr^{-1}) were applied simultaneously.

Table 5.2 Summary of the laboratory experimental design and treatments.

Slope	Treatment	Replicate	Total Water Supply (mm hr^{-1})	Rainfall Intensity (mm hr^{-1})	Upslope Inflow Rate (mm hr^{-1})	Duration (min)
2.5°	Rainfall	1	12	12	0	120
		2	12	12	0	120
	Inflow	1	12	0	12	120
		2	12	0	12	120
	Rainfall + Inflow	1	24	12	12	120
		2	24	12	12	120
7.5°	Rainfall	1	12	12	0	120
		2	12	12	0	120
	Inflow	1	12	0	12	120
		2	12	0	12	120
	Rainfall + Inflow	1	24	12	12	120
		2	24	12	12	120

5.3.2.3 Data acquisition

Sediment flux method

During each run the time of overland flow-initiation was recorded, after which each test lasted for 120 minutes. Total surface overland flow was sampled at the plot outlet every 5 minutes. Overland flow volumes for each sample were determined using a measuring cylinder. Overland flow rates (mL s^{-1}) were subsequently determined by dividing these overland flow volumes by the sampling duration. Samples were then left to settle for six hours to allow deposition of the suspended sediment. The clear supernatant was decanted, and the remaining turbid liquid was transferred to a rectangular foil container and oven-dried at 65.0°C until a constant weight was achieved. The dry sediment mass (in milligrams) was calculated, and the sediment concentration (in mg mL^{-1}) was determined as the ratio of dry sediment mass to the overland flow volume. The sediment yield rate (in mg m^{-2} s^{-1}) was defined as the ratio of dry sediment mass per unit area per sampling duration. The sediment flux data on peat blocks was reported in Li et al. (2018c) which provides a data set for comparison with the laboratory scale SfM data which is, for the first time, presented in this new paper.

SfM Photogrammetry

In addition to the sediment flux approach, high resolution topographic data derived from SfM photogrammetry was acquired before and after each rainfall simulation experiment. Overlapping oblique 2D images of each plot, pre- and post-event, were taken using a FUJIFILM FinePix AX650 16 mega pixel digital camera with focal length set at 6 mm and with automatic exposure enabled. 23 GCPs were positioned along the boundaries of the flume and were marked with high-visibility markers. A local co-ordinate system was used and the relative co-ordinates of the 23 GCPs were determined by measurements and geometric calculation.

Table 5.3 Summary of georeferencing errors (i.e. RMSE on control points) for the laboratory surveys.

Survey	No. of images	No. of GCPs	Georeferencing RMSE (mm)
Rainfall[a] (2.5°)[b]_test 1[c]_pre[d]	38	23	4.5
Rainfall (2.5°)_test 1_post	54	23	4.5
Rainfall (2.5°)_test 2_pre	63	23	4.6
Rainfall (2.5°)_test 2_post	73	23	4.7
Inflow (2.5°)_test 1_pre	57	23	4.5
Inflow (2.5°)_test 1_post	63	23	4.6
Inflow (2.5°)_test 2_pre	48	23	4.2
Inflow (2.5°)_test 2_post	51	23	4.6
Rainfall + Inflow (2.5°)_test 1_pre	51	23	5.1
Rainfall + Inflow (2.5°)_test 1_post	48	23	4.2
Rainfall + Inflow (2.5°)_test 2_pre	54	23	4.5
Rainfall + Inflow (2.5°)_test 2_post	61	23	4.6
Rainfall (7.5°)_test 1_pre	33	23	4.2
Rainfall (7.5°)_test 1_post	52	23	4.6
Rainfall (7.5°)_test 2_pre	43	23	4.4
Rainfall (7.5°)_test 2_post	52	23	4.6
Inflow (7.5°)_test 1_pre	33	23	4.5
Inflow (7.5°)_test 1_post	43	23	4.4
Inflow (7.5°)_test 2_pre	34	23	5.6
Inflow (7.5°)_test 2_post	48	23	4.6
Rainfall + Inflow (7.5°)_test 1_pre	39	23	4.5
Rainfall + Inflow (7.5°)_test 1_post	34	23	5.6
Rainfall + Inflow (7.5°)_test 2_pre	52	23	4.6
Rainfall + Inflow (7.5°)_test 2_post	43	23	5.3

a: three types of laboratory experiments include Rainfall events, Inflow events and Rainfall + Inflow events;
b: two slope gradients include 2.5° and 7.5°;
c: two replicates for each type of simulation experiments include test 1 and test 2;
d: two surveys for each test include survey before and after the laboratory simulation tests.

5.3.3 Data analysis

5.3.3.1 SfM data processing

Images acquired were processed using the commercial software Agisoft PhotoScan. First, image quality was checked visually and by estimating image quality through Photoscan. Any blurred images or those with a quality score < 0.5 were removed. Second, photographs were aligned to produce a sparse point cloud and the default setting with the photo alignment accuracy was set to “highest”. Tie points were refined by gradual selection in Photoscan based on criteria of “reprojection error” and “reconstruction uncertainty”. Third, GCPs were identified in each photograph to georeference the sparse cloud. The residual georeferencing errors were calculated and point-cloud quality was evaluated by summarizing residual errors using root mean squared error (*RMSE*) (Smith et al., 2014). Poorly located GCPs were excluded; however, a minimum of six GCPs that were well distributed over each site remained (Fonstad et al., 2013, Smith et al., 2014). Mean georeferencing uncertainty in the final point clouds was 33 mm for the field data (*RMSE*; Table 5.1) and was 5 mm for the laboratory data (*RMSE*; Table 5.3). Fourth, a dense point cloud was subsequently produced using PhotoScan’s multiview stereo (*MVS*) algorithm. Dense cloud quality was set to “Highest” for laboratory data processing and “medium” for field data processing as a compromise between model quality and processing time. The dense cloud was subsequently edited to remove noise points such as those not on solid surfaces.

5.3.3.2 Point cloud differencing

Lague et al. (2013) provided a detailed review of the main advantages and drawbacks of the approaches normally used (e.g., DEM of difference, C2C, M3C2) to measure the distance between two point clouds. In our study the Cloud-to-cloud differencing was computed using the Multiscale Model to Model Cloud Comparison (M3C2) algorithm due to its ability to quantify the 3-D distance between two point clouds along the normal surface direction and provide a 95% confidence interval based on the point cloud roughness and co-registration uncertainty (Lague et al., 2013). The M3C2 tool is available in the open source CloudCompare software and has been widely used in a range of environments (Lague et al., 2013, Watson et al., 2017, Mallalieu et al., 2017, Barnhart and Crosby, 2013, Gómez-Gutiérrez et al., 2015, Stumpf et al., 2015, Morgan et al., 2017). The general concept behind

M3C2 is to compute Cloud 1 to Cloud 2 distances using a local normal direction that is defined by fitting a plane to all of the points within a sphere that has a diameter *D* (the 'normal diameter') around a given core point *i*. Once the point normal direction is computed, the algorithm subsequently creates a cylinder oriented along the normal direction, with a diameter *d* (the 'projection diameter') specified by the user. All of the points in Cloud 1 and Cloud 2 that reside in the cylinder are spatially averaged to determine mean surface positions, i_1 and i_2, respectively. L_{M3C2} is the distance between i_1 and i_2 and is stored as an attribute of *i* (Lague et al., 2013).

M3C2 requires users to define two main parameters: i) the normal scale *D*, which is used to calculate a surface normal for each point and is dependent upon surface roughness and registration error; ii) the projection scale *d* within which the average surface elevation of each cloud is calculated. In this study, the normal scale *D* for each point cloud was estimated based on a trial-and-error approach similar to that of Westoby et al. (2016), to reduce the estimated normal error, E_{norm} (%), through refinement of a rescaled measure of the normal scale *n*(*i*):

$$n(i) = \frac{D}{\sigma_i(D)} \tag{5.1}$$

where n(*i*) is the normal scale *D* divided by the roughness *σ* measured at the same scale around *i* and where *n*(*i*) falls in the range 20–25, E_{norm} < 2% (Lague et al., 2013). In this study for the field data processing, normal scale *D* ranged from 0.3 to 0.5 m and projection scale *d* was specified as 0.1 m and this scaling was enough to average a minimum of 30 points sampled in each cloud (Lague et al., 2013). For the laboratory data processing, normal scale *D* was fixed at 0.05 m and projection scale *d* was specified as 0.005 m.

Cloud-to-cloud distance was projected onto the original point cloud. In addition to the distance, M3C2 reports the number of points within the projection cylinder (a measure of local point density) and the standard deviation of the points within the cylinder (a measure of local roughness). A spatially variable confidence interval (SVCI) was proposed to account for the precision of the M3C2 distance affected by the local point density, roughness and the registration error (Lague et al., 2013). M3C2 output was subsequently masked to exclude points where change is lower than Level of Detection (LoD) threshold for a 95% confidence level, which is defined as:

$$LOD_{95\%}(d) = \pm 1.96\left(\sqrt{\frac{\sigma_1(d)^2}{n_1} + \frac{\sigma_2(d)^2}{n_2}} + reg\right) \tag{5.2}$$

where σ_1 and σ_2 represent the roughness of each point in sub-clouds of diameter *d* and size n_1 and n_2, and *reg* is the user-specified registration error which is assumed to be isotropic and spatially uniform across the dataset (Lague et al., 2013). The surface-to-surface Interactive Closest Point algorithm implemented in CloudCompare was used to align a patch of two inactive point clouds. The registration error was estimated by a series of tests, and it ranged from 4.5 mm to 5.0 mm for the field models and ranged from 0.7 mm to 0.8 mm for the laboratory models. Distance calculations were masked to exclude points where the change was lower than the $LoD_{95\%}$ threshold.

For each field site, data analyses were conducted on two temporal scales: (a) between individual survey dates and (b) longer-term seasonal to annual change. Survey dates and intervals are presented in Table 5.4. Between 26/10/2016 and 02/11/2017 the 11 repeat topographic surveys yielded 10 short-term survey intervals (e.g., 2–1; 3–2) and a long-term survey interval (11–1). The length of the short-term scale survey intervals ranged from 10 days (26/10/2016–04/11/2016) to 69 days (13/06/2017–21/08/2017). The long-term survey interval was selected to represent potential large topographic changes.

5.3.3.3 Other data analysis

For all points with calculated M3C2 distance above the LoD threshold at 95% confidence level, topographic variables were analyzed for statistical relationships with observed M3C2 changes. The topographic variables examined were aspect, slope, curvature, profile curvature, plan curvature and roughness; these variables were derived from surface analyst tools in ArcGIS 10.4 based on DEM deriving from point clouds gridded at 0.01 m for field models and 0.001 m for laboratory models. The variables were extracted to point datasets that were tested for normality using the Anderson–Darling normality test. Spearman's rank correlation and stepwise regression were used to test for relationships between topographic factors and topographic change.

Six meteorological variables were calculated to determine the meteorological influence on observed temporal variability of topographic change for field short-term surveys. The calculated variables included: (i) number of days between SfM surveys, (ii) number of rainy days, (iii) total rainfall (mm), (iv) maximum 15–minute rainfall intensity, (v) mean temperature, (vi) number of days below freezing (i.e. 0 °C; calculated as the number of days in which at least one value below 0 °C was registered in the 10–minute interval

temperature data set) and (vi) number of frost cycles. Datasets were tested for normality using the Anderson–Darling normality test and the Spearman's rank correlation was used to find the relationship between meteorological variables and topographic changes.

5.4 Results

5.4.1 Field results

5.4.1.1 M3C2 differences of peat surface from multi-temporal field surveys

M3C2 differences above Level of Detection threshold at 95% confidence level ($LoD_{95\%}$) over different survey intervals are given in Table 5.4. Net topographic changes estimated for the whole study period were highly variable. A net negative topographic change was monitored in the peat hagg (Site 1, Model 11–1, median = 14 mm, RMS = 19 mm) and the peat gully wall (Site 2, Model 11–1, median = 13 mm, RMS = 23 mm). In contrast, a net positive topographic change was monitored in the riparian area (Site 3, Model 11–1, median = 30 mm, RMS = 35 mm) and the peat gully head (Site 4, Model 9–1, median = 22 mm, RMS = 29 mm) (Table 5.4).

From 26/10/2016 to 04/11/2016, the net topographic change was negative for the Site 1, 2 and 3 (Model 2–1), but was positive for the Site 4 (Model 2–1). During the period of 04/11/2016–30/11/2016, the peat surface for Sites 1, 2 and 3 experienced a positive net topographic change, with a median net increase in the surface height of 14, 18 and 17 mm, respectively. There was a positive net topographic change for Sites 1, 2 and 3 from 21/12/2016 to 22/02/2016 (Model 5–4). However, a net negative topographic change was monitored for all four sites over the period of 22/02/2017–07/04/2017 (Model 6–5 for Sites 1, 2 and 3, and Model 4–3 for Site 4).

Table 5.4 Median net, positive and negative topographic changes (mm) with root mean square (RMS) (mm) over different survey intervals for each field site. The long-term survey intervals are highlighted with bold.

Sites	Model*	Differencing period	Net change		Positive change		Negative change	
			Median	RMS**	Median	RMS	Median	RMS
Site 1	2–1	26/10/2016–04/11/2016	–16	24	14	16	–18	25
	3–2	04/11/2016–30/11/2016	14	19	15	18	–17	24
	4–3	30/11/2016–21/12/2016	23	37	23	37	–11	12
	5–4	21/12/2016–22/02/2017	10	15	13	15	–13	15
	6–5	22/02/2017–07/04/2017	–30	42	13	14	–40	45
	7–6	07/04/2017–02/05/2017	12	16	14	17	–13	15

Sites	Model*	Differencing period	Net change		Positive change		Negative change	
			Median	RMS**	Median	RMS	Median	RMS
	8–7	02/05/2017–13/06/2017	–14	19	14	16	–16	19
	9–8	13/06/2017–21/08/2017	–10	17	15	18	–14	16
	10–9	21/08/2017–27/09/2017	32	33	36	36	–17	20
	11–10	27/09/2017–02/11/2017	–11	16	16	19	–13	15
	11–1	**26/10/2016–02/11/2017**	**–14**	**19**	**15**	**20**	**–16**	**19**
	2–1	26/10/2016–04/11/2016	–15	22	16	19	–19	23
	3–2	04/11/2016–30/11/2016	18	21	18	21	–14	16
	4–3	30/11/2016–21/12/2016	–13	18	18	22	–15	16
	5–4	21/12/2016–22/02/2017	12	17	14	16	–15	17
	6–5	22/02/2017–07/04/2017	–14	19	16	21	–17	18
Site 2	7–6	07/04/2017–02/05/2017	–12	18	13	14	–15	20
	8–7	02/05/2017–13/06/2017	–15	18	14	17	–16	19
	9–8	13/06/2017–21/08/2017	10	17	14	18	–13	15
	10–9	21/08/2017–27/09/2017	–12	15	13	15	–13	15
	11–10	27/09/2017–02/11/2017	14	20	16	20	–14	19
	11–1	**26/10/2016–02/11/2017**	**–13**	**23**	**18**	**21**	**–19**	**24**
	2–1	26/10/2016–04/11/2016	–12	14	11	11	–12	14
	3–2	04/11/2016–30/11/2016	17	18	17	18	–19	26
	4–3	30/11/2016–21/12/2016	–14	17	13	18	–15	16
	5–4	21/12/2016–22/02/2017	11	13	12	14	–12	12
	6–5	22/02/2017–07/04/2017	–11	12	–	–	–11	12
Site 3	7–6	07/04/2017–02/05/2017	11	12	12	12	–11	11
	8–7	02/05/2017–13/06/2017	–14	17	12	14	–15	17
	9–8	13/06/2017–21/08/2017	12	16	15	18	–12	12
	10–9	21/08/2017–27/09/2017	–14	16	12	13	–15	16
	11–10	27/09/2017–02/11/2017	30	40	30	40	–	–
	11–1	**26/10/2016–02/11/2017**	**30**	**35**	**32**	**36**	**–14**	**15**
	2–1	26/10/2016–04/11/2016	26	34	26	34	–12	14
	3–2	04/11/2016–22/02/2017	10	21	19	25	–14	17
	4–3	22/02/2017–07/04/2017	–12	17	13	16	–14	18
	5–4	07/04/2017–02/05/2017	11	14	12	13	–14	16
Site 4	6–5	02/05/2017–13/06/2017	13	21	16	22	–14	17
	7–6	13/06/2017–21/08/2017	–18	23	16	19	–19	23
	8–7	21/08/2017–27/09/2017	15	21	18	22	–13	16
	9–8	27/09/2017–26/10/2016	–16	24	14	25	–19	24
	9–1	**26/10/2016–02/11/2017**	**22**	**29**	**25**	**29**	**–22**	**25**

Note: * Model shows comparisons over different survey intervals; ** RMS is the square root of the arithmetic mean of the squares of the set of values.

The spatial distribution and histogram of M3C2 differences for short-term and long-term comparisons are shown in Figure 5.3 through Figure 5.6. M3C2 distances ranged from negative values (red colour) that showed eroded sediment, to positive values (blue colour) that indicated deposited

sediment. Topographic changes were mainly observed over short-term intervals when intense rainfall (i.e. Figure 5.5 (j)), flow wash (i.e. Figure 5.3 (a) and Figure 5.4 (a)), needle-ice production (i.e. Figure 5.3 (b), Figure 5.4 (b) and Figure 5.5 (b)), surface desiccation (i.e. Figure 5.3 (e) and Figure 5.4 (e)) or surface swelling (i.e. Figure 5.6 (a)) was observed. On 30/11/2016 field survey showed that needle-ice was formed within the upper layer of the peat surface on Site 1 (hagg), Site 2 (gully wall) and Site 3 (riparian area) (Table 5.1). As a result the calculated M3C2 distance showed positive values across the three sites (Figure 5.3 (b), Figure 5.4 (b) and Figure 5.5 (b)). Drying and cracking of the peat surface was observed during the field campaign on 07/04/2017, resulting in a negative topographic change across the field sites (Figure 5.3 (e), Figure 5.4 (e) and Figure 5.6 (c)). Water recharging and surface welling processes were evident on Site 4 (gully headcut) during the survey on 04/11/2016, leading to positive topographic change across much of the site (Figure 5.6 (a)).

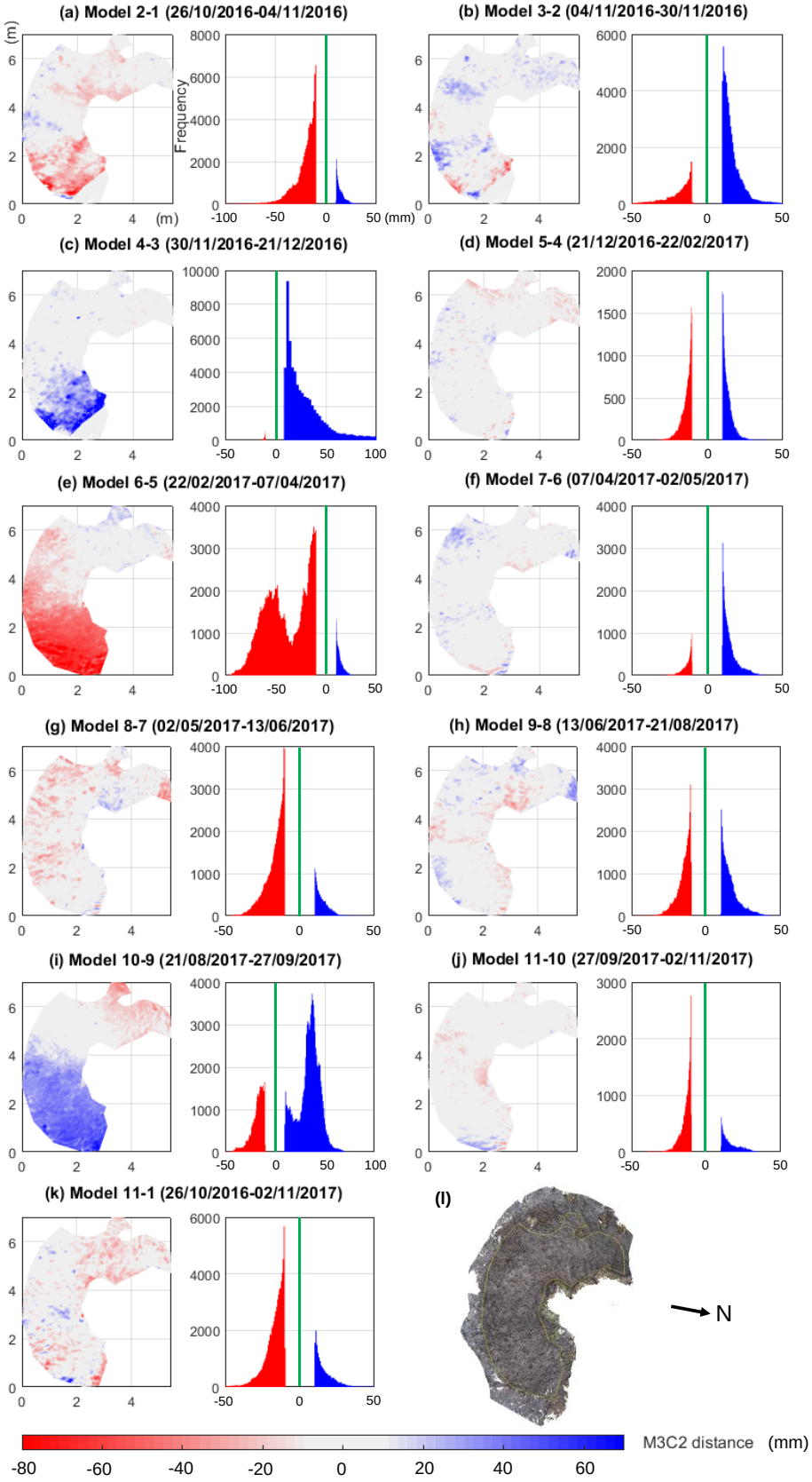

Figure 5.3 M3C2 distances and histograms over different survey intervals at both short-term (a–j) and long-term (k) scales for the Site 1 (hagg). Grey areas have non-significant changes. (l) Top view on the feature of interest (with boundary marked as yellow).

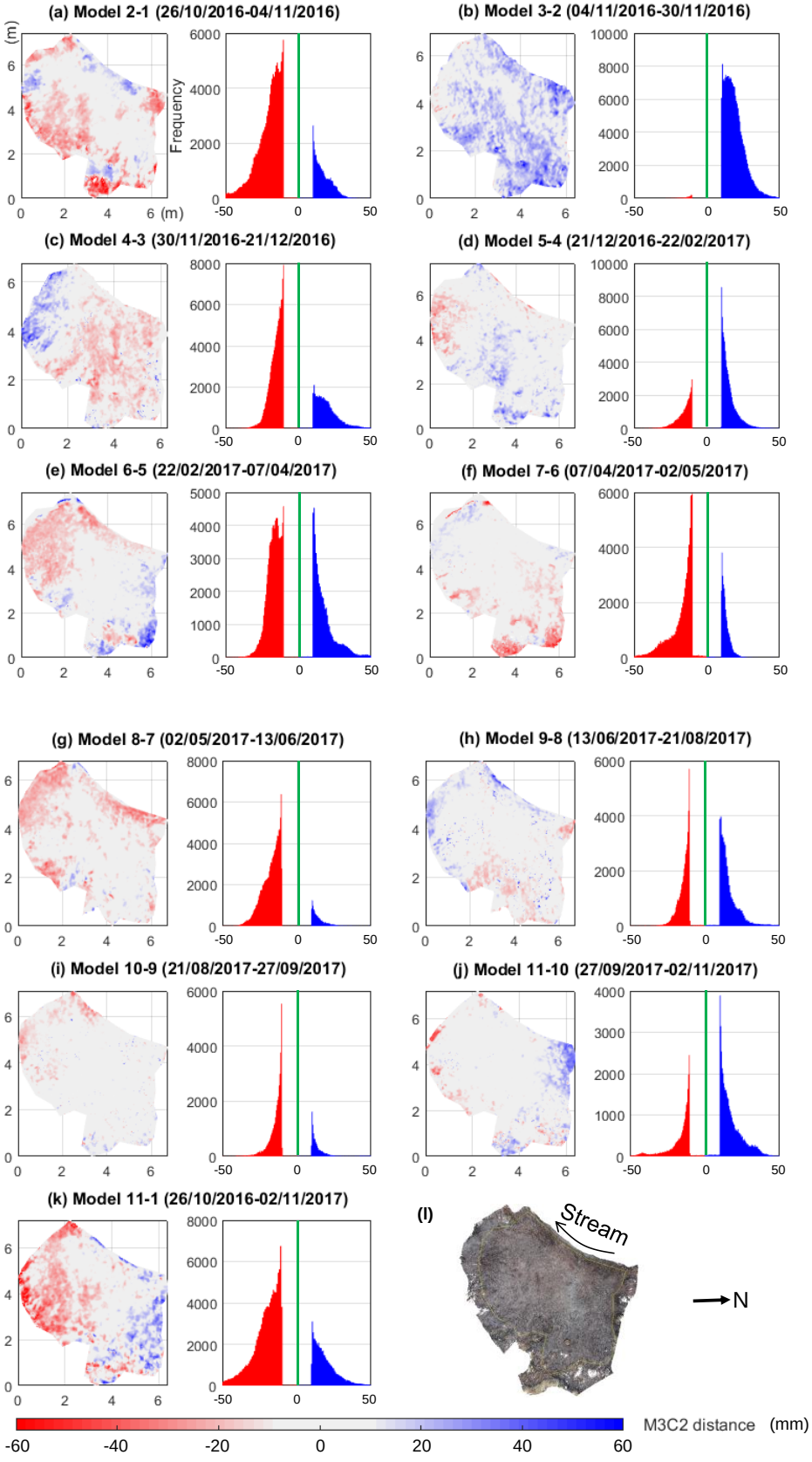

Figure 5.4 M3C2 distances and histograms over different survey intervals at both short-term (a–j) and long-term (k) scales for the Site 2 (gully wall). Grey areas have non-significant changes. (l) Top view on the feature of interest (with boundary marked as yellow).

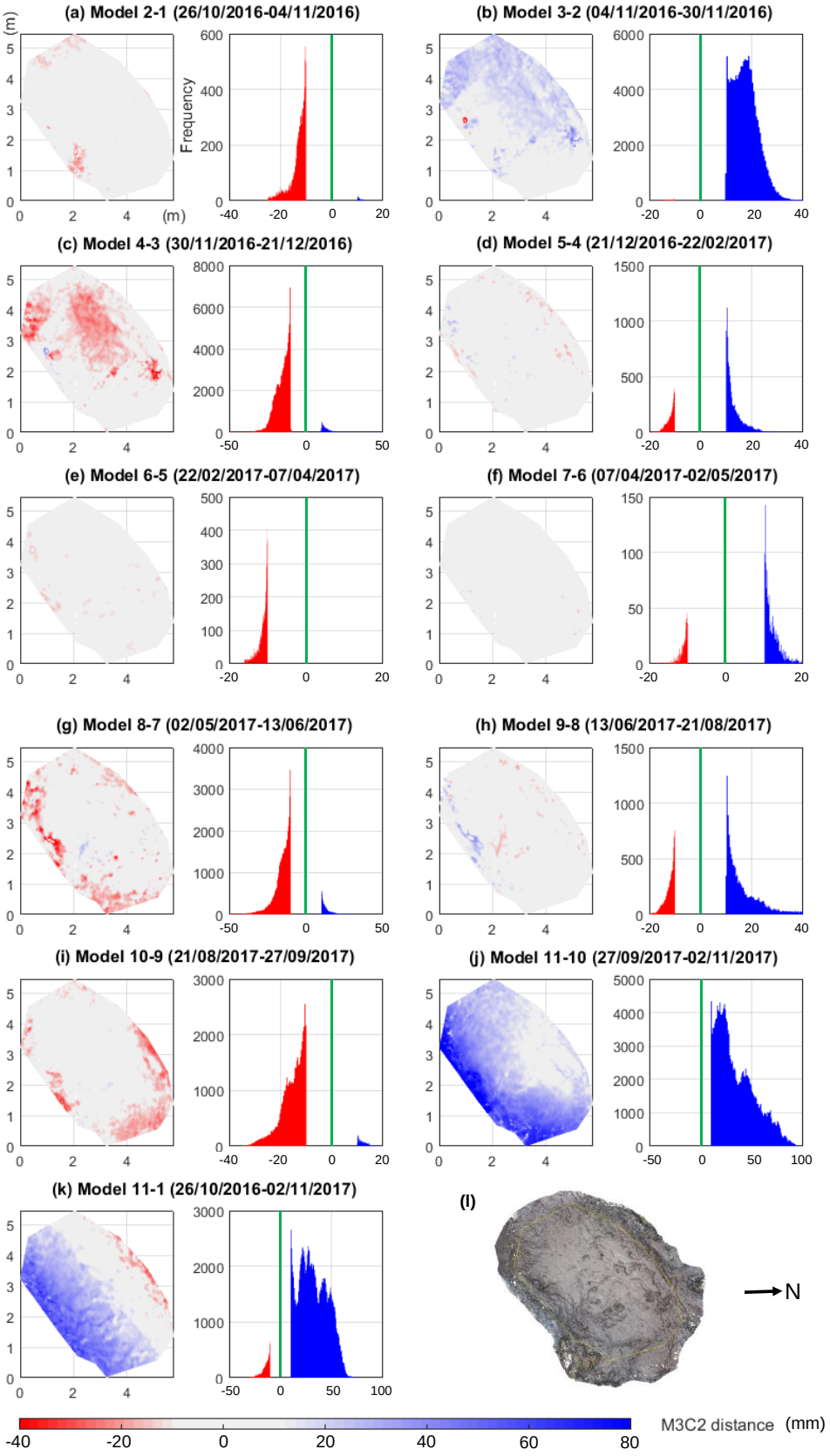

Figure 5.5 M3C2 distances and histograms over different survey intervals at both short-term (a–j) and long-term (k) scales for the Site 3 (riparian flat area). Grey areas have non-significant changes. (l) Top view on the feature of interest (with boundary marked as yellow).

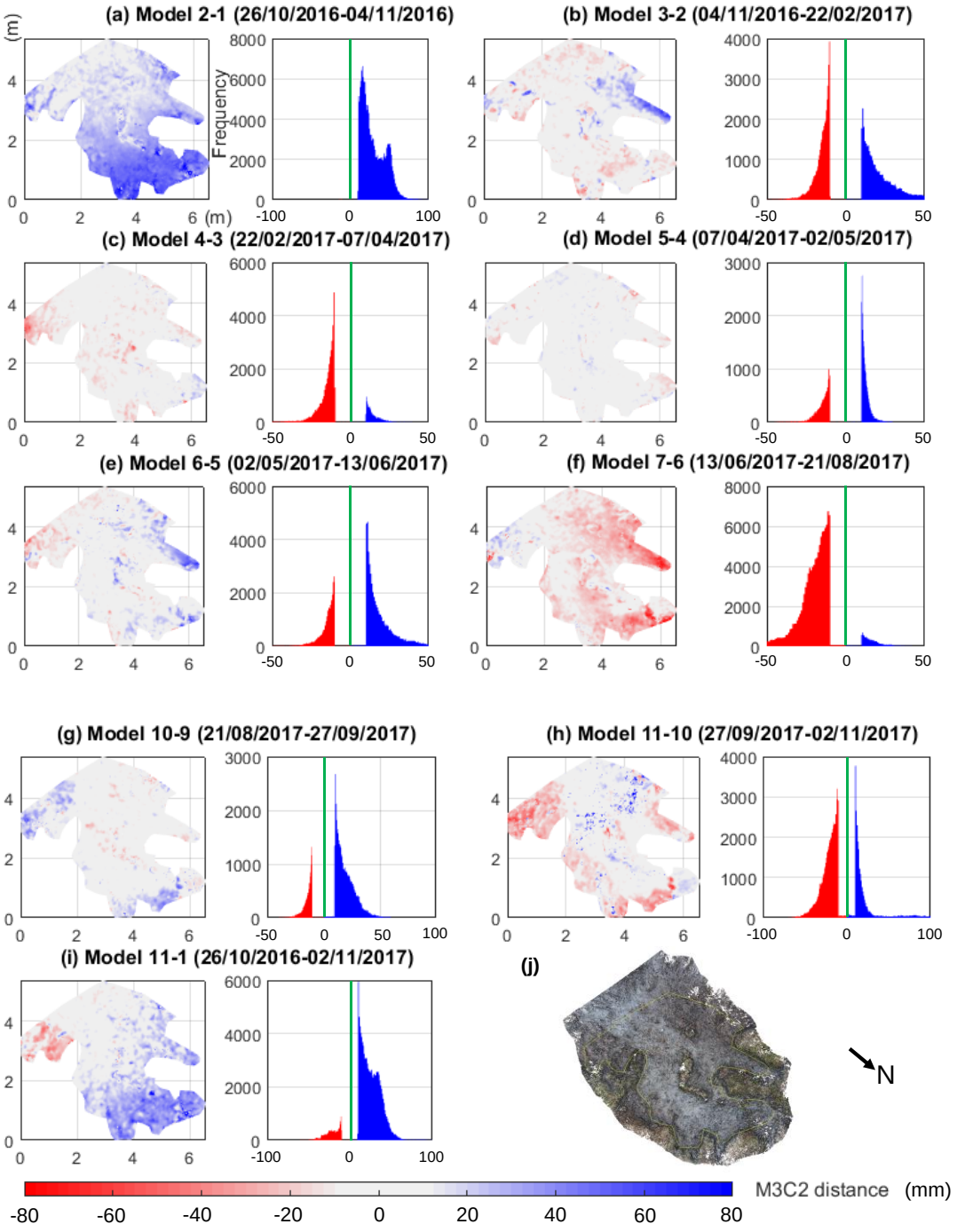

Figure 5.6 M3C2 distances and histograms over different survey intervals at both short-term (a–h) and long-term (i) scales for the Site 4 (gully head). Grey areas have non-significant changes. (j) Top view on the feature of interest (with boundary marked as yellow).

5.4.1.2 Relationships between spatial patterns and topographic variables

Aspect, slope and surface roughness were the most significantly correlated topographic variables for almost all of the topographic changes (Table 5.5). Although statistically significant for many intervals, neither curvature nor plan curvature were the most significant predictor of topographic change in any survey interval. Profile curvature was the most significant topographic predictor only for Site 2, Model 9–8.

For the positive topographic changes, roughness was positively correlated to M3C2 distance; while for the negative topographic changes, roughness was negatively correlated to M3C2 distance (Table 5.5). This relationship is presented in more detail in Figure 5.7 (a–b) where the effect of roughness on topographic change is evident. These results suggest that rougher cells are indicative of more active topographic change. The Spearman's rank topographic change – roughness correlation coefficients for the short-term surveys were generally greater than those of the long-term surveys. For example, Model 4–3 (Site 1) had coefficient of 0.555 and 0.529 for the correlation between roughness and total and positive topographic changes, respectively, compared to 0.280 and 0.315 produced by Model 11–1 (Table 5.5). Slope had strong negative correlations with negative topographic change (Table 5.6), indicating that erosion increases with an increase in slope gradient (Figure 5.7 (c)).

Table 5.5 Spearman's rank correlation coefficients between topographic variables and observed topographic change. Significant correlations ($p < 0.05$) are indicated with an asterisk while the strongest relationship for each survey period is also highlighted in bold.

Sites	Model		Aspect	Slope	Curvature	Profile curvature	Plan curvature	Roughness
Site 1	2–1	Total	**0.185***	–0.000	0.015*	–0.014*	0.014*	0.037*
		Positive	0.041*	–0.006	0.018*	–0.013	0.018*	**0.304***
		Negative	0.126*	–0.007	0.012*	–0.011*	0.011*	**–0.170***
	3–2	Total	0.090*	**–0.104***	0.026*	–0.027*	0.015*	–0.000
		Positive	0.062*	–0.094*	0.015*	–0.018*	0.009*	**0.194***
		Negative	0.061*	–0.151*	0.012	–0.018*	–0.014	**–0.285***
	4–3	Total	–0.127*	0.208*	0.008*	–0.007	0.005	**0.555***
		Positive	–0.128*	0.223*	0.004	–0.003	0.002	**0.529***
		Negative	**–0.234***	–0.045*	0.056*	–0.063*	0.025	–0.085*
	5–4	Total	**0.293***	–0.114*	0.020*	–0.032*	0.003	0.121*
		Positive	0.109*	0.065*	0.016	–0.022*	0.004	**0.134***
		Negative	–0.007	0.011	0.019*	–0.027*	0.005	**–0.048***

Sites	Model		Aspect	Slope	Curvature	Profile curvature	Plan curvature	Roughness
Site 2	6–5	Total	**0.139***	0.065*	0.010*	–0.008*	0.009*	0.000
		Positive	0.026*	**0.040***	0.003	–0.008	–0.004	0.007
		Negative	**0.176***	–0.037*	0.000	0.000	–0.001	0.073*
	7–6	Total	0.150*	**–0.169***	0.047*	–0.048*	0.028*	0.131*
		Positive	0.087*	0.096*	0.013*	–0.012*	0.008	**0.151***
		Negative	–0.022*	**–0.224***	0.016	–0.028*	–0.011	–0.124*
	8–7	Total	–0.042*	0.030*	0.053*	–0.040*	0.054*	**–0.178***
		Positive	–0.008	**0.053***	0.014	–0.014	0.008	–0.015
		Negative	0.015*	–0.119*	0.029*	–0.024*	0.027*	**–0.135***
	9–8	Total	–0.012*	–0.033*	0.053*	–0.052*	0.034*	**0.078***
		Positive	–0.103*	**0.123***	0.012	–0.013*	0.006	0.060*
		Negative	–0.012*	**–0.109***	0.027*	–0.023*	0.020*	–0.058*
	10–9	Total	–0.136*	**–0.211***	0.014*	–0.017*	0.006*	0.028*
		Positive	**–0.180***	0.037*	0.013*	–0.008*	0.017*	–0.145*
		Negative	–0.047*	**0.055***	0.019*	–0.021*	0.009	–0.034*
	11–10	Total	**–0.341***	0.210*	0.056*	–0.039*	0.062*	0.062*
		Positive	–0.158*	0.230*	0.026*	–0.029*	0.013	**0.255***
		Negative	–0.202*	**–0.221***	0.032*	–0.020*	0.039*	–0.205*
	11–1	Total	–0.017*	–0.024*	0.052*	–0.055*	0.036*	**0.280***
		Positive	–0.001	0.144*	0.015	–0.016	0.012	**0.315***
		Negative	**–0.078***	–0.067*	0.039*	–0.043*	0.022*	0.040*
	2–1	Total	–0.013*	**–0.070***	0.036*	–0.038*	0.018*	–0.067*
		Positive	0.051*	**0.099***	0.014*	–0.015*	0.004	0.071*
		Negative	0.043*	–0.156*	0.027*	–0.028*	0.014*	**–0.239***
	3–2	Total	–0.094*	0.123*	0.006*	–0.006*	0.005*	**0.297***
		Positive	–0.103*	0.138*	0.005*	–0.006*	0.003	**0.334***
		Negative	0.110*	–0.176*	0.006	–0.003	0.009	**–0.246***
	4–3	Total	–0.052*	–0.017*	0.004	0.006*	0.025*	**0.254***
		Positive	–0.105*	0.094*	0.002	0.002	0.014*	**0.151***
		Negative	0.030*	**–0.089***	0.017*	–0.014*	0.018*	0.000
	5–4	Total	–0.008*	0.118*	0.021*	–0.024*	0.010*	**0.126***
		Positive	–0.083*	0.050*	0.008*	–0.009*	0.004	**0.124***
		Negative	0.066*	0.002	0.015*	–0.020*	0.001	**–0.163***
	6–5	Total	–0.032*	0.139*	–0.004	0.004	0.002	**0.161***
		Positive	–0.132*	–0.017*	–0.008*	0.008*	–0.003	**0.246***
		Negative	**–0.063***	–0.047*	0.004	–0.005	0.002	0.035*
	7–6	Total	0.078*	**–0.159***	0.071*	–0.077*	0.030*	–0.141*
		Positive	0.040*	0.090*	0.008	–0.009	0.002	**0.168***
		Negative	**0.142***	–0.101*	0.060*	–0.067*	0.024*	–0.073*
	8–7	Total	0.007*	–0.061*	0.011*	–0.010*	0.014*	**0.121***
		Positive	–0.071*	0.065*	0.012	–0.022*	0.002	**0.123***
		Negative	–0.022*	**–0.143***	0.006	–0.004	0.008*	0.042*
	9–8	Total	–0.047*	–0.056*	0.068*	**–0.073***	0.040*	–0.030*
		Positive	–0.057*	0.065*	0.044*	–0.039*	0.043*	**0.101***
		Negative	0.029*	–0.100*	0.032*	–0.038*	0.011*	**–0.169***

Sites	Model		Aspect	Slope	Curvature	Profile curvature	Plan curvature	Roughness
		Total	0.042*	**0.128***	0.027*	–0.027*	0.023*	0.059*
	10–9	Positive	–0.060*	0.120*	0.046*	–0.038*	0.045*	**0.308***
		Negative	0.104*	–0.048*	0.017*	–0.019*	0.008	**–0.271***
		Total	–0.038*	–0.048*	0.014*	–0.012*	0.009*	**0.102***
	11–10	Positive	–0.084*	**0.097***	0.008	–0.008	0.006	0.005
		Negative	0.067*	–0.016*	0.009	–0.011	0.001	**–0.105***
		Total	–0.030*	0.097*	0.027*	–0.027*	0.016*	**0.109***
	11–1	Positive	–0.033*	0.091*	0.008	–0.005	0.007	**0.177***
		Negative	–0.030*	–0.076*	0.019*	–0.018*	0.012*	**–0.129***
		Total	–0.068*	–0.004	0.000	0.004	0.005	**0.171***
	2–1	Positive	0.052	**0.245***	0.024	–0.007	0.074	0.227*
		Negative	–0.026*	**–0.231***	–0.004	0.014	0.008	–0.159*
		Total	**–0.161***	–0.029*	0.002	0.007*	0.011*	0.102*
	3–2	Positive	**–0.157***	–0.061*	–0.002	0.009*	0.007*	0.053*
		Negative	0.275*	–0.283*	0.007	0.001	0.021	**–0.460***
		Total	0.057*	**0.071***	0.029*	–0.051*	–0.001	0.024*
	4–3	Positive	–0.063*	0.159*	0.050*	–0.056*	0.040*	**0.376***
		Negative	0.023*	–0.006	0.023*	–0.030*	0.005	**0.103***
		Total	0.125*	0.207*	0.010	–0.013	0.004	**0.430***
	5–4	Positive	0.007	0.296*	0.013	–0.018	0.004	**0.410***
		Negative	0.061*	**–0.067***	0.036*	–0.029*	0.035*	–0.024*
		Total	**–0.104***	–0.032*	0.005	–0.007	0.002	–0.065*
	6–5	Positive	–	–	–	–	–	–
		Negative	**–0.065***	–0.025*	0.001	–0.002	0.002	–0.033*
		Total	0.200*	0.079*	0.050	–0.063*	0.025	**0.362***
Site 3	7–6	Positive	0.040	0.219*	0.043	–0.066	0.010	**0.326***
		Negative	0.052	–0.321*	0.007	0.025	0.011	**–0.341***
		Total	0.040*	–0.136*	0.033*	–0.029*	0.030*	**–0.170***
	8–7	Positive	–0.092*	0.182*	0.026*	–0.023*	0.022	**0.201***
		Negative	–0.094*	–0.193*	0.023*	–0.022*	0.016*	**–0.203***
		Total	0.159*	0.352*	0.028*	–0.041*	0.009	**0.464***
	9–8	Positive	–0.045*	0.187*	0.034*	–0.034*	0.019*	**0.432***
		Negative	–0.052*	**–0.183***	0.023	–0.021	0.017	–0.171*
		Total	**0.111***	–0.011*	0.011*	–0.009*	0.012*	0.079*
	10–9	Positive	–0.148*	**0.166***	0.003	–0.004	0.009	0.072*
		Negative	**0.075***	–0.067*	0.008	–0.012*	0.005	–0.036*
		Total	0.232*	**0.363***	0.007*	–0.013*	–0.001	0.170*
	11–10	Positive	0.298*	**0.326***	0.014*	–0.017*	0.005*	0.093*
		Negative	–	–	–	–	–	–
		Total	0.351*	**0.426***	0.001	–0.008	–0.007	0.050*
	11–1	Positive	0.070*	**0.463***	0.011*	–0.013*	0.005*	0.072*
		Negative	0.111*	**–0.433***	–0.053	0.076	–0.022	–0.259*
		Total	0.091*	0.028*	–0.002	0.003	0.001	**0.180***
Site 4	2–1	Positive	0.093*	0.030*	–0.003	0.003	0.001	**0.185***
		Negative	–0.012	–0.209*	0.004	0.012	0.029	**–0.222***

Sites	Model		Aspect	Slope	Curvature	Profile curvature	Plan curvature	Roughness
		Total	0.121*	0.069*	0.045*	–0.046*	0.033*	**0.122***
	3–2	Positive	0.089*	**0.200***	0.006	–0.007	0.006	0.060*
		Negative	–0.063*	**–0.155***	0.031*	–0.035*	0.020*	–0.154*
		Total	–0.025*	**–0.091***	0.030*	–0.031*	0.020*	0.015*
	4–3	Positive	0.028*	**0.084***	0.015	–0.014	0.005	0.066*
		Negative	–0.056*	**–0.212***	0.018*	–0.021*	0.014*	–0.201*
		Total	0.009	**–0.100***	0.046*	–0.051*	0.025*	0.068*
	5–4	Positive	0.066*	**0.131***	0.012	–0.014*	0.006	0.101*
		Negative	0.011	**–0.063***	0.036*	–0.034*	0.023*	–0.059*
		Total	0.090*	**–0.023***	0.021*	–0.012*	0.031*	0.000
	6–5	Positive	0.134*	**0.179***	0.005	0.000	0.010*	0.068*
		Negative	–0.078*	–0.206*	0.032*	–0.030*	0.029*	**–0.276***
		Total	**–0.108***	–0.010*	0.035*	–0.042*	0.012*	0.046*
	7–6	Positive	0.037*	**0.063***	0.024*	–0.023*	0.020*	0.058*
		Negative	**–0.137***	–0.088*	0.029*	–0.035*	0.010*	–0.033*
		Total	**0.123***	–0.101*	0.015*	–0.014*	0.010*	0.080*
	8–7	Positive	**0.155***	–0.003	0.007	–0.007	0.004	0.079*
		Negative	–0.053*	–0.135*	0.007	–0.014	–0.003	**–0.170***
		Total	**–0.095***	0.010*	0.061*	–0.066*	0.039*	–0.047*
	9–8	Positive	0.090*	0.195*	0.061*	–0.048*	0.067*	**0.196***
		Negative	–0.114*	–0.107*	0.042*	–0.052*	0.015*	**–0.172***
		Total	0.001	0.009*	0.006*	–0.005	0.010*	**0.089***
	9–1	Positive	0.015*	0.045*	0.004	–0.002	0.009*	**0.133***
		Negative	**–0.276***	0.024	–0.009	0.004	–0.012	–0.212*

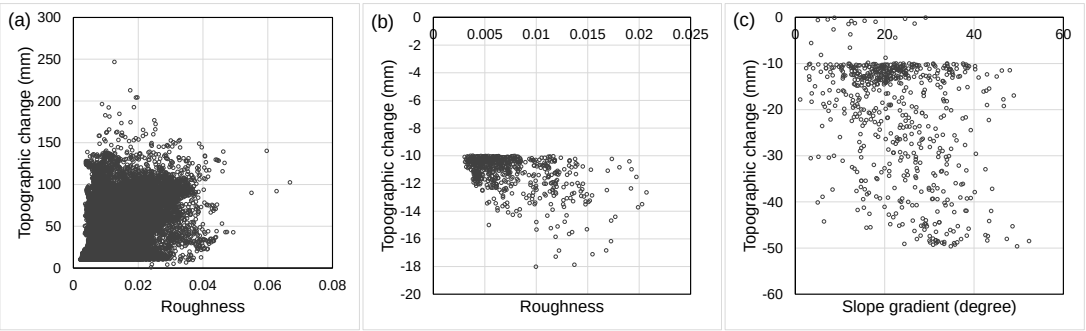

Figure 5.7 Relationships between topographic change and (a–b) roughness and (c) slope. The results were derived from models of (a) Site 1: 4–3; (b) Site 3: 7–6; (c) Site 3: 3–2. Roughness was calculated from the dense points of the start of the survey interval.

5.4.1.3 Relationships between meteorological variables and topographic change

Meteorological variables for different survey intervals are presented in Table 5.6. A total of 2012.0 mm of precipitation, mainly of long-duration and low intensity, was recorded on 266 days during the whole 373 day survey period (Table 5.6). Maximum 15–minute rainfall intensity ranged from 0.2 mm to 7.2 mm. Mean temperature during the period of 04/11/2016–30/11/2016 was lowest (1.5 ºC), and it gradually increased from 22/02/2017. The winter of 2016 had 38 freezing days with sub-zero temperatures recorded.

Table 5.6 Summary of meteorological data for both short-term and long-term monitoring periods. Frost cycles indicate the number of times soil surface temperature fell below 0 ºC and also returned above 0 ºC; both have to occur to count as one cycle.

Scale	Monitoring interval	Number of days (rainy days)	Total rainfall (mm)	Maximum rainfall (mm/15')	Mean temperature (ºC)	Days, T < ºC	Frost cycles
Short-term	26/10/2016–04/11/2016	10 (4)	14.6	0.2	6.4	4	6
	04/11/2016–30/11/2016	27 (19)	103.6	2.2	1.5	7	20
	30/11/2016–21/12/2016	22 (17)	50.6	1.4	4.8	3	3
	21/12/2016–22/02/2017	64 (45)	225.4	2.0	1.7	31	44
	22/02/2017–07/04/2017	45 (36)	320.8	3.0	4.4	10	6
	07/04/2017–02/05/2017	26 (12)	20.0	0.2	6.1	6	5
	02/05/2017–13/06/2017	43 (26)	225.4	2.2	11.2	1	1
	13/06/2017–21/08/2017	70 (52)	457.0	3.4	13.5	0	0
	21/08/2017–27/09/2017	38 (30)	226.4	7.2	–	–	–
	27/09/2017–02/11/2017	37 (30)	396.4	3.6	–	–	–
Long-term	04/11/2016–22/02/2017	112 (80)	379.6	2.2	2.6	41	66
	26/10/2016–02/11/2017	373 (266)	2012.0	7.2	–	–	–

Spearman's rank correlations between the six meteorological variables and median net, positive and negative topographic changes showed that the relationships were generally not significant ($p > 0.05$). However, on the gully head (Site 4) negative topographic change was significantly correlated with

total rainfall ($p < 0.05$). Further regression analysis (Figure 5.8) showed that a linear relationship ($y = –0.0011x – 1.1969$, $n = 8$, $R^2 = 0.519$, $p < 0.05$) performed well in describing the relationship between topographic change (y) and total rainfall (x) for Site 4.

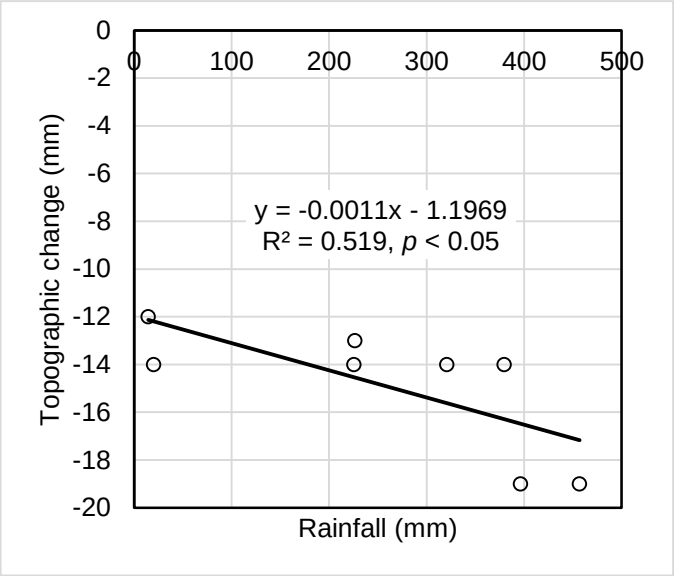

Figure 5.8 Relationships between topographic change and rainfall on Site 4 (gully head).

5.4.2 Laboratory results

5.4.2.1 M3C2 differences of peat surface

The georeferencing errors calculated by the Agisoft Photoscan software ranged from 4.2 to 5.6 mm under the laboratory conditions (Table 5.3). M3C2 differences above Level of Detection threshold at 95% confidence level for different treatments are given in Table 5.7. The net median topographic change ranged from –5 mm to 5 mm (Table 5.7). In general a net negative topographic change was monitored for the Rainfall and Rainfall + Inflow treatments; in contrast, a net positive topographic change was monitored for the Inflow treatments (Table 5.7).

Table 5.7 Summary of the median net, positive and negative topographic changes (mm) with root mean square (RMS) (mm) for laboratory models.

Model	Net change		Positive change		Negative change	
	Median	RMS[d]	Median	RMS	Median	RMS
Rainfall[a] (2.5°)[b]_test 1[c]	–5	6	6	9	–5	6
Rainfall (2.5°)_test 2	–4	6	4	5	–5	7
Inflow (2.5°)_test 1	4	8	5	8	–6	7
Inflow (2.5°)_test 2	–3	5	4	5	–5	6
Rainfall + Inflow (2.5°)_test 1	–5	7	5	6	–6	7
Rainfall + Inflow (2.5°)_test 2	4	5	4	5	–4	5
Rainfall (7.5°)_test 1	4	7	5	7	–4	6
Rainfall (7.5°)_test 2	–4	5	4	5	–4	5
Inflow (7.5°)_test 1	3	6	5	6	–5	6
Inflow (7.5°)_test 2	5	6	5	6	–5	7
Rainfall + Inflow (7.5°)_test 1	–4	7	4	5	–5	7
Rainfall + Inflow (7.5°)_test 2	–5	6	5	6	–5	6

a: three types of laboratory experiments include Rainfall events, Inflow events and Rainfall + Inflow events;
b: two slope gradients include 2.5° and 7.5°;
c: two replicates for each type of simulation experiments include test 1 and test 2;
d: RMS is the square root of the arithmetic mean of the squares of the set of values.

Figure 5.9 gives the spatial patterns of the significant M3C2 distances (> LoD 95%) and histograms of the differences. Some treatments (e.g., 2.5°R1, 2.5°RF1, 7.5°R2 and 7.5°RF2) mainly show negative topographic changes while others (e.g., 2.5°F1, 7.5°R1, 7.5°F1 and 7.5°F2) show greater positive topographic changes (Figure 5.9). These results suggest that simulated rainfall and simulated rainfall + inflow events cause both spatially distributed erosion and deposition as captured by SfM. However, the simulated inflow events had positive topographic changes under both the 2.5° and 7.5° conditions.

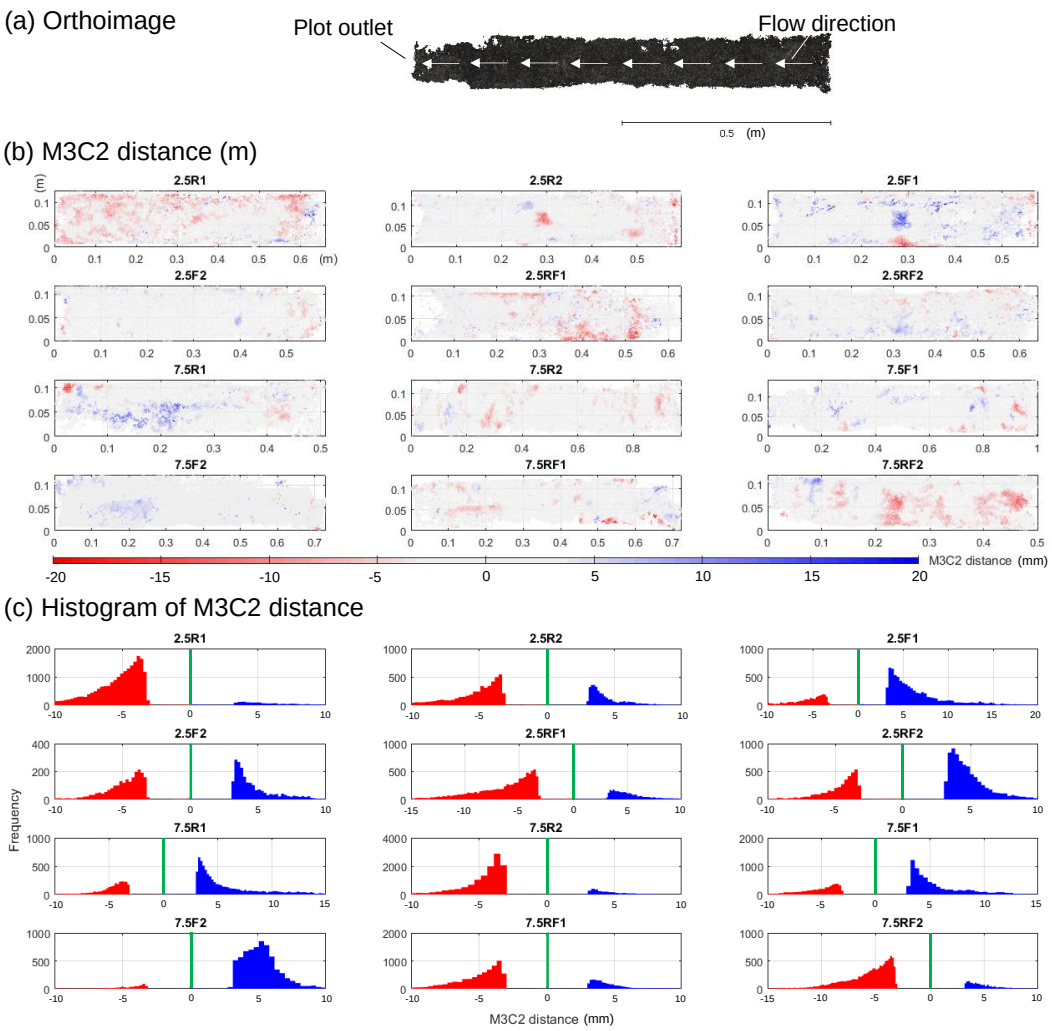

Figure 5.9 Spatial patterns of the significant M3C2 distances (a) and histogram of differences (b) at event scales for laboratory peat blocks. Grey areas have non-significant changes. Two slopes (2.5° and 7.5°), three treatments including *Rainfall* (R), *Inflow* (F) and *Rainfall + Inflow* (RF) and two replicates for each (1 and 2) were examined.

5.4.2.2 Comparison of peat erosion rates measured by SfM and sediment fluxes

Figure 5.10 shows the peat loss data, expressed in grams, derived from both the sediment fluxes and SfM methods. Only erosion was measured by the sediment flux method and the total amount of peat loss (dry weight) ranged from 0.26 g to 2.43 g for different treatments. However, both positive and negative topographic changes were found for the SfM technique, indicating spatially distributed erosion / deposition patterns. The SfM method resulted in an estimated mean peat deposition rate of 7.02 g (0.7 mm topographic change), with standard deviation as 48.29 g (4.3 mm), compared with a mean peat loss rate of 1.05 g (0.1 mm), with standard deviation as 0.55 g

(0.1 mm) derived from the sediment fluxes. The standard deviation of mean topographic change measured by the SfM method was much greater than the sediment flux method, showing a much greater magnitude of topographic change. From the figures showing M3C2 distances and histogram of differences (Figure 5.10), there were areas with both positive and negative topographic changes on the peat block and these features were well described by the SfM method.

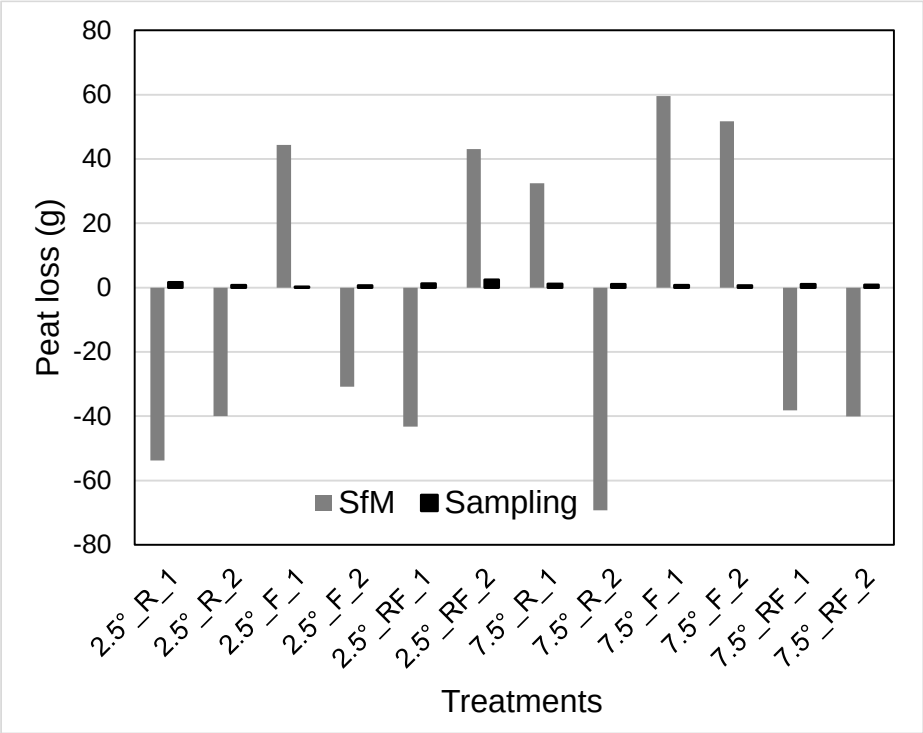

Figure 5.10 Summary of peat loss measured by sampling method and SfM techniques for the three treatments (*Rainfall*, *Inflow* and *Rainfall* + *Inflow*). Positive values show erosion while negative values show deposition. Two slopes (2.5° and 7.5°), three treatments including *Rainfall* (R), *Inflow* (F) and *Rainfall* + *Inflow* (RF) and two replicates for each (1 and 2) were examined.

5.4.2.3 Relationships between spatial patterns and topographic variables

The Spearman's rank correlation coefficients are presented in Table 5.8, with the most significant topographic factors highlighted in bold. For all of the M3C2 comparisons curvature, roughness and slope were the most significant topographic variables ($p < 0.01$) (Table 5.8). Although statistically significant for many models, none of aspect, profile curvature and plan curvature were the most significant predictor of topographic change in any model. Curvature showed significantly negative correlations with topographic

change for all three treatments (R, F and RF) demonstrating that topographic change decreased with an increase in curvature.

Table 5.8 Spearman's rank correlation coefficients between topographic variables and observed topographic change for the laboratory peat blocks. Significant correlations ($p < 0.05$) are indicated with an asterisk while the strongest relationship for each survey period is also highlighted in bold.

Model		Aspect	Slope	Curvature	Profile curvature	Plan curvature	Roughness
2.5R1	Total	–0.007	–0.090*	**–0.154***	0.142*	–0.128*	–0.120*
	Positive	–0.033	**0.234***	–0.106*	0.104*	–0.072*	–0.152*
	Negative	0.004	**–0.222***	–0.110*	0.104*	–0.089*	–0.073*
2.5R2	Total	0.003	–0.066*	**–0.131***	0.113*	–0.117*	–0.114*
	Positive	–0.101*	**0.308***	–0.097*	0.064*	–0.127*	0.260*
	Negative	0.017	**–0.175***	–0.031*	0.025	–0.026	–0.094*
2.5F1	Total	–0.025*	0.050*	**–0.132***	0.105*	–0.129*	–0.106*
	Positive	0.003	**0.162***	–0.079*	0.048*	–0.096*	–0.125*
	Negative	–0.015	**0.072***	0.033	–0.035	0.011	–0.039*
2.5F2	Total	–0.079*	–0.072*	**–0.152***	0.149*	–0.120*	–0.033*
	Positive	–0.064*	**0.142***	–0.053*	0.051*	–0.059*	–0.058*
	Negative	0.014	**–0.093***	0.002	–0.011	–0.012	–0.010
2.5RF1	Total	0.052*	–0.114*	**–0.116***	0.105*	–0.098*	–0.104*
	Positive	0.053*	**0.217***	–0.037*	0.014	–0.055*	–0.184*
	Negative	0.028*	**–0.221***	–0.055*	0.050*	–0.040*	0.039*
2.5RF2	Total	–0.072*	–0.023*	**–0.184***	0.167*	–0.167*	–0.045*
	Positive	–0.066*	**0.189***	–0.121*	0.108*	–0.110*	–0.005
	Negative	–0.015	**–0.200***	–0.111*	0.094*	–0.109*	0.021
7.5R1	Total	–0.096*	**0.291***	–0.186*	0.157*	–0.177*	0.077*
	Positive	–0.134*	**0.437***	–0.185*	0.150*	–0.185*	0.137*
	Negative	–0.019	–0.140*	0.015	–0.015	0.025	**–0.207***
7.5R2	Total	–0.013	–0.040*	**–0.082***	0.080*	–0.067*	0.003
	Positive	–0.052*	0.086*	–0.058*	0.057*	–0.041*	**0.109***
	Negative	0.032*	–0.122*	–0.034*	0.036*	–0.025*	**–0.165***
7.5F1	Total	0.080*	0.110*	–0.147*	0.136*	–0.119*	**–0.205***
	Positive	–0.064*	**0.174***	–0.102*	0.098*	–0.081*	–0.132*
	Negative	0.038*	–0.043*	–0.036*	0.038*	–0.023	**–0.065***
7.5F2	Total	0.019	0.009	**–0.109***	0.106*	–0.082*	0.002
	Positive	0.013	**0.122***	–0.068*	0.061*	–0.059*	–0.003
	Negative	0.081*	**–0.273***	–0.058	0.045	–0.033	–0.047
7.5RF1	Total	0.074*	0.090*	–0.084*	0.076*	–0.077*	**–0.104***
	Positive	–0.054*	**0.159***	–0.055*	0.044*	–0.057*	0.135*
	Negative	0.056*	–0.045*	–0.049*	0.048*	–0.046*	**–0.140***
7.5RF2	Total	0.038*	0.023*	**–0.052***	0.049*	–0.042*	–0.005*
	Positive	–0.100*	0.080*	–0.062*	0.071*	–0.045	**0.230***
	Negative	0.023*	–0.073*	–0.021*	0.019*	–0.018	**–0.102***

For the positive topographic changes, roughness was positively correlated to M3C2 distance; while for the negative topographic changes, roughness was negatively correlated to M3C2 distance (Table 5.8). This relationship is presented in more detail in Figure 5.11 (a–b) where the effect of roughness on topographic change is evident. These results suggest that rougher cells are indicative of more active topographic change. Slope showed strong negative correlations with negative topographic change (Table 5.6), indicating that erosion increases with an increase in slope gradient (Figure 5.11 (c)).

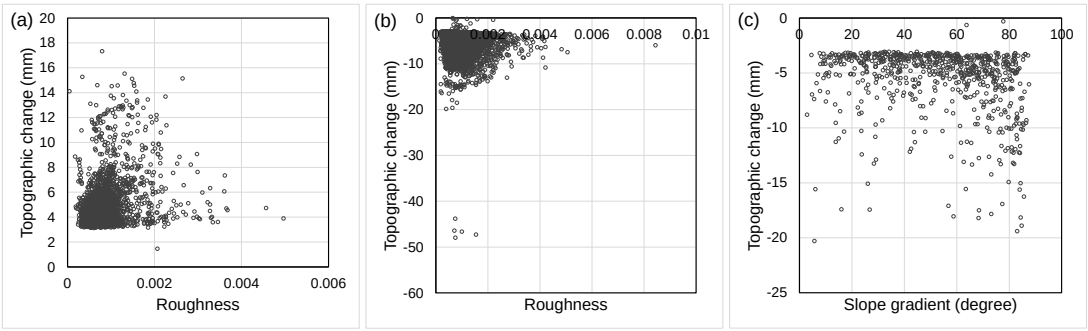

Figure 5.11 Relationships between topographic change and (a–b) roughness and (c) slope. The results were derived from models of (a) 7.5RF2; (b) 7.5R2; (c) 7.5F2. Roughness was calculated from the dense points of the start of the survey interval.

5.5 Discussion

5.5.1 SfM reconstructions of topographic changes

Geomorphic processes such as: i) water and aeolian erosion/deposition; ii) freezing and needle ice expansion and desiccation shrinkage; and iii) shrink–swelling and oxidation are operate on peat hillslopes (Grayson et al., 2012, Evans and Warburton, 2007, Glendell et al., 2017). The topographic change measured by the SfM technique is an aggregation of all of these processes across survey areas. In this study the ‘positive M3C2 distance’ reflects topographic change that could be caused by both deposition and swelling processes; while ‘negative M3C2 distance’ could also be attributed to both erosion and shrink processes.

5.5.1.1 3D reconstruction of topographic changes at plot scale (field experiments)

The error we obtained during the manual registration of the point clouds (mean value of 33 mm) is within the range of registration errors found by

other studies in natural terrain (Glendell et al., 2017). Glendell et al. (2017) reported a root mean square error based on GCPs ranging from 11 mm to 291 mm, with a mean value of 46 mm for different types of erosion features. Our study showed that the topographic changes observed over one year ranging from –14 to 30 mm for the four field sites. These values are moderate in comparison with the globally reported negative topographic change rates (24 ± 8 mm yr^{-1}) measured using erosion pins (Evans and Warburton, 2007, Grayson et al., 2012). Glendell et al. (2017) used ground photography SfM in ten upland peat sites distributed across England and Wales to measure erosion. They found the mean topographic change rate for the gully floor of different sites ranged from –286 mm to 31 mm yr^{-1} and the mean value was –33 mm yr^{-1}.

A net deposition of 30 mm was estimated for a relatively flat bare peat surface (Site 3) for the survey period from 26/10/2016 to 02/11/2017. This result is not in agreement with those previous studies (Imeson, 1974, Tallis and Yalden, 1983, Anderson, 1986) reporting a surface retreat rate of 1–41 mm yr^{-1} on low angled bare peat surfaces from similar blanket peat environments derived from erosion pin data. The discrepancy may be caused by the differences in the geomorphological context or the approaches to measure topographic change. Erosion pins measure erosion or deposition directly through observed changes in the peat surface at a given point (Grayson et al., 2012, Tuukkanen et al., 2016) and the point measurements are subsequently interpolated over relatively small areas. However, significant spatial variation even over small areas (Grayson et al., 2012) affects the accuracy and precision of erosion rates based on erosion pins. In addition, the pin method suffers from problems of disturbance and damage to the peat surface caused by repeated pin measurement. Consequently, erosion pin measurements are typically taken over long time periods to obtain high signal to noise ratio and more meaningful results. SfM is capable of providing fully distributed estimates of topographic change across a large area with minor disturbance of the peat surface. Grayson et al. (2012) compared the use of erosion pin and terrestrial laser scanning techniques for measuring erosion across a peatland site in northern England and found very different erosion rates: a net surface lowering of 38 mm measured using pins but a net deposition of 3–7 mm was calculated from laser scanning. However, SfM is still subject to a wide range of controls on surface elevation over short time periods so that the consideration of signal and noise is still pertinent.

5.5.1.2 3D reconstruction of topographic changes at plot scale (laboratory experiments)

Both positive and negative topographic changes were observed using SfM for simulated rainfall and simulated rainfall + inflow events. However, only positive topographic changes were captured for simulated inflow events. This means that simulated inflow events appeared to cause a higher net level of deposition-related topographic change than erosional denudation. Our previous studies showed that the effect of shallow overland flow on peat erosion, in the absence of rainfall, was low (Li et al., 2018c). Positive topographic changes could be explained by saturation-related surface upwelling processes pushing peat particles upwards, or more likely it is due to the fact that eroded peat is loose and less compact that when it was in situ and so re-deposition of such loose peat materials could result in positive topographic change.

Peat loss data estimated with sediment fluxes at the plot outlet and SfM methodologies were not comparable with each other (Figure 5.10). Deposition-related change measured by SfM was 7.02 ± 48.29 g (0.7 ± 4.3 mm), in comparison with erosion-related change derived from the sediment flux method of 1.05 ± 0.55 g (0.1 ± 0.1 mm). The two approaches measure different things and are suitable for different applications. For many applications surface change is used as a proxy for erosion; while for other applications the mass lost is a key parameter of interest.

5.5.2 Spatial and temporal evolution of eroding headwater peatlands

The main headcut of the tributary (Site 4) experienced net accumulation during the whole study period, with a median net increase in the peat surface height of 22 mm (Table 5.4). This result suggests that incision dynamics and headward migration of the gullies was not active during the whole study period. The main reason is probably that the headcut is covered with dense vegetation on the upper hillslopes (Figure 5.1), which may limit rapid overland flow and prevents the expansion of the gully network. Negative topographic change mainly occurred at the base of the headcuts due to wash of flow accumulated from upper positions. Among the four study sites, the lateral-bank headcut (Site 2) had the most significant negative topographic changes and net surface lowering for the majority of surveys. Field observations showed that the location of the steep lateral-bank gully wall (Site 2) was strongly linked with flowpaths that concentrated and directed overland flow from the upper gentle hillslopes to the main channel

(Figure 5.1), resulting in active progress of gully incision. These results confirm that gully networks can expand rapidly in peatlands (Bower, 1960b). It is thus very important to reduce the hydrological connectivity and slope steepness of gully walls in order to control peatland gully erosion.

A net increase in the peat surface height was observed for the surveyed sites in November 2016 (see Figure 5.4 (b) for an example). Low temperatures observed during this month (Table 5.6) were accompanied by significant ice on the surface which led to an expansion of the peat surface. In addition, diurnal freezing was common in November 2016 with temperature frequently fluctuating above and below zero (Figure 5.2) which was ideal for needle ice growth. Freezing and thawing occurred multiple times and as such was important in producing loose particles and aggregates on the surface. The subsequent rainfall events in December caused erosion of the available peat materials prepared by previous needle-ice freezing and thawing, leading to a net surface lowering (Figure 5.4 (c)). These results are in agreement with those reported by Li et al. (2018b) who found that needle ice production is a primary process contributing to upland peat erosion by enhancing peat erodibility during runoff events following thaw. A net decrease in the peat surface height was observed for all four sites from 22/02/2017 to 07/04/2017 (Table 5.4). Over this period there was a general increase in the mean temperature. The long periods of dry conditions in April 2017 (Table 5.6) resulted in desiccation and drying and cracking of the peat surface and a corresponding surface lowering. Our study showed that short term topographic changes allow useful inference of processes, which are similar to those reported by Evans and Warburton (2007) based on high temporal resolution measurement of peat surface elevation.

A comparison of consecutive surveys with longer-term survey intervals that integrate multiple events reveals different patterns (Table 5.3 and Figures 5.3–5.6). In this study, the main topographic change was observed between a single short-term interval when intense rainfall, flow wash, needle ice production or surface desiccation was observed. However, several changes observed at the short-term scale were cancelled out by further topographic changes in the opposite direction (i.e. erosion followed by deposition) that cannot be discerned from longer monitoring intervals. When attempting to determine topographic changes and earth surface processes, an event-scale survey resolution that can capture important drivers (i.e. heavy rainfall event, needle ice production, serious desiccation) is therefore important. The

stronger control of roughness observed at the event-scale exemplifies the importance of event-scale monitoring. These results obtained from upland peatlands, are in agreement with those reported by Vericat et al. (2014) in a humid badland, who found that an event-scale survey resolution was important for detecting geomorphological changes and could yield better understanding of the driving processes than long-term survey intervals which integrate over multiple process-responses making individual drivers more difficult to determine.

5.5.3 Relationships between spatial patterns and topographic variables

From the relationships identified between spatial patterns of topographic change and topographic variables, there are four key factors that should be highlighted. First, a significant relationship between topographic change and surface roughness was observed consistently at both the field plot scale (Table 5.5) and laboratory macroscale (Table 5.8). Roughness was positively correlated to the positive topographic change; while was negatively correlated to negative topographic change. The main reasons are: i) an increased roughness of bare peat surfaces has important feedbacks on sediment transport mechanisms by reducing overland flow velocity; and ii) surface roughness at the studied small scales provides insights into the erosion agents (e.g., wind-driven rain, surface wash, frost action and desiccation) and the relative magnitude and direction of the sediment transfer process (Evans and Warburton, 2007, Smith and Warburton, 2018). In addition, this study highlights the importance of roughness in particular for short-term surveys during which needle-ice production, desiccation and rainsplash and surface wash take place. Over the long-term scale the relationship was less pronounced. The main reason is probably that both the topographic change and roughness of bare peat surfaces are driven by key natural drivers (rainfall, surface wash, wind action, needle-ice production and desiccation) that take place at event-scales (Evans and Warburton, 2007, Smith and Warburton, 2018). However, as roughness changes soon after the initial survey, over longer timescales topographic changes are less strongly related to initial roughness and other topographic variables (i.e. slope or aspect) become more important (Table 5.5, see Model 11–1 for an example). Our study is in agreement with Vericat et al. (2014) who found via a series of event-scale surveys that roughness had a significant linear relationship with topographic change in a sub-humid, highly erodible badland. From the multi-temporal perspective these studies

suggest that roughness is an important factor in the development of humid peatlands and other environments such as sub-humid badlands. In addition, the importance of roughness is enhanced at particular times of year such as during frost events (needle-ice freezing and thawing) in winter, desiccation in a dry summer period and heavy rainfall events in early autumn. Surface roughness controls on spatial patterns of topographic change are also illustrated by laboratory event-scale surveys before and after the rainfall simulation experiments (Table 5.8). Second, the relationship between slope and topographic change was also important (Figure 5.7 and 5.11) and would be expected (Grayson et al., 2012, Fox and Bryan, 2000). The positive correlation of slope with drainage density reflects the dominant role of fluvial action in initiating peat erosion (Mosely, 1972). Third, a significant relationship between curvature and topographic change was evident especially for the laboratory micro peat block scale (Table 5.8). Fourth, a significant relationship between aspect and topographic change was found at the field plot scale. For some models (i.e. Site 1: Model 5–4) aspect was the main driver of change (Table 5.6). The west-facing part of the peat hagg was actively eroded, suggesting that the prevailing westerly wind and lateral rain were important processes on the peat hagg (Evans and Warburton, 2007). More needle-ice formation was found during winter months on the north-facing gully wall than the other three field sites.

5.5.4 Implications of SfM applications for peat erosion study

In this study we used SfM photogrammetry for peat laboratory flumes and field sites with different geomorphological features. SfM is a technique that is cheap, fast and easy to use in terms of data acquisition and post-processing. SfM provides fully distributed estimates of topographic change and datasets for quantification of controls and drivers. In addition, SfM has the advantage of removing surface disturbance which is difficult to avoid when using many conventional and invasive methods such as erosion pins.

In future, a more detailed understanding of the processes driving observed erosion and deposition patterns could be informed by a segregation of the sediment budget according to the driving process, achieved either by visual inspection, analysis of localised volumetric changes (Wheaton et al., 2013) or roughness analysis (Smith and Warburton, 2018).

Compared to sediment flux at the outlet of bounded plots, SfM is capable of capturing microscale processes that are important in producing variable topographic change patterns during sheet wash even at the very fine (0.13 m^2) scale. The high-resolution topographic data derived from SfM provides

insights into both the quantities and also the potential controls and drivers of such geomorphic changes.

In this study we used permanent GCPs to reduce errors derived from disturbance and damage to the peat during repeat surveying of the coordinates of GCPs. However, future work is required to reduce error for field SfM surveys in peatlands, and for other environments (Borrelli et al., 2017) where erosion or deposition is only a few cm or mm per year.

Numerical models, such as the USLE (May et al., 2010), CAESAR model (Coulthard et al., 2000) and the PESERA–PEAT model (Li et al., 2016b) have been tested in blanket peatlands and are capable of predicting some runoff–erosion relationships. However, incorporating some of the important erosion processes into peat erosion models remains a challenge either due to difficulties in the parametrization of processes that are not fully understood or, as is often the case, a lack of field data for model calibration and validation. Erosion models depend on Digital Elevation Models (DEMs) and their modelling abilities have usually been applied at large-scales (regional, national and global scales) with relatively low resolution DEMs to shorten calculation time. However, since processing time is decreasing with growing computer capacity, there is an increasing trend towards high resolution and small-scale erosion modelling (Kaiser et al., 2014). In this context, the use of SfM techniques provides new possibilities. High resolution DEMs derived from SfM techniques at centimeter-scale or even higher resolution enables sediment budget estimation and erosion features (e.g. rill formation, gully incisions) to be depicted more precisely. The M3C2 and volumetric change data can be used for peat erosion modelling, as predicted peat erosion rate (e.g., surface retreat rate, peat loss volumes) can be validated by SfM measurements.

5.5.5 Limitations

Topographic change in the peat surface can occur through changes in peat density that could result from lower density peat being deposited at the peat surface from upslope, or from swell-shrink and freeze-thaw processes that make the peat less dense at the surface. Future longer (at least annual) timescales of monitoring should be undertaken to capture longer term signals that stand out from the noise of surface oscillations caused by short-term peat density changes.

The size of the peat blocks used in the laboratory was fairly small but meant that it was feasible to obtain undisturbed samples for laboratory treatment,

and to produce quantifiable results with good levels of experimental control. However, it should be noted that the bounded plots produce erosion rates declining with rainfall simulation due to the previously weathered peat particles being splashed and transported by overland flow, resulting in a detachment-limited condition (Li et al., 2018c).

The four field survey plots were selected to represent typical erosion features in blanket peatlands. However, peat loss measurements at one scale are not representative of sediment yield at another scale. A direct extrapolation of plot scale erosion rates up the catchment scale can be problematic (De Vente and Poesen, 2005, Parsons et al., 2006a) since bank erosion (Small et al., 2003) and mass movements (Evans and Warburton, 2007, Evans et al., 2006) form an important part of the catchment sediment budget in upland peat catchments. More field monitoring is needed as a basis for scaling erosion rates from one specific area to larger or smaller areas.

5.6 Conclusions

The net topographic change for the field sites was –14 to +30 mm yr^{-1}. Headward migration of the gully head was not active due to the dense vegetation cover on the upper hillslopes. The lateral-bank headcut had the most significant negative topographic changes since flowpaths were concentrated and well connected. Needle-ice formation on the peat surface resulted in a significant expansion of the upper peat layer; while drying and cracking of the peat surface led to a corresponding surface lowering. The main topographic change was observed between surveys that occurred only a few weeks apart when intense rainfall, flow wash, needle ice production or surface desiccation occurred. Thus we advocate that repeated SfM surveys that capture change between events or seasons will be beneficial and cost effective for understanding longer-term peat erosion dynamics. SfM can provide high spatial resolution data to understand long term erosion and processes at event timescales.

Aspect, slope and surface roughness are significant predictors of topographic change at field plot scale. Slope, curvature and roughness are significantly correlated with topographic change at laboratory macroscale.

On the laboratory peat blocks a mean peat loss rate of 0.1 mm (SD: 0.1 mm) was measured by the plot outlet yield sampling method, compared with a mean peat deposition rate of 0.7 mm (SD: 4.3 mm) derived from the SfM

methodology. Hence we have shown that microscale processes are important in producing variable topographic change patterns during sheet wash that can be captured well by SfM methods.

Acknowledgements

The work was jointly funded by the China Scholarship Council and the University of Leeds (File No. 201406040068). Jonathan Carrivick and Lee Brown are thanked for providing the Geodimeter and tinytag temperature loggers used in this study. Special acknowledgement is given to David Ashley who helped prepare the laboratory experimental materials and field set-up. Santiago Clerici and Sarah Hunt are gratefully acknowledged for their time and assistance involved in field work. Duncan Quincey, Scott Watson and Joe Mallalieu are thanked for providing advice on using Agisoft Photoscan and CloudCompare to undertake data analysis. We are grateful to Claudio Bravo L. and Yi-Min Chang Chien (University of Leeds) for providing help in data visualization.

References

ANDERSON, P. 1986. Accidental moorland fires in the Peak District: a study of their incidence and ecological implications. *Report to the Peak District Moorland Restoration Project Peak District Planning Board***,** 164.

BARNHART, T. B. & CROSBY, B. T. 2013. Comparing two methods of surface change detection on an evolving thermokarst using high-temporal-frequency terrestrial laser scanning, Selawik River, Alaska. *Remote Sensing,* 5**,** 2813-2837.

BONN, A., ALLOTT, T., EVANS, M., JOOSTEN, H. & STONEMAN, R. 2016. *Peatland restoration and ecosystem services: science, policy and practice*, Cambridge University Press.

BORRELLI, P., ROBINSON, D. A., FLEISCHER, L. R., LUGATO, E., BALLABIO, C., ALEWELL, C., MEUSBURGER, K., MODUGNO, S., SCHÜTT, B. & FERRO, V. 2017. An assessment of the global impact of 21st century land use change on soil erosion. *Nature Communications,* 8**,** 2013.

BOWER, M. 1960a. The erosion of blanket peat in the southern Pennines. *East Midland Geographer,* 13**,** 22-33.

BOWER, M. 1960b. Peat erosion in the Pennines. *Advancement of Science,* 64**,** 323-331.

BOWER, M. 1961. The distribution of erosion in blanket peat bogs in the Pennines. *Transactions and Papers (Institute of British Geographers),* 29**,** 17-30.

BOWYER-BOWER, T. & BURT, T. 1989. Rainfall simulators for investigating soil response to rainfall. *Soil Technology,* 2**,** 1-16.

BURT, T. & GARDINER, A. 1984. Runoff and sediment production in a small peat-covered catchment: some preliminary results. *Catchment Experiments in Fluvial Geomorphology* Norwich, England: Geo Books.

DE VENTE, J. & POESEN, J. 2005. Predicting soil erosion and sediment yield at the basin scale: Scale issues and semi-quantitative models. *Earth-Science Reviews,* 71**,** 95-125.

ELTNER, A., KAISER, A., ABELLAN, A. & SCHINDEWOLF, M. 2017. Time lapse structure from motion photogrammetry for continuous geomorphic monitoring. *Earth Surface Processes and Landforms,* 42**,** 2240-2253.

EVANS, M., ALLOTT, T., HOLDEN, J., FLITCROFT, C. & BONN, A. 2005. Understanding gully blocking in deep peat. *Moors for the Future Report.* Derbyshire.

EVANS, M., BURT, T., HOLDEN, J. & ADAMSON, J. 1999. Runoff generation and water table fluctuations in blanket peat: evidence from UK data spanning the dry summer of 1995. *Journal of Hydrology,* 221**,** 141-160.

EVANS, M. & LINDSAY, J. 2010a. High resolution quantification of gully erosion in upland peatlands at the landscape scale. *Earth Surface Processes and Landforms,* 35**,** 876-886.

EVANS, M. & LINDSAY, J. 2010b. Impact of gully erosion on carbon sequestration in blanket peatlands. *Climate Research,* 45**,** 31-41.

EVANS, M. & WARBURTON, J. 2005. Sediment budget for an eroding peat ‐ moorland catchment in northern England. *Earth Surface Processes and Landforms,* 30**,** 557-577.

EVANS, M. & WARBURTON, J. 2007. *Geomorphology of upland peat: erosion, form and landscape change,* Oxford, UK, John Wiley & Sons.

EVANS, M., WARBURTON, J. & YANG, J. 2006. Eroding blanket peat catchments: global and local implications of upland organic sediment budgets. *Geomorphology,* 79**,** 45-57.

FONSTAD, M. A., DIETRICH, J. T., COURVILLE, B. C., JENSEN, J. L. & CARBONNEAU, P. E. 2013. Topographic structure from motion: a new development in photogrammetric measurement. *Earth Surface Processes and Landforms,* 38**,** 421-430.

FOX, D. M. & BRYAN, R. B. 2000. The relationship of soil loss by interrill erosion to slope gradient. *Catena,* 38**,** 211-222.

FRANCIS, I. 1990. Blanket peat erosion in a mid ‐ wales catchment during two drought years. *Earth Surface Processes and Landforms,* 15**,** 445-456.

GLENDELL, M., MCSHANE, G., FARROW, L., JAMES, M. R., QUINTON, J., ANDERSON, K., EVANS, M., BENAUD, P., RAWLINS, B. & MORGAN, D. 2017. Testing the utility of structure ‐ from ‐ motion photogrammetry reconstructions using small unmanned aerial vehicles and ground photography to estimate the extent of upland soil erosion. *Earth Surface Processes and Landforms,* 42**,** 1860-1871.

GÓMEZ-GUTIÉRREZ, Á., DE SANJOSÉ-BLASCO, J. J., LOZANO-PARRA, J., BERENGUER-SEMPERE, F. & DE MATÍAS-BEJARANO, J. 2015. Does HDR pre-processing improve the accuracy of 3D models obtained by means of two conventional SfM-MVS software

packages? The case of the Corral del Veleta Rock Glacier. *Remote Sensing,* 7**,** 10269-10294.

GRAYSON, R., HOLDEN, J., JONES, R., CARLE, J. & LLOYD, A. 2012. Improving particulate carbon loss estimates in eroding peatlands through the use of terrestrial laser scanning. *Geomorphology,* 179**,** 240-248.

HOLDEN, J. & BURT, T. 2002a. Infiltration, runoff and sediment production in blanket peat catchments: implications of field rainfall simulation experiments. *Hydrological Processes,* 16**,** 2537-2557.

HOLDEN, J. & BURT, T. 2002b. Laboratory experiments on drought and runoff in blanket peat. *European Journal of Soil Science,* 53**,** 675-690.

HOLDEN, J. & BURT, T. 2003. Hydrological studies on blanket peat: the significance of the acrotelm - catotelm model. *Journal of Ecology,* 91**,** 86-102.

HOLDEN, J., KIRKBY, M. J., LANE, S. N., MILLEDGE, D. G., BROOKES, C. J., HOLDEN, V. & MCDONALD, A. T. 2008. Overland flow velocity and roughness properties in peatlands. *Water Resources Research,* 44**,** W06415.

IMESON, A. 1974. The origin of sediment in a moorland catchment with particular reference to the role of vegetation. *Institute of British Geographers Special Publication,* 6**,** 59-72.

ISERLOH, T., RIES, J., ARNÁEZ, J., BOIX-FAYOS, C., BUTZEN, V., CERDÀ, A., ECHEVERRÍA, M., FERNÁNDEZ-GÁLVEZ, J., FISTER, W. & GEIßLER, C. 2013. European small portable rainfall simulators: A comparison of rainfall characteristics. *Catena,* 110**,** 100-112.

JAMES, M. & ROBSON, S. 2012. Straightforward reconstruction of 3D surfaces and topography with a camera: Accuracy and geoscience application. *Journal of Geophysical Research: Earth Surface,* 117**,** F03017.

KAISER, A., NEUGIRG, F., ROCK, G., MÜLLER, C., HAAS, F., RIES, J. & SCHMIDT, J. 2014. Small-scale surface reconstruction and volume calculation of soil erosion in complex Moroccan gully morphology using structure from motion. *Remote Sensing,* 6**,** 7050-7080.

KLØVE, B. 1998. Erosion and sediment delivery from peat mines. *Soil and Tillage Research,* 45**,** 199-216.

LABADZ, J., BURT, T. & POTTER, A. 1991. Sediment yield and delivery in the blanket peat moorlands of the Southern Pennines. *Earth Surface Processes and Landforms,* 16**,** 255-271.

LAGUE, D., BRODU, N. & LEROUX, J. 2013. Accurate 3D comparison of complex topography with terrestrial laser scanner: Application to the Rangitikei canyon (NZ). *ISPRS Journal of Photogrammetry and Remote Sensing,* 82**,** 10-26.

LI, C., GRAYSON, R., HOLDEN, J. & LI, P. 2018a. Erosion in peatlands: Recent research progress and future directions. *Earth-Science Reviews,* 185**,** 870-886.

LI, C., HOLDEN, J. & GRAYSON, R. 2018b. Effects of needle ice production and thaw on peat erosion processes during overland flow events. *Journal of Geophysical Research: Earth Surface,* 123**,** 2107-2122

LI, C., HOLDEN, J. & GRAYSON, R. 2018c. Effects of rainfall, overland flow and their interactions on peatland interrill erosion processes. *Earth Surface Processes and Landforms,* 43**,** 1451-1464.

LI, P., HOLDEN, J. & IRVINE, B. 2016a. Prediction of blanket peat erosion across Great Britain under environmental change. *Climatic Change,* 134**,** 177-191.

LI, P., HOLDEN, J., IRVINE, B. & GRAYSON, R. 2016b. PESERA‐PEAT: a fluvial erosion model for blanket peatlands. *Earth Surface Processes and Landforms,* 41**,** 2058-2077.

LI, P., HOLDEN, J., IRVINE, B. & MU, X. 2017. Erosion of Northern Hemisphere blanket peatlands under 21st‐century climate change. *Geophysical Research Letters,* 44**,** 3615-3623.

MALLALIEU, J., CARRIVICK, J. L., QUINCEY, D. J., SMITH, M. W. & JAMES, W. H. 2017. An integrated Structure-from-Motion and time-lapse technique for quantifying ice-margin dynamics. *Journal of Glaciology***,** 1-13.

MARTÍNEZ-MURILLO, J., NADAL-ROMERO, E., REGÜÉS, D., CERDÀ, A. & POESEN, J. 2013. Soil erosion and hydrology of the western Mediterranean badlands throughout rainfall simulation experiments: a review. *Catena,* 106**,** 101-112.

METOFFICE 2018. Maps of climate variables for months, seasons and years https://www.metoffice.gov.uk/climate/uk/summaries/anomacts.

MICHELETTI, N., CHANDLER, J. H. & LANE, S. N. 2015a. Investigating the geomorphological potential of freely available and accessible structure‐from‐motion photogrammetry using a smartphone. *Earth Surface Processes and Landforms,* 40**,** 473-486.

MICHELETTI, N., CHANDLER, J. H. & LANE, S. N. 2015b. Structure from motion (SFM) photogrammetry. *In:* CLARKE, L. E. & NIELD, J. M. (eds.) *Geomorphological Techniques (Online Edition).* London: British Society for Geomorphology.

MORGAN, J. A., BROGAN, D. J. & NELSON, P. A. 2017. Application of Structure-from-Motion photogrammetry in laboratory flumes. *Geomorphology,* 276**,** 125-143.

MOSELY, M. 1972. Gully systems in blanket peat, Bleaklow, North Derbyshire. *East Midland Geographer,* 5**,** 235-244.

NATIONALRIVERFLOWARCHIVE 2018. Catchment daily rainfall record of Snaizeholme Beck at Low Houses (1961-2015) https://nrfa.ceh.ac.uk/data/station/meanflow/27047.

PARSONS, A. J., BRAZIER, R. E., WAINWRIGHT, J. & POWELL, D. M. 2006a. Scale relationships in hillslope runoff and erosion. *Earth Surface Processes and Landforms,* 31**,** 1384-1393.

PARSONS, A. J., WAINWRIGHT, J., BRAZIER, R. E. & POWELL, D. M. 2006b. Is sediment delivery a fallacy? *Earth Surface Processes and Landforms,* 31**,** 1325-1328.

PROSDOCIMI, M., BURGUET, M., DI PRIMA, S., SOFIA, G., TEROL, E., COMINO, J. R., CERDÀ, A. & TAROLLI, P. 2017. Rainfall simulation and Structure-from-Motion photogrammetry for the analysis of soil water erosion in Mediterranean vineyards. *Science of the Total Environment,* 574**,** 204-215.

ROTHWELL, J. J., LINDSAY, J. B., EVANS, M. G. & ALLOTT, T. E. 2010. Modelling suspended sediment lead concentrations in contaminated peatland catchments using digital terrain analysis. *Ecological Engineering,* 36**,** 623-630.

SMALL, I., ROWAN, J. & DUCK, R. 2003. Long-term sediment yield in Crombie Reservoir catchment, Angus; and its regional significance within the Midland Valley of Scotland. *Hydrological Sciences Journal,* 48**,** 619-635.

SMITH, M., CARRIVICK, J., HOOKE, J. & KIRKBY, M. 2014. Reconstructing flash flood magnitudes using 'Structure-from-Motion': A rapid assessment tool. *Journal of Hydrology,* 519**,** 1914-1927.

SMITH, M., CARRIVICK, J. & QUINCEY, D. 2016. Structure from motion photogrammetry in physical geography. *Progress in Physical Geography,* 40**,** 247-275.

SMITH, M. & WARBURTON, J. 2018. Microtopography of bare peat: a conceptual model and objective classification from high‐resolution topographic survey data. *Earth Surface Processes and Landforms,* 43**,** 1557-1574.

SMITH, M. W. & VERICAT, D. 2015. From experimental plots to experimental landscapes: topography, erosion and deposition in sub‐humid badlands from structure‐from‐motion photogrammetry. *Earth Surface Processes and Landforms,* 40**,** 1656-1671.

SNAPIR, B., HOBBS, S. & WAINE, T. 2014. Roughness measurements over an agricultural soil surface with Structure from Motion. *ISPRS Journal of Photogrammetry and Remote Sensing,* 96**,** 210-223.

STÖCKER, C., ELTNER, A. & KARRASCH, P. 2015. Measuring gullies by synergetic application of UAV and close range photogrammetry—A case study from Andalusia, Spain. *Catena,* 132**,** 1-11.

STUMPF, A., MALET, J.-P., ALLEMAND, P., PIERROT-DESEILLIGNY, M. & SKUPINSKI, G. 2015. Ground-based multi-view photogrammetry for the monitoring of landslide deformation and erosion. *Geomorphology,* 231**,** 130-145.

TALLIS, J. & YALDEN, D. 1983. Peak District Moorland Restoration Project Phase 2 Report. *Peak District National Park Authority, Bakewell*.

TUUKKANEN, T., STENBERG, L., MARTTILA, H., FINÉR, L., PIIRAINEN, S., KOIVUSALO, H. & KLØVE, B. 2016. Erosion mechanisms and sediment sources in a peatland forest after ditch cleaning. *Earth Surface Processes and Landforms,* 41**,** 1841-1853.

VERICAT, D., SMITH, M. & BRASINGTON, J. 2014. Patterns of topographic change in sub-humid badlands determined by high resolution multi-temporal topographic surveys. *Catena,* 120**,** 164-176.

WATSON, C. S., QUINCEY, D. J., SMITH, M. W., CARRIVICK, J. L., ROWAN, A. V. & JAMES, M. R. 2017. Quantifying ice cliff evolution with multi-temporal point clouds on the debris-covered Khumbu Glacier, Nepal. *Journal of Glaciology,* 63**,** 823-837.

WESTOBY, M. J., DUNNING, S. A., HEIN, A. S., MARRERO, S. M. & SUGDEN, D. E. 2016. Interannual surface evolution of an Antarctic blue-ice moraine using multi-temporal DEMs. *Earth Surface Dynamics,* 4**,** 515.

WHEATON, J. M., BRASINGTON, J., DARBY, S. E., KASPRAK, A., SEAR, D. & VERICAT, D. 2013. Morphodynamic signatures of braiding mechanisms as expressed through change in sediment storage in a gravel‐bed river. *Journal of Geophysical Research: Earth Surface,* 118**,** 759-779.

XU, J., MORRIS, P. J., LIU, J. & HOLDEN, J. 2018. PEATMAP: Refining estimates of global peatland distribution based on a meta-analysis. *Catena,* 160**,** 134-140.

YU, Z. 2012. Northern peatland carbon stocks and dynamics: a review. *Biogeosciences,* 9**,** 4071-4085.

Chapter 6
Sediment and fluvial particulate carbon flux from an eroding peatland catchment in northern England

6.1 Abstract

Erosion and the associated loss of carbon is a major environmental concern in many peatlands and remains difficult to accurately quantify beyond the plot scale. Erosion was measured in an upland blanket peatland catchment (0.017 km^2) in northern England using Structure-from-Motion (SfM) photogrammetry, sediment traps and stream sediment sampling. A net median topographic change of –27 mm yr^{-1} was recorded by SfM over the 12-month monitoring period for the 598 m^2 surveyed area. Substantial amounts of peat were captured in sediment traps during summer storm events after two months of dry weather where desiccation of the peat surface occurred. The magnitude of topographic change for nested catchments determined by SfM (mean value: 5.3 mm, standard deviation: 5.2 mm) was very different to the areal average derived from sediment traps (mean value: –0.3 mm, standard deviation: 0.1 mm). Thus direct interpolation of peat erosion from local net topographic change into sediment yield at the catchment outlet appears problematic. Peat loss measured at the hillslope scale was not representative of that at the catchment scale. Stream sediment sampling suggested that the yields of suspended sediment and particulate organic carbon were 926.3 t km^{-2} yr^{-1} and 340.9 t km^{-2} yr^{-1} respectively, with highest losses occurring during the autumn. Both freeze–thaw during winter and desiccation during long periods of dry weather in spring and summer were identified as important peat weathering processes during the study. Such weathering was a key enabler of subsequent fluvial peat loss from the catchment.

KEY WORDS: peatlands; erosion; sediment; POC; SfM; topographic change; desiccation

6.2 Introduction

Peatlands cover approximately 4.23 million km^2 (2.84%) of the world's land area (Xu et al., 2018b). They store an equivalent of around two thirds of carbon stored in the atmosphere (Yu et al., 2010). Peatlands in the UK are highly valued because they provide a wide range of ecosystem services such as water supply (Xu et al., 2018a), biodiversity and recreation (Holden et al., 2007, Bonn et al., 2009) and the largest terrestrial carbon pool (Cannell et al., 1993, Milne and Brown, 1997). Though peatlands form a significant carbon reserve, they are fragile ecosystems and can be degraded under a wide range of internal and external pressures (Parry et al., 2014). Numerous studies have suggested that peatlands can be both sinks and sources of carbon to the environment (Clay et al., 2012, Holden et al., 2007). Land management practices and pollution have led to disturbance of peat surfaces, resulting in large areas being extensively eroded (Evans and Warburton, 2007, Li et al., 2016b, Li et al., 2018a) or under increasing erosion risk (Li et al., 2016a, Li et al., 2017) in many peatlands of the UK. The physical disturbance of peat by weathering processes (e.g., freeze–thaw and desiccation) and erosive forces (e.g., water and wind) has the potential to significantly affect the ability of peat to sequester carbon (Evans and Warburton, 2007).

Fluvial organic carbon fluxes in both particulate and dissolved forms are important links between terrestrial peatland carbon stores and ocean carbon sink (Hope et al., 1997). Fluvial carbon is also subject to oxidation representing an important link between terrestrial and atmospheric carbon pools (Pawson et al., 2012). While dissolved organic carbon (DOC) fluxes have been well studied (Worrall et al., 2003, Worrall et al., 2009, Evans et al., 2006), particulate organic carbon (POC) losses from peatlands has been much less studied (Pawson et al., 2012, Hope et al., 1997, Billett et al., 2010). In less severely eroded or intact peatland systems, POC is usually 5–50% of the total organic carbon load (Hope et al., 1997, Dawson et al., 2002). However, for eroding headwater catchments the POC flux represents an even larger proportion of fluvial organic carbon export (Pawson et al., 2008, Evans and Warburton, 2005). For example, Pawson et al. (2008) reported that POC flux from an eroding site in the English Peak District represented over 80% of the total organic carbon fluxes (107 g C m^{-2} yr^{-1}) from the system. A similar magnitude of POC flux has been historically reported from other eroding peat systems in northern England (Crisp, 1966, Evans and Warburton, 2005). In headwater systems, active erosion forms

such as gullies typically export large amounts of POC to peatland streams (Evans et al., 2006, Evans and Warburton, 2007, Evans and Lindsay, 2010). Assessing the temporal patterns of POC from eroding peatlands has the potential to provide insight into the controls on fluvial carbon flux from these systems (Pawson et al., 2012). It can also provide important baseline data to assess effects of restoration projects on carbon fluxes in the fluvial system.

Weathering processes such as frost action and desiccation play an important role in supplying erodible peat particles for fluvial transport (Evans and Warburton, 2007, Li et al., 2018a). Frost weathering resulting from the freezing and thawing of water between peat particles is common in cool, high latitude or high altitude climates which support many peatlands, and plays a vital role in breaking up the peat surface during winter months (Francis, 1990, Labadz et al., 1991, Evans and Warburton, 2007, Li et al., 2018b). Its major expression is in the form of needle-ice which is important in producing eroding peat faces (Tallis, 1973, Luoto and Seppälä, 2000, Grab and Deschamps, 2004) with ice crystal growth gradually weakening and finally breaking peat soil aggregates and the subsequent warming and thawing weakening or loosening the fractured peat. The growth of needle ice can lead to a ‘fluffy’ peat surface that is loose and granular and vulnerable to being flushed off by overland flow events (Li et al., 2018b, Evans and Warburton, 2007). Surface desiccation during extended periods of dry weather is another important weathering process for producing erodible peat (Burt and Gardiner, 1984, Evans et al., 1999, Francis, 1990, Holden and Burt, 2002). Francis (1990) monitored erosion in a mid-Wales blanket peat catchment (Plynlimon) during two drought years (1983–1984) and found that frost action appeared to be of relatively little importance; and instead summer desiccation was far more significant. Li et al. (2016a) modelled the effect of future climate change on UK peatlands and found that peat desiccation is likely to become more important in blanket peatlands as a result of warmer summers. However, additional field monitoring data is required to parameterize models of the temporal dynamics of peat erosion and their responses to climate change (Li et al., 2017).

Different peat erosion processes are active at different spatial scales (Li et al., 2018a). For example, rainsplash, interrill and rill erosion are the dominant erosion processes studied at fine scales (erosion plots) (Holden et al., 2008, Li et al., 2018c, Li et al., 2018b, Holden and Burt, 2002, Grayson et al., 2012). For larger hillslopes and small and medium-size catchment scales, gully erosion and mass movements become more important, yielding

large quantities of sediment (Evans and Warburton, 2007, Evans et al., 2006, Evans and Warburton, 2005). At the large basin scale long-term erosion and sediment deposition processes are potentially more important due to large sediment sinks (footslopes and floodplains) (De Vente and Poesen, 2005). Little is known about the scale dependency of peat erosion. Further research is needed on the role of streams as sediment sources and (temporal) sinks. Multi-scale studies to facilitate spatial upscaling of erosion rates and provide data on the spatial connections between different units at each scale are necessary.

This paper addresses the above-mentioned key knowledge gaps by assessing the hydrosedimentary dynamics of a peat-dominated catchment over the course of a year, with particular focus on the role of suspended sediment load and fluvial carbon flux in the catchment response. The specific objectives are to (i) to measure fluvial suspended sediment and POC fluxes from an eroding headwater peatland system; (ii) to describe the dynamics of suspended sediment transport at different temporal scales (seasonal and monthly); and (iii) to compare peat erosion rates measured by different techniques (sediment traps, SfM photogrammetry, sediment sampling) at different scales (plot, mini-catchment and catchment).

6.3 Materials and methods

6.3.1 Study area

Extensive peat erosion in the UK occurs across many upland systems but particularly in the Pennine region of England (Bower, 1960; 1961; Evans and Warburton, 2007). Fleet Moss (54°14´55´´N, 2°12´53´´W) is an area of approximately 1.0 km^2 with deep blanket peat at an altitude of 550–580 m in the Yorkshire Dales National Park in North Yorkshire, England (Figure 6.1). The vegetation is dominated primarily by *Eriophorum vaginatum*, *Calluna vulgaris* and *Empetrum nigrum*. The research catchment (0.017 km^2) within Fleet Moss (Figure 6.2) has a large area of exposed bare peat with a range of erosion forms (interrill and rill erosion and gullying). There are well developed and connected Type 1 and Type 2 gully systems as classified by Bower (1960). On the flatter interfluve areas (slopes less than 5°), Type 1 dissection usually occurs with gullies branching and intersecting in an intricate dendritic network. On steeper slopes (exceeding 5°), Type 2 dissection dominates with a system of sparsely branched drainage gullies incised through the peat and aligned nearly parallel to each other.

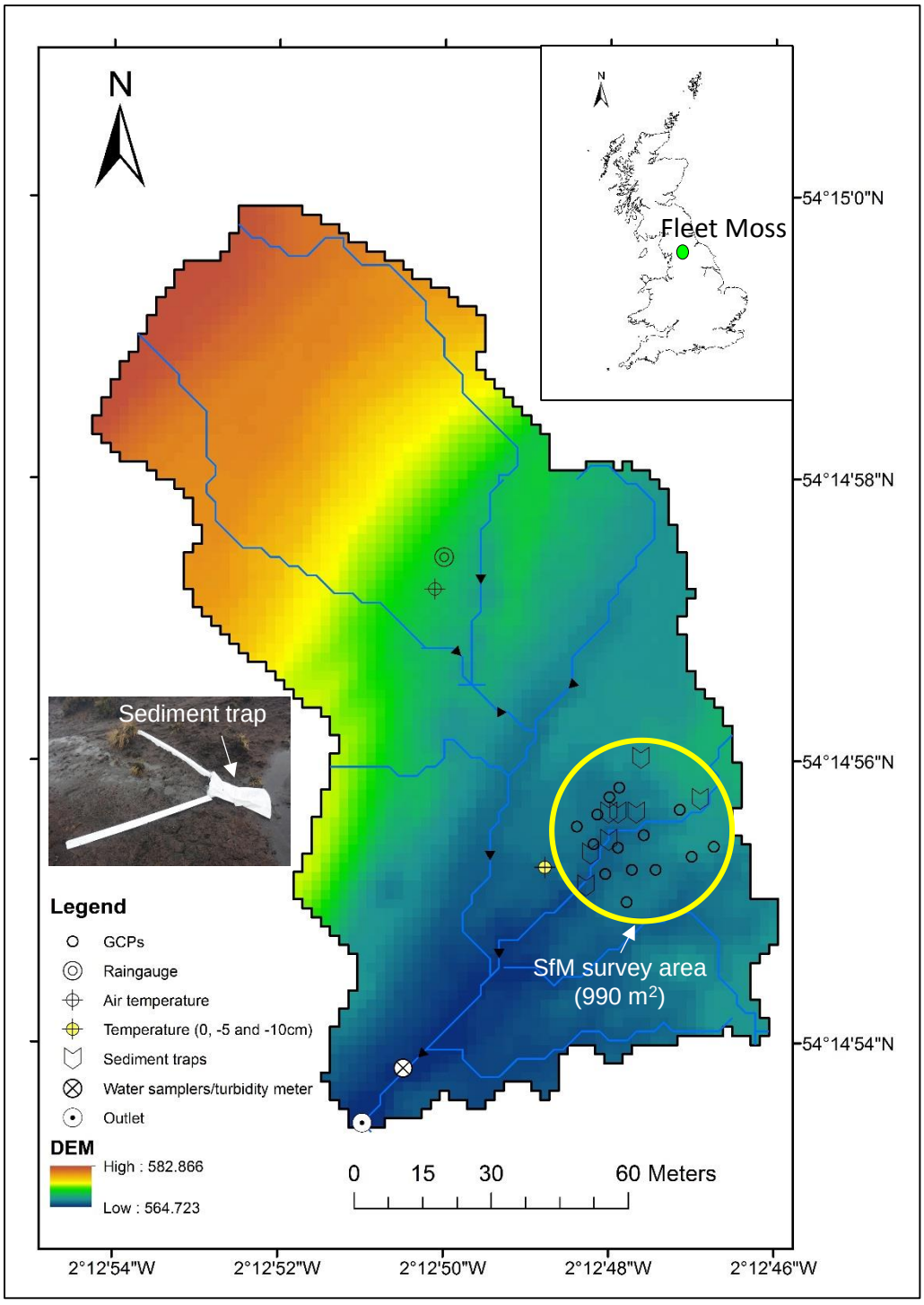

Figure 6.1 Map showing the position of Fleet Moss within the UK and the locations of field instruments in the research catchment (1.7 ha). Within the catchment there was a mini-catchment (990 m^2) where sediment traps were distributed and SfM surveys were conducted. An example sediment trap is shown in the inset photograph.

6.3.2 Data acquisition: monitoring and sampling

Data on climate parameters, discharge, sediment, POC and topographic changes were collected between October 2016 and November 2017. Discharge, sediment and POC were measured at the outlet of the research catchment (1.7 ha). For a 990 m^2 area within the 1.7 ha catchment, sediment was collected by traps and SfM surveys were conducted (Figure 6.1).

6.3.2.1 Climate data

Rainfall was logged every 15 minutes with a tipping bucket raingauge during the course of the study. Temperature was measured using Tinytag Plus 2 loggers (resolution 0.01 ºC) at 10-minute intervals from 26/10/2016 to 20/07/2017. The soil temperatures were recorded at surface, 5 cm and 10 cm depth. Air temperature was also measured using a Tinytag Plus 2 logger housed in a radiation shield approximately 1.5 m above the ground surface. A logger failure meant temperature was not recorded after 20/07/2017.

6.3.2.2 Topographic change measured by SfM Photogrammetry

SfM photogrammetry is a technique that is low cost and quick to use in terms of data acquisition and post-processing and thus was used to measure topographic change. Over the study period (26/10/2016–02/11/2017), a mini-catchment (990 m^2) was surveyed six times (Table 6.1). Since weather conditions during field campaigns significantly influence data quality (Snapir et al., 2014, Stöcker et al., 2015), image acquisition was arranged under conditions with no rain, no snow cover or no sunny weather to avoid producing strong shadows on images. Areas near the catchment boundary were subject to poorer quality SfM data (point clouds were sparse with large empty areas or vegetated points). Therefore, the SfM data analysis focused on a 598 m^2 central part of the catchment (yellow boundary shown in Figure 6.2).

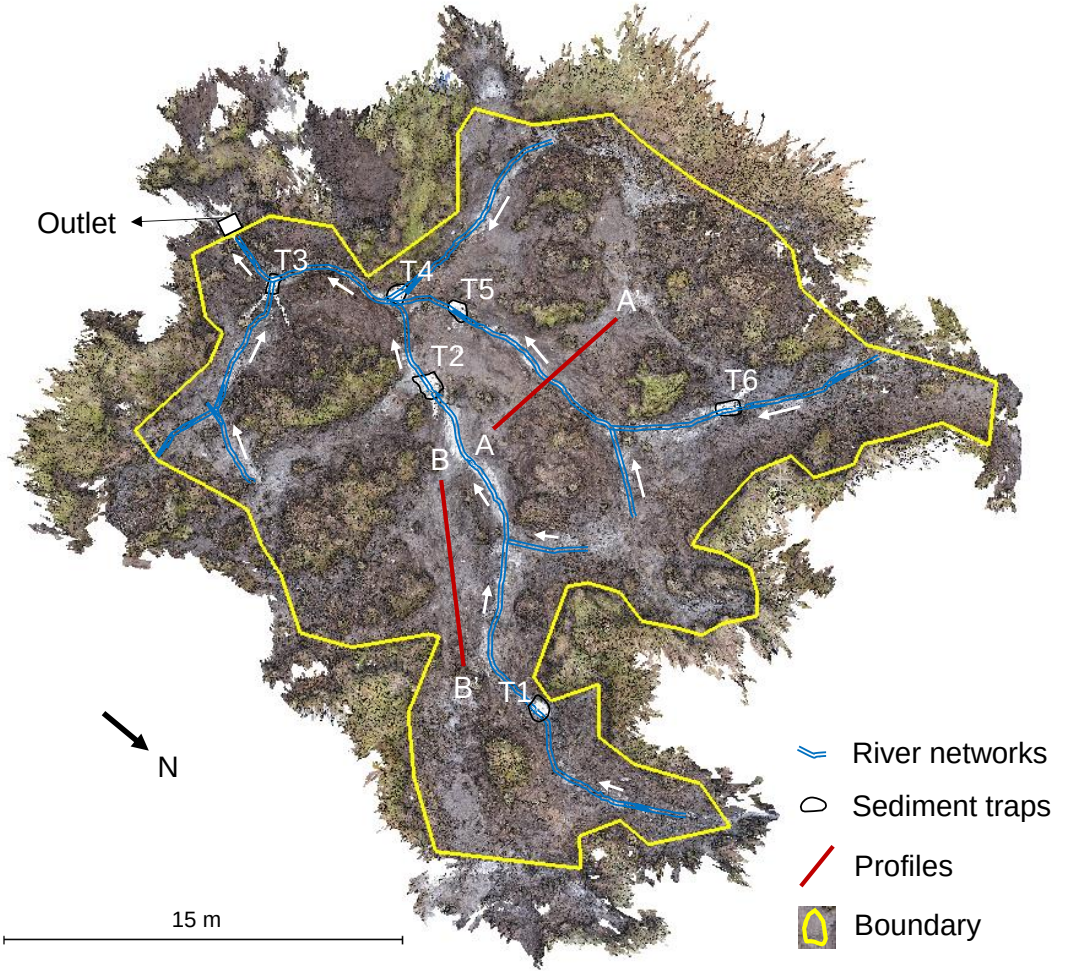

Figure 6.2 Orthophoto of the small-catchment (990 m^2) and the SfM focus area (with boundary outlined with yellow) (598 m^2). The sediment traps are numbered T1–T6. While the transect profiles are labelled A-A' and B-B' shown by the red lines.

Table 6.1 Summary of georeferencing errors (i.e. RMSE on control points) for the field surveys.

Survey date	No. of images	No. of GCPs	Georeferencing RMSE (mm)
04/11/2016	197	6	43.9
02/05/2017	166	6	33.3
13/06/2017	104	6	42.8
21/08/2017	197	6	49.2
27/09/2017	165	6	37.1
02/11/2017	208	6	36.8

Abundant high quality images were taken at positions and angles that have sufficient coverage of the peat erosion features of interest. In specific erosion features (i.e. gully heads, peat hagg), the density of images from additional perspectives was increased for further detailed reconstruction. The camera used was a Sony ILCE-6000 24 mega pixel digital camera with a 16 mm focal length. Camera settings varied based on light conditions, with exposure between 160 and 320 ISO, F-stop between f/4 and f/4.5 and exposure time between 1/160 and 1/80 second. Fourteen permanent Ground Control Points (GCPs) made of rebar (0.5–1.0 m in length) with a painted white top (high contrast with the dark peat surface) were placed around and within the feature of interest. The rebar was hammered deep into the substrate below the peat. A geodimeter was used and full surveys of the relative coordinates of all the GCPs were carried out at the start of the monitoring period.

Images acquired were processed using the commercial software Agisoft PhotoScan, to produce a dense point cloud based on the workflows described in Li et al. (accepted). Poorly located GCPs were excluded; however, a minimum of six GCPs that were well distributed over each site remained (Fonstad et al., 2013, Smith et al., 2014). Point-cloud quality was evaluated by summarizing residual errors using root mean squared error (*RMSE*) (Smith et al., 2014), and mean georeferencing uncertainty was 40.5 mm (Table 6.1). The derived dense point clouds contained both bare peat surface and vegetation points. Vegetation was filtered through selecting vegetation points based on RGB values embedded in the point cloud and the filtering was conducted in the open source CloudCompare software. Cloud-to-cloud differencing was computed using the Multiscale Model to Model Cloud Comparison (M3C2) algorithm that quantifies 3-D distance between two point clouds along the normal surface direction and provide a 95% confidence interval based on the point cloud roughness and co-registration uncertainty (Lague et al., 2013). M3C2 requires two main user-defined parameters: i) the normal scale *D*, which is used to calculate a surface normal for each point and is dependent upon surface roughness and registration error; ii) the projection scale *d* within which the average surface elevation of each cloud is calculated. In this study, the normal scale *D* for each point cloud was estimated based on a trial-and-error approach similar to that of Westoby et al. (2016) and was fixed at 0.5 m. The projection scale *d* was specified as 0.1 m and this scaling was enough to average a minimum of 30 points sampled in each cloud (Lague et al., 2013). M3C2 output was

subsequently masked to exclude points where change is lower than level of Level of Detection (LoD) threshold for a 95% confidence level ($LoD_{95\%}$), which is defined as:

$$LOD_{95\%}(d) = \pm 1.96\left(\sqrt{\frac{\sigma_1(d)^2}{n_1} + \frac{\sigma_2(d)^2}{n_2}} + reg\right) \quad (6.1)$$

where σ_1 and σ_2 represent the roughness of each point in sub-clouds of diameter d and size n_1 and n_2, and reg is the user-specified registration error which is assumed to be isotropic and spatially uniform across the dataset (Lague et al., 2013). The surface-to-surface Interactive Closest Point algorithm implemented in CloudCompare was used to align a patch of two inactive point clouds. The registration error was estimated by a series of tests and it ranged from 7.0 to 8.0 mm for the field models. Data analyses were conducted between individual survey dates with dates and intervals presented in Table 6.1 and Table 6.2. Between 26/10/2016 and 02/11/2017 the 6 repeat topographic surveys yielded 5 survey intervals (e.g., 2–1; 3–2), and a long-term survey interval (6–1) which was selected to represent potential large topographic changes (Table 6.2).

6.3.2.3 Peat eroded through fluvial processes

A series of sediment traps were used to measure the quantity of peat eroded by fluvial processes from different parts of the catchment from 04/11/2016 to 21/08/2017 (Figure 6.2). The traps were made of weaved polypropylene bags which allow water to drain through the sack, but any peat transported in suspension would be trapped. The trapping efficiency was assessed in the laboratory by pouring 1 L peat solution (100 g L^{-1}) into a polypropylene bag over a plastic box and allowing water to seep for 24 hours. The collected solution was poured into weighed beakers, oven-dried, and weighed. The trapping efficiency of the sacks determined by this experiment was greater than 90%. In the field the trapped peat materials were weighed as field moisture weight. Five subsamples were collected and sealed in plastic bags, returned to the laboratory, oven-dried, and weighed. The moisture contents of the subsamples were calculated, then averaged and multiplied by the field moisture peat weight, allowing the estimation of field dried peat weight. The traps installed in the field were renewed periodically.

6.3.2.4 Stream discharge and catchment sediment yield

Steam discharge (Q) was monitored at a cross-section with a ‘U’ shape at the outlet of the research catchment (1.7 ha) using automatic pressure sensors. Unfortunately the water level data collected by the logger could not

be used as the shallow nature of the channels resulted in poor quality data due to issues with temperature compensation. Therefore daily discharge data were interpolated from the rainfall-runoff relationship (rainfall x study area). Previous studies in UK headwater blanket peatlands have shown the runoff coefficient to be > 80% (Evans et al., 1999, Holden et al., 2012, Marc and Robinson, 2007, Holden et al., 2017). Over the research catchment in this study there are large areas of bare peat and thus evapotranspiration is expected to be low. The runoff coefficient was therefore assumed to be 0.9 in this small headwater peatland catchment.

An automatic sampler was used to take samples once per day at 13:00 (UTC +2) from 26 October 2016 to 01 November 2017. Samples collected from automatic samplers were filtered through Whatman GF/F 47 mm (0.7 µm) circle filter papers in the laboratory. Total suspended sediment concentrations (SSCs) were measured by oven-drying at 105 °C to constant weight. All water samples contained both inorganic and organic fractions. POC was determined by first conducting loss-on-ignition tests in a muffle furnace at 375 °C for 16 hours to give organic matter content that was then converted to POC using the method of Ball (1964).

The suspended sediment yield (Q_s: kg d^{-1}) was calculated by $Q_s = SSC \times Q$, where SSC (kg m^{-3}) and Q (m^3 d^{-1}) are suspended sediment concentration and discharge, respectively. The values of suspended sediment yield Q_s were regressed against discharge Q using measured daily data for different months and the total study period. A power function, $Q_s = aQ^b$, widely used to estimate transport, where a and b are empirical constants, was applied to form a Q_s fit for different months. The POC yield (Q_{POC}: kg d^{-1}) and the rating curve for Q_{POC} were calculated in the same way with Q_s.

6.3.3 Data analysis

Regression analysis was used to identify the relationship between SS or POC loads and daily discharge. Test results were considered significant at $p < 0.05$. The area-specific sediment yields measured from plots, a series of nested mini-catchments, and stream sampling measurements for the whole study area were compared.

6.4 Results

6.4.1 Peat surface topographic change measured by SfM

M3C2 differences above Level of Detection threshold at 95% confidence level ($LoD_{95\%}$) over different survey intervals are given in Table 6.2. The

spatial distribution and histogram of M3C2 differences for different comparisons are shown in Figure 6.3. M3C2 distances ranged from negative values marked with red colour to positive values marked with blue colour. In this study the 'positive M3C2 distance' more accurately reflects topographic change that could be caused by both deposition and swelling processes; while 'negative M3C2 distance' could also be attributed to both erosion and shrink processes (Grayson et al., 2012, Evans and Warburton, 2007, Glendell et al., 2017).

Table 6.2 Summary of the median net, positive and negative topographic changes (mm) with root mean square error (RMS) (mm) for comparisons over different survey intervals. The long-term survey intervals are highlighted with bold.

Model	Differencing epoch	Net change			Positive change			Negative change		
		Median	RMS	Area (m^2 and %*)	Median	RMS	Area (m^2 and %**)	Median	RMS	Area (m^2 and %**)
2–1	04/11/2016–02/05/2017	–18	85	414.3 (69%)	50	82	198.1 (48%)	–65	88	216.2 (52%)
3–2	02/05/2017–13/06/2017	–29	66	461.8 (77%)	46	71	229.8 (32%)	–43	64	349.3 (68%)
4–3	13/06/2017–21/08/2017	21	66	431.9 (72%)	39	65	299.0 (60%)	–41	69	243.4 (40%)
5–4	21/08/2017–27/09/2017	–21	62	438.5 (73%)	38	65	245.3 (40%)	–36	59	310.8 (60%)
6–5	27/09/2017–02/11/2017	24	64	433.6 (73%)	40	64	300.8 (63%)	–40	63	232.8 (37%)
6–1	**04/11/2016–02/11/2017**	**–27**	**90**	**413.3** (69%)	**50**	**84**	**205.5 (42%)**	**–71**	**95**	**302.6 (58%)**

* Percentage of the area above the $LoD_{95\%}$.
** Percentage of the area with significant changes.
Note: RMS is the square root of the arithmetic mean of the squares of the set of values.

From 04/11/2016 to 02/05/2017, there are large areas of the peat surface (69%) showing significant change (i.e. M3C2 distance > $LoD_{95\%}$). Net topographic change was –18 mm, with a high variability as shown in the large root mean square (RMS) of the M3C2 distance (Table 6.2). The magnitude of the negative topographic change was high, yielding a median change of 65 mm, which was much greater than the median positive topographic change (50 mm) (Table 6.2). This period had the greatest total rainfall but low rainfall intensity and 57 days of temperatures below 0 ºC. These conditions may cause surface expansion due to freezing. The spatial variability of the changes showed that negative topographic change mainly occurred on hillslopes along the main stream networks (Figure 6.3 (a)), with 52% of the total area that is above the $LoD_{95\%}$ (Table 6.2). In contrast,

positive topographic change was found predominantly on the north-east, north-west and southern edge areas of the catchment (Figure 6.3 (a)) where overland flow paths were not connected and bare peat areas are surrounded by dense vegetation cover (Figure 6.2).

The next survey interval (Model 3–2: 02/05/2017–13/06/2017) experienced greater topographic changes in both magnitude (median = –29 mm) and extent (77% of the total area, 461.8 m^2) (Table 6.2) than the first survey interval (Model 2–1). The median negative topographic change was 43 mm, which was slightly lower than that of the positive topographic change (46 mm). However, negative topographic changes occurred more extensively, with 68% of the area above $LoD_{95\%}$ (Table 6.2). This dominance resulted in a net negative change over the whole study area, although some positive topographic change was observed in the upper stream areas, i.e. north-east and south parts of the catchment (Figure 6.3 (b)). Model 4–3 (from 13/06/2017 to 21/08/2017) had a longer time interval (70 days) than the previous interval (Model 3–2, 43 days), but displayed smaller areas with significant topographic changes (72%) within the catchment (Table 6.2). Positive topographic change was more extensive (60% of the area), leading to a net positive topographic change (Table 6.2 and Figure 6.3 (c)). A small zone of negative change was evident in the central-south part of the study area (Figure 6.3 (c)). For Model 5–4 (21/08/2017–27/09/2017), 73% of the area is above the $LoD_{95\%}$, among which 60% of the area is dominated by negative topographic change. The magnitude of the positive and negative topographic change was similar, ranging from 36 to 38 mm (Table 6.2). Finally, the survey interval from 27/09/2017 to 02/11/2017 (Model 6–5) demonstrated 73% of the catchment area had significant change. The median positive topographic change (40 mm) was the same as that of the median negative topographic change (Table 6.2). However, positive topographic change was more extensive (63% of area) compared to the area with negative topographic change (37%).

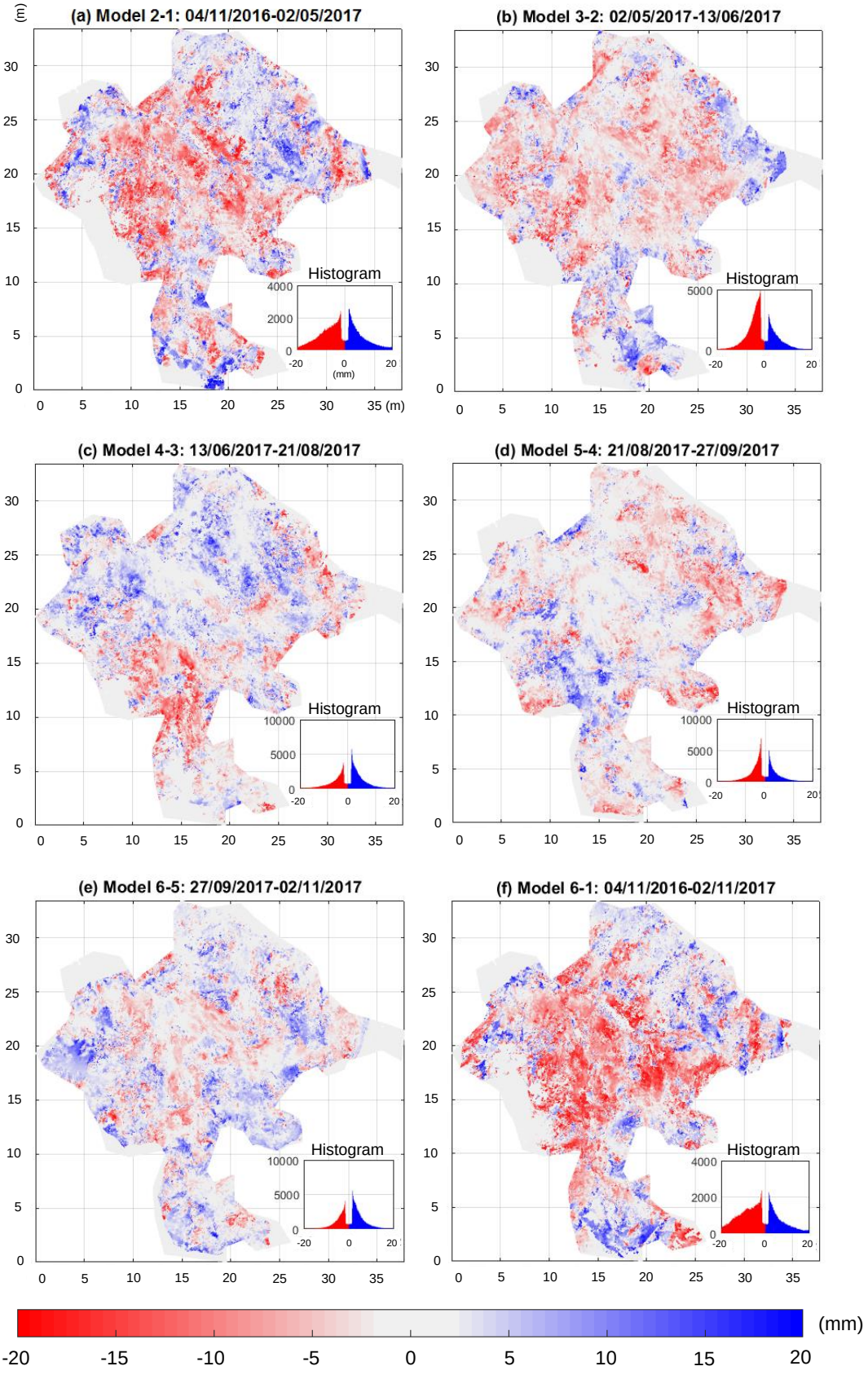

Figure 6.3 M3C2 distances and histograms over different survey intervals (a–f) for the studied catchment. Grey areas have non-significant changes.

The topographic change between the first survey (04/11/2016) and last survey (02/11/2017) (364 days, Model 6–1) was significant over 69% of the area. Positive topographic change was present in 42% of the area above the $LoD_{95\%}$ while negative topographic change was dominant in extent (58%). The median negative topographic change rate was 71 mm, which was much greater than the median positive topographic change rate (50 mm). Zones of intense negative topographic change were observed on the hillslopes, while there was a clear zone of deposition visible along the main drainage lines (Figure 6.3 (f)).

Two example transects were examined over the catchment where topographic changes were significant. Figure 6.4 shows the vertical difference between a series of surface elevation profiles across the profile AA' and BB'. For profile AA' the elevation was initially high at approximately 2.0 m, 3.1–4.0 m and 9.5 m distance along the profile on 04/11/2016 (Figure 6.4 (a), grey line), however, these sections experienced pronounced negative topographic changes during the subsequent field surveys. The maximum vertical displacement was about 500 mm at 3.2 m along the transect. For the sections between 0 and 1.8 m and 4.0 and 5.5 m along the transect, the surface elevation surveyed on 04/11/2016 was significantly lower than for the later surveys, indicating positive topographic changes occurred after the first field survey. For profile BB', there was significant surface lowering at a distance 9.0 to 10.0 m along the transect with a maximum vertical displacement of ~700 mm. The survey on 13/06/2017 recorded surface elevation significantly higher at 5.0–7.0 m along the transect than those of the other surveys.

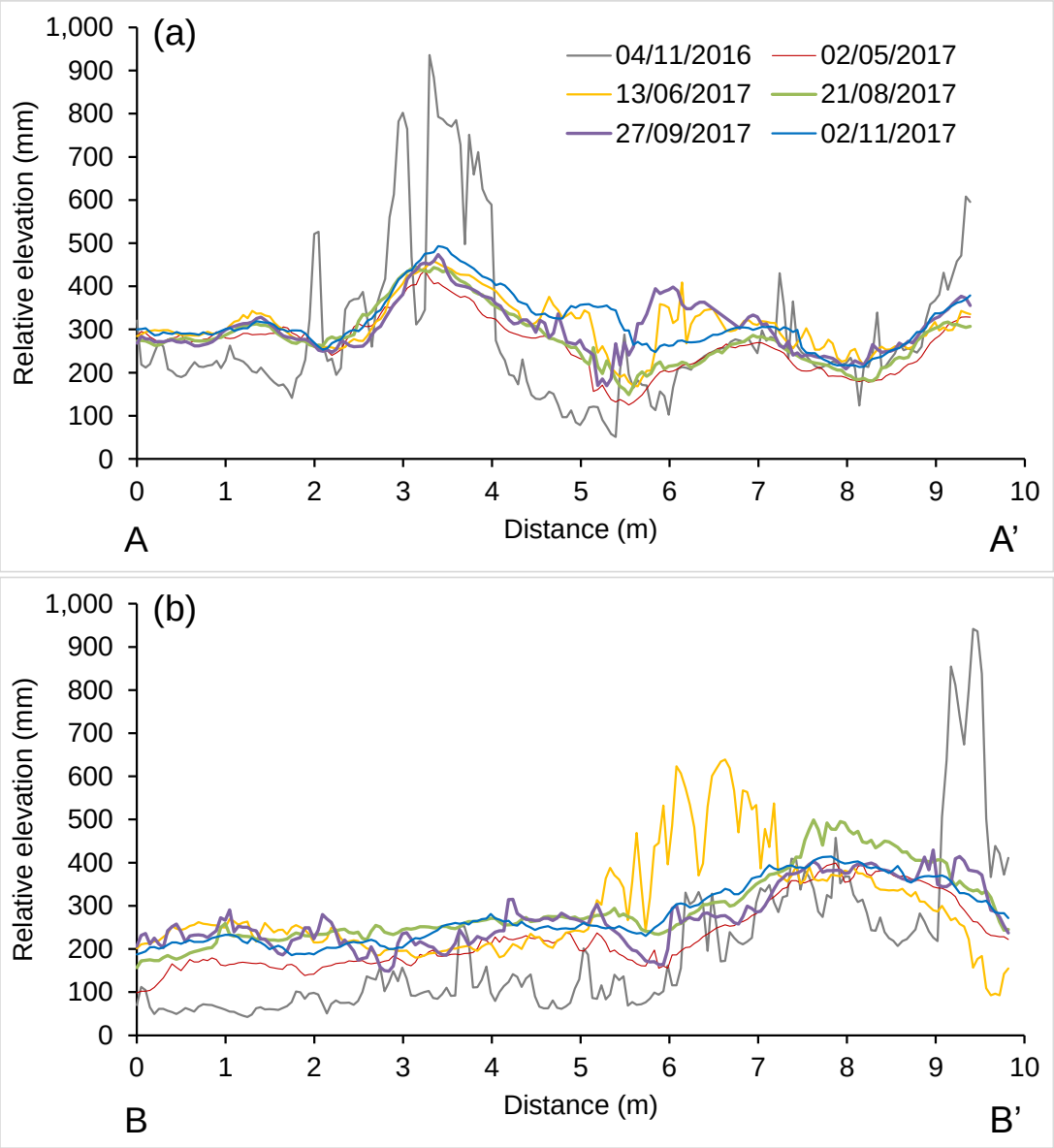

Figure 6.4 2-D peat profiles of (a) AA' and (b) BB' revealing topographic change over the monitored period. For the location of the cross-section, see Figure 6.2.

6.4.2 Sediment production measured by sediment traps

6.4.2.1 Loss measured by sediment traps on the tributaries

Over the 10-month period of sediment trap observation, they captured 30.75 kg of peat (oven-dry weight). The sediment trapped during the intervals 13/06/2017–21/08/2017, 04/11/2016–23/03/2017 and 23/03/2017–07/04/2017 was high, with 10.71 kg, 9.60 kg and 8.53 kg captured, respectively (Table 6.3). In contrast, the sediment trapped between 07/04/2017 and 13/06/2017 was only 1.91 kg. Among the six sediment traps

T3 and T5 generally collected more sediment than other traps (Table 6.3), indicating that source areas of T3 and T5 were more actively eroding.

Table 6.3 Summary of peat loss rates and net topographic change measured by sediment traps. '–' indicates not reported. Peat loss obtained from sediment traps was converted to an estimate of net topographic change using peat bulk density values from the study site.

Monitoring interval	Sediment traps	Peat loss rate (kg)	Peat loss (g m^{-2} d^{-1})	Net topographic change (mm)
04/11/2016–23/03/2017	T1	1.24	0.4	0.3
	T2	1.01	0.1	0.1
	T3	2.27	0.4	0.5
	T4	0.84	0.1	0.1
	T5	2.65	0.2	0.2
	T6	1.59	0.3	0.3
	Total	**9.60**		
23/03/2017–07/04/2017	T1	0.87	2.5	0.2
	T2	0.62	0.5	0.0
	T3	2.40	3.4	0.6
	T4	1.26	1.6	0.1
	T5	1.65	1.2	0.1
	T6	1.73	3.3	0.3
	Total	**8.53**		
07/04/2017–13/06/2017	T1	0.41	0.3	0.1
	T2	0.13	0.0	0.0
	T3	0.37	0.1	0.0
	T4	–	–	–
	T5	0.77	0.1	0.0
	T6	0.23	0.1	0.0
	Total	**1.91**		
13/06/2017–21/08/2017	T1	–	–	–
	T2	1.17	0.2	0.1
	T3	3.21	1.0	0.4
	T4	2.35	0.7	0.3
	T5	2.83	0.5	0.2
	T6	1.15	0.5	0.2
	Total	**10.71**		

Over the full monitoring period T3 had the highest peat loss rate of 0.6 g m^{-2} d^{-1}, followed by T6 (0.5 g m^{-2} d^{-1}) and T1 (0.4 g m^{-2} d^{-1}). The total sediment captured by T2 was lowest, with 0.1 g m^{-2} d^{-1}. Among the different monitoring periods the interval 23/03/2017–07/04/2017 had the highest peat

loss rate; while 07/04/2017 to 13/06/2017 had the smallest peat losses (Table 6.3).

6.4.2.2 Comparing SfM and sediment trap data

The sediment trap data allowed a comparison of ground recession to be made with SfM measurements. The peat loss data, expressed in kilograms and surface change (mm), derived from both the sediment traps and SfM is shown in Figure 6.5. The peat loss (dry weight) rate measured by the sediment traps ranged from 0.0 kg to 4.7 kg, with a mean value of 1.8 kg (standard error of mean is 0.3 kg) but does not take into account any deposition that may take place. In contrast, the SfM measurements indicated both positive and negative values, allowing not only areas of erosion and deposition to be identified but also periods of time. The SfM method resulted in an estimated mean peat deposition rate of 93.3 ± 55.5 kg (5.3 ± 5.2 mm), compared with a mean peat loss rate of 1.8 ± 0.3 kg (0.3 ± 0.1 mm) derived from the sediment traps (Figure 6.5). The standard deviation of mean topographic change measured by the SfM method was much greater than the sediment trap data, showing a much greater magnitude of topographic change. From the M3C2 distances and histogram of differences (Figure 6.3), there were both erosional and depositional areas within the catchment and these features were well captured by SfM.

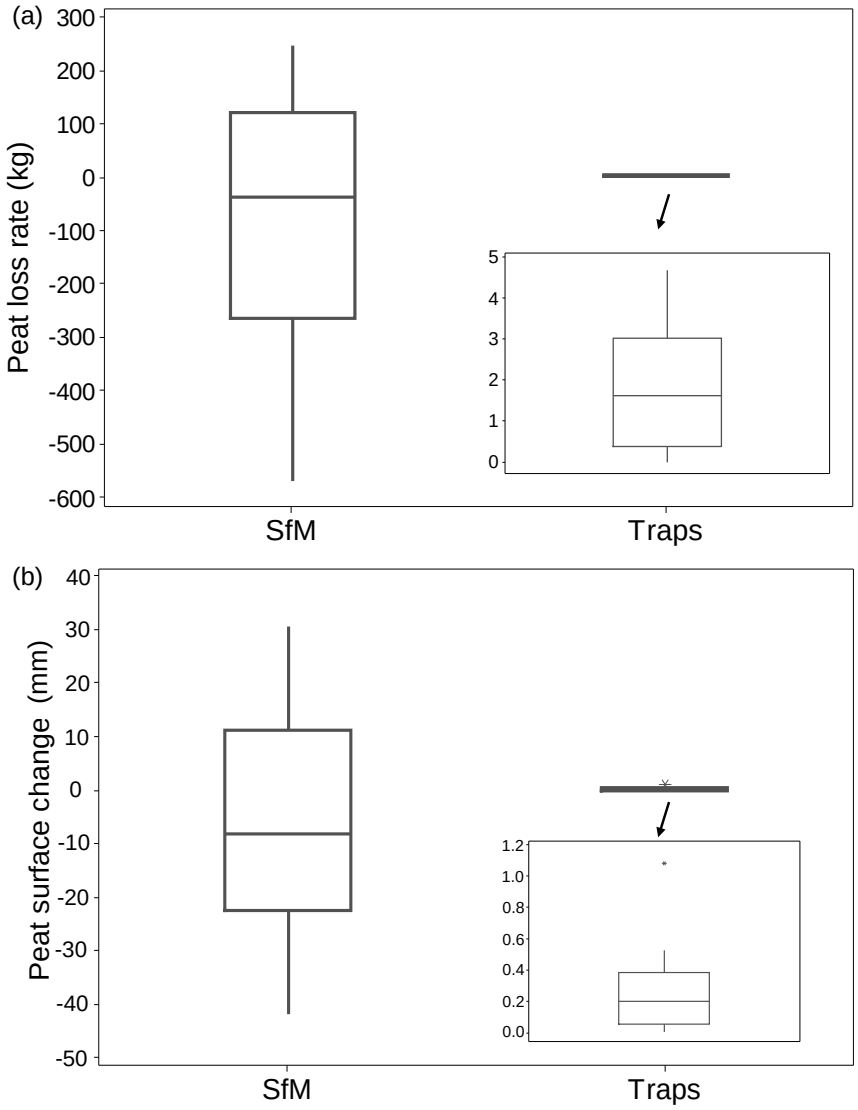

Figure 6.5 Summary of (a) peat loss (positive values show erosion; negative values show deposition) and (b) surface change (positive values show deposition; negative values show erosion) measured by SfM and sample trap methods.

6.4.3 Stream discharge and suspended sediment loads

6.4.3.1 Empirical suspended sediment-transport rating curves

A power law ($Q_s = aQ^b$) performed well in describing the relationship between suspended sediment yield (Q_s) and discharge (Q). However, the sediment rating curves differed between different months (Figure 6.6). High uncertainty of the regression equations was found from February to June 2017. The values of coefficients *a* and *b*, which indicate erodibility and erosive power of flow, respectively, varied significantly among different

months. The regression curve for the whole study period was Q_s = $49505Q^{1.0441}$ (n = 176, R^2 = 0.6817, p < 0.05).

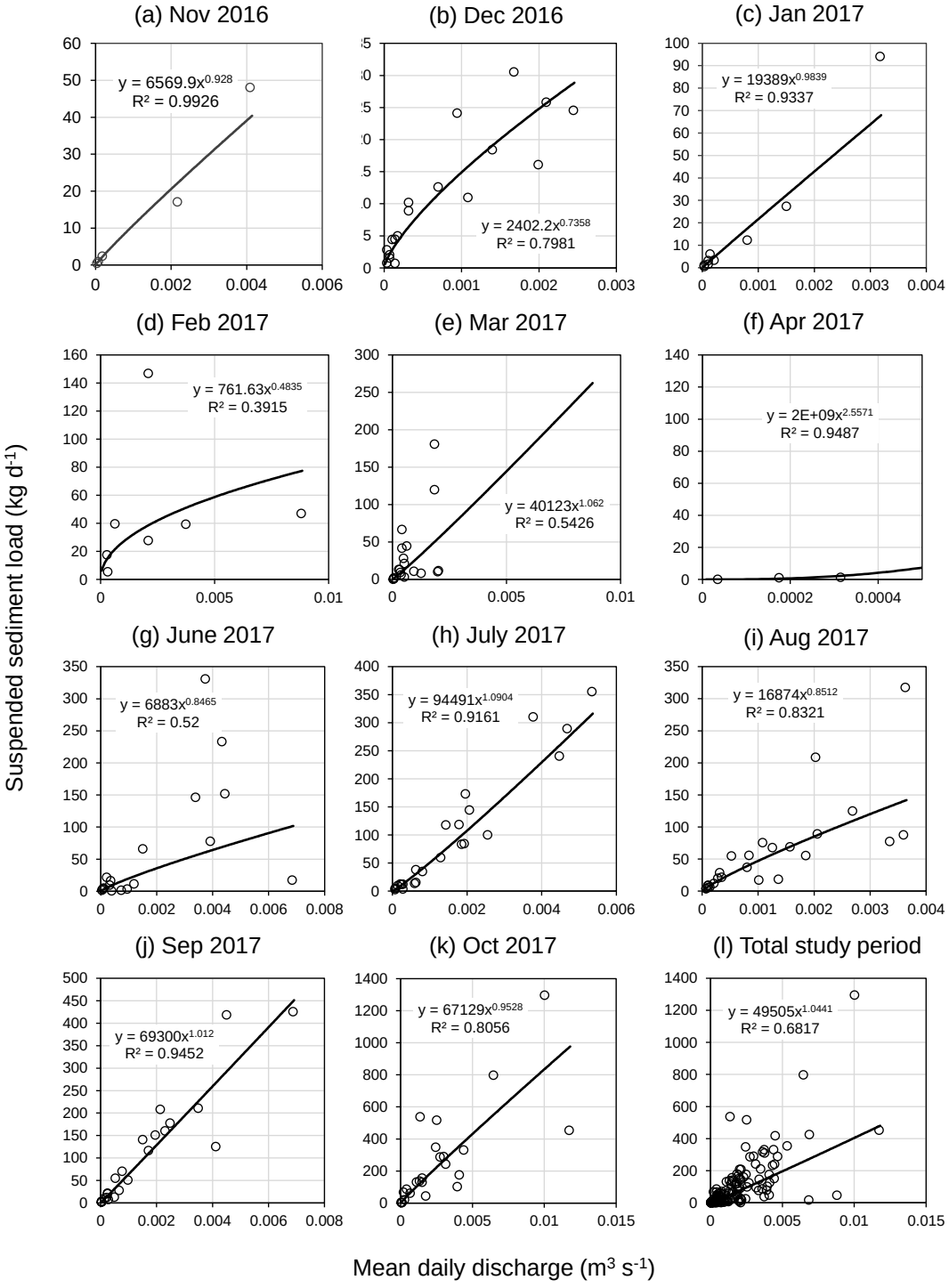

Figure 6.6 Sediment rating curves for months from November 2016 to October 2017 and for the full study period.

6.4.4.2 Stream discharge and suspended sediment (SS) loads

Mean daily stream discharge for the 12-month monitoring period was 0.0013 m^3 s^{-1} (Table 6.4). Flows ranged over two orders of magnitude, with a minimum mean discharge of 0.0001 m^3 s^{-1} and a maximum mean discharge of 0.0021 m^3 s^{-1}. There were 53 days when discharge exceeded 0.0021 m^3 s^{-1} during the study period (Figure 6.7). The majority of high flows occurred in the autumn months (September and October) and early spring 2017 (March).

Suspended sediment (SS) loads ranged from 0.002 to 6.236 t with a total value of 14.822 t (Table 6.4). Despite some breaks in the record, some seasonal patterns can be identified. Both SS and POC loads were low during late spring months (April and May) and increased in the late summer and autumn and were highest in October. For most of April to June 2017, discharge was maintained at a low level and very little sediment was transported to the catchment outlet. However, there were two high flow events (daily mean discharge rate > 0.0060 m^3 s^{-1}) in late May and June which mobilised a considerable amount of sediment (Figure 6.7).

Table 6.4 Summary of suspended sediment load and POC load during different months, seasons and whole monitoring period.

	Mean discharge (m^3 s^{-1})	SS load (t)	POC load (t)
November 2016	0.0006	0.069	-
December 2016	0.0006	0.204	-
January 2017	0.0005	0.150	-
February 2017	0.0011	0.323	0.114
March 2017	0.0012	0.592	0.194
April 2017	0.0001	0.002	0.000
May 2017	0.0005	0.002	0.000
June 2017	0.0014	1.100	0.400
July 2017	0.0012	2.237	0.838
August 2017	0.0009	1.475	0.550
September 2017	0.0012	2.431	0.912
October 2017	0.0021	6.236	2.444
Winter 2016	0.0009	0.677	0.114
Spring 2017	0.0008	0.596	0.195
Summer 2017	0.0017	4.813	1.788
Autumn 2017	0.0023	8.667	3.357
Whole monitoring period	0.0013	14.822	5.454

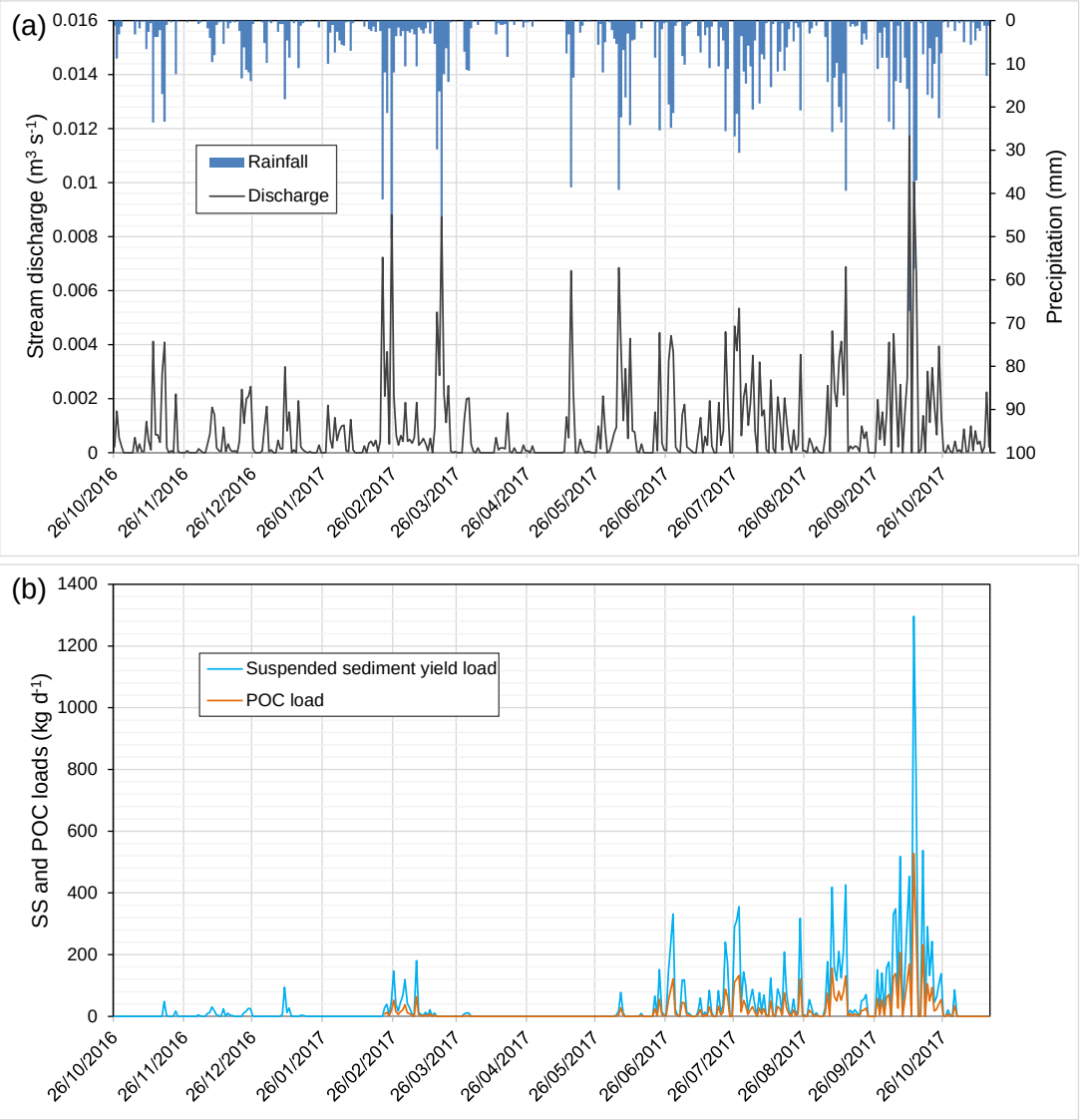

Figure 6.7 Daily rainfall, discharge, suspended sediment and particulate organic carbon loads during the monitoring period of 26/10/2016–15/11/2017 from the catchment outlet.

6.4.4.3 Particulate organic carbon loads

The relationship between POC load (Q_{POC}) and discharge (Q) was well described by a power law ($Q_{POC} = aQ^b$) (Figure 6.8). Similar to the SS rating curves, the POC rating curves had high uncertainty from February to June 2017. The values of coefficients a and b varied significantly among different months. The regression curve for the whole study period was $Q_{POC} = 15776Q^{1.0061}$ (n = 144, R^2 = 0.6245, $p < 0.05$). POC loss ranged from 0.000 to 2.444 t per month, and the total POC flux was 5.454 t which accounted for 36.8% of the total suspended sediment load (Table 6.4).

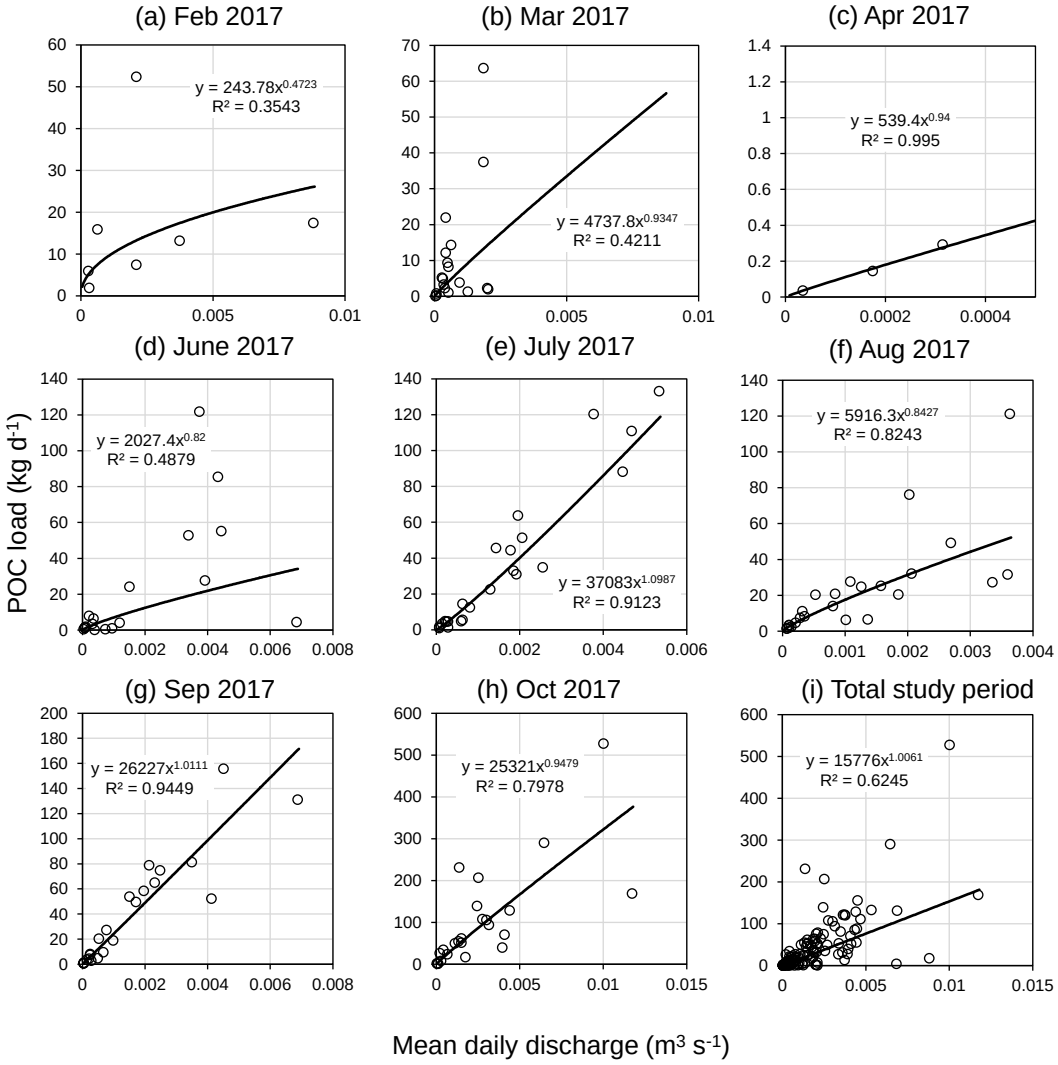

Figure 6.8 POC rating curves for months from February 2017 to October 2017 and for the total study period.

6.4.4 Scale effect of sediment production in headwater peatlands

The relationship between sediment yield and area was described in Figure 6.9. At the fine scale with area ranging from 1×10^{-5} to 1×10^{-3} km^2, sediment yield generally decreased with increasing area. The sediment yield at the outlet of the whole study area was highest.

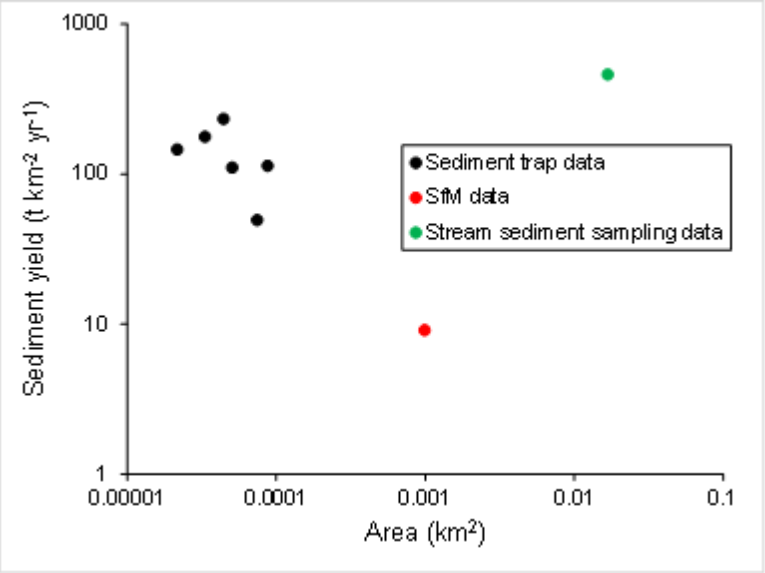

Figure 6.9 Area-specific sediment yield estimates over the 12-month monitoring period at Fleet Moss.

6.5 Discussion

6.5.1 Temporal evolution of eroding headwater peatlands

The study winter (Dec/Jan/Feb) was cold with a mean temperature of 2.3 ºC. A total of 55 freezing days occurred between 26/10/2016 and 07/04/2017. Diurnal freezing was common in November 2016 with temperature frequently fluctuating above and below zero and needle ice was formed and caused expansion of the peat surface. The large amount of peat material captured by the sediment traps during the period 23/03/2017–07/04/2017 may have been related to a period of heavy rainfall from 30 to 31 March which occurred on the peat surface preconditioned by freeze–thaw weathering. During the dry period from April to May 2017, hillslope peat exhibited substantial desiccation. Surface desiccation also affected deposited peat within the river channels and overbank areas. Field observations showed that on the desiccated peat surface the upper dried curst was generally concave in shape and detached from the intact peat below, a classic feature also reported by Evans and Warburton (2007). Cracks often connected in the form of polygons and were up to 12 cm deep. The peat loss rate measured by sediment traps during the period of 07/04/2017–13/06/2017 was the lowest (Table 6.3) during the study as there was a lack of rainfall. However, the sediment trapped during the subsequent period with higher rainfall totals (13/06/2017–21/08/2017) was extremely

high (Table 6.3). These results are in agreement with those reported in other blanket peatland environments showing that surface desiccation during extended periods of dry weather is an important weathering process for producing erodible peat (Burt and Gardiner, 1984, Evans et al., 1999, Francis, 1990, Holden and Burt, 2002). Similar seasonal patterns of sediment captured have also been reported by Francis (1990) and Labadz et al. (1991) who found little peat sediment removed during the summer or late winter/spring, and the majority captured in the autumn and early winter.

6.5.2 Scale effect of sediment production in headwater peatlands

Peat erosion decreased with increasing area at the fine scale for areas less than 1×10^{-3} km^2 (Figure 6.9) where the erosion processes are dominated by rill and interrill erosion (Li et al., 2018a). This could be caused by decreasing sediment delivery ratios with increasing area (Walling and Webb, 1996). The fact that sediment yield was highest for the whole study area (0.017 km^2) suggests that gully erosion, channel bank erosion and flushing of deposited materials could be important sediment sources at larger scales. There are numerous studies showing that bank erosion (Small et al., 2003), gully erosion and mass movements (Evans and Warburton, 2007, Evans et al., 2006) form an important part of the catchment sediment budget in upland peat catchments. The erosion and transport of mineral materials might become even more important at larger scales as mineral sediment accounted for 63.2% of the total sediment yield. Mineral sediments in these upland systems may be loosened and mobilized in different ways and may not require freeze–thaw and desiccation to make them available for transport.

This study showed that peat loss measurements at one scale are not representative of sediment yield at another scale level. Therefore, direct extrapolation of plot scale interrill and rill erosion rates up the catchment scale can be problematic (De Vente and Poesen, 2005, Parsons et al., 2006). More monitoring, experimental and modelling studies are needed as a basis for scaling erosion rates from one specific area to larger or smaller areas. In addition, it is suggested that monitoring of peat erosion processes should utilize standardized procedures to allow comparisons of data obtained from different study areas (Prosdocimi et al., 2016).

6.5.3 Sediment production estimated from topographic change measured by SfM and sediment traps

The error obtained during the manual registration of the SfM point clouds (mean value of 41 mm) (Table 6.1) is within the range of registration errors (i.e. 11–291 mm, mean 46 mm) found by other studies in natural terrain (Glendell et al., 2017). Although both positive and negative net topographic changes were observed over different survey intervals, the net topographic change observed over the whole monitoring period was –27 mm (Table 6.2). This value is in agreement with the globally reported negative topographic change rates (24 ± 8 mm yr^{-1}) measured using erosion pins (Evans and Warburton, 2007, Grayson et al., 2012); and those (–286 mm to +31 mm yr^{-1}; mean value of –33 mm yr^{-1}) measured using SfM (Glendell et al., 2017).

Peat erosion measurement using sediment traps and SfM have different applications. For many applications mass loss captured by sediment traps or estimated by river sediment yield studies is a key parameter of interest; while for other applications surface change is used as a proxy for erosion. It should be noted from mass balance principles that all things being equal, the estimates of mass loss using different methods should be comparable. However, in this study peat loss data estimated from the sediment traps and SfM techniques were not comparable with each other (Figure 6.5). Deposition-related change measured by SfM was 93.3 ± 55.5 kg (5.3 ± 5.2 mm), in comparison with erosion-related change derived from the sediment traps of 1.8 ± 0.3 kg (0.3 ± 0.1 mm). The discrepancy could be explained by two reasons. The first explanation is associated with wind erosion, oxidation loss of the peat and shrinkage of the peat by compression that can cause topographic change captured by SfM but not by sediment traps. For example, 30–81% of surface lowering has previously been attributed to peat wastage in upland peat environments (Francis, 1990, Evans and Warburton, 2007, Evans et al., 2006) though it is thought that this estimate probably includes both oxidation loss (i.e. true wastage) and compression of the peat associated with loss of water and collapse of the pore structure leading to higher bulk density values. In addition, eroded peat is loose and less compact than when it was *in situ* and so re-deposition of such loose peat materials could result in positive topographic change which is well captured by SfM. However, such changes to peat bulk density would not often be accounted for in stream sediment sampling or sediment trap data which examines dry mass loss.

6.5.4 Loss of organic sediment from the catchment

The estimated annual total suspended sediment load leaving the catchment was calculated as 14.8 tonnes per year, equivalent to 926.3 t km^{-2} yr^{-1}. This value at Fleet Moss is much greater than those reported from other upland blanket peatlands (generally less than 200 t km^{-2} yr^{-1}, cited in Li et al. (2018a)). The estimated POC load was 5.5 t yr^{-1}, equivalent to 340.9 tonnes of organic carbon km^{-2} yr^{-1} and accounted for 36.8% of the total suspended sediment load. The POC flux is greater than those reported (0.12–38.9 t C km^{-2} yr^{-1}) in other peatland catchments in the UK (Francis, 1990, Labadz et al., 1991, Hutchinson, 1995, Dawson et al., 2002, Dawson et al., 1995, Holden, 2006, Worrall et al., 2003). It is recognised that the discharge from the catchment was not continuously gauged due to instrument errors and that continuous gauging combined with storm event sediment sampling would improve the stream sediment flux estimates for Fleet Moss. Nevertheless, the evidence presented using multiple data sources suggests that there is a very high erosion and organic carbon loss rate from the system and high localized rates of topographic change measured in only 12 months (i.e. 500–700 mm in some places). Thus Fleet Moss is rapidly eroding, exporting large amounts of sediment and particulate carbon and could be a hot spot target for restoration intervention to stabilize the peatland and reduce future erosion.

6.6 Conclusions

The net topographic change for the studied catchment within Fleet Moss derived from SfM was –27 mm yr^{-1} during the 12 month monitoring period. A comparison of topographic changes for a series of nested small watersheds derived from SfM and sediment traps showed significant differences with a positive topographic change (mean: 5.3 mm, SD: 5.2 mm) determined by the SfM and a negative topographic change (mean: –0.3 mm, SD: 0.1 mm) from the sediment traps. This difference indicates that it is problematic to directly interpolate peat erosion rates measured by local net topographic change that can be as high as 500–700 mm into sediment yield at the catchment outlet, without considering sediment sinks within the catchment budget. The total suspended sediment yield and POC load were 926.3 t km^{-2} yr^{-1} and 340.9 t C km^{-2} yr^{-1}, respectively. Desiccation and freeze–thaw processes were identified as playing key roles in breaking up the peat surface prior to removal by fluvial processes. The greatest sediment and organic carbon losses occurred during the autumn following a two month period of dry

weather in spring during which desiccation was observed and summer period when bare peat was exposed to warmer weather and more desiccation. Frost action played an important role in providing available sediment during the winter months via needle-ice formation and thaw. Peat loss measured at the hillslope scale was not representative of that at catchment scale within which bank erosion, mass movements and transport of eroded mineral sediment could also be important.

Acknowledgements

The work was jointly funded by the China Scholarship Council and the University of Leeds (File No. 201406040068). Jonathan Carrivick and Lee Brown are thanked for providing the Geodimeter and tinytag temperature loggers used in this study. Special acknowledgement is given to David Ashley who helped prepare the laboratory experimental materials and field set-up. Santiago Clerici and Sarah Hunt are much acknowledged for their time and assistance involved in field work. Mark Smith, Duncan Quincey, Scott Watson and Joe Mallalieu are thanked for providing advice on using Agisoft Photoscan and Cloudcompare to undertake data analysis. Demonstrations from Josh Greenwood for water sample (POC) analysis in the laboratory is much appreciated. We are grateful to Claudio Bravo L. for providing help in data visualization. Jeff Warburton (Department of Geography, Durham University) is thanked for sharing experience and providing advice for the design of sediment traps.

References

BALL, D. 1964. Loss ‐ on ‐ ignition as an estimate of organic matter and organic carbon in non ‐ calcareous soils. *Journal of soil science,* 15**,** 84-92.

BILLETT, M., CHARMAN, D., CLARK, J., EVANS, C., EVANS, M., OSTLE, N., WORRALL, F., BURDEN, A., DINSMORE, K. & JONES, T. 2010. Carbon balance of UK peatlands: current state of knowledge and future research challenges. *Climate Research,* 45**,** 13-29.

BONN, A., ALLOTT, T., HUBACEK, K. & STEWART, J. 2009. *Drivers of environmental change in uplands*, Routledge.

BOWER, M. 1960. The erosion of blanket peat in the southern Pennines. *East Midland Geographer,* 13**,** 22-33.

BURT, T. & GARDINER, A. 1984. Runoff and sediment production in a small peat-covered catchment: some preliminary results. *Catchment Experiments in Fluvial Geomorphology* Norwich, England: Geo Books.

CANNELL, M., DEWAR, R. & PYATT, D. 1993. Conifer plantations on drained peatlands in Britain: a net gain or loss of carbon? *Forestry: An International Journal of Forest Research,* 66**,** 353-369.

CLAY, G. D., DIXON, S., EVANS, M. G., ROWSON, J. G. & WORRALL, F. 2012. Carbon dioxide fluxes and DOC concentrations of eroding blanket peat gullies. *Earth Surface Processes and Landforms,* 37**,** 562-571.

CRISP, D. 1966. Input and output of minerals for an area of Pennine moorland: the importance of precipitation, drainage, peat erosion and animals. *Journal of Applied Ecology,* 3**,** 327-348.

DAWSON, J., BILLETT, M., NEAL, C. & HILL, S. 2002. A comparison of particulate, dissolved and gaseous carbon in two contrasting upland streams in the UK. *Journal of Hydrology,* 257**,** 226-246.

DAWSON, J., HOPE, D., CRESSER, M. & BILLETT, M. 1995. Downstream changes in free carbon dioxide in an upland catchment from northeastern Scotland. *Journal of Environmental Quality,* 24**,** 699-706.

DE VENTE, J. & POESEN, J. 2005. Predicting soil erosion and sediment yield at the basin scale: Scale issues and semi-quantitative models. *Earth-Science Reviews,* 71**,** 95-125.

EVANS, M., BURT, T., HOLDEN, J. & ADAMSON, J. 1999. Runoff generation and water table fluctuations in blanket peat: evidence from UK data spanning the dry summer of 1995. *Journal of Hydrology,* 221**,** 141-160.

EVANS, M. & LINDSAY, J. 2010. Impact of gully erosion on carbon sequestration in blanket peatlands. *Climate Research,* 45**,** 31-41.

EVANS, M. & WARBURTON, J. 2005. Sediment budget for an eroding peat‐moorland catchment in northern England. *Earth Surface Processes and Landforms,* 30**,** 557-577.

EVANS, M. & WARBURTON, J. 2007. *Geomorphology of upland peat: erosion, form and landscape change,* Oxford, UK, John Wiley & Sons.

EVANS, M., WARBURTON, J. & YANG, J. 2006. Eroding blanket peat catchments: global and local implications of upland organic sediment budgets. *Geomorphology,* 79**,** 45-57.

FONSTAD, M. A., DIETRICH, J. T., COURVILLE, B. C., JENSEN, J. L. & CARBONNEAU, P. E. 2013. Topographic structure from motion: a new development in photogrammetric measurement. *Earth Surface Processes and Landforms,* 38**,** 421-430.

FRANCIS, I. 1990. Blanket peat erosion in a mid‐wales catchment during two drought years. *Earth Surface Processes and Landforms,* 15**,** 445-456.

GLENDELL, M., MCSHANE, G., FARROW, L., JAMES, M. R., QUINTON, J., ANDERSON, K., EVANS, M., BENAUD, P., RAWLINS, B. & MORGAN, D. 2017. Testing the utility of structure‐from‐motion photogrammetry reconstructions using small unmanned aerial vehicles and ground photography to estimate the extent of upland soil erosion. *Earth Surface Processes and Landforms,* 42**,** 1860-1871.

GRAB, S. W. & DESCHAMPS, C. L. 2004. Geomorphological and geoecological controls and processes following gully development in alpine mires, Lesotho. *Arctic, Antarctic, and Alpine Research,* 36**,** 49-58.

GRAYSON, R., HOLDEN, J., JONES, R., CARLE, J. & LLOYD, A. 2012. Improving particulate carbon loss estimates in eroding peatlands through the use of terrestrial laser scanning. *Geomorphology,* 179**,** 240-248.

HOLDEN, J. 2006. Sediment and particulate carbon removal by pipe erosion increase over time in blanket peatlands as a consequence of land drainage. *Journal of Geophysical Research: Earth Surface (2003–2012),* 111.

HOLDEN, J. & BURT, T. 2002. Infiltration, runoff and sediment production in blanket peat catchments: implications of field rainfall simulation experiments. *Hydrological Processes,* 16**,** 2537-2557.

HOLDEN, J., GREEN, S. M., BAIRD, A. J., GRAYSON, R. P., DOOLING, G. P., CHAPMAN, P. J., EVANS, C. D., PEACOCK, M. & SWINDLES, G. 2017. The impact of ditch blocking on the hydrological functioning of blanket peatlands. *Hydrological processes,* 31**,** 525-539.

HOLDEN, J., KIRKBY, M. J., LANE, S. N., MILLEDGE, D. G., BROOKES, C. J., HOLDEN, V. & MCDONALD, A. T. 2008. Overland flow velocity and roughness properties in peatlands. *Water Resources Research,* 44**,** W06415.

HOLDEN, J., SHOTBOLT, L., BONN, A., BURT, T., CHAPMAN, P., DOUGILL, A., FRASER, E., HUBACEK, K., IRVINE, B. & KIRKBY, M. 2007. Environmental change in moorland landscapes. *Earth-Science Reviews,* 82**,** 75-100.

HOLDEN, J., SMART, R. P., DINSMORE, K. J., BAIRD, A. J., BILLETT, M. F. & CHAPMAN, P. J. 2012. Natural pipes in blanket peatlands: major point sources for the release of carbon to the aquatic system. *Global Change Biology,* 18**,** 3568-3580.

HOPE, D., BILLETT, M. F., MILNE, R. & BROWN, T. A. 1997. Exports of organic carbon in British rivers. *Hydrological Processes,* 11**,** 325-344.

HUTCHINSON, S. M. 1995. Use of magnetic and radiometric measurements to investigate erosion and sedimentation in a British upland catchment. *Earth Surface Processes and Landforms,* 20**,** 293-314.

LABADZ, J., BURT, T. & POTTER, A. 1991. Sediment yield and delivery in the blanket peat moorlands of the Southern Pennines. *Earth Surface Processes and Landforms,* 16**,** 255-271.

LAGUE, D., BRODU, N. & LEROUX, J. 2013. Accurate 3D comparison of complex topography with terrestrial laser scanner: Application to the Rangitikei canyon (NZ). *ISPRS Journal of Photogrammetry and Remote Sensing,* 82**,** 10-26.

LI, C., GRAYSON, R., HOLDEN, J. & LI, P. 2018a. Erosion in peatlands: Recent research progress and future directions. *Earth-Science Reviews,* 185**,** 870-886.

LI, C., GRAYSON, R., SMITH, M. & HOLDEN, J. accepted. Patterns and drivers of peat erosion via using Structure-from-Motion photogrammetry at field plot and laboratory scales. *Earth Surface Processes and Landforms*.

LI, C., HOLDEN, J. & GRAYSON, R. 2018b. Effects of needle ice production and thaw on peat erosion processes during overland flow events. *Journal of Geophysical Research: Earth Surface,* 123**,** 2107-2122

LI, C., HOLDEN, J. & GRAYSON, R. 2018c. Effects of rainfall, overland flow and their interactions on peatland interrill erosion processes. *Earth Surface Processes and Landforms,* 43**,** 1451-1464.

LI, P., HOLDEN, J. & IRVINE, B. 2016a. Prediction of blanket peat erosion across Great Britain under environmental change. *Climatic Change,* 134**,** 177-191.

LI, P., HOLDEN, J., IRVINE, B. & GRAYSON, R. 2016b. PESERA‐PEAT: a fluvial erosion model for blanket peatlands. *Earth Surface Processes and Landforms,* 41**,** 2058-2077.

LI, P., HOLDEN, J., IRVINE, B. & MU, X. 2017. Erosion of Northern Hemisphere blanket peatlands under 21st‐century climate change. *Geophysical Research Letters,* 44**,** 3615-3623.

LUOTO, M. & SEPPÄLÄ, M. 2000. Summit peats ('peat cakes') on the fells of Finnish Lapland: continental fragments of blanket mires? *The Holocene,* 10**,** 229-241.

MARC, V. & ROBINSON, M. 2007. The long-term water balance (1972-2004) of upland forestry and grassland at Plynlimon, mid-Wales. *Hydrology and Earth System Sciences,* 11**,** 44-60.

MILNE, R. & BROWN, T. 1997. Carbon in the vegetation and soils of Great Britain. *Journal of Environmental Management,* 49**,** 413-433.

PARRY, L. E., HOLDEN, J. & CHAPMAN, P. J. 2014. Restoration of blanket peatlands. *Journal of Environmental Management,* 133**,** 193-205.

PARSONS, A. J., BRAZIER, R. E., WAINWRIGHT, J. & POWELL, D. M. 2006. Scale relationships in hillslope runoff and erosion. *Earth Surface Processes and Landforms,* 31**,** 1384-1393.

PAWSON, R., EVANS, M. & ALLOTT, T. 2012. Fluvial carbon flux from headwater peatland streams: significance of particulate carbon flux. *Earth Surface Processes and Landforms,* 37**,** 1203-1212.

PAWSON, R., LORD, D., EVANS, M. & ALLOTT, T. 2008. Fluvial organic carbon flux from an eroding peatland catchment, southern Pennines, UK. *Hydrology and Earth System Sciences,* 12**,** 625-634.

PROSDOCIMI, M., CERDÀ, A. & TAROLLI, P. 2016. Soil water erosion on Mediterranean vineyards: A review. *Catena,* 141**,** 1-21.

SMALL, I., ROWAN, J. & DUCK, R. 2003. Long-term sediment yield in Crombie Reservoir catchment, Angus; and its regional significance within the Midland Valley of Scotland. *Hydrological Sciences Journal,* 48**,** 619-635.

SMITH, M., CARRIVICK, J., HOOKE, J. & KIRKBY, M. 2014. Reconstructing flash flood magnitudes using 'Structure-from-Motion': A rapid assessment tool. *Journal of Hydrology,* 519**,** 1914-1927.

SNAPIR, B., HOBBS, S. & WAINE, T. 2014. Roughness measurements over an agricultural soil surface with Structure from Motion. *ISPRS Journal of Photogrammetry and Remote Sensing,* 96**,** 210-223.

STÖCKER, C., ELTNER, A. & KARRASCH, P. 2015. Measuring gullies by synergetic application of UAV and close range photogrammetry—A case study from Andalusia, Spain. *Catena,* 132**,** 1-11.

TALLIS, J. 1973. Studies on southern Pennine peats: V. Direct observations on peat erosion and peat hydrology at Featherbed Moss, Derbyshire. *The Journal of Ecology,* 61**,** 1-22.

WALLING, D. E. & WEBB, B. 1996. *Erosion and Sediment Yield: Global and Regional Perspectives: Proceedings of an International Symposium Held at Exeter, UK, from 15 to 19 July 1996*, IAHS.

WESTOBY, M. J., DUNNING, S. A., HEIN, A. S., MARRERO, S. M. & SUGDEN, D. E. 2016. Interannual surface evolution of an Antarctic blue-ice moraine using multi-temporal DEMs. *Earth Surface Dynamics,* 4**,** 515.

WORRALL, F., BURT, T., ROWSON, J., WARBURTON, J. & ADAMSON, J. 2009. The multi-annual carbon budget of a peat-covered catchment. *Science of the Total Environment,* 407**,** 4084-4094.

WORRALL, F., REED, M., WARBURTON, J. & BURT, T. 2003. Carbon budget for a British upland peat catchment. *Science of the Total Environment,* 312**,** 133-146.

XU, J., MORRIS, P. J., LIU, J. & HOLDEN, J. 2018a. Hotspots of peatland-derived potable water use identified by global analysis. *Nature Sustainability,* 1**,** 246.

XU, J., MORRIS, P. J., LIU, J. & HOLDEN, J. 2018b. PEATMAP: Refining estimates of global peatland distribution based on a meta-analysis. *Catena,* 160**,** 134-140.

YU, Z., LOISEL, J., BROSSEAU, D. P., BEILMAN, D. W. & HUNT, S. J. 2010. Global peatland dynamics since the Last Glacial Maximum. *Geophysical Research Letters,* 37.

Chapter 7
Discussion and conclusions

The previous four chapters have presented the results of this study along with detailed interpretations and discussion. This chapter discusses the key findings from each respective chapter, which are linked together into a complete body of work, in light of a current understanding of upland peat erosion. It also provides a synthesis of the implications of the research findings, limitations and suggestions for further work. The chapter ends with the main conclusions from the research.

7.1 Summary of key findings

The sections presented below relate to the aims and objectives specified in Chapter 1. However, the sections below are re-constructed under several cross-cutting themes because detailed discussions around the individual objectives are found within each respective results chapter.

7.1.1 Different phases of peat erosion

Peat erosion is a two-phase process including supply of a friable and highly erodible peat surface layer by freeze–thaw and desiccation (Evans and Warburton, 2007, Li et al., 2018b, Lindsay et al., 2014), and its subsequent transport by agents such as water and wind (Li et al., 2018a). Rainsplash and runoff energy are active erosion agents for water erosion processes involving splash erosion, interrill erosion, rill erosion, pipe erosion and ditch/channel erosion (Li et al., 2018c, Evans and Warburton, 2007, Holden, 2006). This thesis, which coupled laboratory-based experiments and field monitoring, examined the combined effects of sediment supply (rainsplash, freeze–thaw and desiccation) and sediment transport by water erosion processes (interrill erosion, rill erosion and gully erosion), to reveal the relative importance of these controls (Figure 7.1). Overall, bare peat surfaces on blanket peatlands are much more susceptible to erosion if they are firstly weathered by frost action (this was particularly demonstrated for needle-ice through laboratory experiments, Chapter 4) and desiccation (based on field data but not directly studied as a phenomenon in its own right; Chapter 6). Raindrops subsequently provide energy for detaching the weathered peat (Chapter 3) and were shown to be very important in increasing erosion rates on weathered peat surfaces. Where saturation-

excess overland flow occurs, which can often be across most of the peatland system (Holden and Burt, 2002a), the transport of peat materials interacts with raindrop impact but ultimately leads to a range of surface erosion processes including interrill erosion (Chapter 3), rill erosion (Chapter 4) and gully development (Chapter 5).

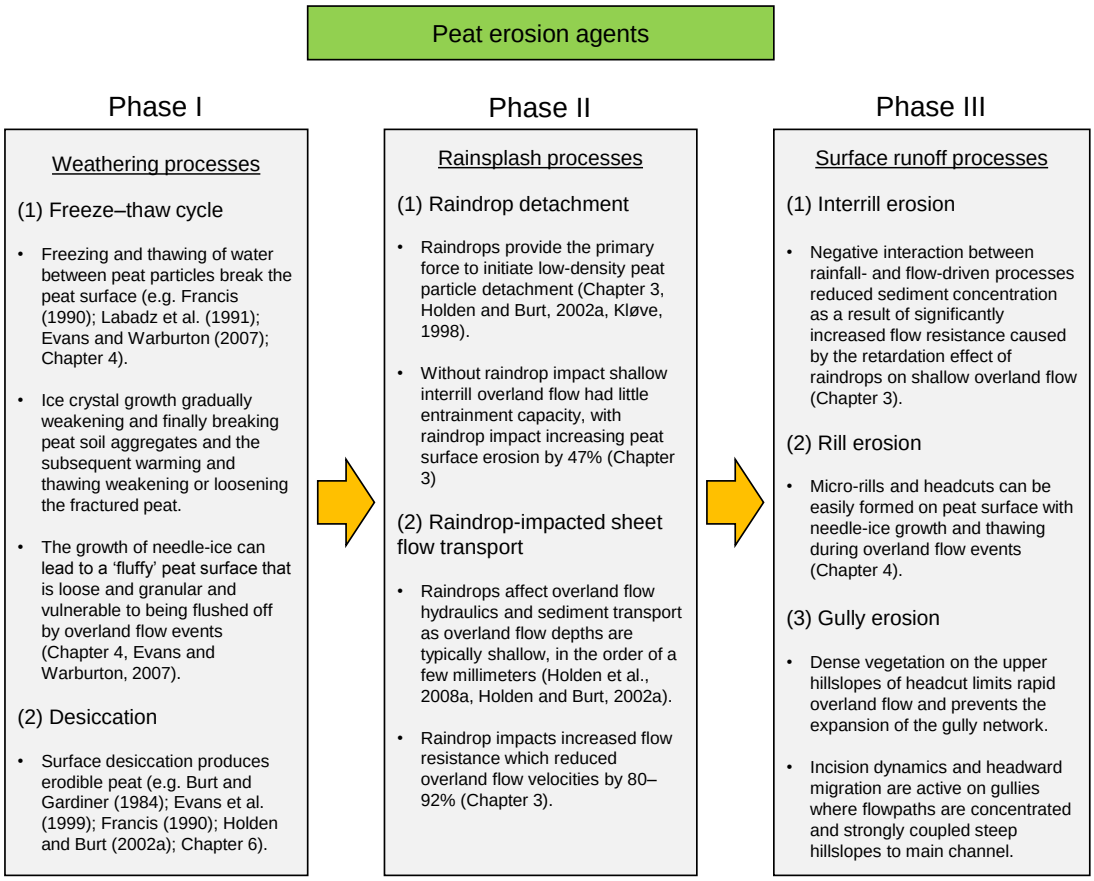

Figure 7.1 Peat erosion agents and the dominant processes for different phases.

Phase 1: Weathering processes

Antecedent conditions such as freeze–thaw or desiccation activity are very important in controlling peat erodibility and thus erosional response to a given rainfall event. Without the impacts of rainsplash and weathering processes (freeze–thaw and desiccation), sheet or rill flow has limited effect on increasing peat erosion (Chapter 3 and 4).

Freeze–thaw processes (needle-ice processes)

Chapter 4 updated our understanding by quantitatively measuring how needle ice affects peat erodibility, overland flow hydraulic characteristics and sediment production processes. Needle ice processes (NI) reduced bulk density and increased porosity, resulting in enhanced peat infiltration

capacity and increased time taken to generate overland flow. NI increased peat erodibility and decreased the inherent resistance of peat to water erosion, producing nearly six times greater peat losses compared to Non-NI treatments.

Chapter 5 showed that cold conditions in the winter of 2016 resulted in a net surface topographic rise first and lowering afterwards via freeze–thaw processes. Chapter 6 showed that large amount of peat material was captured by the sediment traps during the period 23/03/2017–07/04/2017 and this was related to a period of heavy rainfall on a previously freeze–thaw weathered peat surface with loose particles and aggregates.

Desiccation processes

Structure-from-Motion (SfM) data showed that there was a surface lowering during the dry periods (April and May) of 2017 resulting from drying and cracking of the peat surface (Chapter 5). Chapter 6 suggested that surface desiccation during the dry periods affected peat surfaces from hillslopes, and later resulted in deposited peat within the river channels and overbank areas. The peat loss rate measured by sediment traps was lowest during the dry periods, while it was much higher during the subsequent wet period and autumn (Table 6.3). These results indicate that surface desiccation during extended periods of dry weather is an important weathering process for producing erodible peat (Burt and Gardiner, 1984, Evans et al., 1999, Francis, 1990, Holden and Burt, 2002a).

Phase 2: Rainsplash erosion processes

Rainsplash plays an important role in detaching peat particles for flow transport (Chapter 3). For treatments with raindrop impact (*Rainfall* and *Rainfall + Inflow*), sediment concentrations typically demonstrated an initial sharp increase followed by a gradual decrease to constant level (Chapter 3, Figure 3.3). The increase corresponded to the period when peat aggregates previously weathered by freeze–thaw and desiccation (Francis, 1990, Labadz et al., 1991, Shuttleworth et al., 2017) were detached and splashed by raindrop impact. The erosion pattern appeared to be transport-limited in the initial stage of runoff generation due to the limited ability of overland flow with low rate to mobilise and export loose sediments on the surface. The erosive force of splash decreased with the increase in flow depth and resistance to detachment. Despite an increase in the overland flow rate and the associated transport capacity, the peat loss rate in the steady-state overland flow stage was generally lower than the initial peak rate,

demonstrating that the erosion rate experienced a switch from a transported-limited to a detachment-limited system. Peak sediment concentration occurred during the rising limb of overland flow graphs (Chapter 3, Figure 3.3) and this was also reported by Kløve (1998) and Holden and Burt (2002a).

Phase 3: Surface runoff erosion processes

Interrill erosion processes

Chapter 3 highlights the effects of rainfall, overland flow and their interactions on peatland interrill erosion processes. Raindrop impact, which was calculated as the difference in erosion between the *Rainfall* and *Inflow* treatments, significantly increased sediment yields with an average increase of 47% (Chapter 3). Raindrop impact significantly reduced the overland flow velocity on the gentler slope gradient (2.5° and 7.5°) by increasing surface roughness as represented by Manning's *n* friction factor.

For peat soils, the interaction between rainfall and flow driven erosion processes are important in affecting flow hydraulics and sediment, in particular under gentle slopes and shallow overland flow conditions. A negative interaction was observed to reduce sediment concentration that primarily results from significantly increased flow resistance caused by the retardation effect of raindrops on shallow overland flow (Chapter 3, Table 3.7). In addition, interaction resulted in a decrease in stream power that was responsible for a decrease in sediment concentration as erosion was found to be positively correlated with the stream power.

Rill erosion processes

There is a higher risk of rill formation on peat surfaces after needle ice processes (NI) since micro-rills and headcuts typically occurred in laboratory experiments (Chapter 4). Peat blocks with NI treatments had greater hydraulic roughness and lower flow velocity resulting from localized micro-waterfalls, which may indicate a lower sediment transport capacity. However, significantly greater sediment was measured on peat blocks with NI treatments, indicating that rill flow with relatively lower velocity is still capable of transporting more peat materials when such materials are available.

Gully erosion processes

In the field study at Fleet Moss there were well developed and connected Type 1 and Type 2 gully systems as classified by Bower (1960a). Gullies in

headwater systems typically export large amounts of sediment and particulate organic carbon (POC) to peatland streams (Evans et al., 2006, Evans and Warburton, 2007, Evans and Lindsay, 2010). Chapter 5 showed that a lateral-bank headcut experienced significant surface lowering during the study period, mainly because it was strongly linked with flowpaths that concentrated and directed overland flow from the upper gentle hillslopes to the main channel (Figure 5.1). Consequently, gully incision was actively progressed, confirming that gully networks can expand rapidly in peatlands (Bower, 1960b). Local net topographic change for some places within the gullies studied was as 500–700 mm over the year (Figure 6.4). It is thus very important to reduce the hydrological connectivity and slope steepness of gully walls in order to control peatland gully erosion. In contrast, the main headcut of the tributary experienced net accumulation with a median net increase in the peat surface height of 22 mm during the whole study period (Table 5.4). This result suggests that incision dynamics and headward migration of the gullies was not active. The headcut was covered with dense vegetation on the upper hillslopes (Figure 5.1) which may have limited rapid overland flow, protected the peat from weathering or reduced particle transport by entrapment and prevented the expansion of the gully network.

7.1.2 Scale-dependency of peat erosion

The active sources and sinks of sediment in peatlands can be developed by a conceptual model based on this research and previous studies. Different erosion processes are active at different spatial scales, and different sediment sinks and sources appear from plot to catchment scale (Figure 7.2). Weathering processes such as frost action (Chapter 4–6) and desiccation (Chapter 5–6) are important in supplying erodible peat particles. Rainsplash (Chapter 3), interrill (Chapter 3) and rill erosion (Chapter 4) are the dominant erosion processes studied at fine erosion plot scales. For larger hillslope and small and medium-size catchment scales, gully erosion (Chapter 5–6) and mass movements (Evans and Warburton, 2007, Evans et al., 2006, Evans and Warburton, 2005) become more important. At the large basin scale long-term erosion and sediment deposition processes are more important due to large sediment sinks (footslopes and floodplains).

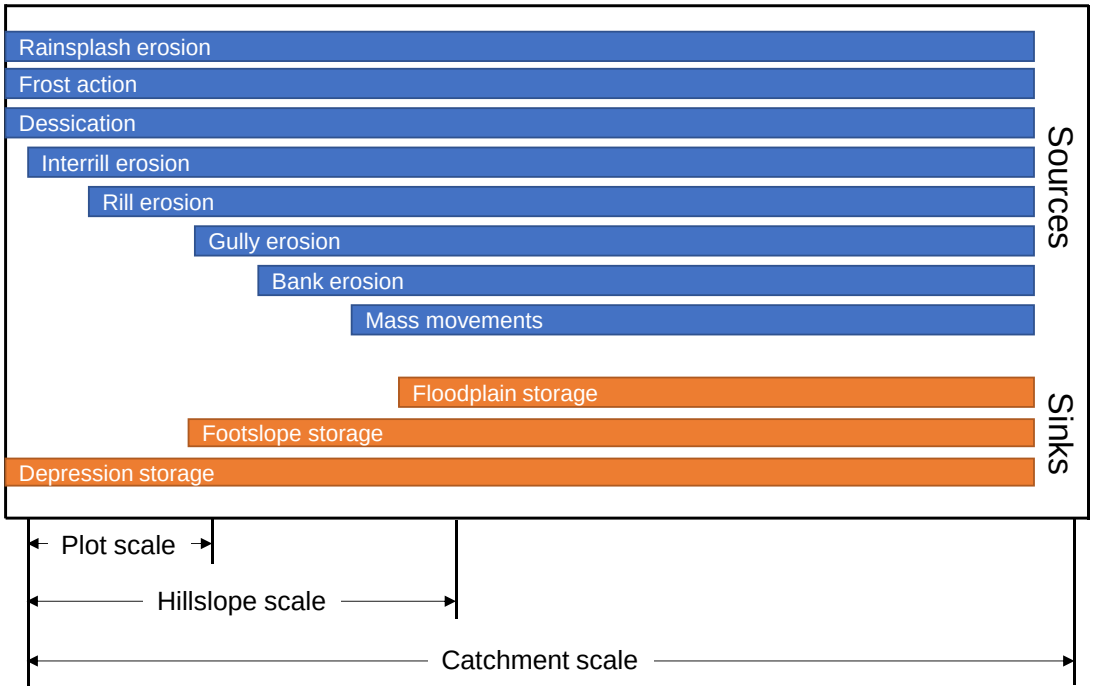

Figure 7.2 Conceptual model of active peat erosion processes at various spatial scales and contributing sediment sources and sinks for peatlands environments (modified to represent peat erosion features from the original semi-arid study by De Vente and Poesen (2005)).

In Chapter 2 a meta-analysis of peat erosion rates from the existing published literature was conducted (Figure 2.5 (a); Section 2.6). A comparison of sediment yields at different scales indicated significant differences between scales, probably caused by extrapolating data from very fine and fine scales to catchment scales. This study collected erosion or sediment yield data at scales not normally studied, i.e. very fine erosion plot scale (0.13 m^2), fine field scale (ranging from 20 to 90 m^2), small catchment scale (598 m^2) and catchment scale (1.7 ha). Data collection at these scales, particularly 50 m^2 to 2 ha has rarely occurred in previous peatland erosion studies. At the fine scale (areas less than 100 m^2) where interrill erosion and rill erosion dominated, peat erosion decreased with increasing area (Figure 6.9) possibly due to decreasing sediment delivery ratios (Walling and Webb, 1996). However, sediment yield at the catchment scale had no significant relationship with area since the combined effects of all active and interacting erosion and sediment deposition processes are complicated (Chapter 2). The percentage of POC flux as a proportion of total sediment flux was 36.8% (Chapter 6) and this value is in agreement with the range of 24.5–50.0% reported in previous blanket peat studies (Hutchinson, 1995, Francis, 1990, Worrall et al., 2003). The higher content of mineral materials (63.2%) in the

total sediment measured at larger scales would affect the scaling relationship (Chapter 6) as mineral sediment weathering and mobilization may be driven by different processes to those driving peat erodibility.

7.1.3 Peat erosion measurements

In this research numerous direct and indirect methods have been used to measure peat erosion, including bounded plots with rainfall and overland flow simulation experiments (Chapter 3 and 4), sediment traps (Chapter 6), catchment outlet sampling (Chapter 6) and high-resolution SfM surveying (Chapter 3–6). Bounded plots and laboratory simulation experiments allow the measurement of peat erosion rates and processes over short time periods in a controlled way (Chapter 3 and 4). The plot scale studies as shown in this research, together with those of previously published studies, have significantly improved our understanding of peatland hydrological and erosional processes (Holden and Burt, 2002a, Holden and Burt, 2002b, Holden and Burt, 2003, Holden et al., 2008, Li et al., 2018c, Li et al., 2018b, Kløve, 1998). Plot scale studies under laboratory rainfall simulations or natural field rainfall conditions remain an important research methodology for future peat erosion studies. However, plot scale studies usually allow the measurement of the peat loss reaching the plot outlet, which is then averaged for the entire plot area (Chapter 3 and 4) with the data integrating all upslope processes at a single point; thus it is difficult to assess the spatial variation of erosion and deposition within the plot and the drivers (Chapter 5).

SfM photogrammetry was used at different spatial scales in this study, ranging from laboratory peat blocks (Chapter 4 and 5) to field plots with different geomorphological features (Chapter 5), and to small headwater catchment scale (Chapter 6). SfM has the advantage of avoiding surface disturbance by the observer which is often problematic when using conventional methods such as erosion pins. In addition, SfM provides fully distributed estimates of topographic change and datasets for quantification of controls and drivers (Chapter 5). However, the magnitude of topographic change determined by SfM and traditional methods such as sediment sampling (Chapter 5) and sediment traps (Chapter 6) was not comparable. For example, for the headwater catchment the topographic change determined by SfM (mean value: 5.3 mm, standard deviation: 5.2 mm) was very different to the areal average derived from the sediment traps (mean value: –0.3 mm, standard deviation: 0.1 mm) (Chapter 6). The discrepancy could be result from the sediment sampling method or sediment traps failed

to detect local net topographic change that can be high (Figure 6.4) and those changes in opposite directions (positive/negative) may or may not cancel each other out at the catchment outlet scale.

In Chapter 5, the main topographic change was observed between a single short-term interval when intense rainfall, flow wash, needle ice production or surface desiccation was observed. However, several changes observed at the short-term scale were cancelled out by further topographic changes in the opposite direction (i.e. erosion followed by deposition) that cannot be discerned from longer monitoring intervals. When attempting to determine topographic changes and earth surface processes, an event-scale survey resolution that can capture important drivers (i.e. heavy rainfall event, needle ice production, serious desiccation) is therefore important.

7.1.4 Relationship between peat erosion and carbon loss

Peatlands store large amounts of the world's soil carbon (Yu et al., 2010), while these fragile ecosystems are vulnerable to degradation (Parry et al., 2014), leading to enhanced carbon release to the environment (Clay et al., 2012, Holden et al., 2007). In Chapter 6 the estimated POC load from the headwater catchment at Fleet Moss was 5.5 t yr^{-1}, equivalent to 340.9 tonnes of organic carbon km^{-2} yr^{-1} and accounting for 36.8% of the total suspended sediment load (926.3 t km^{-2} yr^{-1}). The sediment and POC fluxes at Fleet Moss appear to be much greater than those of other upland blanket peatlands reported in the literature showing values generally less than 200 t km^{-2} yr^{-1} for sediment flux and below 40 t km^{-2} yr^{-1} for POC flux (Chapter 2). These results suggest that Fleet Moss is an erosion hot spot where restoration intervention should aim to reduce future erosion.

7.2 Implications of research findings

The findings of this research have practical implications relating to erosion and hydrology of peatlands, peat erosion model development and restoration of eroded upland peatlands. Large amounts of sediment and POC were exported from the rapidly eroding Fleet Moss system (Chapter 6), suggesting that the peat surface would disappear due to fluvial erosion within approximately 100 years assuming the peat has an average depth of three metres. This study provides important baseline data to assess effects of planned future restoration projects on carbon fluxes in the fluvial system at the site. Within Fleet Moss there were areas of 0.7 m peat loss in one year (Chapter 6). Such a large topographical change rate could have a

major impact on the hydrological integrity of the peatland and may dramatically change local hydraulic gradients. The areas with higher surface roughness and slope are indicative of more active topographic change (Chapter 5) and thus should be priority areas for implementing restoration practices to reduce erosion.

Numerical models, such as the USLE (May et al., 2010) and the CAESAR model (Coulthard et al., 2000) have been tested in blanket peatlands and are capable of predicting some runoff–erosion relationships. Recent modelling projections using the PESERA–PEAT model (Li et al., 2016b) have suggested that many blanket peatlands in the Northern Hemisphere will be more susceptible to erosion under climate change and land management practices (Li et al., 2017). However, incorporating some of the important erosion processes into peat erosion models remains a challenge either due to difficulties in the parameterization of processes that are not fully understood or, as is often the case, a lack of field data for model calibration and validation. This present study therefore has important implications for model development and the ability of models to upscale across landscapes:

(1) Chapter 3 demonstrated that spatially distributed models of blanket peatlands that predict stream power and which can incorporate rainsplash – flow interactions would be useful for predicting future slope development in blanket peatlands.

(2) The interaction between rainfall and flow driven erosion processes are important in affecting flow hydraulics and sediment, in particular under gentle slopes and shallow overland flow conditions (Chapter 3). Consequently, to improve process-based interrill erosion modelling, the interaction between rainfall and flow driven erosion processes should be considered. However, further work is required to acquire an extensive dataset for parameterization across different soils (i.e. for application across non-peat soils) and slope conditions.

(3) Needle ice is a primary process contributing to upland peat erosion by enhancing peat erodibility and modifying overland flow hydraulics including overland flow velocity and hydraulic roughness during runoff events that follow thaw (Chapter 4). Models of overland flow-induced peat erosion should have a winter component that properly accounts for the effects of freeze–thaw (Li et al., 2016b) and especially needle ice processes, in order to successfully predict hillslope erosion and

sediment yield for watersheds in areas influenced by freezing and thawing.

(4) There is an increasing trend towards high resolution and small-scale erosion modelling (Kaiser et al., 2014). In this context, the use of SfM techniques provides new possibilities (Chapter 5 and 6). High resolution DEMs derived from SfM techniques at centimetre-scale or even higher resolution enables sediment budget estimation and erosion features (e.g. rill formation, gully incision) to be depicted more precisely.

Raindrop impact was found to play an important role in affecting peat overland flow and erosion processes for gentle slopes and shallow overland flow conditions (Chapter 3). From a restoration perspective, covering gently sloping bare peat surfaces by vegetation, brash or stabilizing geo-textiles (Parry et al., 2014) should help reduce erosion under typical rainfall intensities by weakening the impact of rainsplash. Needle ice processes significantly increased peat erosion risk during overland flow events (Chapter 5). This highlights that reducing bare areas of upland peat may play an important role in reducing peat erosion through protecting it from the disruptive effects of needle ice processes.

Gully incision was actively progressed via headward retreat on the lateral-bank headcut studied that strongly directed overland flow from the upper gentle hillslopes to the main channel (Chapter 5, Figure 5.1). In contrast, incision dynamics and headward migration was not active on the main headcut of the tributary that is covered with dense vegetation on the upper hillslopes (Chapter 5, Figure 5.1). Consequently, reducing hydrological connectivity and slope steepness of gullies is important to control gully erosion.

7.3 Limitations

Diverse geomorphic processes such as interrill and rill erosion/deposition, aeolian erosion/deposition, shrink–swelling, needle ice expansion and desiccation shrinkage are simultaneously operating on peat hillslopes (Grayson et al., 2012, Evans and Warburton, 2007, Glendell et al., 2017). The topographic change measured by the SfM technique is an aggregation of all of these processes across survey areas. In Chapters 5 and 6 the ‘positive M3C2 distance’ more accurately reflects topographic change that could be caused by both deposition and swelling processes; while a

‘negative M3C2 distance’ could also be attributed to both erosion and shrink/oxidation processes. Future work could be done to verify peat surface conditions (e.g. peat moisture, temperature, bulk density) between survey periods and thus establish the effects of swell–shrink processes in the observed patterns.

In order to produce quantifiable results with good levels of experimental control, bounded plots with rainfall and inflow simulation techniques were used in Chapters 3 and 4. The size of the peat blocks used was fairly small (1 m × 0.13 m) but this meant that it was feasible to obtain undisturbed peat blocks for careful collection, transport and storage in the laboratory. However, there are two main drawbacks with the very fine scale study. First, in Chapter 3 the main active erosion process on the surface of the peat blocks was interrill erosion due to the fact that the supplied water input was insufficient for the peat surface to develop into a rill. Future work could look at rill development and also wind assisted splash effects. Second, for some cases for natural peat deposits the depth of the friable upper layer disturbed by needle ice may sometimes be 10 cm or more (Evans and Warburton, 2007) and so the experiments in Chapter 4 may underrepresent roughness effects that occur in the field, particularly where there is a much larger scale hummocky peat surface or where previous desiccation has created surface polygon features. There may also have been other effects on surface roughness if repeated diurnal needle ice and thaw processes had been simulated and so these processes require further investigation.

Due to time limits this PhD thesis focused on certain surface erosion processes. However, subsurface erosion process (i.e. pipe erosion) and wind erosion could also be important in catchment sediment budgets but were not studied. The operation of these processes may also partially explain some of discrepancies between net topographic change and sediment yield measurements at different scales. At Fleet Moss the monitoring of discharge, sediment and POC was limited to one year (2016/2017) with long periods of dry weather that were important in producing erodible peat. However, this period may not be representative of multi-year fluctuations and temporal uncertainty could be reduced by continuous and prolonged monitoring. That said, given that climate change predictions suggest a reduced role for needle ice in many parts of the British Isles and an enhanced role of desiccation by the 2090s (Li et al., 2016a), the findings from the catchment study could be a useful indicator of concern for the future as sediment flux appeared to be extremely high following

desiccation during the study year and much greater than in the rainfall period (albeit a shorter period) following winter needle ice.

7.4 Future work

Since peat erosion consists of complex interacting process that are variable in both space and time and are influenced by numerous internal and external factors, there are still many unanswered questions. More peat erosion research is required in terms of:

(1) Under wet and windy conditions, wind-driven rain is important in peat surface erosion through the detachment and transport of peat particles (Warburton, 2003, Foulds and Warburton, 2007). More significant effects could be expected with higher kinetic energy levels closer to those experienced where natural rainfall is driven by strong wind. Future work could examine overland flow interactions with wind-driven rainsplash erosion and its contribution to total erosion as rainfall on blanket peatlands is often associated with strong winds (Evans and Warburton, 2007).

(2) Future work should be carried out to examine the effects of both the number and duration of needle ice processes on peat erodibility and the contribution to total erosion. Chapter 4 used simulated upslope inflow and excluded responses to raindrop impact, while under natural rainfall conditions raindrops provide the primary force to initiate peat particle detachment (Chapter 3). Thus, more significant effects of needle ice processes on increasing peat erosion could be expected under combined rainfall and overland flow conditions and exploration of these processes could be undertaken in future work. More attention should paid to examining the effects of desiccation on hydrological and erosional processes on desiccated peat blocks in the laboratory due to the apparently important role of desiccation on producing erodible peat materials suggested by findings in Chapter 6.

(3) Peat loss measurements at one scale are not representative for sediment yield at another scale level (Chapter 6). Therefore, direct extrapolation of plot scale interrill and rill erosion rates up the catchment scale can be problematic. More future work is needed for monitoring, experimental and modelling studies as a basis for scaling erosion rates from one specific area to larger or smaller areas. In addition, it is suggested that monitoring of peat erosion processes

should utilize standardized procedures to allow comparisons of data obtained from different study areas.

7.5 Conclusions

This thesis coupled laboratory-based experiments and field monitoring and used a range of direct and indirect methods, to examine sediment supply (rainsplash, freeze–thaw and desiccation) and sediment transport by water erosion processes and the drivers at various spatial and temporal scales. The main conclusions are:

- Both raindrop impact and the interaction between rainfall and flow driven erosion processes were important in affecting peat overland flow and erosion processes for gentle slopes and shallow overland flow conditions. Sediment yield generally increased with overland flow rate but sediment exhaustion and the detachment-limited interrill erosion pattern meant no linear relationship was found. Instead, stream power was found to be a good predictor of peat erosion.
- Needle-ice processes dramatically increased peat erodibility and reduced peat stability, and significantly reduced the surface flow velocity mainly through increased hydraulic roughness and changed surface microtopographic features, with micro-rills and headcuts developing. Peat erosion rates for the needle ice treatments showed a significant linear relationship with stream power.
- The net topographic change was –14 to +30 mm yr^{-1} for field plot sites with a peat hagg, gully wall, riparian area and gully head; and was –27 mm yr^{-1} for a headwater catchment at Fleet Moss. The incision dynamics and headward migration of the gully head was not active due to the dense vegetation cover on the upper hillslopes; while the lateral-bank headcut had significant negative topographic changes since flowpaths were concentrated and well connected.
- The topographic change patterns during both short-term and long-term surveys were well captured using SfM. Repeated SfM surveys that capture main change during events (intense rainfall, flow wash, needle ice production or surface desiccation) will be beneficial and cost effective for understanding longer-term peat

erosion dynamics. Surface roughness is a significant predictor of topographic change at both field plot scale and laboratory macroscale, and thus is important in controlling geomorphological processes and developments of peatlands.

- ❖ SfM produced significantly different topographic change compared to sediment traps on nested watersheds in the field (5.3 ± 5.2 mm vs –0.3 ± 0.1 mm); and sediment yield sampling on laboratory peat blocks (0.7 ± 4.3 mm vs –0.1 ± 0.1 mm). The difference suggested that direct interpolation of peat erosion rate measured at one scale to another scale could be problematic without considering sediment deposition, reworking and organic sediment oxidation processes; peat 'wastage' could be important during dry periods or when reworked, deposited peat becomes exposed.
- ❖ The total suspended sediment yield and POC load were 926.3 t km^{-2} yr^{-1} and 340.9 t C km^{-2} yr^{-1}, respectively, suggesting very high rates of active erosion at Fleet Moss. The greatest sediment and POC losses were found during the autumn. Both freeze–thaw during winter and desiccation during long periods of dry weather in spring and summer were identified as important peat weathering processes during the particular year of study.
- ❖ Bare peat surfaces are much more susceptible to erosion after being subjected to needle ice processes and desiccation. The weathered peat is subsequently detached by raindrops for transport by raindrop-impacted saturation-excess overland flow, ultimately leads to a range of spatially distributed surface erosion processes including interrill erosion, rill erosion and gully development.

The findings of this thesis have practical implications relating to upland erosion control in terms of: i) providing important baseline data to assess effects of restoration projects on fluvial carbon fluxes from an actively eroding headwater catchment; and ii) improving model parameterization through incorporation of basic erosion processes that are currently under-represented in erosion models to better predict slope development in blanket peatlands under future climate change and land management practices. However, future work is required to establish long-term and multi-scale in-situ monitoring programmes.

References

BOWER, M. 1960a. The erosion of blanket peat in the southern Pennines. *East Midland Geographer,* 13**,** 22-33.

BOWER, M. 1960b. Peat erosion in the Pennines. *Advancement of Science,* 64**,** 323-331.

BURT, T. & GARDINER, A. 1984. Runoff and sediment production in a small peat-covered catchment: some preliminary results. *Catchment Experiments in Fluvial Geomorphology* Norwich, England: Geo Books.

CLAY, G. D., DIXON, S., EVANS, M. G., ROWSON, J. G. & WORRALL, F. 2012. Carbon dioxide fluxes and DOC concentrations of eroding blanket peat gullies. *Earth Surface Processes and Landforms,* 37**,** 562-571.

DE VENTE, J. & POESEN, J. 2005. Predicting soil erosion and sediment yield at the basin scale: Scale issues and semi-quantitative models. *Earth-Science Reviews,* 71**,** 95-125.

EVANS, M., BURT, T., HOLDEN, J. & ADAMSON, J. 1999. Runoff generation and water table fluctuations in blanket peat: evidence from UK data spanning the dry summer of 1995. *Journal of Hydrology,* 221**,** 141-160.

EVANS, M. & LINDSAY, J. 2010. Impact of gully erosion on carbon sequestration in blanket peatlands. *Climate Research,* 45**,** 31-41.

EVANS, M. & WARBURTON, J. 2005. Sediment budget for an eroding peat ‐ moorland catchment in northern England. *Earth Surface Processes and Landforms,* 30**,** 557-577.

EVANS, M. & WARBURTON, J. 2007. *Geomorphology of upland peat: erosion, form and landscape change,* Oxford, UK, John Wiley & Sons.

EVANS, M., WARBURTON, J. & YANG, J. 2006. Eroding blanket peat catchments: global and local implications of upland organic sediment budgets. *Geomorphology,* 79**,** 45-57.

FOULDS, S. A. & WARBURTON, J. 2007. Significance of wind-driven rain (wind-splash) in the erosion of blanket peat. *Geomorphology,* 83**,** 183-192.

FRANCIS, I. 1990. Blanket peat erosion in a mid ‐ wales catchment during two drought years. *Earth Surface Processes and Landforms,* 15**,** 445-456.

GLENDELL, M., MCSHANE, G., FARROW, L., JAMES, M. R., QUINTON, J., ANDERSON, K., EVANS, M., BENAUD, P., RAWLINS, B. & MORGAN, D. 2017. Testing the utility of structure ‐ from ‐ motion photogrammetry reconstructions using small unmanned aerial vehicles and ground photography to estimate the extent of upland soil erosion. *Earth Surface Processes and Landforms,* 42**,** 1860-1871.

GRAYSON, R., HOLDEN, J., JONES, R., CARLE, J. & LLOYD, A. 2012. Improving particulate carbon loss estimates in eroding peatlands through the use of terrestrial laser scanning. *Geomorphology,* 179**,** 240-248.

HOLDEN, J. 2006. Sediment and particulate carbon removal by pipe erosion increase over time in blanket peatlands as a consequence of land

drainage. *Journal of Geophysical Research: Earth Surface (2003–2012),* 111.

HOLDEN, J. & BURT, T. 2002a. Infiltration, runoff and sediment production in blanket peat catchments: implications of field rainfall simulation experiments. *Hydrological Processes,* 16**,** 2537-2557.

HOLDEN, J. & BURT, T. 2002b. Laboratory experiments on drought and runoff in blanket peat. *European Journal of Soil Science,* 53**,** 675-690.

HOLDEN, J. & BURT, T. 2003. Hydrological studies on blanket peat: the significance of the acrotelm ‐ catotelm model. *Journal of Ecology,* 91**,** 86-102.

HOLDEN, J., KIRKBY, M. J., LANE, S. N., MILLEDGE, D. G., BROOKES, C. J., HOLDEN, V. & MCDONALD, A. T. 2008. Overland flow velocity and roughness properties in peatlands. *Water Resources Research,* 44**,** W06415.

HOLDEN, J., SHOTBOLT, L., BONN, A., BURT, T., CHAPMAN, P., DOUGILL, A., FRASER, E., HUBACEK, K., IRVINE, B. & KIRKBY, M. 2007. Environmental change in moorland landscapes. *Earth-Science Reviews,* 82**,** 75-100.

HUTCHINSON, S. M. 1995. Use of magnetic and radiometric measurements to investigate erosion and sedimentation in a British upland catchment. *Earth Surface Processes and Landforms,* 20**,** 293-314.

KAISER, A., NEUGIRG, F., ROCK, G., MÜLLER, C., HAAS, F., RIES, J. & SCHMIDT, J. 2014. Small-scale surface reconstruction and volume calculation of soil erosion in complex Moroccan gully morphology using structure from motion. *Remote Sensing,* 6**,** 7050-7080.

KLØVE, B. 1998. Erosion and sediment delivery from peat mines. *Soil and Tillage Research,* 45**,** 199-216.

LABADZ, J., BURT, T. & POTTER, A. 1991. Sediment yield and delivery in the blanket peat moorlands of the Southern Pennines. *Earth Surface Processes and Landforms,* 16**,** 255-271.

LI, C., GRAYSON, R., HOLDEN, J. & LI, P. 2018a. Erosion in peatlands: Recent research progress and future directions. *Earth-Science Reviews,* 185**,** 870-886.

LI, C., HOLDEN, J. & GRAYSON, R. 2018b. Effects of needle ice production and thaw on peat erosion processes during overland flow events. *Journal of Geophysical Research: Earth Surface,* 123**,** 2107-2122

LI, C., HOLDEN, J. & GRAYSON, R. 2018c. Effects of rainfall, overland flow and their interactions on peatland interrill erosion processes. *Earth Surface Processes and Landforms,* 43**,** 1451-1464.

LI, P., HOLDEN, J. & IRVINE, B. 2016a. Prediction of blanket peat erosion across Great Britain under environmental change. *Climatic Change,* 134**,** 177-191.

LI, P., HOLDEN, J., IRVINE, B. & GRAYSON, R. 2016b. PESERA ‐ PEAT: a fluvial erosion model for blanket peatlands. *Earth Surface Processes and Landforms,* 41**,** 2058-2077.

LI, P., HOLDEN, J., IRVINE, B. & MU, X. 2017. Erosion of Northern Hemisphere blanket peatlands under 21st ‐ century climate change. *Geophysical Research Letters,* 44**,** 3615-3623.

LINDSAY, R., BIRNIE, R. & CLOUGH, J. 2014. Peat bog ecosystems: weathering, erosion and mass movement of blanket bog. Edinburgh: International Union for the Conservation of Nature.

PARRY, L. E., HOLDEN, J. & CHAPMAN, P. J. 2014. Restoration of blanket peatlands. *Journal of Environmental Management,* 133**,** 193-205.

SHUTTLEWORTH, E. L., CLAY, G. D., EVANS, M. G., HUTCHINSON, S. M. & ROTHWELL, J. J. 2017. Contaminated sediment dynamics in peatland headwater catchments. *Journal of Soils and Sediments,* 17**,** 1-11.

WALLING, D. E. & WEBB, B. 1996. *Erosion and Sediment Yield: Global and Regional Perspectives: Proceedings of an International Symposium Held at Exeter, UK, from 15 to 19 July 1996*, IAHS.

WARBURTON, J. 2003. Wind-splash erosion of bare peat on UK upland moorlands. *Catena,* 52**,** 191-207.

WORRALL, F., REED, M., WARBURTON, J. & BURT, T. 2003. Carbon budget for a British upland peat catchment. *Science of the Total Environment,* 312**,** 133-146.

YU, Z., LOISEL, J., BROSSEAU, D. P., BEILMAN, D. W. & HUNT, S. J. 2010. Global peatland dynamics since the Last Glacial Maximum. *Geophysical Research Letters,* 37.

Appendix A
Supplementary information

Supplementary information for Chapters 4 is included below.

A.1 Chapter 4 Effects of needle ice on peat erosion processes during overland flow events

The supporting information includes three supplementary tables and a figure: (1) Supplementary Table 4.1: Summary of the experimental design and treatments; (2) Supplementary Table 4.2: Basic physical and chemical characteristics of the tested peat soils for the NI and Non-NI treatments; and (3) Supplementary Table 4.3: The measured sediment concentration, sediment yield rate and peat anti-scouribility capacity for the NI and Non-NI treatments under different slopes and scouring rates; (4) Supplementary Figure 4.1: M3C2 distance and histogram of differences, and roughness for the peat blocks with and without needle ice growth.

A.1.1 Experimental design and treatments

Supplementary Table 4.1 Summary of the experimental design and treatments.

Slopes	**Designed flow rate (L min^{-1})**	**Treatment***	**Replicates**	**Upslope inflow rate (L min^{-1})**		**Duration** (min)**
				Mean	STDev	
2.5°	0.5	NI	1	0.55	0.02	20
			2	0.49	0.01	20
		Non-NI	1	0.50	0.01	20
			2	0.50	0.02	20
			3	0.48	0.02	20
	1.0	NI	1	1.07	0.02	30
			2	0.95	0.00	20
		Non-NI	1	1.06	0.05	30
			2	1.02	0.03	10
			3	0.97	0.00	10
	2.0	NI	1	2.00	0.04	10
			2	2.00	0.01	10
		Non-NI	1	1.97	0.10	10
			2	2.03	0.00	10
			3	1.98	0.03	10
7.5°	0.5	NI	1	0.50	0.01	20
			2	0.50	0.01	20
		Non-NI	1	0.50	0.01	20

Slopes	Designed flow rate (L min^{-1})	Treatment*	Replicates	Upslope inflow rate (L min^{-1})		Duration** (min)
			2	0.50	0.01	10
			3	0.49	0.01	20
	1.0	NI	1	1.12	0.07	30
			2	1.01	0.01	30
			3	0.95	0.00	20
		Non-NI	1	1.04	0.01	30
			2	1.08	0.01	30
			3	1.04	0.01	10
	2.0	NI	1	1.96	0.08	10
			2	1.99	0.06	10
			3	1.99	0.06	10
		Non-NI	1	2.03	0.00	10
			2	2.03	0.00	10

1) * Needle ice treatments include treatment with needle ice processes (NI) and without needle ice processes (Non-NI);
2) ** Duration indicates time since overland flow generation (min).

A.1.2 Basic physical and chemical characteristics of the tested peat soils

Supplementary Table 4.2 Basic physical and chemical characteristics of the tested peat soils for the NI and Non-NI treatments

Basic physical and chemical characteristics		Non-NI		NI	
		Median	StDev	Median	StDev
Bulk density (g cm^{-3})		0.19	0.01	0.17	0.01
Porosity (%)		86.5	1.0	90.0	0.7
Moisture (%)		87.2	0.9	52.6	7.9
pH		3.7	0.1	3.7	0.1
Size and shape parameters of peat particles	Length (µm)	18.4	8.9	31.42	11.47
	Width (µm)	10.8	4.6	17.39	6.10
	Perimeter (µm)	49.3	23.2	89.46	33.81
	Circularity	0.83	0.06	0.80	0.03
	Convexity	0.97	0.02	0.97	0.01
	Solidity	0.94	0.03	0.93	0.02
	Aspect Ratio	0.69	0.01	0.61	0.03
	Elongation	0.31	0.01	0.39	0.03

Circularity (0–1) quantifies how close the peat particles are to perfect circles with 1 being a perfect circle; Convexity (0–1) measures the surface roughness of peat particles.

A.1.3 Sediment concentration, sediment yield rate and peat anti-scouribility capacity data

Supplementary Table 4.3 The measured sediment concentration, sediment yield rate and peat anti-scouribility capacity for the NI and Non-NI treatments under different slopes and scouring rates.

Slopes	Designed flow rate (L min^{-1})	Treatment	Replicates	SC	SY	AS
2.5°	0.5	NI	1	74.5	305.0	24.3
			2	162.0	654.1	7.0
			Mean	118.3	479.6	15.6
		Non-NI	1	86.3	309.2	13.9
			2	33.5	189.2	31.1
			Mean	59.9	249.2	22.5
	1.0	NI	1	74.5	713.2	13.2
			2	136.6	1109.9	7.5
			Mean	105.6	911.6	10.3
		Non-NI	1	90.2	1002.2	9.9
			2	46.4	694.2	22.1
			3	74.7	560.7	15.9
			Mean	70.4	752.4	16.0
	2.0	NI	1	610.3	16424.7	2.7
			2	1126.5	8256.1	2.6
			Mean	868.4	12340.4	2.7
		Non-NI	1	59.8	1003.1	16.4
			2	85.4	2279.3	18.4
			3	59.5	950.0	18.8
			Mean	68.2	1410.8	17.9
7.5°	0.5	NI	1	125.1	735.6	11.6
			2	483.2	3507.5	2.3
			Mean	304.2	2121.6	7.0
		Non-NI	1	96.7	365.0	11.3
			2	50.1	188.8	24.2
			Mean	73.4	276.9	17.8
	1.0	NI	1	366.1	3718.9	3.5
			2	1393.2	12876.6	1.6
			3	802.8	7001.0	3.4
			Mean	854.1	7865.5	2.8
		Non-NI	1	108.6	1048.7	10.4
			2	326.3	3197.5	4.1
			3	114.7	1341.0	10.5
			Mean	183.2	1862.4	8.3
	2.0	NI	1	2229.4	72061.8	0.7
			2	100.4	2842.1	12.4
			3	186.6	4856.8	6.2
			Mean	838.8	26586.9	6.4
		Non-NI	1	119.9	1898.0	9.0
			2	53.2	1639.2	19.3

Slopes	Designed flow rate (L min^{-1})	Treatment	Replicates	SC	SY	AS
			Mean	86.5	1768.6	14.1

Abbreviations: SC, Sediment concentration (mg L^{-1}); SY, Sediment yield rate (mg m^{-2} min^{-1}); AS, peat anti-scouribility capacity (L g^{-1}).

A.1.4 M3C2 distance and roughness data

A description of SfM data acquisition, processing in Agisoft Photoscan and differencing in CloudCompare is provided below.

[Methods]

The peat blocks of NI and Non-NI treatments were put into individual soil flumes with 23 ground control points (*GCPs*) positioned along the boundaries and marked with high-visibility bookmarkers (Figure S1a). A local co-ordinate system was used and the relative co-ordinates of the 23 *GCPs* were determined. Overlapping 2D images (Figure S1b) were taken using a FUJIFILM FinePix AX650 16 mega pixel digital camera with focal length set at 6 mm and with automatic exposure enabled. Images acquired were processed using the commercial software Agisoft PhotoScan. The default settings with the photo alignment accuracy set to “highest” and the dense cloud quality set to “highest” were used to produce dense point clouds. The residual georeferencing errors were calculated by subtracting the GPS co-ordinates of each GCP from the point cloud, and point-cloud quality was evaluated by summarizing residual errors using root mean squared error (RMSE) [*Smith et al*., 2014]. For the tests, the georeferencing errors for the peat blocks of NI and Non-NI treatments were 0.004589 m and 0.004021 m, respectively.

The Multiscale Model to Model Cloud Comparison (M3C2) algorithm [*Lague et al*., 2013] in the open source CloudCompare software was used to compute cloud-to-cloud differencing and roughness of both clouds (NI and Non-NI). M3C2 requires users to define two main parameters: i) the normal scale D, which is used to calculate a surface normal for each point and is dependent upon surface roughness and registration error; ii) the projection scale d within which the average surface elevation of each cloud is calculated. For our tests, the normal scale D for each point cloud was estimated based on a trial-and-error approach similar to that of *Westoby et al*. [2016] and was fixed at 0.05 m. The projection scale d was specified as 0.005 m and this scaling was enough to average a minimum of 30 points sampled in each cloud [*Lague et al*., 2013]. A Level of Detection (LoD)

threshold for a 95% confidence level [*Lague et al*., 2013] was used to exclude points with non-significant changes.

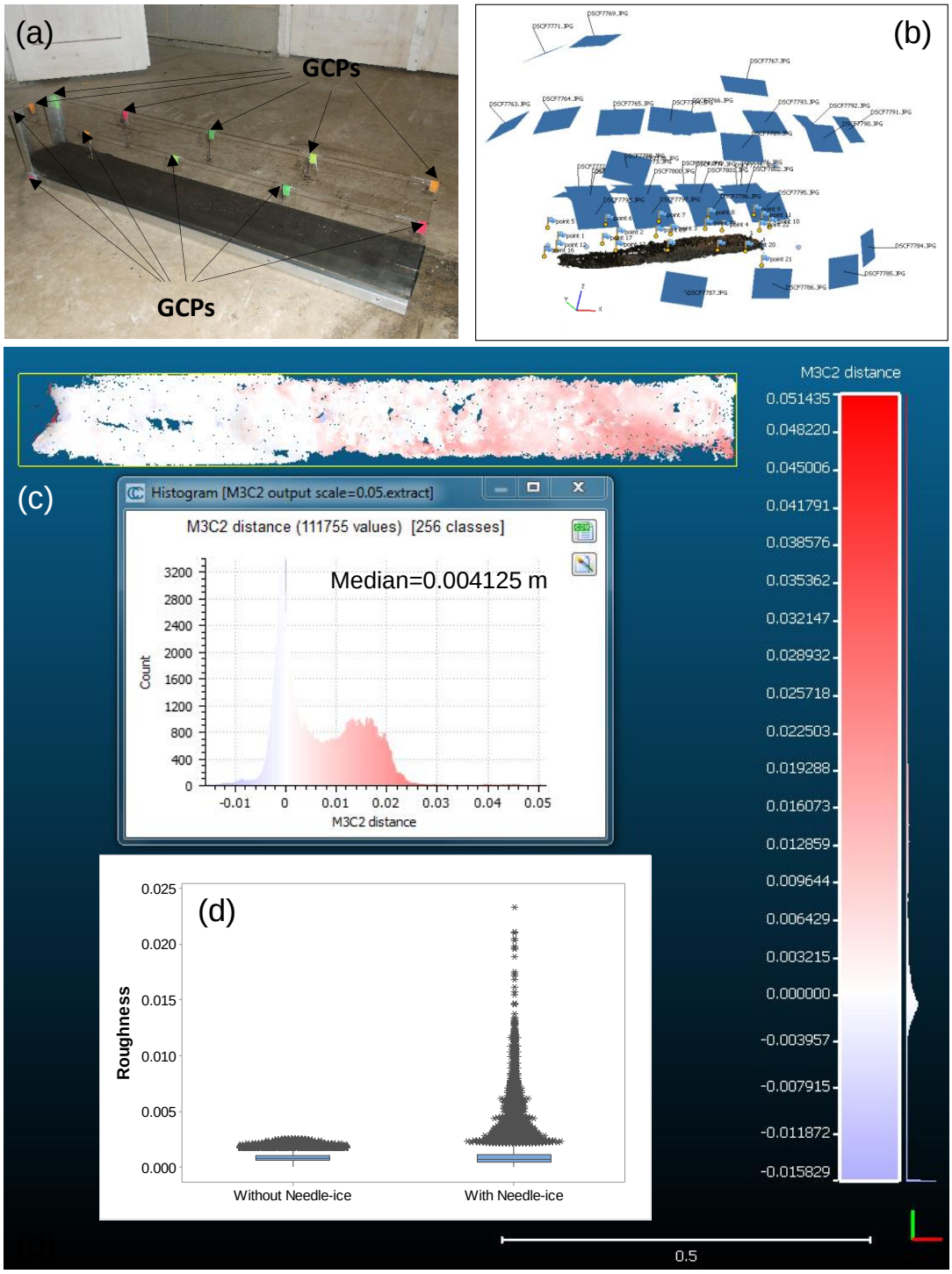

Supplementary Figure 4.1 (a) Distribution of ground cover points (GCPs) along the boundaries of the soil flume; (b) Dense points of the surface of peat block with needle ice formation. The locations of images and GCPs are shown in Agisoft PhotoScan; (c) M3C2 distance and histogram of differences for the peat blocks with and without needle ice growth; (d) Roughness of the peat blocks without needle ice (Mean = 0.000887, Stdev = 0.000388) and with needle ice (Mean = 0.001008, Stdev = 0.001071).